Leibniz-Institut für Katalyse e.V. an der Universität Rostock

CO_2 Fischer-Tropsch Synthesis: Unleashing the Power of Data Science and Machine Learning for Sustainable Hydrocarbon Production

Dissertation

In Kumulativer Form
zur Erlangung des akademischen Grades
Doctor rerum naturaliun (Dr. rer. nat.)
der Mathematisch-Naturwissenschaftlichen Fakultät
der Universität Rostock

vorgelegt von

Aleksandr Fedorov

geb. am 23.04.1991 in Amurskaya Oblast, Russland

Rostock, 2024

https://doi.org/10.18453/rosdok_id00005013

Die vorliegende Arbeit entstand in der Zeit von April 2021 bis März 2024 am Leibniz-Institut für Katalyse e.V. an der Universität Rostock unter der Betreuung von Dr. David Linke (Bereichsleitung Katalysatorentwicklung und Reaktionstechnik)

This thesis was performed in the Leibniz Institute for Catalysis at the University of Rostock in the period from April 2021 to March 2024 and was supervised by Dr. David Linke (the head of department of Catalyst Discovery and Reaction Engineering).

1. Gutachter

Dr. David Linke

Leibniz-Institut für Katalyse e.V., Rostock, Germany

2. Gutachter

Prof. Dr. Evgeny Pidko

Delft University of Technology, Delft, the Netherlands

Tag der Einreichung: 8. April 2024

Tag der mündlichen Prüfung: 22. Oktober 2024

Prüfungsrechtliche Erklärung

Ich, Aleksandr Fedorov, versichere, dass ich die Arbeit selbständig verfasst, nicht anderweitig für Prüfungszwecke vorgelegt, alle benutzten Quellen und Hilfsmittel angegeben sowie wörtliche und sinngemäße Zitate als solche gekennzeichnet habe.

Plagiarism Declaration in Accordance with Examination Rules

I herewith declare that I have worked on this thesis independently. Furthermore, it was not submitted to any other examining committee. All sources and aids used in this thesis, including literal and analogous citations, have been identified.

Rostock, March 2024

Dedicated to the thousands of individuals who have coded for open-source projects for free. It is due to their efforts that scientific work with powerful tools is possible.

Acknowledgements

I would like to express my deepest gratitude to my supervisor, Dr. David Linke, for his unwavering support and guidance throughout this journey. His expertise, patience, and constructive feedback have been invaluable in shaping this work. I can say with confidence that I have grown significantly as a scientist under his leadership. I am proud to have been his PhD student.

Heartfelt thanks to my colleagues for their support and assistance in completing the current work. Specifically, I would like to thank Dr. Henrik Lund for XRD measurements and help with the analysis of the results, Axel Radtke for helping in fixing and improving the catalytic setup, Dr. Vita A. Kondratenko for performing TAP experiments, Dr. Armin Springer for recording SEM images, Dr. Hanan Atia for TPR-H_2 investigation, Reinhard Ecklet for BET analysis, Anja Simmula for ICP measurement. I would like to express my gratitude to Prof. Dr. Evgenii V. Kondratenko for fruitful discussions and constructive criticism, which made my work better. I want to give special thanks to the colleagues of the InnoSyn project in which this work was carried out, particularly Dr. Anna Perechodjuk, Philipp Andreas Graefe, Dr. Sebastian Wohlrab, Dr. Uwe Rodemerck, and Prof. Dr. Reinhard Rauch.

I feel great gratitude to current and former employees of LIKAT, particularly Dr. Tatiana Otroshchenko, Dr. Qiyang Zhang, Dr. Anna Zanina, Laura Kraußer, Dr. Dan Zhao, Dr. Mariana Armbruster, Dr. Qingxin Yang, Lin Xu, Dr.-Ing. Zeynep Aydin, Dr. Nils Ortner, Karin Buchholz, Dr. Martin Holena, Dr. Elka Kraleva, and Dr. Nikolaos Moustakas for always having time to help as well as warm and friendly work environment.

I want to thank the friends and muchachos, who have appeared during the period of completing the work, particularly Dr. José Balena Gabriel Filho, Mikhail Bednov, Dr. Sebastian Cisneros, Phong Dam, Hilario Diego Huerta, Aleksandrs Kalamasnikovs, Frau Aleksandra Khomutetckaia, Dr. Vladislav Kochetov, Vyacheslav Petchenko, Alexandra Rossiyskaya, Sebastian Smyczek, Constanza Terazzi, and Dr. Vasily Tulsky for their encouragement, moral support, and having fun days in Rostock.

I am indebted to my wife Dr. Elizaveta Fedorova for her unwavering love, understanding, and encouragement throughout this endeavor. Her belief in me has been my source of strength and motivation.

I acknowledge German Federal Ministry of Education and Research (BMBF) through the project InnoSyn (FKZ: 03SF0616B) for the financial support that made this work possible.

Zusammenfassung

Der Anstieg der Kohlendioxidemissionen, der zum Klimawandel und zur Umweltzerstörung führt, motiviert zur Entwicklung neuer Technologien zur Lösung dieses Problems. Die CO_2-Hydrierung zu höheren Kohlenwasserstoffen (CO_2-Fischer-Tropsch-Synthese (CO_2-FTS)) kann als eine mögliche Lösung dieses Problems angesehen werden. Das Interesse an der CO_2-Hydrierung hat dazu geführt, dass die Zahl der wissenschaftlichen Veröffentlichungen über die Untersuchung von CO_2-FT-Katalysatoren und damit auch die Menge der veröffentlichten Daten gestiegen ist. Es ist vielversprechend, die gesammelten Daten auszuwerten und zu analysieren, um Korrelationen zwischen Katalysatoreigenschaften und Aktivität zu finden und verborgenes Wissen über CO_2-FTS aus der Literatur zu extrahieren. Die Analyse von CO_2-FTS-Daten ist jedoch mit zusätzlicher Komplexität verbunden, die sich aus zwei Faktoren ergibt: (i) eine breite Vielfalt von Produkten (CO, Methan, niedere Olefine, höhere Kohlenwasserstoffe etc.) und (ii) die katalytischen Daten wurden unter verschiedenen Reaktionsbedingungen gewonnen. Moderne Methoden der Datenanalyse und des maschinellen Lernens (ML) könnten bei der Analyse dieser Art von Daten helfen. Diese Arbeit konzentriert sich auf die Untersuchung der CO_2-FTS mit Hilfe dieser modernen Methoden.

Der erste Teil der Arbeit ist der Analyse der Literaturdaten über CO_2-Hydrierungskatalysatoren für die Kohlenwasserstoffproduktion gewidmet. Es wurde festgestellt, dass die Schlüsselparameter der Katalysatorselektivität wie die Kettenwachstumswahrscheinlichkeit nur geringfügig von den Reaktionsbedingungen abhängen. Stattdessen bestimmen hauptsächlich die Katalysatorzusammensetzung, die Präparationsmethode und die Reduktionsvorbehandlung die Katalysatorselektivität. Die mit der Random-Forest-Regression durchgeführte Feature-Importance-Analyse hat gezeigt, dass die Promatierung von Katalysatoren auf Fe-Basis mit Alkalimetallen (wie K und Na) im Vergleich zu anderen Ansätzen (Reaktionsbedingungen, Reduktionsvorbehandlung, Vorhandensein anderer Promotoren etc.) die wirksamste Maßnahme zur Verbesserung der Katalysatorselektivität ist. Für die RWGS-Reaktion wurde ihre Annäherung an das Gleichgewicht analysiert. Die erzielten Ergebnisse deuten darauf hin, dass es einen zusätzlichen Weg für eine direkte CO_2-Hydrierung zu höheren Kohlenwasserstoffen über die FT-Reaktion gibt.

Der zweite Teil der vorliegenden Arbeit ist einer experimentellen Validierung des direkten Weges der Bildung höherer Kohlenwasserstoffe aus CO_2 gewidmet. Zu diesem Zweck wurden typische promotiert Katalysatoren auf Fe-Basis nach der Methode der organischen Verbrennung hergestellt und unter CO_2-FT-Bedingungen getestet. Die Analyse der erhaltenen katalytischen Daten ermöglichte es, das

Vorhandensein des direkten Weges für einige katalytische Systeme zuverlässig zu bestätigen. Die Untersuchung der erhaltenen Katalysatoren mit physikalisch-chemischen Methoden zeigte, dass bestimmte Eisenkarbide in der Lage sind, CO_2 direkt zu höheren Kohlenwasserstoffen zu hydrieren. Daher sollte das Konzept, Eisenoxid als wesentliche aktive Komponente für die Katalyse der RWGS in der CO_2-FTS zu benötigen, überprüft werden.

Der letzte Teil der Arbeit ist der Entwicklung neuer Ansätze für die kinetische Modellierung der CO_2-Hydrierung unter Verwendung neuronaler gewöhnlicher Differentialgleichungen (ODE) gewidmet, indem künstliche neuronale Netzmodelle (ANN) mit nur wenigen Daten trainiert werden, die für die Entwicklung kinetischer Modelle typisch sind. Es wurde festgestellt, dass die Einschränkung der neuronalen ODE durch die Integration des allgemeinen Wissens über Thermodynamik und Kinetik die Erstellung zuverlässiger kinetischer Modelle auf der Grundlage von ANN für den Prozess der CO_2-Hydrierung zu Kohlenwasserstoffen ermöglicht. Der neue Ansatz wurde durch numerische Experimente validiert und erfolgreich für die Modellierung der CO_2-FTS unter Verwendung realer experimenteller Daten angewendet. Es wurden einige Ideen zur Rekonstruktion und Aufklärung des mechanistischen Modells der CO_2-FTS aus den erhaltenen neuronalen ODE-Modellen vorgestellt.

Abstract

An increase in carbon dioxide emissions resulting in the climate change and environmental degradation motivates to develop new technologies for solving this problem. CO_2 hydrogenation to higher hydrocarbons (CO_2 Fischer-Tropsch synthesis (CO_2-FTS)) may be considered as a potential solution of this problem. The interest in CO_2 hydrogenation has led to a rise in the number of scientific publications regarding the investigation of CO_2-FT catalysts and, thus, the amount of published data. It becomes attractive to evaluate and analyze the accumulated data to find the correlations between catalyst properties and activity as well as extract hidden knowledge about CO_2-FTS from the literature. However, the analysis of CO_2-FTS data comes with additional complexity that arises from two factors: (i) a wide range of the products (CO, methane, light olefins, higher hydrocarbons etc.) and (ii) the catalytic data were obtained under different reaction conditions. Modern data science and machine learning (ML) methods could help in the analysis of such type of data. This work focuses on the investigation of the CO_2-FTS using these modern methods.

The first part of the work is devoted to analyzing of the literature data about CO_2 hydrogenation catalysts for hydrocarbon production. It was found that the key parameters of the catalyst selectivity such as the chain growth probability only slightly depend on the reaction conditions. Instead, the catalyst composition, preparation, and reduction pre-treatment mainly define the catalyst selectivity. Feature importance analysis performed by the random forest regression demonstrated that doping Fe-based catalysts with alkaline metals (like K and Na) is the most effective measure for improving catalyst selectivity compared to other approaches (reaction conditions, reduction pretreatment, presence of other dopants etc.). For the RWGS reaction its approach to equilibrium was analyzed. The obtained results indicate the presence of an additional route of a direct CO_2 hydrogenation to higher hydrocarbons via the FT reaction.

The second part of the present thesis is devoted to an experimental validation of the presence of the direct route of the higher hydrocarbon formation from CO_2. For this, typical promoted Fe-based catalysts were prepared by the organic combustion method and tested under CO_2-FT condition. The analysis of the obtained catalytic data allowed one to reliably confirm the presence of the direct route for some catalytic systems. The investigation of the obtained catalysts by physicochemical methods demonstrated that certain iron carbides are able to directly hydrogenate CO_2 to higher hydrocarbons. Thus, the concept of requiring iron oxide as an essential active component for catalyzing the RWGS in CO_2-FTS should be reviewed.

The last part of work is devoted to developing new approaches for kinetic modelling of CO_2 hydrogenation using neural ordinary differential equations (ODE) by training artificial neural network (ANN) models with only small data that are typical for the kinetic model development. It was found that the constraining of neural ODE by integrating the general knowledge about thermodynamics and kinetics allows one to build reliable kinetic models based on ANN for the process of CO_2 hydrogenation to hydrocarbons. The new approach was validated by the numerical experiments and successfully applied for modelling of the CO_2-FTS using real experimental data. Some ideas for reconstructing and elucidating the mechanistic model of CO_2-FTS from the obtained neural ODE models were presented.

Table of Contents

List of Abbreviations

ANN – artificial neural network

ANOVA – analysis of variance

ASF – Anderson-Schulz-Flory

CCS – carbon capture and storage

CV- cross validation

DFT – density functional theory

FTS – Fischer-Tropsch synthesis

GHSV – gas hourly space velocity

HOMO – highest occupied molecular orbital

HTFT – high temperature Fischer-Tropsch

LHHW – Langmuir-Hinshelwood-Hougen-Watson

LSTM – long short-term memory networks

LTFT – low temperature Fischer-Tropsch

LUMO – lowest unoccupied molecular orbital

ML – machine learning

MLR – multiple linear regression

NN – neural network

OCM – oxidation coupling of methane

ODE – ordinary differential equation

PCA – principal component analysis

PCR – principal component regression

PLS – partial least square

RWGS – reverse water gas shift

SVM – support vector machine

SVR – support vector regression

TAP – temporal analysis of products

XPS – X-ray photoelectron spectroscopy

ΔH_{298K} – standard enthalpy of a reaction at 298 K

1. Introduction

1.1. CO_2 Emission Problem

Over the past century, there has been a significant rise in global energy production, primarily driven by the combustion of fossil fuels such as coal, oil, and natural gas [1]. This increase in energy supply has undoubtedly provided numerous benefits, powering economic growth, improving living standards, and enabling technological advancements. However, it has also led to a range of interconnected problems that cannot be ignored. They include resource depletion, air pollution, and the significant issue of CO_2 emissions leading to environmental degradation. The CO_2 emission problem arises from the significant contribution (around 75 %) of carbon dioxide as a greenhouse gas [2], which traps heat in the Earth's atmosphere and enhances the greenhouse effect. Greenhouse gases have the unique property of being transparent to incoming sunlight but absorbing and re-emitting a portion of the outgoing infrared radiation formed in the form of heat from warm land and oceans [3]. Re-emitting a portion of the infrared radiation results in the additional warming of the planet that contributes to the greenhouse effect. The above problem of the climate change and CO_2 emissions can be illustrated in Figure 1, which shows the temporal dependencies of monthly temperature anomaly, annual CO_2 emissions worldwide, and global atmospheric CO_2 concentrations.

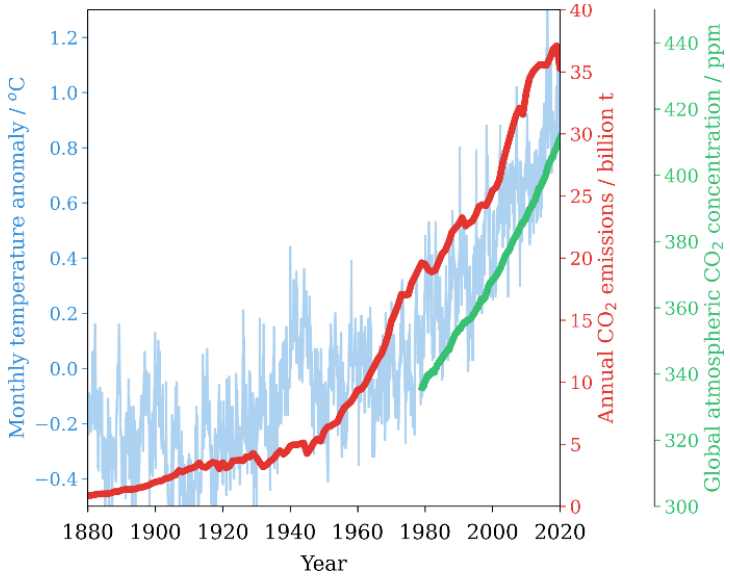

Figure 1. The combined land-surface air and sea-surface water mean temperature anomaly is given as the deviation from the 1951–1980 (blue line) [4, 5]; CO_2 emissions from fossil fuels and industry (red line) [6]; Atmospheric carbon dioxide concentration (green line) [7].

The excessive accumulation of CO_2 emissions is a significant environmental problem with far-reaching consequences for ecosystems, weather patterns, sea levels etc. Addressing this problem is crucial for mitigating climate change and ensuring a sustainable future.

1.2. CO_2 Storage and Utilization

A dramatic rise in the CO_2 emission motivates academia and industry to be looking for the solutions for reducing carbon dioxide emission. The main strategy involves capturing and storing it or converting carbon dioxide into valuable products in a manner that reduces its environmental impact. Given the existence of different sources of CO_2, ranging from high-concentrated flue gas with 5-50 % of CO_2 to the ambient air with a CO_2 concentration of around 400 ppm, various technologies are being developed for the capture of carbon dioxide. These technologies are based on different physical and chemical processes including cryogenic distillation [8], permeation through membranes (polymer based and inorganic membranes) [9, 10], absorption into liquid solutions (amine-based solution [11], alkaline hydroxides [12]), adsorption onto a solid (alumina, zeolite, activated carbon) [13], algal and microbiological systems (consuming CO_2 during photosynthesis or metabolic processes) [1, 14].

In the case of atmospheric air, with its relatively low concentration of carbon dioxide (<0.04%), the direct separation of CO_2 from it can be achieved using solid sorbents containing amines or basic absorbents ($Ca(OH)_2$, KOH etc.) that chemically react and chemosorb carbon dioxide [15]. However, current technologies face efficiency challenges including processing large volumes of air, leading to high energy consumption and material costs [1].

Another step is to use the concentrated source of carbon dioxide for the storage or conversion into valuable organic products. The Carbon Capture and Storage (CCS) technologies involves capturing CO_2 emissions and storing it underground, preventing its release into the atmosphere [16]. The captured CO_2 can be injected into suitable geological formations, such as depleted oil and gas reservoirs [17] or deep saline aquifers [18], where it can be securely stored for long periods.

Utilizing concentrated sources of CO_2 to produce organic compounds represents a promising strategy for circular economy, as it not only helps to reduce CO_2 emissions but also enables the generation of valuable products with commercial potential [19-21]. CO_2 hydrogenation is the most promising approach. Since carbon dioxide is thermodynamically stable molecule [22], converting CO_2 requires to use active catalysts as well as hard reducing agents (usually H_2). Such methods of CO_2 hydrogenation include CO formation, methanation reaction, methanol production as well as higher hydrocarbon formation via

Fischer-Tropsch synthesis (FTS). The interest in CO_2 hydrogenation can be clearly seen in a rise in the number of publications according to Google Scholar web portal (Figure 2).

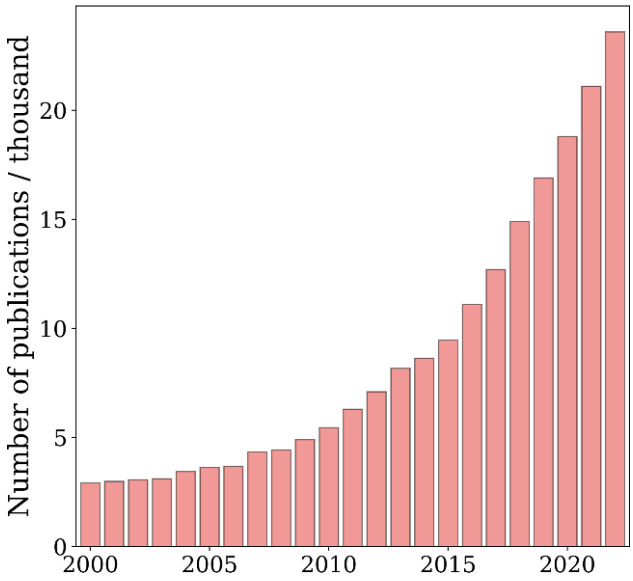

Figure 2. The number of publications on the topic "CO_2 hydrogenation" searched on Google Scholar web portal.

The reaction of CO_2 hydrogenation into CO (reverse water gas shift reaction (RWGS), $CO_2 + H_2 \rightleftarrows CO + H_2O$, $\Delta H_{298K} = 41.2$ kJ mol^{-1}) is carried out to produce CO for syngas (the mixture of CO and H_2) that further can be used to produce methanol, dimethyl ether, as well as higher hydrocarbons via Fischer-Tropsch synthesis (FTS). Such processes are called two-step (indirect) ones because the RWGS reaction and sequential conversion of syngas to valuable organic compounds are carried out in two different reactors. The RWGS reaction is an endothermic reaction and that is why higher temperatures are required for increasing the equilibrium conversion of CO_2 and suppressing side reactions like methane formation from CO_2 [23]. On the other hand, higher reaction temperature promotes carbon deposition resulting from the Boudouard reaction ($2CO \rightleftarrows C + CO_2$, $\Delta H_{298K} = -172$ kJ mol^{-1}) [24, 25] and active component sintering resulting in the catalyst deactivation [26]. As catalysts for the RWGS reaction, transition metals and their oxides (Fe_3O_4, Cu-ZnO, Ni, Co-CeO_2 etc.), Nobel metals (It, Pt, Rh etc.), carbides (Mo_2C, MoC_2, V_8C_7) can be used [27, 28].

The direct conversion of CO_2 to valuable products in one step (using only a single reactor) has gained significant attention due to its feasibility. Firstly, it worth mentioning the process of CO_2 hydrogenation to methane (methanation reaction, $CO_2 + 4H_2 \rightleftarrows CH_4 + H_2O$, $\Delta H_{298K} = -165$ kJ mol^{-1}). It is an exothermic reaction and, thus, lower temperature are favorable for increasing the yield of methane.

However, since CO_2 is a stable molecule, the process typically occurs at elevated temperatures and pressures, with the aid of a suitable catalyst. Commonly used catalysts include transition metals such as nickel and ruthenium supported on Al_2O_3 or SiO_2 [29]. These catalysts enhance the reaction kinetics and improve the selectivity towards methane formation.

Another attractive process is CO_2 hydrogenation to methanol ($CO_2 + H_2 \rightleftarrows CH_3OH + H_2O$, ΔH_{298K} = -49.5 kJ mol^{-1}). Methanol has gained attention as a potential alternative fuel due to its favorable properties. It has a high energy content per unit volume, making it an efficient fuel source. Methanol can be easily stored, transported, and distributed [1]. Moreover, CH_3OH is a valuable chemical compound used as a feedstock in various industrial processes, including the production of formaldehyde, acetic acid, olefins, aromatics, and synthetic fuels [30-32]. The process of converting CO_2 to methanol has certain limitations especially if we compare it to the traditional process of CO hydrogenation to CH_3OH. Thermodynamic analysis of CO_2/CO to methanol processes made in the work [33] demonstrated that equilibrium conversion for CO_2 hydrogenation is much lower than for CO one. So, at 250 °C and 50 bar, the equilibrium conversions are around 19 and 55 % for CO_2 and CO hydrogenation, respectively. Moreover, higher amount of water obtained in the process of CO_2 hydrogenation compared to CO is one of the reasons for lower productivity of CO_2 to methanol process due to water-induced catalyst deactivation [34, 35]. A Cu-based catalyst supported on ZnO is the most suitable for the CO_2 to methanol process due to its high activity and selectivity to desired product [20, 36]. Different promoters such as Al, Cr, Ga, Zr, K, Ba, La etc. are also investigated which demonstrate an increase in catalyst selectivity and activity [37-39].

CO_2 hydrogenation to higher hydrocarbons also known as direct CO_2 Fischer-Tropsch synthesis (CO_2-FTS) may be also considered as a potential solution for reducing CO_2 dioxide emission problem [40]. It represents an extension of the classical FTS suggested by Franz Fischer and Hans Tropsch in 1923 [41] where CO-H_2 mixture is used. The process of direct CO_2-FTS allows one to produce hydrocarbons (olefins and paraffins) in a wide range. The interest in light olefins C_2-C_4 formed in the process is caused by their role as fundamental blocks of chemical industry [42] as well as by C_{5+} hydrocarbons being versatile feedstocks that could be used for the production of synthetic fuel or as value-added compounds for high-octane gasoline, synthetic lubricants, new polymers etc. [43, 44].

All the above processes belong to the concept of Power-to-X technologies [1, 33]. Power-to-X is a concept that involves the conversion of electrical power, typically generated from renewable sources, into various energy carriers or chemical products. The basic idea behind Power-to-X is to utilize an

excess of renewable electricity during periods of high generation or low demand and convert it into a form that can be stored and used when needed. This helps to address the intermittent nature of renewable energy sources and contributes to a more flexible and sustainable energy system. One common application of Power-to-X is the production of hydrogen through electrolysis, where water is split into hydrogen and oxygen using renewable electricity. The hydrogen can then be used as a clean fuel for various purposes, such as fuel cell vehicles or industrial processes as well as a reducing reagent for converting CO_2 into valuable compounds (syngas, CH_4, methanol, sustainable fuels etc.) by the reactions discussed above. The concept of the Power-to-X for the example of CO_2 hydrogenation to higher hydrocarbons is shown in Figure 3.

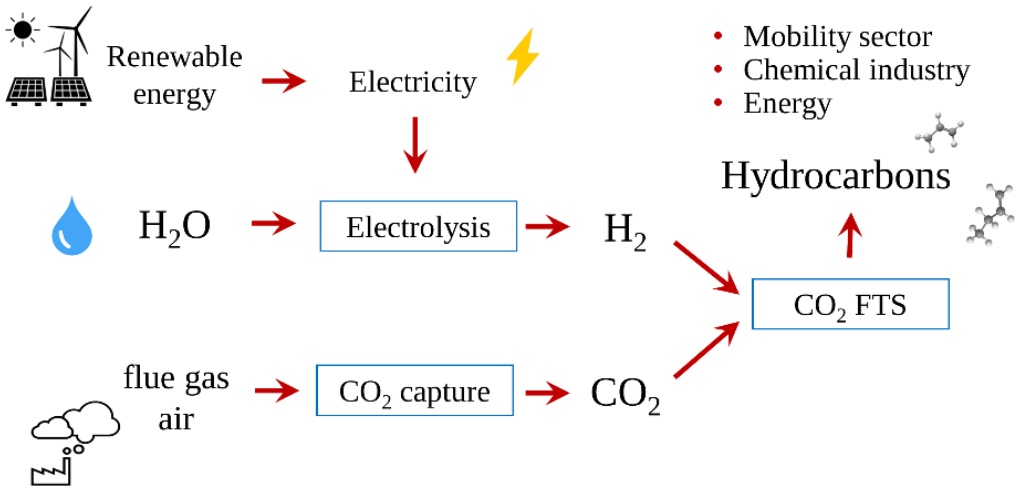

Figure 3. The concept of Power-to-X on the example of FTS.

The Power-to-X concept offers opportunities to integrate different sectors of the energy system, including electricity, transportation, and industry, fostering a more integrated and sustainable approach to energy production, storage, and utilization. While Power-to-X technologies show promising potential, there are still challenges to overcome, including cost-effectiveness, scalability, and the availability of infrastructure [45]. CO_2 hydrogenation plays a crucial role in the Power-to-X concept for converting carbon dioxide into valuable fuels and chemicals. Moreover, this process faces issues related to catalysts. Catalysts need to efficiently activate and convert CO_2, exhibit high selectivity towards desired products, be cost-effective, and maintain stability under severe and dynamic reaction conditions which are related non-stable generation of renewable energy. The present work is focused on an investigation of CO_2-FTS that is why the next chapter describes this process in more details.

1.3. CO_2 Fischer-Tropsch Synthesis

It is generally accepted that the process of CO_2 hydrogenation to higher hydrocarbons proceeds into two stages [46, 47]: CO_2 hydrogenation to CO via RWGS reaction followed by CO hydrogenation to hydrocarbons via FT mechanism:

$$CO_2 + H_2 \rightleftarrows CO + H_2O,\ \Delta H_{298K} = 41.2\ kJ\ mol^{-1}, \quad (RWGS) \quad (1)$$

$$CO + 2H_2 \rightleftarrows -CH_2- + H_2O,\ \Delta H_{298K} = -163\ kJ\ mol^{-1}, \quad (CO\text{-}FT) \quad (2)$$

Fe-based catalysts are typically used for the process of CO_2-FTS because they can catalyze both reactions [40, 48, 49]. A more detailed description of the limitations of the process in terms of thermodynamics and kinetics, mechanistic aspects, used catalysts and kinetic modelling of the overall process is given below.

1.3.1. Thermodynamic Aspects

The first stage of CO_2-FTS is the RWGS reaction which is an endothermic reaction and, thus, higher temperature is beneficial to increase the conversion of carbon dioxide. Wherein, there is no influence of pressure on the equilibrium conversion since the number of gas moles is the same on both sides of the RWGS reaction. Thermodynamic analysis performed by Riedel et al. [40] reveals that equilibrium conversion reaches approximately 23% at 300 °C and increases to 45% at 400 °C. However, elevated reaction temperature also leads to increased carbon deposition due to the Boudouard reaction leading to catalyst deactivation. So, Lucas Brübach et al. [50] observed an increased rate of the catalyst deactivation at 320 °C. Despite the constrain in equilibrium conversion of the RWGS reaction, the overall conversion of CO_2-FTS is usually higher because CO-FT reaction shifts the equilibrium conversion of the RWGS [46]. It is related to that the second stage of CO-FT reaction does not have thermodynamic limitation [51]. So, the equilibrium conversion of CO_2 in the case of considering both RWGS and CO-FT reactions (CH_4 and C_3H_8 were selected as the products of the second stage) calculated in the work [40] was around 75 % and slightly depended on temperature. It is agreed with the results of thermodynamic analysis performed by Torrente-Murciano et al. in the work [52].

More detailed thermodynamic analysis of CO_2 hydrogenation to olefins were performed by Yao et al. [53] (only olefins and CO were considered as product of carbon dioxide hydrogenation). They found that the CO_2 equilibrium conversion decreases with increasing temperature from 100 to 450 °C but increases at temperatures from 450 to 1000 °C. Wherein, the selectivity to overall olefins is nearly 100%

below 400 °C and dramatically decreases at higher temperatures. They concluded that the optimal temperature for the production of light olefins (C_2-C_6) is in the range from 300 to 400 °C while lower temperature (< 300 °C) favors higher olefin selectivity. These results are also in agreement with thermodynamic analysis made by Chen and Yang [51]. Increasing the reaction pressure and the molar ratio of H_2:CO_2 positively affects CO_2 conversion with the most favorable H_2:CO_2 ratio being around 3-4 [53].

In summary, the thermodynamic constraint of the RWGS reaction in CO_2-FTS results in a lower partial pressure of carbon monoxide along the reactor compared to traditional CO-FTS. Consequently, the overall rate of the CO_2-FTS process is reduced relative to CO-FTS, challenging for the development of highly selective and active catalysts for direct CO_2 hydrogenation into higher hydrocarbons via the FT mechanism. Overcoming this challenge is crucial for advancing the technology of CO_2 conversion into valuable hydrocarbons through FT reactions.

1.3.2. Product Distribution

The second stage of CO_2-FTS is CO hydrogenation to higher hydrocarbons via classical FT mechanism. Because this reaction is a polymerization process [54], it has a kinetic limitation, and the distribution of hydrocarbon products can be described by the Anderson-Schulz-Flory (ASF) distribution [55-57]:

$$W_n = n(1-\alpha)^2\alpha^{n-1} \quad (3)$$

where W_n is the mass fraction of hydrocarbon with carbon number n, α is the chain growth probability. The physical meaning of the chain growth probability is that it is a ratio of prolongation rate r_p to the sum of rates of prolongation and termination r_t [58, 59]:

$$\alpha = \frac{r_p}{r_p + r_t} \quad (4)$$

By applying natural logarithm to the Expression 3 we can obtain the general formula that can be used for estimating the parameter α from the catalytic data by plotting in the corresponding ASF coordinates (n, $\log\frac{W_n}{n}$):

$$\log\frac{W_n}{n} = n\log\alpha + \log\frac{(1-\alpha)^2}{\alpha} \quad (5)$$

According to the ASF equation (Expression 3), only one parameter is needed to describe the distribution of hydrocarbon selectivity products. It means that there are direct correlations between the values of

hydrocarbon selectivity (S_1, $S_{2\text{-}4}$, S_{5+} etc.). Figure 4 shows the dependence between theoretical mass fraction of hydrocarbons and the chain growth probability.

One can see that higher values of the chain growth probability correspond to lower selectivity to CH_4. Thus, higher α contributes to suppressing undesired methane formation. Due to statistical nature of hydrocarbon production, there is a constraint in the maximum mass fraction of the target hydrocarbons. For example, the maximum theoretical value of the mass fraction to lower hydrocarbons C_2-C_4 is around 56.8 % that corresponds to the chain growth probability being equal to 0.47. Wherein, the fraction of CH_4 is 28.1 % in this case. Thus, it is fundamentally impossible to carry out the process of FT with close to 100 % of selectivity to desired fraction of hydrocarbons (like gasoline, diesel, or light hydrocarbons) and refining processes of primary FT products are required to improve yields and selectivity to the desired fractions.

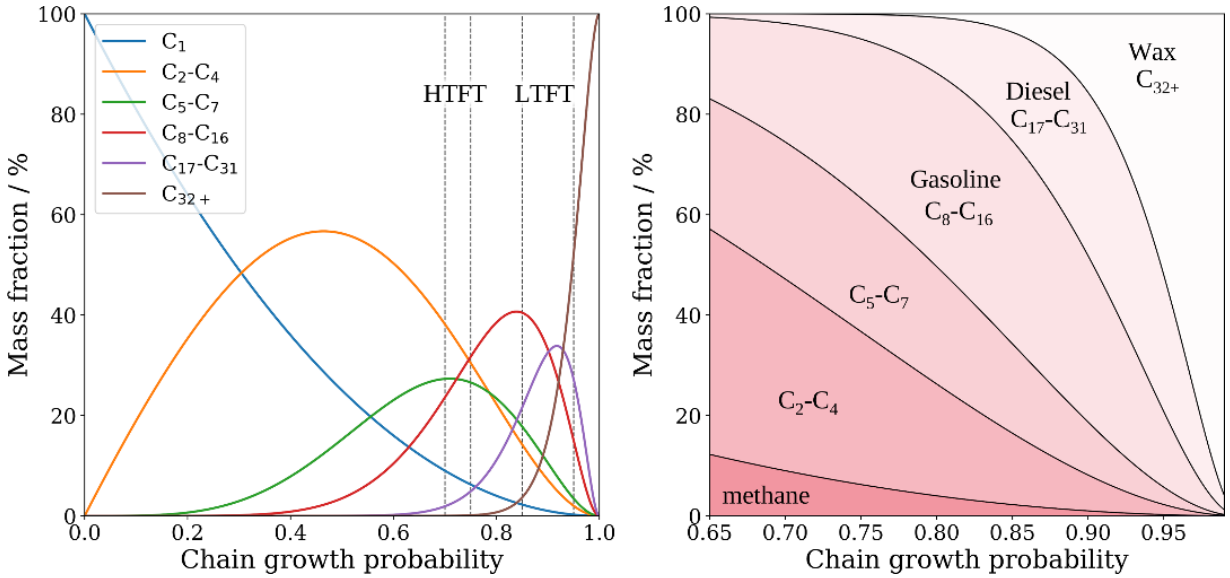

Figure 4. The dependencies between theoretical mass fraction of hydrocarbons in different range and the chain growth probability calculated by ASF distribution (left). The mass fraction of the key products of FTS as a function of the chain growth probability (right). HTFT – high temperature FT, LTFT - high temperature FT. Adapted from [33].

Here, it is also worth noting that there are deviations from the ASF distribution in the products of FT synthesis that have been summarized in a review [60]. Firstly, an increase in methane selectivity compared to the theoretical ASF distribution can be observed [61-64]. One of the explanations is the presence of an additional reaction of methane formation from CO_2 not via FT mechanism but via the Sabatier reaction ($CO_2 + 4H_2 \rightleftarrows CH_4 + H_2O$) [40, 48, 65, 66]. Another reason may be a split of α-olefines (by breaking a double bond) with higher carbon number that leads to additional methane production [67].

On the other hand, Wojciechowski and Sarup [68, 69] explained enhanced methane selectivity by using a separate parameter of the termination probability for the CH_4 formation. So, the rate constant for the termination of methane is 10 times higher than for higher hydrocarbons (C_2, C_3 etc.). Another deviation is related to a decrease in C_2 hydrocarbon selectivity compared to the ASF distribution [61-64]. The observed decrease may be due to high reactivity of C_2H_4 or surface C_2-intermediates participating in the chain growth compared to olefins with a higher carbon number [70, 71].

1.3.3. Catalysts

Co- and Fe-based catalysts are usually used for catalyzing the process of the traditional CO-FTS [72, 73]. For this reason, they are also investigated for CO_2-FTS. But in the case of the direct CO_2-FTS, the catalysts have to be active not only in the CO-FT reaction, but also in the RWGS one. Co-based catalysts are known to be inactive in the RWGS reaction [74] and produce mainly methane from CO_2 [75, 76]. Fe-based catalysts are more promising materials because they can catalyze both reactions [46]. It is discussed that the RWGS reaction occurs on Fe_3O_4, while iron carbides formed in situ under reaction conditions are responsible for catalyzing the CO-FT reaction [46, 71]. Unpromoted Fe-based catalysts are reported to produce a lot of methane in CO_2-FTS [77-79]. For this reason, there are efforts to suppress undesired methane formation by doping the catalysts with different promoters [67, 80-86]. However, it is worth mentioning that the suppression of CH_4 formation can also be achieved by using a proper preparation method. Albrecht et al. showed [48] that a cellulose templating method allowed one to obtain unpromoted Fe-based catalyst with low selectivity to methane (CO_2 conversion was 23 %, selectivity to CH_4 was 14 %). In other work [65], Skrypnik et al. demonstrated that a promoter-free Fe-based catalyst prepared by decomposition of iron oxalate shows good performance in CO_2-FTS (CO_2 conversion was 25 %, methane selectivity $< 10\%$, C_{2+} hydrocarbon selectivity – around 50 %). Nevertheless, the doping Fe-based catalysts with promoters is still the more popular approach for improving the performance of the catalysts.

Alkali metals, particularly K, are widely used as promoters for Fe-based catalysts in CO_2-FTS. The addition of alkali metals has shown significant improvements in catalyst performance, leading to an increase in CO_2 conversion, an increase in selectivity towards olefins and higher hydrocarbons, and a reduction of the methane selectivity [82, 87-89]. Numerous studies have investigated the effect of alkali dopants on CO_2-FT catalysts. Numpilai Thanapha et al. [81] demonstrated that the presence of K decreases the hydrogenation activity of the catalyst that was explained by increasing the bond strength of between the catalyst and adsorbed CO_x. It leads to increasing CO adsorption and weakening the bond

energy of C–O facilitating the dissociation of the adsorbed carbon monoxide. In addition to an increase in the strength of CO adsorption, doping with alkaline metal decreases H_2 adsorption leading to suppressing of the hydrogenation ability [70, 90]. It has been supported by in situ XPS and DFT calculations [88, 91], where the effect of changing of the absorption strength of the CO/CO_2 and H_2 was explained by the donation of electron density to iron carbide leading to an increase in its basicity. Additionally, alkali metals facilitate the formation of Fe_5C_2 and increase its stability, as observed for alkali-modified catalysts, where the activity correlates with the alkali content and the amount of iron carbide [92, 93]. Thus, such catalysts are able to accelerate the formation of Fe_5C_2 which is an active phase in CO-FT reaction. The influence of alkaline metal amount on the performance of Fe-based catalysts has been investigated [78, 87, 89, 90]. Increasing the potassium content in the Fe-based catalysts leads to an increase in CO_2 conversion and selectivity to C_{2+} hydrocarbons, olefins content, accompanied by a decrease in methane selectivity. However, further increase in K content (to above 5%) results in a decrease in the activity of promoted Fe-based catalysts [78, 90]. Therefore, there is an optimal potassium content in the catalyst, which is around 1-2% according to the works [87, 89]. Because doping with K and Na are perspective for CO_2-FTS catalysts, the influence of the nature of alkaline metals (Li, Na, K, Rb, and Cs) is also investigated [94-96]. First, it is worth noting that among all alkali metals, only Li has a weak effect on improving catalyst performance. A more detailed analysis of the influence of alkali metals indicates that they contribute local electronic modifications of iron in iron carbides [94] that explains the positive effect of these dopants and allows decreasing the contribution of the direct methane formation from CO_2.

Other dopants used for CO_2-FT catalysts are transition metals like Cu [82], Co [81], Mn [80], Zn [84] etc. [67, 83] which increase the performance and stability of CO_2-FT catalysts. Cu is commonly used as a promoter in CO_2 hydrogenation due to its ability to reduce iron oxides, increase surface basicity, and decrease CH_4 formation [40, 97]. Since Cu increases the reducibility of iron particles, it leads to rise in the dispersion of active component [98]. Moreover, in recent work [44] it was shown that doping with Cu can lead to a synergy of Fe and Cu caused by CO insertion over interfacial sites between copper and iron carbides leading to the efficient chain growth of FT-intermediates. The authors managed to achieve a selectivity to long-chain olefins (C_{4+}=) of around 67 % under 1 bar and 320 °C. For the comparison, Xu Cui et al. reported [99] the selectivity to C_{4+} olefins was around 41 % for Fe-based catalyst promoted with Zn and Na (reaction temperature was 320 °C, pressure – 30 bar). As previously discussed, Co-based catalysts are not active in the RWGS reaction and produce a lot of methane in the process of CO_2 hydrogenation. However, using Co as a dopant for Fe-based catalysts can increase the overall conversion of

carbon dioxide. So, Satthawong et al. demonstrated [100] that doping Fe-K catalyst with Co increased CO_2 conversion from 27.0 to 35.8 % while maintaining the hydrocarbon selectivity (i.e. without a rise of CH_4 selectivity). But further increasing the amount of Co in the Fe-K catalyst led to an increase in methane production. Doping Fe-based catalysts with Mn is observed to increase light olefin content [88]. It was discussed that Mn acts as a structural promoter which increases the reducibility of iron oxide, catalyst basicity, and, thus, enhances iron carbide formation [49, 101]. Some authors report a synergic effect between Mn and K in the promoted Fe catalysts [102]. Doping Fe-based catalysts with Zn allows improving the stability of the catalysts. Zn was reported to be a structural promoter which suppresses the oxidation of iron carbides to oxides by water and carbon dioxide [84].

1.3.4. Mechanistic Aspects

The discussion about the mechanistic aspects of the CO_2-FTS should start from the reaction pathways occurring in the process. The information about reaction pathways can be obtained from the analysis of the catalytic data presented in the conversion-selectivity plots that were done in works [48, 65, 95, 103]. The authors concluded that the process of CO_2-FT proceeds into two stages: the RWGS reaction followed by CO hydrogenation to hydrocarbons via classical FT mechanism. But they also found that in addition to these two routes, there are additional pathways of undesired methane formation. One of them is a methanation reaction ($CO_2 + H_2 \rightleftarrows CH_4 + H_2O$). In the work [95], Skrypnik et al. suggested that this reaction occurs over the surface of Fe_3O_4 and can be suppressed by promoting of Fe-based catalysts with alkaline metals. Another undesired route of methane formation is the hydrogenolysis of long-chain α-olefins that was discussed in the work [65]. Figure 5 summarized the main pathways occurring over Fe-based catalysts in the CO_2 hydrogenation to higher hydrocarbons. It is also worth mentioning the presence of additional side reactions occurring in CO_2-FTS including olefin hydrogenation and carbon deposition [68]. The hydrogenation of olefins formed in the CO_2-FTS results in the formation of saturated hydrocarbons. Carbon deposition or coking refers to the deposition of carbonaceous species on the catalyst surface, leading to catalyst deactivation [40]. These side reactions can affect the overall product selectivity and catalyst performance in FTS processes.

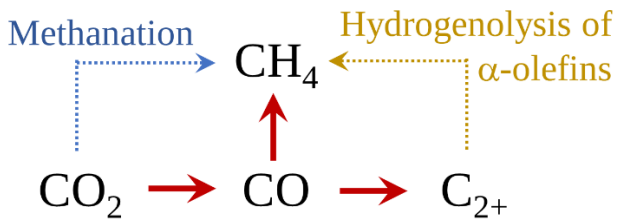

RWGS: $CO_2 + H_2 \rightleftarrows CO + H_2O$

CO-FT: $CO + 2H_2 \rightleftarrows -CH_2- + H_2O$

Methanation: $CO_2 + 4H_2 \rightleftarrows CH_4 + 2H_2O$

Hydrogenolysis: $R\text{-}CH{=}CH_2 + 2H_2 \rightleftarrows R\text{-}CH_3 + CH_4$

Figure 5. The main reaction pathways occurring over Fe-based catalysts in CO_2 hydrogenation.

Because the RWGS and CO-FT reactions are main routes of hydrocarbon production in CO_2-FTS, it is worth discussing the main mechanisms describing both reactions in more details. Regarding the RWGS reaction, two generally accepted mechanisms were proposed and discussed in the literature: redox and associative mechanisms [104-106]. In the redox pathway [105], adsorbed molecule of CO_2* dissociated into adsorbed CO* and O*. Obtained adsorbed CO* is desorbed from the surface of the catalyst. Later, H_2 reacts with adsorbed atoms of O* to produce water and reduces the catalyst surface. In the case of the associative mechanism [106], adsorbed CO_2* react with atom of H* with the formation of formate species COOH* on the surface of the catalyst. Formate is reduced by the additional atom of H* on the surface with further desorption of CO and H_2O. Elementary steps of the redox and associative mechanisms are presented in Figure 6.

Redox mechanism	**Associative mechanism**
$CO_2 + * \rightleftarrows CO_2*$	$CO_2 + * \rightleftarrows CO_2*$
$CO_2* + * \rightleftarrows CO* + O*$	$H_2 + * \rightleftarrows H_2*$
$H_2 + O* \rightleftarrows H_2O*$	$H_2* + * \rightleftarrows 2H*$
$H_2O* \rightleftarrows H_2O + *$	$CO_2* + H* \rightleftarrows COOH* + *$
$CO* \rightleftarrows CO + *$	$COOH* + H* \rightleftarrows CO + H_2O + 2*$

Figure 6. Redox and associative mechanisms of the RWGS reaction adapted from [104]. * stands for surface site.

CO formed in the RWGS from CO_2 is converted to hydrocarbons via CO-FT reaction. In general, the FT polymerization process can be described by several steps including initiation, prolongation, and termination. In the initiation stage , the initial chain monomers are generated from adsorbed CO on the surface of iron carbides by reacting with hydrogen. The propagation stage involves reaction between

adsorbed FT monomers and growing chains. Termination stage implies the formation of FT products from the growing chain. Depending on the nature of FT monomers and C-C coupling reactions, the following generally accepted mechanisms are distinguished: carbide, enolic, and CO insertion mechanisms (see Figure 7).

The carbide mechanism is one of the first mechanisms suggested for describing FT process [107]. The FT monomer in this case is -CH_2- intermediate (methylene) formed from dissociative adsorption of CO followed by hydrogenation of C* surface species [108-110]. Paraffins and olefins are formed from the growing chains (alkyl species) by their hydrogenation and dehydrogenation (β-hydride elimination), respectively (the termination stage). Certain transition metals can dissociate CO to form metal carbides, while metals that have low dissociation ability of CO (such as Cu, Pd, Ag, Ir, Pt, and Au) are typically inactive in FTS. Similarly, metals that readily dissociate CO but form overly stable oxides and carbides also exhibit low FTS activity [111]. One of the problem with the carbide mechanism that it cannot explain the presence of oxygenates in the products of FTS [112].

In the CO insertion mechanism, CO is the FT monomer which reacts with alkyl species to form acyl species leading to the chain growth (Figure 7). Acyl species are hydrogenated resulting in the formation of enlarged alkyl species and H_2O. Paraffins and olefins are formed from alkyl species like in the carbide mechanism. The termination of acyl species leads to the formation oxygenates [113]. In this mechanism, adsorbed CO acts as a monomer of FT that is analogous to the hydroformylation mechanism [114]. However, the CO insertion mechanism has remained postulated but has not been validated due to experimental limitations [115] for a long time but DFT study made by Mingkun Zhuo et al. [116] demonstrated a potential opportunity of the existence of such the mechanism. But, in the recent work [117] Yusheng Zhang et al. claimed an experimental evidence of CO-insert mechanism at low temperature over Co-based catalyst.

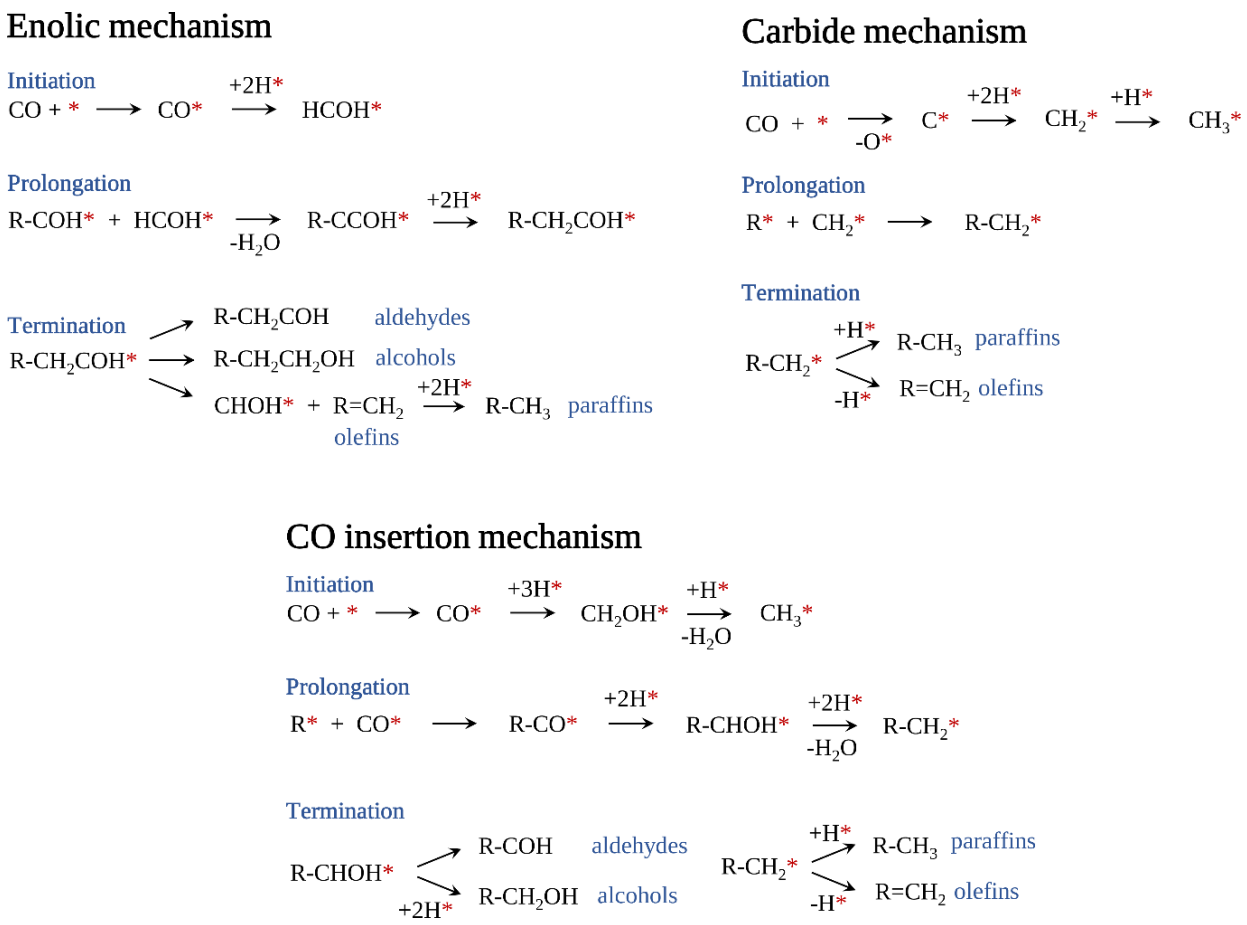

Figure 7. The schemes of enolic, carbide, and CO insertion mechanisms [108-110].

The enolic mechanism suggests that surface HCOH monomers are formed through the hydrogenation of chemisorbed CO, and chain growth occurs through condensation reactions under water elimination. R-CH_2COH surface species are responsible for producing branched hydrocarbons. The R-CH_2COH species are terminated that leads to the formation of olefins and paraffins as well as oxygenates according to the mechanism (Figure 7).

In addition to the discussed mechanisms of FTS, there are other mechanisms that have been explored and discussed in the literature including formate, alkyl, alkenyl, alkylidene–hydride–methylidyne mechanisms. Comprehensive reviews on these various FTS mechanisms can be found in the following works [108, 109].

1.3.5. Kinetic Modelling

Kinetic modeling of heterogeneous catalytic reactions holds significant importance in applied science, particularly in the field of chemical engineering. Reliable models are essential for accurately describing catalytic processes, enabling scale-up and optimization of industrial plants in chemical

engineering [118]. The kinetic models of the classical FTS process have been extensively studied. Reviews covering the kinetic modeling of classical CO-FT can be found elsewhere [68, 109]. While there is a wealth of research on the kinetics of CO-FT, this section specifically focuses on the of CO_2-FTS. In general, models describing the kinetics of CO_2 hydrogenation to higher hydrocarbons can be categorized into empirical models, e.g. using Langmuir-Hinshelwood-Hougen-Watson (LHHW) expressions, and detailed micro-kinetics models. These models provide different levels of complexity and detail in capturing the reaction mechanisms and rate dependencies.

All reported kinetic models are based on the generally accepted two-stage mechanism of direct CO_2-FTS consisting of the RWGS and CO-FT reactions. Moreover, due to a wide range of FT products, researchers made some assumptions and simplifications to facilitate the development of kinetic models. Riedel et al. [40] were the first who developed an empirical kinetic model of CO_2-FTS over K-promoted Fe-based catalyst. In addition to two stages, they also considered a direct route of CO_2 hydrogenation to higher hydrocarbons. To simply the model, only C_3H_8 was considered as a pseudo-product of FT process. They found that the contribution of direct pathway of CO_2 hydrogenation is low and can be neglected in kinetic modelling. The same kinetic model was applied for describing the CO_2 hydrogenation to higher hydrocarbons over a Fe-based catalyst promoted with K and Mn [119]. In the work [50], Brübach et al. developed a new kinetic model of CO_2 hydrogenation over supported Fe-based catalyst. For development of the kinetic model, they considered the associative and carbide mechanisms describing the RWGS and CO-FT reactions, respectively. They assumed that the reaction between adsorbed CO_2 and an adsorbed H atom is the rate-determining step in the associative mechanism and that the decomposition of enolic species ($HCOH^* + * \rightleftarrows CH^* + OH^*$) is the rate-determining step of CO-FT reaction. Enolic species were assumed to be formed from the hydrogenation of adsorbed CO with H_2. For describing the products of FT process (hydrocarbons), they also considered only one organic compound (C_4). In the work [120], Ali Nakhaei Pour et al. investigated the process of CO_2 hydrogenation over Fe/Cu/K catalyst. Based on the results of kinetic modelling and the screening of different sets of reaction mechanism and rate-determining stages, they found that a model based on the associative mechanism of the RWGS reaction and enol mechanism of the CO-FT gave the best fit of the experimental data. According to their kinetic model the chain growth is limited by the reaction between adsorbed CO and H to form enol species.

The development of the kinetic models predicting the distribution of hydrocarbons is a difficult task for simulating of CO_2 hydrogenation to hydrocarbons. The complexity of it arises from that the kinetic models should satisfy the kinetic limitations discussed above (see section 1.3.2). Panzone et al.

[121] suggested a semi-empirical model to describe the formation of products (paraffins, olefins, and alcohols) in CO_2 hydrogenation using the ASF distribution (one distribution for an type of the products). For describing the rates of the RWGS and CO-FT reactions, they used the resembling expressions developed by Riedel et al. [40] but slightly modified them by adding additional parameters. Later Panzone et al. [112] also developed a more detailed kinetic model of CO_2 hydrogenation to higher hydrocarbons. They assumed two different active sites responsible for the RWGS and CO-FT reactions, respectively. For describing the RWGS reaction, the redox mechanism was assumed. In the case of the CO-FT reaction, CO insertion, and alkyl (one of the variants of the carbide mechanism) mechanisms were used for describing the distribution of the CO_2 hydrogenation products. Two mechanisms of CO-FT reaction were chosen to explain the observed deviation from the ASF distribution in the hydrocarbon selectivity. Moreover, the obtained model was able to describe the product formation of paraffins and olefins as well as alcohols. Another detailed kinetic model of CO_2 hydrogenation to higher hydrocarbons over K-promoted Fe-based supported catalyst was developed by Brübach et al. in the work [122]. For the RWGS reaction they used the redox mechanism as well as the alkyl mechanism for FTS. They demonstrated that using of one type of active site for describing both reactions is enough for a reliable description of the overall process.

As summary, kinetic modelling of the process of CO_2 hydrogenation to higher hydrocarbons is a complicated task. The kinetic models have to satisfy a wide range of the requirements including thermodynamic and kinetic limitations, as well as accurately predict the distribution of products. Due to the complexity and a wide range of products, simplifications and assumptions are often made to facilitate the model development. The development of accurate kinetic models for predicting hydrocarbon distribution remains a challenging task in CO_2-FTS.

1.3.6. Industrial Variants of Fischer-Tropsch Synthesis

The process of the direct CO_2 hydrogenation to higher hydrocarbons via FT is still on its way to industrial implementation. However, it is important to discuss industrial variants of plants for the classical FT synthesis because they could make a basis for the CO_2-FTS technology. A discussed above (see section 1.3.2), there is a constraint in the maximum selectivity to target products (light olefins, gasoline etc., see Figure 4) and refining of the primary products is required to increase their yield. In the case of traditional FTS, two industrially applied variants are distinguished: low and high temperature FT (LTFT and HTFT, respectively). The comparison of both technologies is presented in the Table 1.

In the case of the LTFT process, slurry or fixed bed reactors are used and the typical value of the chain growth probability is in a range from 0.85 to 0.95 that favors the wax production [33]. Because higher hydrocarbons are the predominant products, the refining processes of primary products of LTFT process includes hydrocracking of heavy products (wax) and hydrotreating. In contrast, the HTFT process is carried out in fluidized bed reactors and at higher temperature and produces short-chain paraffins and olefins (the chain growth probability is in a range from 0.70-0.75). The refining process in this case is oligomerization and hydrogenation. It is worth noting that the refining processes of primary products for LTFT and HTFT are rather complicated. More detailed information about refining processes of primary products of CO-FTS were summarized in the reviews [123, 124].

Table 1. The comparison of LTFT and HTFT technologies.

Parameter	LTFT	HTFT
Temperature	190-250 °C	300-350 °C
Reactor type	Slurry or fixed bed	Fluidized bed
Catalyst	Co- or Fe-based	Fe-based
Typical α	0.85-0.95	0.70-0.75
Main products	Long chain paraffins	Short-chain paraffins, olefins
Product refining	Hydrocracking, hydrotreatment etc.	Oligomerization, hydrogenation etc.

1.4. Data Science and Machine Learning in Catalysis

1.4.1. Main Features and Applications

In recent days, there has been a rapid rise in applying the modern data science and machine learning (ML) methods for solving many complicated tasks in different fields of academia, industry, and business. In healthcare, ML is used for diagnosing diseases [125], predicting patient outcomes, and drug discovery [126]. In finance, ML aids in fraud detection, risk assessment, and algorithmic trading [127]. ML also plays a crucial role in recommender systems used by e-commerce platforms to provide personalized product recommendations [128, 129]. Additionally, ML is used in natural language processing for sentiment analysis, chatbots, and language translation [130, 131], in image and video recognition [132], autonomous vehicles [133], and optimizing supply chain operations [134]. These are just a few examples highlighting the diverse and impactful applications of ML across different sectors. In general, there are several types of ML, including [135]:

- Supervised Learning: In supervised learning, the algorithm learns from labeled data where the input features and their corresponding target labels are provided. The goal is to train a model that can make accurate predictions or classifications on unseen data.
- Unsupervised Learning: In unsupervised learning, the algorithm learns from unlabeled data where only input features are available. The objective is to discover patterns, relationships, or structures in the data without any predefined labels.
- Reinforcement Learning: Reinforcement learning involves an agent that learns to make decisions in an environment to maximize a reward signal. The agent learns through trial and error, exploring different actions and receiving feedback in the form of rewards or penalties.
- Deep Learning: Deep learning is a subset of machine learning that utilizes neural networks with multiple layers to learn and represent complex patterns and relationships in data. Deep learning has been particularly successful in areas such as image recognition, natural language processing, and speech recognition.
- Ensemble Learning: Ensemble learning combines multiple individual models to make predictions or classifications. By aggregating the predictions of multiple models, ensemble learning can often achieve better performance and more robust results compared to using a single model.

These are some of the commonly used types of machine learning, and each type has its own advantages and applications depending on the problem at hand. This study focuses on the supervised learning since it is the most applicable approach used in catalysis and related fields. The ML model development process have the following stages [136-138]:

- Problem Formulation: In this stage, the objective of the machine learning model is defined clearly. It involves understanding the problem, determining the target variable, and defining the success criteria.
- Data Collection: This stage involves gathering the required data for training the machine learning model. Data can be collected from various sources such as databases, scientific literature, experiments.
- Data Preprocessing: In this stage, the collected data are cleaned, transformed, and prepared for analysis. It involves handling missing values, dealing with outliers, normalizing or standardizing the data, and addressing any other data quality issues.

- Feature Selection: In this stage, relevant features or variables are selected from the dataset that more likely have an impact on the target variable. It helps in reducing the dimensionality of the data and improving model performance.
- Model Training and Validation: In this stage, the selected machine learning model is trained on the prepared dataset. The data is divided into training and validation sets, and the model learns patterns and relationships from the training data. The model's performance is evaluated using the validation data to ensure its generalization.
- Model Evaluation and Deployment: In this final stage, the trained model is evaluated on unseen data or a separate test dataset to assess its performance and generalization capability. If the model meets the desired criteria, it can be deployed for real-world use, where it makes predictions or classifications on new, unseen data.

It is worth dwelling in more details on the section of model training and validation. In general, ML model can be presented as a complex function $y_{model} = f(x_{exp}, \theta)$. Training of ML models involves iteratively adjusting the model's parameters θ using a labeled dataset x_{exp} to minimize the difference between predicted y_{model} and actual y_{exp} outcomes (minimizing the loss function). Mean squared error is a popular loss function used in the regression:

$$\frac{1}{N}\sum_{i=1}^{N}\left(y_{exp} - y_{model}\right)^2 \quad (6)$$

Here, it is worth mention the overfitting problem [136-138]. Overfitting occurs when a ML model learns the training data too well, capturing noise and random variations instead of the underlying patterns. This leads to poor generalization, causing the model to perform poorly on unseen data. It is often a result of an overly complex model or a lack of sufficient training data. The overfitting problem is particularly pronounced when dealing with small data sets, where the limited amount of data enhances the risk of the model memorizing noise or outliers rather than capturing meaningful patterns. To avoid building overfitted models, cross-validation (CV) is usually applied [139]. CV is a technique used to assess the performance and generalization ability of machine learning models. It involves dividing the available data into multiple subsets or folds, using some of them for training the model and the remaining ones for evaluating the model. By repeating this process with different combinations of training and evaluation data, cross-validation provides a more robust estimation of the model's performance and helps to identify potential issues such as overfitting.

1.4.2. Machine Learning Methods

There is a wide pool of different machine learning algorithms and methods which can be distinguished into two groups: linear and non-linear methods. The linear methods include multiple linear regression (MLR) [140], Lasso regression (MLR with L1 regularization) [141], principal component analysis and regression (PCA and PCR) [142], partial least squares (PLS) regression etc. [142, 143] MLR is a linear regression where the line equation is used to fit a data set. The classical estimation of an apparent activation energy from the catalytic data presented in the corresponding coordinates (log k and 1000/RT) is a simple example of MLR in only one variable (it is 1000/RT in this case). PCA is mainly applied for reducing the dimension of the input variables and transforming them into new variables with lower dimension (also called principal components). Using principal components as input variables for MLR is the principal component regression (PCR). The extension of PCR is the PLS regression that incorporates information about the response variable in addition to the predictor variables. Unlike PCR, which focuses on capturing variance in the predictor variables, PLS seeks to maximize the covariance between the predictor variables and the response variable. This makes PLS particularly useful in situations where there are strong relationships between the predictor and response variables and can lead to more accurate predictions.

Linear ML methods have several advantages that make them appealing for various applications. Firstly, they offer simplicity and interpretability, allowing users to understand and explain the relationships between variables. Secondly, linear models are computationally efficient, making them suitable for large datasets and real-time applications. Additionally, linear models are robust to noise and outliers, providing stable predictions even in the presence of noisy data. They also facilitate feature importance analysis, enabling identification of the most influential variables in the model, but only for linear dependencies. Furthermore, linear models tend to have good generalization capabilities, meaning they can make accurate predictions on unseen data. However, it is obvious that they cannot generalize non-linear dependencies in the data which is one of their key disadvantages [136-138].

Non-linear ML models are able to generalize non-linear dependencies, therefore, they found a wide application in different fields. These methods include support vector regression (SVR), tree-based ML algorithms, artificial neural networks (ANN) etc. [136-138, 143] SVR is a machine learning algorithm that uses support vector machines (SVM) to perform regression tasks [144]. It aims to find a hyperplane that best fits the data while minimizing the error. Using different kernels (polynomial, redial basis function, sigmoid function etc. [145]) to transform the input data into a higher-dimensional space allows SVR

to capture nonlinear relationships between features and target variables. It can efficiently model complex patterns and improve the flexibility and accuracy of regression predictions especially with the small data [146].

Tree-based machine learning methods, including decision trees [147], random forests [148], AdaBoost [149], XGBoost etc. [149, 150], utilize a hierarchical structure of interconnected nodes to make predictions. In a decision tree, each internal node represents a feature or attribute, and each branch represents a possible value or outcome. The model splits the data based on these features until it reaches the leaf nodes, which provide the final predictions (see Figure 8). Random forests or similar AdaBoost and XGBoost methods combine multiple decision trees to make more robust and accurate predictions by aggregating the results. Tree-based methods handle both numerical and categorical data and can capture complex interactions between variables, making them effective for both classification and regression tasks. One of the useful properties of tree-based models is an opportunity to determine feature importance of the input variables from the obtained ML models. A disadvantage of tree-based methods is their limited generalization ability and potentially inaccurate predictions for unseen data in the task of the regression.

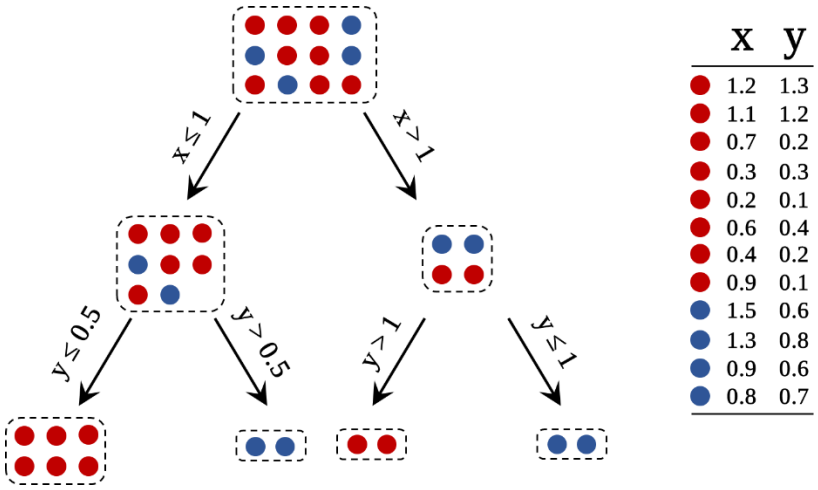

Figure 8. The example of the decision tree for binary classification (red or blue).

Artificial neural networks (ANNs) are widely utilized as powerful machine learning tools due to their capability as universal approximators [151]. Due to the flexibility of the constructing different structures of the ANNs, there are a lot of different variants of ANN architectures including feedforward NNs [152], convolutional NNs [153], graph NNs [154], long short-term memory networks (LSTM) [155], physics-informed NNs [156], neural ordinary differential equations etc. [135, 157] Because of this, NNs have found their application in solving a wide range of problems.

Non-linear ML models offer several advantages over linear models. Firstly, they provide increased flexibility, allowing for the capture of complex relationships and patterns in the data. This flexibility enables non-linear models to better handle highly non-linear and intricate data structures. Secondly, non-linear models can effectively capture feature interactions, which is particularly important when dealing with complex and interconnected variables. However, non-linear models are more complex and require more data and computational resources for training than linear models. Non-linear models, especially those with high complexity, are more prone to overfitting, where they learn the training data too well and struggle to generalize to unseen data. In addition, it is often more challenging to interpret and understand the obtained models compared to linear ones, making it difficult to gain insights into the underlying relationships and mechanisms in the data [136-138].

1.4.3. Applications in Catalysis and Material Science

The scope of applying data science and ML in material science and particularly in catalysis is quite wide. In general, the following directions can be distinguished. Firstly, it is worth highlighting the usage of ML in the analysis of existing scientific publications. It can be natural language processing with Word2vec (a special type of NNs) for revealing the latent knowledge from the material science literature [158]. Another one is to use ChatGPT [131] as a chemistry assistant for text mining and the prediction of metal-organic frameworks [159]. Here, it is also worth noting works related to an extraction of an existing data presented in scientific publications in the form of figures by autonomous frameworks (like ChartOCR [160], LineEx [161]) based on ML models. It allows one to fast extract the data from the literature and use them for further analysis.

ML models can be used for the prediction of the properties of compounds and materials calculated by ab initio methods (for example, DFT) [162]. Even so these properties can be calculated via these methods, they require a lot of computation. ML models can help in an accelerated estimation of target properties. For example, Casey et al. [163] used 3D convolutional ANNs for predicting energic properties of organic compounds (energy formation, dipole moment, HOMO-LUMO band gap etc.). Huang et al. [164] used deep learning methods for predicting the formation energies of inorganic compounds. In other work [165], Singh et al. used ANNs for predicting chemical reaction barriers.

One of the attractive directions for ML is to develop regression models for predicting catalytic properties based on the catalyst composition and structure. For example, Madaan et al. [166] used linear PLS regression for predicting the performance of the catalysts for oxidative dehydrogenation of butane.

They used a series of descriptors including unique features representing the parameters of Slater-type function of atoms that allowed them to obtain the linear model with good generalization. Based on the obtained results, they experimentally validated the model by preparing the most perspective catalysts suggested by the PLS model. Suzuki et al. in the work [167] performed the analysis of the catalytic data presented in the literature about oxidative coupling of methane for predicting the catalyst performance using XGBoost models. Smith et al. [168] used PCA and NNs for predicting activity and selectivity of catalysts in the RWGS reaction. They found that Au-based catalysts supported on CeO_2 and promoted with Li, Na, and Mg are the most perspective candidates. In addition to the development of regression models for predicting the catalyst performance, ML can be used for the analysis and systematization of the catalytic data as well as for elucidating important factors affecting catalyst performance. So, Zavyalova et al. [169] created the database about OCM catalysts from the literature and performed a statistical analysis of the obtained results. Using the analysis of variance (ANOVA) and regression trees, they suggested a new strategy for preparing highly-selective OCM catalysts with the multicomponent composition. In other work [170], Yang et al. used ANOVA and regression trees for the analysis of CO_2-FT catalysts based on the data from literature. They found that doping Fe-based catalysts with alkaline and transition metals allows one to increase CO_2 conversion rate, C_{2+} selectivity, and olefins/paraffins ratio. They also found that electronegativity of the promoters is the key descriptor defining the catalyst activity and selectivity. However, their analysis focused only certain parameters like CH_4 and C_{2+} hydrocarbon selectivity, CO_2 conversion, as well as olefin content but did not consider the chain growth probability. The latter is the key parameter for catalyst selectivity in FT. Moreover, the analysis of an approach to equilibrium of the RWGS reaction was not performed.

Another perspective direction of applying ML is the development of models for kinetic modelling of catalytic reactions [156, 171]. It is worth mentioning physics-informed NNs (PINN) for simulating and solving the system of ordinary and partial differential equations [171]. The key idea is to embed the general knowledge about the process in the loss function. Thus, during the NN training, the obtained regression models satisfy the experimental data as well as the governing differential equations. Gusmão et al. [172] extended this approach for any chemical and catalytic reactions that was called kinetics-informed NNs. Another approach in kinetic model development is to use neural ordinary differential equations (neural ODE) that was suggested by Chen et al. [173]. The key idea is to use traditional NNs for approximating the right part of ODE. Neural ODE is an attractive tool in the kinetic model development because only data are used for kinetic model development [174, 175]. Thus, we do not need to

suggest the reaction mechanisms, assume rate-determining stages, solve the inverse kinetic task. However, it worth noting that the requirement of big data for building reliable ML models is one of the limiting factors restraining application of ML in the kinetic model development.

The above examples demonstrated that data science and ML methods can be successfully used in different fields of material science and catalysis. Data science and ML offer powerful tools for analyzing complex catalytic systems, predicting reaction outcomes, optimizing catalyst design, and accelerating the discovery of new catalytic materials, as well as simulating reaction kinetics. This integration of data science and machine learning in catalysis has the potential to enable more efficient and informed decision-making processes, leading to the development of catalysts with improved performance and selectivity.

2. Objectives and Outline

2.1. Problem Statement and Objectives

As shown in the above literature review, the problem of CO_2 emissions, having the main contribution in the greenhouse effect leading to a climate change, motivates academia and industry to be looking for a solution of this problem. CO_2 hydrogenation to valuable organic compounds may be considered a promising approach not only for reducing CO_2 emissions, but also for generating products with commercial potential. One of these attractive processes is CO_2 hydrogenation to higher hydrocarbons (CO_2-FTS). The interest in this topic has led to a significant rise in the number of scientific publications and, thus, in the amount of the data regarding CO_2-FT catalysts.

According to the literature, the overall process of CO_2-FTS proceeds into two stages: RWGS reaction with CO formation in a gas phase followed by CO hydrogenation to higher hydrocarbons via FT. The first RWGS reaction has the thermodynamic limitation which constrains the overall rate of CO_2-FTS compared to traditional FTS. The second reaction is a typical polymerization process, and hydrocarbon selectivity can be described by the statistical single-parameter ASF distribution. The chain growth probability α (the parameter of the ASF distribution) is key and defines the selectivity of the CO_2-FT catalysts to the target products (higher α corresponds to lower CH_4 selectivity and higher C_{2+} hydrocarbons production). Due to the above limitations, the development of active and selective catalysts for CO_2-FTS is a complex task. Fe-based catalysts are usually used for this process because Fe can catalyze both reactions (iron oxides are responsible for RWGS, iron carbides – CO-FT). The bulk and supported Fe-based catalysts doped by different promoters (K, Na, Cu, Mn, Zn, Co etc.) and prepared by using various preparation methods have been intensively investigated. Due to the large amount of accumulated data on CO_2-FT catalysts in the literature, it becomes attractive to analyze them for searching for relationships between catalyst properties and activity as well as revealing latent knowledge from the literature. However, the challenges in the comparison of the activity of catalysts investigated in the different articles arise from two factors: (i) the multiplicity of the catalytic parameters (CO_2 conversion, CO and CH_4 selectivity, hydrocarbon distribution, olefins content, etc.); (ii) the catalytic data were obtained at different reaction conditions (temperature, pressure, CO_2:H_2 ratio, residence time, etc.). In ideally, the comparison of catalyst activity should be made at the same reaction conditions (temperature, partial pressure of reagents and products, etc.). The recalculation and normalization of the catalytic data from one reaction conditions to others require deep knowledge about reaction kinetics (kinetic law expressions,

activation energy, etc. for each separated catalyst) that are usually unknown. The development of new approaches for normalization of such a type of the data is valuable since it could help in the evaluation and the analysis of the catalytic data of CO_2-FT catalysts.

In addition to the catalyst development, an industrial implementation of the technology also requires the development of reliable kinetic models of CO_2-FTS. The literature review demonstrated that different mechanisms of CO_2-FTS are suggested and discussed. Based on the suggested mechanisms, various kinetic models have been developed (from simple kinetic models based on the two-stage mechanism to detailed microkinetic models of CO_2-FTS describing the whole product distribution). The complexity of the traditional approach in kinetic modelling is related to the performing of the screening of reaction mechanisms and assumptions for converting the detailed mechanisms into LHHW-like kinetic expressions. It is worth mentioning that solving of an inverse kinetic task that is still an untrivial calculation problem. The last one is related to that catalytic data are recorded as integral reactor data (conversion, selectivity) which can only be derived from kinetic rates equations by solving a system of ODEs. The wide range of the CO_2-FT products as well as the thermodynamic and kinetic limitations further complicate the task. Thereby, the development of methods for accelerated constructing of kinetic models is an important task for various scientific and industrial applications including CO_2-FTS.

The modern ML and data science methods were shown in the introduction to be effective tools in solving of a wide range of the tasks in science and industry. Depending on the specific of the task, the different ML methods can be applied which are able to generalize complex non-linear dependencies in the data. Such modern ML and data science methods could be successfully used for the analysis of the catalytic data and development structure-composition-activity regression models. They can help in the organizing, systemizing a big amount of the data, predicting new materials with necessary properties as well as extracting the latent knowledge from the scientific literature. The key advantage of ML methods is that only the data are required for building the predictive models. However, to avoid the overfitting of ML models, applying these methods demands big data which are usually not available in the case of catalytic data. In such a case, to improve significance and effectiveness of the data analysis and ML models two approaches could be considered: (i) the recalculation and normalization of the catalytic data to minimize the correlations between parameters; (ii) the improvement of the ML models by embedding the expert's knowledge into the architecture of the models. The current work was focused on the developing such approaches for the analysis of the scientific literature and kinetic model development of CO_2-FTS.

Thus, the main aim of this work is to investigate in more details CO_2 hydrogenation to higher hydrocarbons using modern data science and ML methods. The following objectives of the present work were set:

1. Extracting and organizing detailed information about catalysts and reaction conditions from the scientific literature with its further analysis by the data science and ML methods as well as an experimental validation of the hypotheses formulated from the data analysis.
2. Developing and investigating new approaches for kinetic modelling of CO_2 hydrogenation with ML.

2.2. Outline

According to the aim and formulated objectives, the first part of the work is devoted to the analysis of the literature data on CO_2 hydrogenation catalysts for hydrocarbon production (see section 3.1). Detailed information about catalysts and reaction conditions was extracted from scientific articles and converted into SQLite database for facilitating the data evaluation and analysis. As the catalytic data of CO_2-FTS include different parameters (CO_2 conversion, CO and hydrocarbon selectivity, olefin content), the first stage involved developing a methodology to convert them into a small number of independent features that define the catalyst activity and selectivity and can be calculated from the data. The next step was to analyze the obtained data for formulating new hypothesizes in CO_2-FTS and find correlations between the suggested features and catalyst properties (composition, preparation methods, reduction pretreatment) as well as reaction conditions (temperature, pressure, CO_2:H_2 ratio, GHSV).

The hypothesis formulated from the data analysis was further validated by catalytic experiments (see section 3.2). This hypothesis relates to the presence of an additional direct pathway of CO_2 hydrogenation to higher hydrocarbons. To validate this statement, we prepared typical Fe-based catalysts with/without dopants (K, Mn, and Al) and tested them under CO_2-FT conditions to obtain catalytic data in the form of a conversion-selectivity dependencies. This analysis allowed us to determine the main reaction pathways occurring in the CO_2-FT process. Additionally, the obtained catalysts were characterized by various physicochemical methods to find correlations between activity and catalyst properties.

The last part of the work focuses on the development of a new method for modelling the kinetics of catalytic reactions using neural ODE (see section 3.3). To address the issue of limited data, the architecture of the neural network models was constrained by integrating general knowledge about the process. Numerical experiments were conducted to validate the proposed approach. Furthermore, we applied this new approach to real experimental data. For this purpose, we prepared supported Fe-based catalysts and tested them in the CO_2 hydrogenation process under a wide range of reaction conditions that are typical for kinetic model development.

3. Summary of Publications

3.1. Data Analysis of CO_2 Hydrogenation Catalysts for Hydrocarbon Production

Aleksandr Fedorov* and David Linke*

Journal of CO_2 Utilization, 2022, 102034, DOI: 10.1016/j.jcou.2022.102034.

Summary:

In this study, the data analysis of the scientific literature about CO_2 hydrogenation catalysts for hydrocarbon production was performed. The detailed information about catalysts and reaction conditions were extracted from the articles and converted into SQLite database. The obtained data were analyzed by applying data science and machine learning methods. The catalytic characteristics (CO_2 conversion, CO and hydrocarbon selectivity, olefin content etc.) were transformed into a small number of independent parameters to improve the significance of the analysis. The key parameters of catalyst selectivity are the chain growth probability α and an excess-methane selectivity γ. The last one describes an increase in CH_4 selectivity compared to the value calculated by the ASF distribution. In addition to these parameters, the thermodynamic ratio (the reaction quotient to the equilibrium constant) of the RWGS reaction was used for the analysis of an approach to the equilibrium. It was found that the suggested parameters (α and γ) only slightly depend on reaction conditions (temperature, pressure, CO_2:H_2 ratio, GHSV) and are mainly defined by the catalyst. By the feature importance analysis, it was found that doping Fe-based catalysts with alkali metals (particularly K and Na) is the most effective measure for improving the catalyst activity and selectivity. The performed analysis of an approach to equilibrium of the RGWS reaction indicates the presence of an additional direct route of CO_2 hydrogenation via FT mechanism at least for some catalytic systems. An experimental validation of such a reaction pathway would be great of interest.

Author contributions:

I extracted the information from the literature and converted it into the database. I contributed a large part of the methodology development and of the data analysis. I performed all the calculations as well as the data preprocessing and evaluation. I took a part in the discussion and making conclusions from the obtained results. I wrote the first draft and co-edited the final manuscript. My contribution was approximately 80 %.

_____ /A. Fedorov/
Signature of the student

_____ /Dr. D. Linke/
Signature of the supervisor

3.2. Elucidating Reaction Pathways occurring in CO_2 Hydrogenation over Fe-based Catalysts

Aleksandr Fedorov*, Henrik Lund, Vita A. Kondratenko, Evgenii V. Kondratenko, David Linke*,

Applied Catalysis B: Environmental, **2023**, 328, 122505, DOI: 10.1016/j.apcatb.2023.122505.

Summary:

In this study, an experimental validation of the presence of a 'hypothetical' direct route of CO_2 hydrogenation to higher hydrocarbons via FT mechanism was made. For this, an analysis of reaction pathways in CO_2 hydrogenation over Fe-based catalysts was performed. Typical Fe-based catalysts promoted with/without different dopants (K, Mn, and Al) were prepared by the organic combustion method and tested under CO_2-FT conditions. By varying the residence time, we obtained the catalytic data in a wide range of CO_2 conversion (2.5-30 %) with small increments of the conversion (~ 2.5 %). It allowed calculating the production/consumption rates of the products/reagents along the catalyst bed. The obtained fresh and spent catalysts were characterized by the physicochemical methods including TPR-H_2, XRD, low temperature N_2 adsorption. It was clearly shown that except for the RWGS, CO-FT, and direct methanation reactions, an additional pathway of hydrocarbon formation from CO_2 via FT mechanism was observed for some catalytic systems. This is an experimental conformation of the hypothesis made from the data analysis. Based on the results of physicochemical characteristics, we concluded that certain iron carbides are able to directly hydrogenate CO_2 to hydrocarbons. Thus, the concept of requiring iron oxides as an essential active component in CO_2-FTS for catalyzing the RWGS should be reviewed.

Author contributions:

I took a part in the plaining of all the experiments. I prepared all the catalysts and tested them under CO_2-FT conditions. I performed all the calculations except for the kinetic modelling of the data obtained in the TAP (temporal analysis of products) experiments. I took a part in the discussion and making conclusions from the obtained results. I wrote the first draft and co-edited the final manuscript. My contribution was approximately 70 %.

_____ /A. Fedorov/
Signature of the student

_____ /Dr. D. Linke/
Signature of the supervisor

3.3. Kinetics-Constrained Neural Ordinary Differential Equations: Artificial Neural Network Models tailored for Small Data to boost Kinetic Model Development

Aleksandr Fedorov*, Anna Perechodjuk, and David Linke*,

Chemical Engineering Journal, **2023**, 477, 146869, DOI: 10.1016/j.cej.2023.146869.

Summary:

In this study, a new method for kinetic modelling of heterogeneous catalytic reactions by the neural ODE was suggested. The key idea is to constrain the architecture of neural ODE by integrating the general knowledge about thermodynamic and kinetics. The effectiveness of the suggested approach was validated by the performing the numerical experiment using the catalytic reaction of CO_2 hydrogenation to methane as an example. It was found that the suggested approach allows one to obtain reliable kinetic models using only small data which are typically used in the kinetic model development. We successfully applied this approach for the development of the kinetic model of a real experimental data: CO_2 hydrogenation to higher hydrocarbons over Fe-based catalyst. We also demonstrated how to use the obtained kinetic model of CO_2-FTS based on neural ODE for reconstructing the mechanistic model for the RWGS reaction as a key reaction in the CO_2-FTS.

Author contributions:

I took a part in the planning of the catalytic tests. I tested the obtained catalyst under CO_2-FT conditions. I developed the theoretical model and performed all the calculations. I took a part in the discussion and making conclusions from the obtained results. I wrote the first draft and co-edited the final manuscript. My contribution was approximately 75 %.

_____ /A. Fedorov/
Signature of the student

_____ /Dr. D. Linke/
Signature of the supervisor

4. Conclusions and Outlook

The present study demonstrates how applying the modern data science and ML in the scientific workflow helps to identify gaps in knowledge, formulate hypotheses, and accelerate the development of data-driven kinetic models.

The first part of work is related to the literature data analysis regarding CO_2-FT catalysts. To address the issue of the catalytic data (see section 2.1), we first developed a methodology for converting the catalytic feathers into a small number of independent parameters. For this, we modified the ASF distribution by incorporating two extra parameters to describe the observed deviations in the hydrocarbon selectivity from the single-parameter ASF. One of the additional parameters is an excess to CH_4 selectivity γ which is responsible for an increase in methane formation beyond the ideal ASF distribution. The last parameter calculated for all the samples from the database was the thermodynamic ratio η (the ration between reaction quotient and equilibrium constant) which was used to investigate an approach to equilibrium of the RWGS reaction. It is worth noting that the analysis of the database demonstrated that only 9 % of publications provided the full information about catalyst activity. The overwhelming majority of publications provided limited information, particularly regarding hydrocarbons distribution. Moreover, it is fundamentally impossible to calculate the values of the suggested parameters of the modified ASF distribution using such type of data. This created the problems in calculating the key parameters of the catalyst selectivity. However, making some assumptions, we managed to develop methods for estimating the key parameters of the catalyst selectivity (α and γ) using such limited data. The lesson learned from it is that we as a community should become better and provide more detailed data and metadata.

The analysis of the influence of the reaction conditions and catalyst properties on the key parameters of the catalyst selectivity α and γ demonstrated that the suggested parameters only slightly depend on the reaction condition (temperature, pressure, H_2:CO_2 ratio, the feed flow rate) and are mainly defined by the catalyst. Analysis of parameters´ importance performed by using random forest to compare the influence of all the catalytic parameters (reaction condition, catalyst composition and properties) on α and γ showed that the doping Fe-based catalysts with alkali metals is the most effective measure for improving these parameters and, thus, catalyst performance. This finding expands our knowledge about the factors affecting the selectivity of CO_2-FT catalysts and may be used for developing the strategy for the screening of highly selective CO_2-FT catalysts.

The thermodynamic ratio η was used to investigate the approach to equilibrium of the RWGS reaction. It is worth mentioning that in the case of generally accepted two-stage mechanism of CO_2-FTS, the value of thermodynamic ratio η must not exceed one. However, when we estimated the values of the thermodynamic ratio for all the samples from the obtained database, we found that the ratio $\eta > 1$ for around 17 % of all the samples from the obtained database. It may be explained by the presence of additional direct (not via CO) routes of hydrocarbons formation from CO_2. More detailed analysis of the obtained results showed that such pathways may be the direct methanation reaction and possibly other direct CO_2 hydrogenation routes to hydrocarbons. This idea led us to postulate a hypothesis regarding the presence of the direct route of CO_2 hydrogenation to C_{2+} hydrocarbons in CO_2-FTS for some catalytic systems.

To validate the formulated hypothesis, a series of the Fe-based catalysts doped by K, Al and/or Mn was prepared by the organic combustion method and investigated in CO_2-FTS. To check the presence of 'hypothetical' direct route of CO_2 hydrogenation to C_{2+} hydrocarbons, the analysis of the reaction pathways occurring in CO_2-FTS was performed. For this purpose, the catalytic data were obtained in a wide range of CO_2 conversion (2.5-30 %) in small increments of conversion (< 5 %) that allowed estimating the rates of reagents consumption and product formation along the catalyst bed without kinetic modelling. It was found that except for the RWGS and CO-FT reactions, additional reaction pathways exist in CO_2-FTS. One of them is the direct route of methane formation from CO_2 that takes place over all the investigated catalysts that agrees with the above literature review. Another one is the direct route of CO_2 hydrogenation to C_{2+} hydrocarbons that plays significant role for certain Fe-based catalysts promoted with K that was demonstrated for the first time. Thus, this is an experimental conformation of the hypothesis formulated from the literature data analysis. Moreover, the XRD analysis of the spent catalysts allowed one to conclude that iron carbides are responsible for catalyzing of the direct rout of CO_2 hydrogenation to C_{2+} hydrocarbons. In addition, it was observed that CH_4 selectivity for non-promoted Fe-based catalyst is much higher than for K-promoted ones. Detailed analysis of the formation rates for each hydrocarbon using the ASF distribution demonstrated that high selectivity of non-promoted Fe catalyst to methane is related to the presence of low selective (to higher hydrocarbons) active sites responsible for the chain growth with α being equal to 0.18 accounting for approximately 86 % of all hydrocarbon formation. It was found that doping of Fe-based catalysts with K allowed to suppress the formation of these sites.

The validated hypothesis formulated from the literature data analysis regarding the presence of the direct route of CO_2 hydrogenation to C_{2+} hydrocarbons expands our knowledge about the role of iron carbide in CO_2-FTS. The concept of requiring iron oxides as an essential active component for catalyzing CO_2-FTS should be reviewed. Furthermore, gaining further insights into the role of iron carbide in the direct route could aid in the design of novel catalytic systems that exhibit enhanced performance and high selectivity towards the desired products. Moreover, understanding the factors influencing the presence of direct route to the CO_2-FT reaction may have a potential opportunity for the control of the contribution of this direct pathway in the overall CO_2-FT process and, thus, bypass the thermodynamic limitation of the CO_2-FT process related to the RWGS reaction. In addition, the obtained results about the main reaction pathways occurring in CO_2-FTS are important for accurate kinetic modeling of the overall process.

The last part of work was devoted to developing new approaches for kinetic modelling with neural ODE. To address the problem of small data in data-driven kinetic model development, the new approach was suggested that is based on constraining the architecture of neural ODE by integrating general knowledge about kinetics and thermodynamics of the chemical process. To validate the suggested approach, the numerical experiment was performed. For this, the typical small training dataset of the catalytic data obtaining from the simulation of CO_2 hydrogenation to methane were generated and used for training neural ODE models. In addition, larger test data were generated for validating the obtained models and the analysis of their generalization in a wide range of the reaction conditions. It was demonstrated that traditional neural ODE model that was used as a baseline performs poorly and does not have a good generalization ability. However, kinetics-constrained neural ODE (KCNODE) suggested in the present work was shown to fit the training and test data correctly. Moreover, it was demonstrated that the KCNODE model with high generalization ability can be also obtained by using ‘noisy’ training datasets. The obtained models were demonstrated to be resistant to overfitting. This resistance to overfitting can be explained by the presence of chemistry knowledge into the architecture of neural ODE. The suggested approach was applied for kinetic model development of the more complex reaction of CO_2 hydrogenation to higher hydrocarbons. For this, a typical Fe-based catalyst doped by K and Cu was prepared by the incipient wetness impregnation method using γ-Al_2O_3. The obtained catalyst was tested in CO_2-FTS under different reaction condition to collect the catalytic data further used for kinetic model development based on improved neural ODE approach. The KCNODE model was successfully developed for describing the CO_2-FTS using the obtained catalytic dataset. It was demonstrated that the obtained model

describes the reagent consumption and the product formation as well as the hydrocarbon distribution correctly. In addition, the obtained KCNODE model was used to derive a mechanistic model of the RWGS reaction. For this, the screening of the different models describing the RWGS/WGS reactions was performed to find expression which is best matching the rates of RWGS estimated by the KCNODE model. Based on the obtained results, a new type of LHHW kinetic expression was suggested which fits the data as well as the best one from the literature but has a fewer number of kinetic parameters.

The devised approach for the kinetic modelling of CO_2 hydrogenation based on neural ODE using only small datasets could significantly expand the scope of applying neural networks and accelerate the kinetic model development. Due to method's ability to train neural ODE models with small data, the suggested approach could be applied for kinetic model development of any catalytic reactions and further investigation for another reaction network systems would be great of interest. Additionally, it's noteworthy that catalyst descriptors can serve as inputs for neural networks. This expansion allows the suggested approach to not only create a kinetic model for a single catalyst but also a universal model for a range of catalysts. This could facilitate the analysis of catalytic data and identification of key descriptors influencing performance. Moreover, ideas used in the present study may be applied for developing new knowledge-constrained neural ODE for solving of a wide range of tasks in different fields where differential equations are applied.

5. References

[1] C. Panzone, R. Philippe, A. Chappaz, P. Fongarland, A. Bengaouer, Power-to-Liquid catalytic CO_2 valorization into fuels and chemicals: focus on the Fischer-Tropsch route, Journal of CO_2 Utilization, 38 (2020) 314-347.

[2] H. Ritchie, M. Roser, P. Rosado, CO_2 and Greenhouse Gas Emissions, Our World in Data.

[3] J.F.B. Mitchell, The “Greenhouse” effect and climate change, Reviews of Geophysics, 27 (1989) 115-139.

[4] J. Hansen, R. Ruedy, M. Sato, K. Lo, Global Surface Temperature Change, Reviews of Geophysics, 48 (2010).

[5] N.J.L. Lenssen, G.A. Schmidt, J.E. Hansen, M.J. Menne, A. Persin, R. Ruedy, D. Zyss, Improvements in the GISTEMP Uncertainty Model, Journal of Geophysical Research: Atmospheres, 124 (2019) 6307-6326.

[6] P. Friedlingstein, M. O'Sullivan, M.W. Jones, R.M. Andrew, L. Gregor, J. Hauck, C. Le Quéré, I.T. Luijkx, A. Olsen, G.P. Peters, W. Peters, J. Pongratz, C. Schwingshackl, S. Sitch, J.G. Canadell, P. Ciais, R.B. Jackson, S.R. Alin, R. Alkama, A. Arneth, V.K. Arora, N.R. Bates, M. Becker, N. Bellouin, H.C. Bittig, L. Bopp, F. Chevallier, L.P. Chini, M. Cronin, W. Evans, S. Falk, R.A. Feely, T. Gasser, M. Gehlen, T. Gkritzalis, L. Gloege, G. Grassi, N. Gruber, Ö. Gürses, I. Harris, M. Hefner, R.A. Houghton, G.C. Hurtt, Y. Iida, T. Ilyina, A.K. Jain, A. Jersild, K. Kadono, E. Kato, D. Kennedy, K. Klein Goldewijk, J. Knauer, J.I. Korsbakken, P. Landschützer, N. Lefèvre, K. Lindsay, J. Liu, Z. Liu, G. Marland, N. Mayot, M.J. McGrath, N. Metzl, N.M. Monacci, D.R. Munro, S.I. Nakaoka, Y. Niwa, K. O'Brien, T. Ono, P.I. Palmer, N. Pan, D. Pierrot, K. Pocock, B. Poulter, L. Resplandy, E. Robertson, C. Rödenbeck, C. Rodriguez, T.M. Rosan, J. Schwinger, R. Séférian, J.D. Shutler, I. Skjelvan, T. Steinhoff, Q. Sun, A.J. Sutton, C. Sweeney, S. Takao, T. Tanhua, P.P. Tans, X. Tian, H. Tian, B. Tilbrook, H. Tsujino, F. Tubiello, G.R. van der Werf, A.P. Walker, R. Wanninkhof, C. Whitehead, A. Willstrand Wranne, R. Wright, W. Yuan, C. Yue, X. Yue, S. Zaehle, J. Zeng, B. Zheng, Global Carbon Budget 2022, Earth Syst. Sci. Data, 14 (2022) 4811-4900.

[7] X. Lan, P. Tans, K.W. Thoning, Trends in globally-averaged CO_2 determined from NOAA Global Monitoring Laboratory measurements. Version 2023-06, 2023.

[8] H. Li, R. Zhang, T. Wang, X. Sun, C. Hou, R. Xu, Y. Wu, Z. Tang, Simulation of H_2S and CO_2 removal from IGCC syngas by cryogenic distillation, Carbon Capture Science & Technology, 3 (2022) 100012.

[9] F. Amirkhani, H.R. Harami, M. Asghari, CO_2/CH_4 mixed gas separation using poly(ether-b-amide)-ZnO nanocomposite membranes: Experimental and molecular dynamics study, Polymer Testing, 86 (2020) 106464.

[10] Y. Ying, Z. Zhang, S.B. Peh, A. Karmakar, Y. Cheng, J. Zhang, L. Xi, C. Boothroyd, Y.M. Lam, C. Zhong, D. Zhao, Pressure-Responsive Two-Dimensional Metal–Organic Framework Composite Membranes for CO_2 Separation, Angewandte Chemie International Edition, 60 (2021) 11318-11325.

[11] R. Augelletti, S. Galli, P. Gislon, M. Granati, G. Monteleone, M.A. Murmura, M.C. Annesini, Biogas upgrading through CO_2 removal by chemical absorption in an amine organic solution: Physical and technical assessment, simulation and experimental validation, Biomass and Bioenergy, 141 (2020) 105729.

[12] A. Taghvaie Nakhjiri, A. Heydarinasab, O. Bakhtiari, T. Mohammadi, Numerical simulation of CO_2/H_2S simultaneous removal from natural gas using potassium carbonate aqueous solution in hollow fiber membrane contactor, Journal of Environmental Chemical Engineering, 8 (2020) 104130.

[13] F. Raganati, F. Miccio, P. Ammendola, Adsorption of Carbon Dioxide for Post-combustion Capture: A Review, Energy & Fuels, 35 (2021) 12845-12868.

[14] G.A. Olah, G.K.S. Prakash, A. Goeppert, Anthropogenic Chemical Carbon Cycle for a Sustainable Future, Journal of the American Chemical Society, 133 (2011) 12881-12898.

[15] F.V. Vázquez, J. Koponen, V. Ruuskanen, C. Bajamundi, A. Kosonen, P. Simell, J. Ahola, C. Frilund, J. Elfving, M. Reinikainen, N. Heikkinen, J. Kauppinen, P. Piermartini, Power-to-X technology using renewable electricity and carbon dioxide from ambient air: SOLETAIR proof-of-concept and improved process concept, Journal of CO_2 Utilization, 28 (2018) 235-246.

[16] M.E. Boot-Handford, J.C. Abanades, E.J. Anthony, M.J. Blunt, S. Brandani, N. Mac Dowell, J.R. Fernández, M.-C. Ferrari, R. Gross, J.P. Hallett, R.S. Haszeldine, P. Heptonstall, A. Lyngfelt, Z. Makuch, E. Mangano, R.T.J. Porter, M. Pourkashanian, G.T. Rochelle, N. Shah, J.G. Yao, P.S. Fennell, Carbon capture and storage update, Energy & Environmental Science, 7 (2014) 130-189.

[17] A. Raza, R. Gholami, R. Rezaee, C.H. Bing, R. Nagarajan, M.A. Hamid, CO_2 storage in depleted gas reservoirs: A study on the effect of residual gas saturation, Petroleum, 4 (2018) 95-107.

[18] J.T. Birkholzer, Q. Zhou, C.-F. Tsang, Large-scale impact of CO_2 storage in deep saline aquifers: A sensitivity study on pressure response in stratified systems, International Journal of Greenhouse Gas Control, 3 (2009) 181-194.

[19] F. Marques Mota, D.H. Kim, From CO_2 methanation to ambitious long-chain hydrocarbons: alternative fuels paving the path to sustainability, Chemical Society Reviews, 48 (2019) 205-259.

[20] W. Wang, S. Wang, X. Ma, J. Gong, Recent advances in catalytic hydrogenation of carbon dioxide, Chemical Society Reviews, 40 (2011) 3703-3727.

[21] M.D. Garba, M. Usman, S. Khan, F. Shehzad, A. Galadima, M.F. Ehsan, A.S. Ghanem, M. Humayun, CO_2 towards fuels: A review of catalytic conversion of carbon dioxide to hydrocarbons, Journal of Environmental Chemical Engineering, 9 (2021) 104756.

[22] T. Reda, C.M. Plugge, N.J. Abram, J. Hirst, Reversible interconversion of carbon dioxide and formate by an electroactive enzyme, Proceedings of the National Academy of Sciences, 105 (2008) 10654-10658.

[23] Y.A. Daza, J.N. Kuhn, CO_2 conversion by reverse water gas shift catalysis: comparison of catalysts, mechanisms and their consequences for CO_2 conversion to liquid fuels, RSC Advances, 6 (2016) 49675-49691.

[24] P. Lahijani, Z.A. Zainal, M. Mohammadi, A.R. Mohamed, Conversion of the greenhouse gas CO_2 to the fuel gas CO via the Boudouard reaction: A review, Renewable and Sustainable Energy Reviews, 41 (2015) 615-632.

[25] A. Goguet, F. Meunier, J.P. Breen, R. Burch, M.I. Petch, A. Faur Ghenciu, Study of the origin of the deactivation of a Pt/CeO_2 catalyst during reverse water gas shift (RWGS) reaction, Journal of Catalysis, 226 (2004) 382-392.

[26] C.-S. Chen, W.-H. Cheng, S.-S. Lin, Study of iron-promoted Cu/SiO_2 catalyst on high temperature reverse water gas shift reaction, Applied Catalysis A: General, 257 (2004) 97-106.

[27] A.M. Bahmanpour, M. Signorile, O. Kröcher, Recent progress in syngas production via catalytic CO_2 hydrogenation reaction, Applied Catalysis B: Environmental, 295 (2021) 120319.

[28] M. González-Castaño, B. Dorneanu, H. Arellano-García, The reverse water gas shift reaction: a process systems engineering perspective, Reaction Chemistry & Engineering, 6 (2021) 954-976.

[29] J. Ashok, S. Pati, P. Hongmanorom, Z. Tianxi, C. Junmei, S. Kawi, A review of recent catalyst advances in CO_2 methanation processes, Catalysis Today, 356 (2020) 471-489.

[30] S.G. Jadhav, P.D. Vaidya, B.M. Bhanage, J.B. Joshi, Catalytic carbon dioxide hydrogenation to methanol: A review of recent studies, Chemical Engineering Research and Design, 92 (2014) 2557-2567.

[31] P. Schwiderowski, H. Ruland, M. Muhler, Current developments in CO_2 hydrogenation towards methanol: A review related to industrial application, Current Opinion in Green and Sustainable Chemistry, 38 (2022) 100688.

[32] X. Jiang, X. Nie, X. Guo, C. Song, J.G. Chen, Recent Advances in Carbon Dioxide Hydrogenation to Methanol via Heterogeneous Catalysis, Chemical Reviews, 120 (2020) 7984-8034.

[33] V. Dieterich, A. Buttler, A. Hanel, H. Spliethoff, S. Fendt, Power-to-liquid via synthesis of methanol, DME or Fischer–Tropsch-fuels: a review, Energy & Environmental Science, 13 (2020) 3207-3252.

[34] F. Pontzen, W. Liebner, V. Gronemann, M. Rothaemel, B. Ahlers, CO_2-based methanol and DME – Efficient technologies for industrial scale production, Catalysis Today, 171 (2011) 242-250.

[35] A. Prašnikar, A. Pavlišič, F. Ruiz-Zepeda, J. Kovač, B. Likozar, Mechanisms of Copper-Based Catalyst Deactivation during CO_2 Reduction to Methanol, Industrial & Engineering Chemistry Research, 58 (2019) 13021-13029.

[36] Y.-F. Zhao, Y. Yang, C. Mims, C.H.F. Peden, J. Li, D. Mei, Insight into methanol synthesis from CO_2 hydrogenation on Cu(111): Complex reaction network and the effects of H_2O, Journal of Catalysis, 281 (2011) 199-211.

[37] J. Ding, M. Wang, H. Liu, Z. Wang, X. Guo, G. Yu, Y. Wang, Influence of La-doping on the CuO/ZrO_2 catalysts with different Cu contents for hydrogenation of dimethyl oxalate to ethylene glycol, New Journal of Chemistry, 45 (2021) 18102-18113.

[38] A. Bansode, B. Tidona, P.R. von Rohr, A. Urakawa, Impact of K and Ba promoters on CO_2 hydrogenation over Cu/Al_2O_3 catalysts at high pressure, Catalysis Science & Technology, 3 (2013) 767-778.

[39] C.S. Santana, L.F. Rasteiro, F.C.F. Marcos, E.M. Assaf, J.F. Gomes, J.M. Assaf, Influence of Al, Cr, Ga, or Zr as promoters on the performance of Cu/ZnO catalyst for CO_2 hydrogenation to methanol, Molecular Catalysis, 528 (2022) 112512.

[40] T. Riedel, G. Schaub, K.-W. Jun, K.-W. Lee, Kinetics of CO_2 Hydrogenation on a K-Promoted Fe Catalyst, Industrial & Engineering Chemistry Research, 40 (2001) 1355-1363.

[41] H. Schulz, Short history and present trends of Fischer–Tropsch synthesis, Appl.Catal.A, 186 (1999) 3-12.

[42] S.A. Chernyak, M. Corda, J.-P. Dath, V.V. Ordomsky, A.Y. Khodakov, Light olefin synthesis from a diversity of renewable and fossil feedstocks: state-of the-art and outlook, Chemical Society Reviews, 51 (2022) 7994-8044.

[43] A. Corma, Inorganic Solid Acids and Their Use in Acid-Catalyzed Hydrocarbon Reactions, Chemical Reviews, 95 (1995) 559-614.

[44] Z. Li, W. Wu, M. Wang, Y. Wang, X. Ma, L. Luo, Y. Chen, K. Fan, Y. Pan, H. Li, J. Zeng, Ambient-pressure hydrogenation of CO_2 into long-chain olefins, Nature Communications, 13 (2022) 2396.

[45] M. Hermesmann, K. Grübel, L. Scherotzki, T.E. Müller, Promising pathways: The geographic and energetic potential of power-to-x technologies based on regeneratively obtained hydrogen, Renewable and Sustainable Energy Reviews, 138 (2021) 110644.

[46] B. Yao, T. Xiao, O.A. Makgae, X. Jie, S. Gonzalez-Cortes, S. Guan, A.I. Kirkland, J.R. Dilworth, H.A. Al-Megren, S.M. Alshihri, P.J. Dobson, G.P. Owen, J.M. Thomas, P.P. Edwards, Transforming carbon dioxide into jet fuel using an organic combustion-synthesized Fe-Mn-K catalyst, Nature Communications, 11 (2020) 6395.

[47] J. Wei, Q. Ge, R. Yao, Z. Wen, C. Fang, L. Guo, H. Xu, J. Sun, Directly converting CO_2 into a gasoline fuel, Nature Communications, 8 (2017) 15174.

[48] M. Albrecht, U. Rodemerck, M. Schneider, M. Bröring, D. Baabe, E.V. Kondratenko, Unexpectedly efficient CO_2 hydrogenation to higher hydrocarbons over non-doped Fe_2O_3, Applied Catalysis B: Environmental, 204 (2017) 119-126.

[49] T. Herranz, S. Rojas, F.J. Pérez-Alonso, M. Ojeda, P. Terreros, J.L.G. Fierro, Hydrogenation of carbon oxides over promoted Fe-Mn catalysts prepared by the microemulsion methodology, Applied Catalysis A: General, 311 (2006) 66-75.

[50] L. Brübach, D. Hodonj, P. Pfeifer, Kinetic Analysis of CO_2 Hydrogenation to Long-Chain Hydrocarbons on a Supported Iron Catalyst, Industrial & Engineering Chemistry Research, 61 (2022) 1644-1654.

[51] J. Chen, C. Yang, Thermodynamic Equilibrium Analysis of Product Distribution in the Fischer–Tropsch Process Under Different Operating Conditions, ACS Omega, 4 (2019) 22237-22244.

[52] L. Torrente-Murciano, D. Mattia, M.D. Jones, P.K. Plucinski, Formation of hydrocarbons via CO_2 hydrogenation – A thermodynamic study, Journal of CO_2 Utilization, 6 (2014) 34-39.

[53] B. Yao, W. Ma, S. Gonzalez-Cortes, T. Xiao, P.P. Edwards, Thermodynamic study of hydrocarbon synthesis from carbon dioxide and hydrogen, Greenhouse Gases: Science and Technology, 7 (2017) 942-957.

[54] F.A.N. Fernandes, Polymerization Kinetics of Fischer-Tropsch Reaction on Iron Based Catalysts and Product Grade Optimization, Chemical Engineering & Technology, 28 (2005) 930-938.

[55] G.V. Schulz, Über die Beziehung zwischen Reaktionsgeschwindigkeit und Zusammensetzung des Reaktionsproduktes bei Makropolymerisationsvorgängen, Zeitschrift für Physikalische Chemie, 30B (1935) 379-398.

[56] P.J. Flory, Molecular Size Distribution in Linear Condensation Polymers1, Journal of the American Chemical Society, 58 (1936) 1877-1885.

[57] R.B. Anderson, R.A. Friedel, H.H. Storch, Fischer-Tropsch Reaction Mechanism Involving Stepwise Growth of Carbon Chain, The Journal of Chemical Physics, 19 (1951) 313-319.

[58] G. Henrici-Olivé, S. Olivé, The Fischer-Tropsch Synthesis: Molecular Weight Distribution of Primary Products and Reaction Mechanism, Angewandte Chemie International Edition in English, 15 (1976) 136-141.

[59] E.S. Lox, G.F. Froment, Kinetics of the Fischer-Tropsch reaction on a precipitated promoted iron catalyst. 2. Kinetic modeling, Industrial & Engineering Chemistry Research, 32 (1993) 71-82.

[60] G.P. Van Der Laan, A.A.C.M. Beenackers, Kinetics and Selectivity of the Fischer–Tropsch Synthesis: A Literature Review, Catalysis Reviews, 41 (1999) 255-318.

[61] S. Wang, T. Wu, J. Lin, Y. Ji, S. Yan, Y. Pei, S. Xie, B. Zong, M. Qiao, Iron–Potassium on Single-Walled Carbon Nanotubes as Efficient Catalyst for CO_2 Hydrogenation to Heavy Olefins, ACS Catalysis, 10 (2020) 6389-6401.

[62] L. Falbo, M. Martinelli, C.G. Visconti, L. Lietti, P. Forzatti, C. Bassano, P. Deiana, Effects of Zn and Mn Promotion in Fe-Based Catalysts Used for CO_x Hydrogenation to Long-Chain Hydrocarbons, Industrial & Engineering Chemistry Research, 56 (2017) 13146-13156.

[63] C.G. Visconti, M. Martinelli, L. Falbo, L. Fratalocchi, L. Lietti, CO_2 hydrogenation to hydrocarbons over Co and Fe-based Fischer-Tropsch catalysts, Catalysis Today, 277 (2016) 161-170.

[64] C.G. Visconti, L. Lietti, E. Tronconi, P. Forzatti, R. Zennaro, E. Finocchio, Fischer–Tropsch synthesis on a Co/Al_2O_3 catalyst with CO_2 containing syngas, Applied Catalysis A: General, 355 (2009) 61-68.

[65] A.S. Skrypnik, Q. Yang, A.A. Matvienko, V.Y. Bychkov, Y.P. Tulenin, H. Lund, S.A. Petrov, R. Kraehnert, A. Arinchtein, J. Weiss, A. Brueckner, E.V. Kondratenko, Understanding reaction-induced restructuring of well-defined $Fe_xO_yC_z$ compositions and its effect on CO_2 hydrogenation, Applied Catalysis B: Environmental, 291 (2021) 120121.

[66] J. Liu, G. Zhang, X. Jiang, J. Wang, C. Song, X. Guo, Insight into the role of Fe_5C_2 in CO_2 catalytic hydrogenation to hydrocarbons, Catalysis Today, 371 (2021) 162-170.

[67] S.-C. Lee, J.-H. Jang, B.-Y. Lee, J.-S. Kim, M. Kang, S.-B. Lee, M.-J. Choi, S.-J. Choung, Promotion of hydrocarbon selectivity in CO_2 hydrogenation by Ru component, Journal of Molecular Catalysis A: Chemical, 210 (2004) 131-141.

[68] B.W. Wojciechowski, The Kinetics of the Fischer-Tropsch Synthesis, Catalysis Reviews, 30 (1988) 629-702.

[69] B. Sarup, B.W. Wojciechowski, Studies of the fischer-tropsch synthesis on a cobalt catalyst i. evaluation of product distribution parameters from experimental data, The Canadian Journal of Chemical Engineering, 66 (1988) 831-842.

[70] C.G. Visconti, M. Martinelli, L. Falbo, A. Infantes-Molina, L. Lietti, P. Forzatti, G. Iaquaniello, E. Palo, B. Picutti, F. Brignoli, CO_2 hydrogenation to lower olefins on a high surface area K-promoted bulk Fe-catalyst, Applied Catalysis B: Environmental, 200 (2017) 530-542.

[71] T. Riedel, H. Schulz, G. Schaub, K.-W. Jun, J.-S. Hwang, K.-W. Lee, Fischer–Tropsch on Iron with H_2/CO and H_2/CO_2 as Synthesis Gases: The Episodes of Formation of the Fischer–Tropsch Regime and Construction of the Catalyst, Topics in Catalysis, 26 (2003) 41-54.

[72] B. H. Davis, M.L. Occelli, Advances in Fischer-Tropsch Synthesis, Catalysts, and Catalysis, CRC Press2009.

[73] G. Jacobs, W. Ma, P. Gao, B. Todic, T. Bhatelia, D.B. Bukur, B.H. Davis, The application of synchrotron methods in characterizing iron and cobalt Fischer–Tropsch synthesis catalysts, Catalysis Today, 214 (2013) 100-139.

[74] T. Riedel, M. Claeys, H. Schulz, G. Schaub, S.-S. Nam, K.-W. Jun, M.-J. Choi, G. Kishan, K.-W. Lee, Comparative study of Fischer–Tropsch synthesis with H_2/CO and H_2/CO_2 syngas using Fe- and Co-based catalysts, Applied Catalysis A: General, 186 (1999) 201-213.

[75] Z. Shi, H. Yang, P. Gao, X. Li, L. Zhong, H. Wang, H. Liu, W. Wei, Y. Sun, Direct conversion of CO2 to long-chain hydrocarbon fuels over K–promoted $CoCu/TiO_2$ catalysts, Catalysis Today, 311 (2018) 65-73.

[76] G.D. Weatherbee, C.H. Bartholomew, Hydrogenation of CO_2 on group VIII metals: IV. Specific activities and selectivities of silica-supported Co, Fe, and Ru, Journal of Catalysis, 87 (1984) 352-362.

[77] Z. You, W. Deng, Q. Zhang, Y. Wang, Hydrogenation of carbon dioxide to light olefins over non-supported iron catalyst, Chinese Journal of Catalysis, 34 (2013) 956-963.

[78] J. Wang, Z. You, Q. Zhang, W. Deng, Y. Wang, Synthesis of lower olefins by hydrogenation of carbon dioxide over supported iron catalysts, Catalysis Today, 215 (2013) 186-193.

[79] N. Boreriboon, X. Jiang, C. Song, P. Prasassarakich, Fe-based bimetallic catalysts supported on TiO_2 for selective CO_2 hydrogenation to hydrocarbons, Journal of CO_2 Utilization, 25 (2018) 330-337.

[80] B. Liang, T. Sun, J. Ma, H. Duan, L. Li, X. Yang, Y. Zhang, X. Su, Y. Huang, T. Zhang, Mn decorated Na/Fe catalysts for CO_2 hydrogenation to light olefins, Catalysis Science & Technology, 9 (2019) 456-464.

[81] T. Numpilai, N. Chanlek, Y. Poo-Arporn, C.K. Cheng, N. Siri-Nguan, T. Sornchamni, M. Chareonpanich, P. Kongkachuichay, N. Yigit, G. Rupprechter, J. Limtrakul, T. Witoon, Tuning Interactions of Surface-adsorbed Species over $Fe{-}Co/K{-}Al_2O_3$ Catalyst by Different K Contents: Selective CO_2 Hydrogenation to Light Olefins, ChemCatChem, 12 (2020) 3306-3320.

[82] S.-R. Yan, K.-W. Jun, J.-S. Hong, M.-J. Choi, K.-W. Lee, Promotion effect of Fe–Cu catalyst for the hydrogenation of CO_2 and application to slurry reactor, Applied Catalysis A: General, 194-195 (2000) 63-70.

[83] A. Aitbekova, E.D. Goodman, L. Wu, A. Boubnov, A.S. Hoffman, A. Genc, H. Cheng, L. Casalena, S.R. Bare, M. Cargnello, Engineering of Ruthenium–Iron Oxide Colloidal Heterostructures: Improved

Yields in CO_2 Hydrogenation to Hydrocarbons, Angewandte Chemie International Edition, 58 (2019) 17451-17457.

[84] C. Zhang, C. Cao, Y. Zhang, X. Liu, J. Xu, M. Zhu, W. Tu, Y.-F. Han, Unraveling the Role of Zinc on Bimetallic Fe_5C_2–ZnO Catalysts for Highly Selective Carbon Dioxide Hydrogenation to High Carbon α-Olefins, ACS Catalysis, 11 (2021) 2121-2133.

[85] N. Chaipraditgul, T. Numpilai, C. Kui Cheng, N. Siri-Nguan, T. Sornchamni, C. Wattanakit, J. Limtrakul, T. Witoon, Tuning interaction of surface-adsorbed species over Fe/K-Al_2O_3 modified with transition metals (Cu, Mn, V, Zn or Co) on light olefins production from CO_2 hydrogenation, Fuel, 283 (2021) 119248.

[86] T. Witoon, V. Lapkeatseree, T. Numpilai, C. Kui Cheng, J. Limtrakul, CO_2 hydrogenation to light olefins over mixed Fe-Co-K-Al oxides catalysts prepared via precipitation and reduction methods, Chemical Engineering Journal, 428 (2022) 131389.

[87] A. Ramirez, L. Gevers, A. Bavykina, S. Ould-Chikh, J. Gascon, Metal Organic Framework-Derived Iron Catalysts for the Direct Hydrogenation of CO_2 to Short Chain Olefins, ACS Catalysis, 8 (2018) 9174-9182.

[88] B. Liu, S. Geng, J. Zheng, X. Jia, F. Jiang, X. Liu, Unravelling the New Roles of Na and Mn Promoter in CO_2 Hydrogenation over Fe_3O_4-Based Catalysts for Enhanced Selectivity to Light α-Olefins, ChemCatChem, 10 (2018) 4718-4732.

[89] J. Wei, J. Sun, Z. Wen, C. Fang, Q. Ge, H. Xu, New insights into the effect of sodium on Fe_3O_4-based nanocatalysts for CO_2 hydrogenation to light olefins, Catalysis Science & Technology, 6 (2016) 4786-4793.

[90] P.S. Sai Prasad, J.W. Bae, K.-W. Jun, K.-W. Lee, Fischer–Tropsch Synthesis by Carbon Dioxide Hydrogenation on Fe-Based Catalysts, Catalysis Surveys from Asia, 12 (2008) 170-183.

[91] X. Liu, C. Zhang, P. Tian, M. Xu, C. Cao, Z. Yang, M. Zhu, J. Xu, Revealing the Effect of Sodium on Iron-Based Catalysts for CO_2 Hydrogenation: Insights from Calculation and Experiment, The Journal of Physical Chemistry C, 125 (2021) 7637-7646.

[92] B. Liang, H. Duan, T. Sun, J. Ma, X. Liu, J. Xu, X. Su, Y. Huang, T. Zhang, Effect of Na Promoter on Fe-Based Catalyst for CO_2 Hydrogenation to Alkenes, ACS Sustainable Chemistry & Engineering, 7 (2019) 925-932.

[93] N. Fischer, R. Henkel, B. Hettel, M. Iglesias, G. Schaub, M. Claeys, Hydrocarbons via CO_2 Hydrogenation Over Iron Catalysts: The Effect of Potassium on Structure and Performance, Catalysis Letters, 146 (2016) 509-517.

[94] Q. Yang, V.A. Kondratenko, S.A. Petrov, D.E. Doronkin, E. Saraçi, H. Lund, A. Arinchtein, R. Kraehnert, A.S. Skrypnik, A.A. Matvienko, E.V. Kondratenko, Identifying Performance Descriptors in CO_2 Hydrogenation over Iron-Based Catalysts Promoted with Alkali Metals, Angewandte Chemie International Edition, 61 (2022) e202116517.

[95] A.S. Skrypnik, H. Lund, Q. Yang, E.V. Kondratenko, Spatial analysis of CO_2 hydrogenation to higher hydrocarbons over alkali-metal promoted iron(ii)oxalate-derived catalysts, Catalysis Science & Technology, (2023).

[96] M.K. Gnanamani, H.H. Hamdeh, W.D. Shafer, S.D. Hopps, B.H. Davis, Hydrogenation of carbon dioxide over iron carbide prepared from alkali metal promoted iron oxalate, Applied Catalysis A: General, 564 (2018) 243-249.

[97] W. Wang, X. Jiang, X. Wang, C. Song, Fe–Cu Bimetallic Catalysts for Selective CO_2 Hydrogenation to Olefin-Rich C_{2+} Hydrocarbons, Industrial & Engineering Chemistry Research, 57 (2018) 4535-4542.

[98] L. Pastor-Pérez, F. Baibars, E. Le Sache, H. Arellano-García, S. Gu, T.R. Reina, CO_2 valorisation via Reverse Water-Gas Shift reaction using advanced Cs doped Fe-Cu/Al_2O_3 catalysts, Journal of CO_2 Utilization, 21 (2017) 423-428.

[99] X. Cui, P. Gao, S. Li, C. Yang, Z. Liu, H. Wang, L. Zhong, Y. Sun, Selective Production of Aromatics Directly from Carbon Dioxide Hydrogenation, ACS Catalysis, 9 (2019) 3866-3876.

[100] R. Satthawong, N. Koizumi, C. Song, P. Prasassarakich, Bimetallic Fe–Co catalysts for CO_2 hydrogenation to higher hydrocarbons, Journal of CO_2 Utilization, 3-4 (2013) 102-106.

[101] M. Amoyal, R. Vidruk-Nehemya, M.V. Landau, M. Herskowitz, Effect of potassium on the active phases of Fe catalysts for carbon dioxide conversion to liquid fuels through hydrogenation, Journal of Catalysis, 348 (2017) 29-39.

[102] Y. Xu, P. Zhai, Y. Deng, J. Xie, X. Liu, S. Wang, D. Ma, Highly Selective Olefin Production from CO_2 Hydrogenation on Iron Catalysts: A Subtle Synergy between Manganese and Sodium Additives, Angewandte Chemie International Edition, 59 (2020) 21736-21744.

[103] J. Zhu, G. Zhang, W. Li, X. Zhang, F. Ding, C. Song, X. Guo, Deconvolution of the Particle Size Effect on CO_2 Hydrogenation over Iron-Based Catalysts, ACS Catalysis, 10 (2020) 7424-7433.

[104] J.A. Loiland, M.J. Wulfers, N.S. Marinkovic, R.F. Lobo, Fe/γ-Al2O3 and Fe–K/γ-Al2O3 as reverse water-gas shift catalysts, Catalysis Science & Technology, 6 (2016) 5267-5279.

[105] C.M. Kalamaras, S. Americanou, A.M. Efstathiou, "Redox" vs "associative formate with –OH group regeneration" WGS reaction mechanism on Pt/CeO_2: Effect of platinum particle size, Journal of Catalysis, 279 (2011) 287-300.

[106] T. Shido, Y. Iwasawa, Reactant-Promoted Reaction Mechanism for Water-Gas Shift Reaction on Rh-Doped CeO_2, Journal of Catalysis, 141 (1993) 71-81.

[107] A. Ekstrom, J. Lapszewicz, On the role of metal carbides in the mechanism of the Fischer-Tropsch reaction, The Journal of Physical Chemistry, 88 (1984) 4577-4580.

[108] S. Saeidi, S. Najari, F. Fazlollahi, M.K. Nikoo, F. Sefidkon, J.J. Klemeš, L.L. Baxter, Mechanisms and kinetics of CO_2 hydrogenation to value-added products: A detailed review on current status and future trends, Renewable and Sustainable Energy Reviews, 80 (2017) 1292-1311.

[109] S. Mousavi, A. Zamaniyan, M. Irani, M. Rashidzadeh, Generalized kinetic model for iron and cobalt based Fischer–Tropsch synthesis catalysts: Review and model evaluation, Applied Catalysis A: General, 506 (2015) 57-66.

[110] B.H. Davis, Fischer–Tropsch Synthesis: Reaction mechanisms for iron catalysts, Catalysis Today, 141 (2009) 25-33.

[111] V. Ponec, W.A. van Barneveld, The Role of Chemisorption of Fischer-Tropsch Synthesis, Industrial & Engineering Chemistry Product Research and Development, 18 (1979) 268-271.

[112] C. Panzone, R. Philippe, C. Nikitine, A. Bengaouer, A. Chappaz, P. Fongarland, Development and Validation of a Detailed Microkinetic Model for the CO_2 Hydrogenation Reaction toward Hydrocarbons over an $Fe–K/Al_2O_3$ Catalyst, Industrial & Engineering Chemistry Research, 61 (2022) 4514-4533.

[113] S.S. Ail, S. Dasappa, Biomass to liquid transportation fuel via Fischer Tropsch synthesis – Technology review and current scenario, Renewable and Sustainable Energy Reviews, 58 (2016) 267-286.

[114] R. Franke, D. Selent, A. Börner, Applied Hydroformylation, Chemical Reviews, 112 (2012) 5675-5732.

[115] H. Schulz, Principles of Fischer–Tropsch synthesis—Constraints on essential reactions ruling FT-selectivity, Catalysis Today, 214 (2013) 140-151.

[116] M. Zhuo, K.F. Tan, A. Borgna, M. Saeys, Density Functional Theory Study of the CO Insertion Mechanism for Fischer−Tropsch Synthesis over Co Catalysts, The Journal of Physical Chemistry C, 113 (2009) 8357-8365.

[117] Y. Zhang, Y. Yao, J. Chang, X. Lu, X. Liu, D. Hildebrandt, Fischer–Tropsch synthesis with ethene co-feeding: Experimental evidence of the CO-insertion mechanism at low temperature, AIChE Journal, 66 (2020) e17029.

[118] G. Yablonsky, V. Bykov, A. Gorban, V. Elokhin, Kinetic Models of Catalytic Reactions, Elsevier1991.

[119] H.D. Willauer, R. Ananth, M.T. Olsen, D.M. Drab, D.R. Hardy, F.W. Williams, Modeling and kinetic analysis of CO_2 hydrogenation using a Mn and K-promoted Fe catalyst in a fixed-bed reactor, Journal of CO_2 Utilization, 3-4 (2013) 56-64.

[120] A.N. Pour, M.R. Housaindokht, H. Monhemi, A new LHHW kinetic model for CO_2 hydrogenation over an iron catalyst, Prog. React. Kinet. Mech., 41 (2016) 159-169.

[121] C. Panzone, R. Philippe, C. Nikitine, L. Vanoye, A. Bengaouer, A. Chappaz, P. Fongarland, Catalytic and Kinetic Study of the CO_2 Hydrogenation Reaction over a Fe–K/Al_2O_3 Catalyst toward Liquid and Gaseous Hydrocarbon Production, Industrial & Engineering Chemistry Research, 60 (2021) 16635-16652.

[122] L. Brübach, D. Hodonj, L. Biffar, P. Pfeifer, Detailed kinetic modeling of CO_2-based Fischer–Tropsch synthesis, Catalysts, 12 (2022) 630.

[123] B.I. Kamara, J. Coetzee, Overview of High-Temperature Fischer−Tropsch Gasoline and Diesel Quality, Energy & Fuels, 23 (2009) 2242-2247.

[124] D. Leckel, Diesel Production from Fischer−Tropsch: The Past, the Present, and New Concepts, Energy & Fuels, 23 (2009) 2342-2358.

[125] P. Singh, N. Singh, K.K. Singh, A. Singh, Chapter 5 - Diagnosing of disease using machine learning, in: K.K. Singh, M. Elhoseny, A. Singh, A.A. Elngar (Eds.) Machine Learning and the Internet of Medical Things in Healthcare, Academic Press2021, pp. 89-111.

[126] J. Vamathevan, D. Clark, P. Czodrowski, I. Dunham, E. Ferran, G. Lee, B. Li, A. Madabhushi, P. Shah, M. Spitzer, S. Zhao, Applications of machine learning in drug discovery and development, Nature Reviews Drug Discovery, 18 (2019) 463-477.

[127] P. Gogas, T. Papadimitriou, Machine Learning in Economics and Finance, Computational Economics, 57 (2021) 1-4.

[128] J.S. Shyam Mohan, H.S. Vedantham, V.C. Vanam, N.P. Challa, Product Recommendation Systems Based on Customer Reviews Using Machine Learning Techniques, in: I. Jeena Jacob, S. Kolandapalayam Shanmugam, S. Piramuthu, P. Falkowski-Gilski (Eds.) Data Intelligence and Cognitive Informatics, Springer Singapore, Singapore, 2021, pp. 267-286.

[129] L. Chen, R. Li, Y. Liu, R. Zhang, D.M.k. Woodbridge, Machine learning-based product recommendation using Apache Spark, 2017 IEEE SmartWorld, Ubiquitous Intelligence & Computing, Advanced & Trusted Computed, Scalable Computing & Communications, Cloud & Big Data Computing, Internet of People and Smart City Innovation (SmartWorld/SCALCOM/UIC/ATC/CBDCom/IOP/SCI), 2017, pp. 1-6.

[130] H. Li, Deep learning for natural language processing: advantages and challenges, National Science Review, 5 (2018) 24-26.

[131] OpenAi, GPT-4 Technical Report, arXiv [cs.CL], (2023).

[132] Z.Q. Zhao, P. Zheng, S.T. Xu, X. Wu, Object Detection With Deep Learning: A Review, IEEE Transactions on Neural Networks and Learning Systems, 30 (2019) 3212-3232.

[133] A. Miglani, N. Kumar, Deep learning models for traffic flow prediction in autonomous vehicles: A review, solutions, and challenges, Vehicular Communications, 20 (2019) 100184.

[134] E. Puskás, Á. Budai, G. Bohács, Optimization of a physical internet based supply chain using reinforcement learning, European Transport Research Review, 12 (2020) 47.

[135] E. Alpaydin, Introduction to Machine Learning, 2nd ed., The MIT Press.

[136] T. Toyao, Z. Maeno, S. Takakusagi, T. Kamachi, I. Takigawa, K.-i. Shimizu, Machine Learning for Catalysis Informatics: Recent Applications and Prospects, ACS Catalysis, 10 (2020) 2260-2297.

[137] M. Erdem Günay, R. Yıldırım, Recent advances in knowledge discovery for heterogeneous catalysis using machine learning, Catalysis Reviews, 63 (2021) 120-164.

[138] P. Schlexer Lamoureux, K.T. Winther, J.A. Garrido Torres, V. Streibel, M. Zhao, M. Bajdich, F. Abild-Pedersen, T. Bligaard, Machine Learning for Computational Heterogeneous Catalysis, ChemCatChem, 11 (2019) 3581-3601.

[139] C. Schaffer, Selecting a classification method by cross-validation, Machine Learning, 13 (1993) 135-143.

[140] L.E. Eberly, Multiple Linear Regression, in: W.T. Ambrosius (Ed.) Topics in Biostatistics, Humana Press, Totowa, NJ, 2007, pp. 165-187.

[141] R. Tibshirani, Regression Shrinkage and Selection Via the Lasso, Journal of the Royal Statistical Society: Series B (Methodological), 58 (1996) 267-288.

[142] W.J. Dunn, D.R. Scott, W.G. Glen, Principal components analysis and partial least squares regression, Tetrahedron Computer Methodology, 2 (1989) 349-376.

[143] J.G. Greener, S.M. Kandathil, L. Moffat, D.T. Jones, A guide to machine learning for biologists, Nature Reviews Molecular Cell Biology, 23 (2022) 40-55.

[144] W.S. Noble, What is a support vector machine?, Nature Biotechnology, 24 (2006) 1565-1567.

[145] S. Amari, S. Wu, Improving support vector machine classifiers by modifying kernel functions, Neural Networks, 12 (1999) 783-789.

[146] S. Salcedo-Sanz, J.L. Rojo-Álvarez, M. Martínez-Ramón, G. Camps-Valls, Support vector machines in engineering: an overview, WIREs Data Mining and Knowledge Discovery, 4 (2014) 234-267.

[147] B. de Ville, Decision trees, WIREs Computational Statistics, 5 (2013) 448-455.

[148] K. Fawagreh, M.M. Gaber, E. Elyan, Random forests: from early developments to recent advancements, Systems Science & Control Engineering, 2 (2014) 602-609.

[149] R.E. Schapire, The Boosting Approach to Machine Learning: An Overview, in: D.D. Denison, M.H. Hansen, C.C. Holmes, B. Mallick, B. Yu (Eds.) Nonlinear Estimation and Classification, Springer New York, New York, NY, 2003, pp. 149-171.

[150] C. Kern, T. Klausch, F. Kreuter, Tree-based Machine Learning Methods for Survey Research, Surv Res Methods, 13 (2019) 73-93.

[151] K. Hornik, M. Stinchcombe, H. White, Multilayer feedforward networks are universal approximators, Neural Networks, 2 (1989) 359-366.

[152] V.K. Ojha, A. Abraham, V. Snášel, Metaheuristic design of feedforward neural networks: A review of two decades of research, Engineering Applications of Artificial Intelligence, 60 (2017) 97-116.

[153] K. O'Shea, R. Nash, An Introduction to Convolutional Neural Networks, arXiv [cs.NE], (2015).

[154] Z. Wu, S. Pan, F. Chen, G. Long, C. Zhang, P.S. Yu, A Comprehensive Survey on Graph Neural Networks, IEEE Transactions on Neural Networks and Learning Systems, 32 (2021) 4-24.

[155] J. Cheng, L. Dong, M. Lapata, Long Short-Term Memory-networks for machine reading, arXiv [cs.CL], (2016).

[156] G.E. Karniadakis, I.G. Kevrekidis, L. Lu, P. Perdikaris, S. Wang, L. Yang, Physics-informed machine learning, Nature Reviews Physics, 3 (2021) 422-440.

[157] R.T.Q. Chen, Y. Rubanova, J. Bettencourt, D.K. Duvenaud, Neural Ordinary Differential Equations, in: S. Bengio, H. Wallach, H. Larochelle, K. Grauman, N. Cesa-Bianchi, R. Garnett (Eds.) Advances in Neural Information Processing Systems, Curran Associates, Inc., 2018.

[158] V. Tshitoyan, J. Dagdelen, L. Weston, A. Dunn, Z. Rong, O. Kononova, K.A. Persson, G. Ceder, A. Jain, Unsupervised word embeddings capture latent knowledge from materials science literature, Nature, 571 (2019) 95-98.

[159] Z. Zheng, O. Zhang, C. Borgs, J.T. Chayes, O.M. Yaghi, ChatGPT Chemistry Assistant for text mining and prediction of MOF synthesis, arXiv [cs.IR], (2023).

[160] J. Luo, Z. Li, J. Wang, C.-Y. Lin, ChartOCR: Data Extraction From Charts Images via a Deep Hybrid Framework, Proceedings of the IEEE/CVF Winter Conference on Applications of Computer Vision (WACV), 2021, pp. 1917-1925.

[161] S.V. P, M.Y. Hassan, M. Singh, LineEX: Data Extraction From Scientific Line Charts, Proceedings of the IEEE/CVF Winter Conference on Applications of Computer Vision (WACV), 2023, pp. 6213-6221.

[162] J.A. Keith, V. Vassilev-Galindo, B. Cheng, S. Chmiela, M. Gastegger, K.-R. Müller, A. Tkatchenko, Combining Machine Learning and Computational Chemistry for Predictive Insights Into Chemical Systems, Chemical Reviews, 121 (2021) 9816-9872.

[163] A.D. Casey, S.F. Son, I. Bilionis, B.C. Barnes, Prediction of Energetic Material Properties from Electronic Structure Using 3D Convolutional Neural Networks, Journal of Chemical Information and Modeling, 60 (2020) 4457-4473.

[164] L. Huang, C. Ling, Practicing deep learning in materials science: An evaluation for predicting the formation energies, Journal of Applied Physics, 128 (2020) 124901.

[165] A.R. Singh, B.A. Rohr, J.A. Gauthier, J.K. Nørskov, Predicting Chemical Reaction Barriers with a Machine Learning Model, Catalysis Letters, 149 (2019) 2347-2354.

[166] N. Madaan, N.R. Shiju, G. Rothenberg, Predicting the performance of oxidation catalysts using descriptor models, Catalysis Science & Technology, 6 (2016) 125-133.

[167] K. Suzuki, T. Toyao, Z. Maeno, S. Takakusagi, K.-i. Shimizu, I. Takigawa, Statistical Analysis and Discovery of Heterogeneous Catalysts Based on Machine Learning from Diverse Published Data, ChemCatChem, 11 (2019) 4537-4547.

[168] A. Smith, A. Keane, J.A. Dumesic, G.W. Huber, V.M. Zavala, A machine learning framework for the analysis and prediction of catalytic activity from experimental data, Applied Catalysis B: Environmental, 263 (2020) 118257.

[169] U. Zavyalova, M. Holena, R. Schlögl, M. Baerns, Statistical Analysis of Past Catalytic Data on Oxidative Methane Coupling for New Insights into the Composition of High-Performance Catalysts, ChemCatChem, 3 (2011) 1935-1947.

[170] Q. Yang, A. Skrypnik, A. Matvienko, H. Lund, M. Holena, E.V. Kondratenko, Revealing property-performance relationships for efficient CO_2 hydrogenation to higher hydrocarbons over Fe-based catalysts: Statistical analysis of literature data and its experimental validation, Applied Catalysis B: Environmental, 282 (2021) 119554.

[171] M. Raissi, P. Perdikaris, G.E. Karniadakis, Physics-informed neural networks: A deep learning framework for solving forward and inverse problems involving nonlinear partial differential equations, Journal of Computational Physics, 378 (2019) 686-707.

[172] G.S. Gusmão, A.P. Retnanto, S.C.d. Cunha, A.J. Medford, Kinetics-informed neural networks, Catalysis Today, (2022).

[173] R.T.Q. Chen, Y. Rubanova, J. Bettencourt, D. Duvenaud, Neural ordinary differential equations, (2018).

[174] S. Kim, W. Ji, S. Deng, Y. Ma, C. Rackauckas, Stiff neural ordinary differential equations, Chaos, 31 (2021) 093122.

[175] O. Owoyele, P. Pal, ChemNODE: A neural ordinary differential equations framework for efficient chemical kinetic solvers, Energy and AI, 7 (2022) 100118.

6. Publications

Journal of CO2 Utilization 61 (2022) 102034

Contents lists available at ScienceDirect

Journal of CO2 Utilization

journal homepage: www.elsevier.com/locate/jcou

Data analysis of CO_2 hydrogenation catalysts for hydrocarbon production

Aleksandr Fedorov *, David Linke *

Leibniz-Institut für Katalyse e.V., Albert-Einstein-Str. 29a, 18059 Rostock, Germany

ARTICLE INFO

Keywords:
CO_2 hydrogenation catalysts
Data analysis
Machine learning
Anderson-Schulz-Flory distribution

ABSTRACT

Literature data of CO_2 hydrogenation catalysts for hydrocarbon production via Fischer-Tropsch synthesis (FTS) were extracted from literature, collected into a SQLite database, and analyzed using data science and machine learning techniques. A challenge was to include performance data obtained by different groups which vary in the applied reaction conditions but vary also in the set of performance indicators that are reported. The thermodynamic ratio was used for analyzing reverse water gas shift reaction as the first stage of CO_2 hydrogenation. A tailored Anderson-Schulz-Flory distribution modified by two additional parameters was suggested based on the data and applied for describing hydrocarbon production. The data analysis indicated the existence of direct CO_2 conversion to hydrocarbons via the FT mechanism for some catalysts. It was shown that the chain growth probability as the key parameter of catalyst selectivity slightly depends on reaction condition (temperature, pressure, H_2:CO_2 ratio) and is mainly defined by catalyst composition, method of catalyst preparation, nature of active sites and pretreatment conditions. With respect to the catalyst composition, it was found that doping catalysts by alkali metals like K or Na is the most effective measure to improve catalyst performance leading to increased chain growth probability, increased olefins content and a decrease of undesired CH_4 formation.

1. . Introduction

The generation of carbon dioxide by combustion gas, liquid, and solid fuels is one of the main reasons for global warming resulting from the greenhouse effect. For reducing and controlling CO_2 emissions in the atmosphere, several strategies are considered [1]. The ones of perspective are clean energy technologies where obtained carbon dioxide is captured and used for valuable compounds production [2,3] by hydrogenation with H_2. Such methods of CO_2 conversion include methanation reaction, alcohol production [4,5], CO_2 Fischer Tropsch synthesis (FTS) [5,6]. The latter approach allows one to obtain hydrocarbons in the form of lower olefins [7,8] or fuels [9,10]. There are interesting two-steps methods to produce high value-added hydrocarbons where obtained hydrocarbons in the CO_2-FTS are converted to olefins, aromatics, or iso-paraffins on zeolite catalysts [11–13].

According to the literature [14,15], the CO_2-FTS proceeds in the two stages:

$$CO_2 + H_2 \rightleftarrows CO + H_2O$$

$$CO + 2H_2 \rightleftarrows -(CH_2)- + H_2O$$

The first stage is the endothermic reverse water gas shift reaction (RWGS) (Equation 1) followed by exothermic hydrogenation CO to hydrocarbons (Equation 2) via FTS in the second stage. The RWGS has a thermodynamic constraint limiting CO_2 conversion to a range of 20–50% for the range of conditions considered for CO_2 FTS [16,17].

The second stage has a kinetic limitation wherein a proportion of hydrocarbons can be described by the well-known Anderson-Schulz-Flory distribution (ASF)* [18–20]:

$$W_n = n(1-\alpha)^2\alpha^{n-1},$$

where n – carbon number, W_n – mass fraction of hydrocarbon with n carbon atoms, α – chain growth probability. The physical meaning of the α parameter is a ratio of prolongation rate to the sum of rates of prolongation and termination [21,22] because FTS is a typical polymerization process [23]. In effect, the chain growth probability α defines hydrocarbons distribution.

It is worth mentioning about the ASF distribution in the logarithmic form:

$$W_n = n(\ln\alpha)^2\alpha^{n-1},$$

that is an approximation to Equation 3 at $\alpha \geq 0.5$. Determination of chain growth probability using both equations from an experimental

* Corresponding author.
E-mail addresses: aleksandr.fedorov@catalysis.de (A. Fedorov), david.linke@catalysis.de (D. Linke).

https://doi.org/10.1016/j.jcou.2022.102034

Available online 17 May 2022

data give approximately the same results.

Iron is the most popular active component in CO_2-FT catalysts because it can catalyze both reactions 1 and 2. Bulk or supported Fe-based catalysts without dopants produce a lot of methane in the process of CO_2-FTS [24]. Because CH_4 is one of the undesirable products, there are many publications about using different dopants for reducing the methane production. Primarily, it is noteworthy that alkali metals [25–27] allow one to significantly improve the catalyst performance by enhancing adsorption of CO_2 on the surface of the catalysts [27]. Other popular dopants are transitional metals like Mn [28], Co [8], Cu [29], Ru [30,31], Zn [32] that increase the performance and stability of CO_2-FT catalysts. Some authors report a synergic effect between transitional and alkali metals [33]. The catalyst preparation method also strongly influences catalyst performance [34].

The CO_2 hydrogenation catalysts must satisfy requirements of high catalytic productivity and stability under reaction condition. A high productivity implies high activity for carbon dioxide conversion, high C_{2+} hydrocarbons selectivity, high olefins-paraffins ratio, and low values of CO and CH_4 selectivity. The stability requires sustaining the catalytic activity under reaction condition as well as mechanical stability. The latter is of special importance when applying a 3-phase slurry reactor where the catalyst attrition rate has to be kept low [29,35,36]. The main parameters of the CO_2-FTS are temperature, pressure, H_2/CO_2 ratio, space velocity, and catalyst reduction pretreatment.

It is a difficult task to compare CO_2-FT catalysts with respect to their performance data that were obtained in different ways and at different reaction condition. Moreover, the multiplicity of catalytic features (CO_2 conversion, selectivity etc.) do not facilitate this task. Ideally, the comparison of catalyst activity should be made at the same reaction condition (temperature, partial pressure of reagents etc.). However, recalculation and normalization of the catalytic data measured at the different condition requires knowledge about the reaction kinetics and activation energy that are usually unknown. Therefore, improved approaches to normalization are valuable. They assist the researcher in understanding dependencies and relationships between catalyst characteristics and activity. Such analysis benefits from applying data science and machine learning methods. These methods can help in analyzing, systematizing a large amount of the data, and predicting new materials under requirement constraints [37]. Besides, machine learning techniques can reveal latent knowledge from the scientific data consisting inside [38].

In the case catalytic data, Smith et al. [39] used neural network for analyzing catalysts for water-gas shift reaction and influence reactions condition and catalyst composition on catalytic activity. Keisuke Suzuki et al. [40] analyzed the catalytic data from the literature on oxidative coupling of methane (OCM), water gas shift, and CO oxidation reactions and created gradient boosting regression models with XGBoost for prediction of catalytic performance. Based on the made analysis, the top 20 promising catalyst candidates for the OCM reaction were suggested for the future investigation. It is worth mention earlier works [41,42] about the analysis of OCM catalyst database that are directed at analysis the literature data. In the case of CO_2 hydrogenation catalyst, Qingxin Yang et al. [43] used regression trees and ANOVA for statistical analysis of the literature data of CO_2 hydrogenation catalysts. It was confirmed that doping iron catalyst by alkaline and transition metals increases C_{2+} selectivity and olefins/paraffins ratio that is completely consistent with the previous results [8,26,44,45]. Authors of that work limited their analysis to some key features like a rate of CO_2 hydrogenation, a rate of C_{2+} production, C_{2+} selectivity, and olefins/paraffins ration but did not consider hydrocarbon distribution and chain growth probability α. The last one is known to be a key parameter of CO_2-FTS.

Thus, the main aim of this investigation is a detailed analysis of the literature data of CO_2 hydrogenation catalysts. For this aim, the data with all information about catalysts such as composition, preparation method, reduction pretreatment condition etc., and the information about catalytic data (reaction condition, conversion and selectivity of products, hydrocarbon distribution etc.) was extracted from scientific articles and converted into an SQL database. The obtained database was used for analyzing and extracting new knowledge about CO_2-FTS catalysts using data science methods. Particular attention was paid to describing CO_2-FT catalytic data with a minimum number of parameters, which helps to minimize correlation between catalytic performance measures and thereby improves the significance of the analysis.

2. Software and hardware specifications

The SQLite database was used for collecting the data [46,47]. Python programming language (version 3.8) was used for calculations [48]. SQLAlchemy was used to interface the database from Python [49]. Scientific libraries SciPy [50], NumPy [51], Pandas [52], Scikit-learn [53] were used for the data evaluation; Plotly [54] was used to visualize the results.

3. Developing a CO_2-FTS-tailored data analysis

3.1. Analysis of RWGS reaction for CO_2-FTS

In this part the methodology of CO_2-FT catalyst analysis is described. Based on the two-stages mechanism of CO_2-FTS, Reactions 1 and 2 were considered separately. In this case of chemical reaction with thermodynamic limitation, the thermodynamic value (equilibrium factor, ratio) η is usually used for analyzing the closeness to equilibrium [33,55,56]. Thermodynamic ratio η of the RWGS reaction can be calculated by the following equation:

$$\eta = \frac{P_{CO}P_{H_2O}}{P_{CO_2}P_{H_2}K},$$

where $_{Pi}$ – partial pressure of i-compound in the flow from the reactor, K – equilibrium constant, that can be calculated by the following equation [57]:

$$K = \exp\left(-\frac{4577.8}{T} + 4.33\right),$$

where T – temperature in Kelvin scale. The partial pressures of CO_2, H_2, CO, and H_2O were estimated by using simple calculation described in the Supporting information. The RWGS reaction is at equilibrium for a thermodynamic ratio of $\eta = 1$. In the case of $\eta < 1$ the reaction rate is directed towards the formation of CO and H_2O (forward reaction).

3.2. Analysis of hydrocarbon distribution

The second stage of CO_2-FTS (Reaction 2) has a kinetic limitation. In theory, hydrocarbon selectivity may be described by only one parameter α of the ASF distribution. It means direct correlations exist between proportions for one hydrocarbon (C_1, C_2 etc.) or any range (e.g., C_{2-4}, C_{5-15}). Fig. 1 shows the dependence between theoretical mass fraction of hydrocarbons in different fraction and chain growth probability α. The calculated values of CH_4 and the fraction of typical products for the different change growth probabilities of Fig. 1 are compared in Table 1.

One can see that there are restrictions of target fraction because of the kinetic limitation imposed by the assumed polymerization mechanism. Moreover, CH_4 proportion strongly depends on chain growth probability. For example, maximum production of C_2-C_4 fraction at $\alpha = 0.47$ corresponds to 28.1% mass fraction of methane. In fact, the desire to decrease CH_4 selectivity leads to hydrocarbon production with higher values carbon number. The chain growth probability α also defines the maximum selectivity of CO_2-FTS and thus is the key parameter of the CO_2 hydrogenation catalyst.

The obtained database contains around 500 experimental data points with catalytic information about CO_2-FT catalysts. All of them have the information about reaction conditions (temperature, pressure, H_2/CO_2

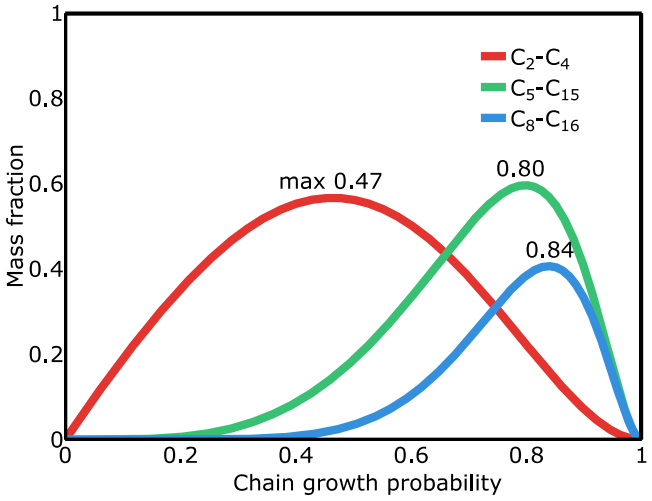

Fig. 1. The dependencies between the chain growth probability and theoretical mass fraction of hydrocarbons in different range (C_2-C_4, C_5-C_{15}, C_8-C_{16}) among all hydrocarbons formed by FTS calculated by Equation 3.

Table 1
Mass fraction of products at different hydrocarbons range for fixed the chain growth probability.

Range	CH_4, %	target fraction, %	other products, %	α[a]
C_2-C_4	28.1	56.7	15.2	0.47
C_5-C_{15}	4.0	59.7	36.3	0.80
C_8-C_{16}	2.6	40.7	56.7	0.84

[a] chain growth probability

ratio, catalyst composition etc.). Concerning catalytic data there are different ways presenting this information in the articles. In general, researchers report only selected data e.g., only C_1, C_{2-4} and C_{5+} selectivity and CO_2 conversion, CO selectivity, and olefins/paraffins ratio. Some works (around 23%) have the information about the chain growth probability. What is reported varies between papers, which creates some difficulties in directly comparing the catalysts. But as will be seen below, even this information is enough to extract some interesting catalytic features of CO_2-FT catalysts. Fig. 2 shows the circle diagram of the information that was reported to describe the hydrocarbon distribution in the analyzed papers. It is also worth mentioning alcohol formation for CO_2-FTS which were reported in ~ 22% articles of the database (for example in [7]). However, most articles do not contain any information about alcohols or other oxygenates.

For comparing the hydrocarbon distributions from different experiments, the data was converted to one line with fixed parameters using linear transformation. Detailed description of this approach can be found in Supporting information. Fig. 3 shows mean hydrocarbon distribution of the CO_2-FT catalysts plotted in ASF coordinates. The 99.7% confidence interval also is presented on Fig. 3. One can clearly see that C_{3+} hydrocarbons correspond to the ASF distribution but CH_4 and C_2 do not. Thus, using only the ASF distribution does not allow one to describe the experimentally observed hydrocarbon distribution of CO_2-FT catalysts accurately. It is necessary to consider deviations at least of C_1 and C_2. Empirically, the hydrocarbon selectivity can be described by the following equations:

$$S_1 = (1 - S_{CO})\left(\gamma + \frac{(1-\gamma)W_1(\alpha)}{1-(1-\delta)W_{2(\alpha)}}\right)$$

$$S_2 = (1 - S_{CO})\left(\frac{(1-\gamma)(1-\delta)W_2(\alpha)}{1-(1-\delta)W_2(\alpha)}\right)$$

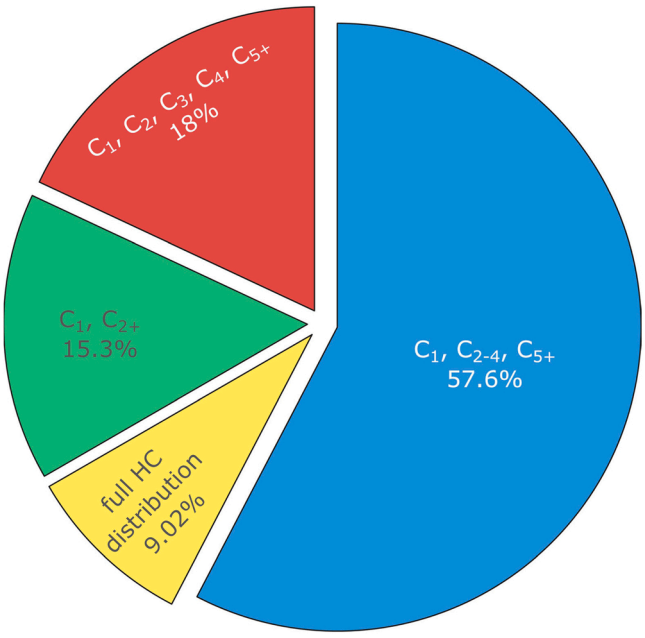

Fig. 2. The circle diagram of the information reported to describe the hydrocarbon distribution in the analyzed papers.

$$S_n = (1 - S_{CO})\left(\frac{(1-\gamma)W_n(\alpha)}{1-(1-\delta)W_2(\alpha)}\right), \text{ at } n = 3, 4 \ldots \infty,$$

where S_i – C_i selectivity, S_{CO} – CO selectivity, n – carbon number, α – chain growth probability. The δ parameter represents a fraction of C_2 responding for a decrease of the ethylene selectivity compared with the value calculated by the ASF distribution. The empirical parameter γ responds an excess of CH_4 selectivity.

One can see that only 9% of the experiments are reported with the full information about hydrocarbon distribution (up to C_{12}). In this part of article, only this data subset was discussed and analyzed.

According to equations 4–6 hydrocarbon selectivity depends on only 4 parameters: $S_{CO}, \alpha, \gamma, \delta$ wherein CO selectivity is usually known. It is worth noting that all the parameters are in a range from 0 to 1. The other parameters of the equations can be calculated by minimization of the following cost function:

$$\sum \left(S_i^{exp} - S_i^{pred}\right)^2$$

The Broyden-Fletcher-Goldfarb-Shanno (BFGS) algorithm [58] was used for minimization of the cost function. The chain growth probability can be also calculated from the slope of a curve describing hydrocarbon distribution for C_{3+} in corresponding ASF coordinates if the information about selectivity distribution exists. The parameter α calculated in this way allows one to calculate the other parameters γ and δ. The advantage of the approach via optimization is that it opens the opportunity to calculate the parameters even when data are given in various ways (S_1, S_2 …, or ranges S_{2-4}, S_{2-6} …). Both approaches give similar results (see Fig. S4). It is worth noting that the majority information about hydrocarbons is given in the form C_1, C_{2-4} and C_{5+} selectivity (see Fig. 2). It is impossible to calculate the three parameters of equations 4–6 by using these data with only two degrees of freedom. However, it was found that a decrease of C_2 selectivity is around 10% (the δ parameter) for most catalysts. By setting δ to 0.1 for those data, α and γ parameters can be calculated from the data having only a two degree of freedom. This approach was checked by the data with the information about hydrocarbons distribution for which these parameters can be calculated directly (see the Supporting information). Thus, using this approximation allowed us to estimate the parameters α and γ even for the data

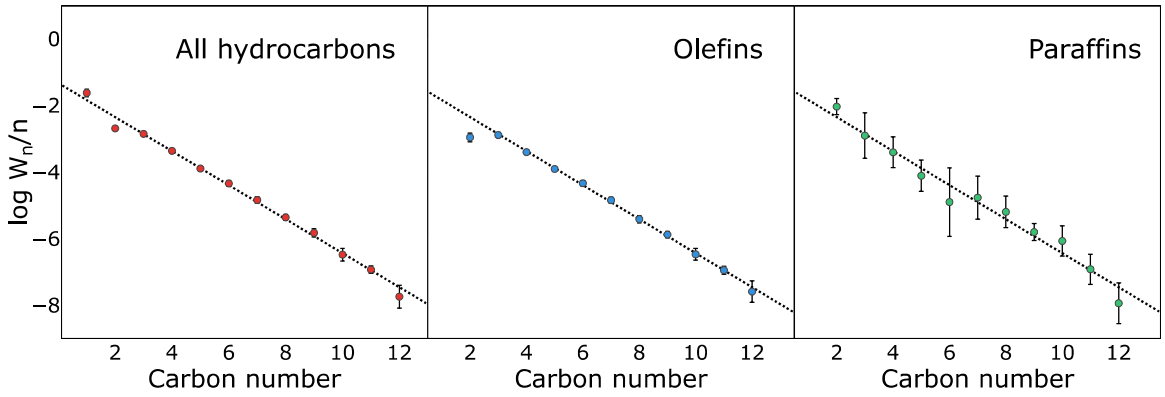

Fig. 3. Hydrocarbon distributions of the CO_2-FT catalysts plotted in ASF coordinates for all hydrocarbons (left), olefins (middle), and paraffins (right).

presented in the form of C_1, C_{2-4} and C_{5+} selectivity or similar representation.

3.3. Descriptor selection analysis

The descriptor selection (feature selection) is the most important stage for building reliable machine learning models. There are different approaches for finding and determining important descriptors, for example Pearson's R correlation coefficient, lasso regression, random forest, gradient boosting etc. [59,60]. For understanding the influence of reaction and catalyst parameters on performance and catalytic activity (CO_2 conversion; CO selectivity, the chain growth probability etc.) the random forest regression was used in this work. The first stage is to present the catalytic data as vectors using the set of descriptors. The following descriptors were considered:

- Temperature reaction, pressure reaction, H_2:CO_2 ratio, GHSV, reduction temperature
- Bulk or supported catalyst, presence of alkali or transition metals (has K or has Me)
- Type of support (Al_2O_3, SiO_2 etc.)
- Cu content, Mn content etc.
- Alkali metals content

Bulk or supported catalyst, presence of alkali or transitional metals, and similar categorial descriptors were presented as 0 and 1. Type of supported was encoded by one-hot (one-of-K) encoding [53]. Other descriptors were presented as real number (temperature, Mn content etc.). The performance of models obtained by 10-fold cross validation is shown in the Supplementary information (see Fig. S20-S21).

For analyzing the deviation of the descriptor contributions two approaches were used. The values of targets parameters were changed by adding random noise in a range ± 5% with subsequent using 10-fold cross validation. The obtained arrays of descriptor contributions were used for calculation of the mean values and the deviations. 5% and 95% quantities were used for determination of a low and high values of deviations. For calculating the correlation of descriptors with target data (positive or negative) a linear regression with L_2-regularization (parameter of regularization was set 10^{-3}) was chosen as the first approximation.

4. Analysis and discussion

4.1. The approach to equilibrium of RWGS reaction

Fig. 4 shows the distribution histogram of the thermodynamic ratio η for all experimental data. One can see that there is data (its portion is around 18%) with a thermodynamic ratio η value of more than 1 and that this is more common for catalysts doped by alkaline metals. It is

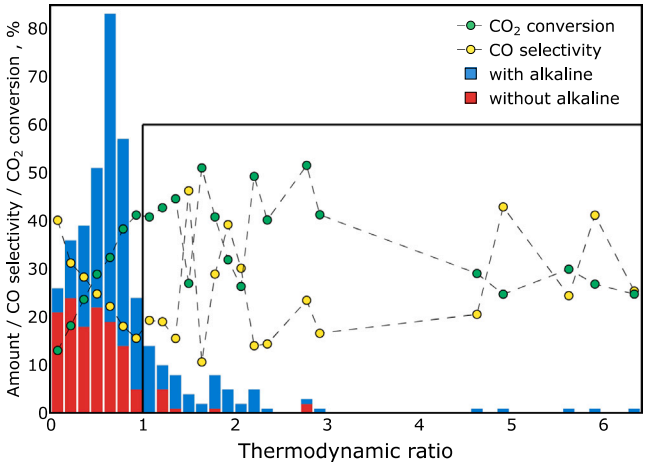

Fig. 4. Histogram of the distribution of alkaline containing/free catalysts and mean values of CO selectivity and CO_2 conversion as a function of the thermodynamic ratio η.

worth noting that the portion of the alkaline-doped catalysts in all catalysts is around 63% whereas it is around 88% in the case of $\eta > 1$. The Fisher's exact test [61] was used for validating the influence catalyst doping by alkali metal on thermodynamic ratio. A significance level was selected equal to 0.01. The two samples of experimental data with $\eta \leq 1$ and $\eta > 1$ were created. Elements of each one were equal to 1 or 0 (1 if a catalyst consists of alkali metals). The calculated p-value was $2.4 \cdot 10^{-5}$ (< 0.01) that allows one to reject a null hypothesis that both distributions are equal. It can be concluded that an increased value of thermodynamic ratio is characteristic of the catalysts doped by alkali metals that was proven by statistics. Possible reasons for $\eta > 1$ are discussed below.

The presented data allow to conclude that the equilibrium of the RWGS reaction for CO_2-FTS on Fe-based catalysts is not established in general. Fig. 4 also shows the mean value CO selectivity $\overline{S}_{CO}$ and CO_2 conversion $\overline{X}_{CO_2}$ for each group (bars of the histogram). One can see that there are correlations between the thermodynamic ratio η and $\overline{S}_{CO}$, $\overline{X}_{CO_2}$ in the case of $\eta \leq 1$. A decrease of CO selectivity accompanied by an increase CO_2 conversion is known to be a consequence of two stages mechanism of CO_2-FTS. It was found and proven by the analysis of the dependence of products selectivity on CO_2 conversion [10, 34, 62–64]. An increase of thermodynamic ratio is accompanied by an increase of $\overline{X}_{CO_2}$ and a decrease of $\overline{S}_{CO}$. A high CO_2 conversion corresponds to a high RWGS reaction rate and, thus, the thermodynamic equilibrium of the RWGS reaction may be achieved.

The cases of $\eta > 1.0$ may results from other reactions leading to

either reduced reagents pressure (CO_2, H_2) or to increased production pressure (CO, H_2O). Such a reaction could be coke formation and subsequent reaction carbon dioxide:

$$C + CO_2 \rightleftarrows 2CO,$$

that has a thermodynamic limitation. The equilibrium constant is around 10^{-8} at 250 °C [65]. The calculated pressure of CO at this temperature and a pressure of CO_2 of 15 bar is only $3.98 \cdot 10^{-4}$ bar which is orders of magnitude below the experimental observation. It is well-known that the Boudouard Reaction usually plays a significant role only at higher temperature (T > 900 °C) [66]. The calculated values for the thermodynamic ratio would be lower if alcohols are formed. However, at typical alcohol selectivity (5% MeOH) the thermodynamic ratio would hardly change. For example, in the case of using $ZnFeO_x$-5.76Na catalyst for CO_2-FTS [67] oxygenates selectivity was 4.9%. Assuming that the main product of oxygenates are alcohols, thermodynamic ratio was calculated and was 0.48. If alcohol selectivity was ignored the estimated value would be 0.52. In the case K-Fe/ZrO_2 catalyst [7], the values of ratio are 0.99 and 1.33. Methanol selectivity was 20% in last case.

The reason of an increase of η may be methanation reaction (direct CO_2 hydrogenation to CH_4). Only the catalysts with $\eta > 1.5$ were considered for further analysis to avoid an influence of systematic errors in the experimental data (measurement the reaction temperature, determination of product concentrations etc.) and in the estimation of thermodynamic ratio (see Table S1). Firstly, it is worth pointing out the Co-containing catalysts investigated in works [68,69]. In this work [69], the calculated values of η are in a range from 1.53 to 5.83 wherein excess of CH_4 selectivity γ are in (0.06, 0.90). In the work [68], the thermodynamic ratio is around 1.85 with γ value is 0.95 for the Co-based catalyst. The Co-based catalysts are known to be hardly active in RWGS reaction and but to have high hydrogenation ability. This may explain the high values of η an increase of which may be also relate to methanation reaction. The high hydrogenation ability is confirmed by the data about the fraction of olefins in C_2-C_4 hydrocarbons that are practically absent for these Co-containing catalysts. Secondly, a rise of the thermodynamic ratio (in a range of 1.72–2.98) is also found for Fe-based catalyst supported on carbon nanotubes [70,71] doped with or without alkaline metals. Wherein the values of γ are low (not more than 0.17) and even equal to zero in some cases. A similar behavior is also found for several bulk and supported Fe-based catalysts doped by alkaline metals [11,17,31,55]. The data with high values of η and low ones of γ cannot be explained by the methanation reaction. However, a direct hydrogenation of CO_2 to hydrocarbons may explain this phenomenon as was discussed in [14]. So, Zhenhong He et al. [72] demonstrated for Co/MnO_x catalysts this direct CO_2 hydrogenation to hydrocarbons without CO production. They suggested that the reduction of adsorbed CO_2 by hydrogen to CH_2 and CH_3 monomers proceeds via formation of $CO_2^{\delta-}$, $HCOO^-$, $-CH_2OH$, and/or CH_3O^- intermediates.

Fig. 5 presents different pathways for CO_2 hydrogenation. The pathways 1–2 are the two-stage CO_2-FT process via RWGS reaction and subsequent hydrogenation of CO to hydrocarbons. They cannot describe the increase of the thermodynamic ratio for those cases where the influence of the methanation reaction is weak. The Reaction 3 (see Fig. 5) is a direct hydrogenation of CO_2 to hydrocarbons that can lead to $\eta > 1$. Thus, the analysis of the literature data of CO_2-FT catalysts indicates the presence of a direct path of CO_2 hydrogenation to hydrocarbons.

4.2. Analysis of CO-FT reaction

The hydrocarbons selectivity of Fe-based catalysts for CO_2 hydrogenation was shown to correspond to the ASF distribution except for a decrease of ethylene selectivity and an increase of CH_4 one (see Fig. 3). This result suggests that for the calculation chain growth probability only C_{3+} hydrocarbons should be used. In practice, the various hydrocarbons ranges were used for calculating chain growth probability. So, for examples, in work [73] C_1-C_5 were used, C_1-C_7 [74], C_2-C_7 [75], C_3-C_{10} [76]. There are also some works without description of the calculation methods like here [44,77].

It is worth mentioning that some papers report deviations from ASF distribution, like for Fe-Mn-K catalyst in this work [9] or for Co/MnO_x in this one [72]. Thus, one should carefully check the applicability of the ASF distribution for describing hydrocarbon selectivity. In the case of our data, this ASF approximation is reasonable for most CO_2-FT catalysts as proven by the analysis shown in Fig. 3 and Fig. S3.

There are some reasons for the increased methane selectivity in comparison to the theoretical ASF distribution (see Fig. 3). The first one is hydrogenolysis of olefins [31,34]. The other reason may be direct hydrogenation of CO_2 (or CO) to CH_4 not via FT that were discussed in several works [14,34,62,64]. Fig. 3 also presents olefin and paraffin distribution in corresponding coordinates. It shows a decrease in ethylene selectivity compared with the value calculated by the ASF distribution that does exist in the case of paraffin distribution. It is worth noting the larger confidence intervals for the paraffins compared to olefins. It may relate to a higher error of quantifying long paraffins in presence of the corresponding olefins which when mainly olefins are formed (an excess of olefins is common for the data published with the full hydrocarbon distribution information). Also, for C_{12+} paraffins it becomes experimentally challenging to prevent partial condensation which could affect the accuracy of online analysis data. Concerning ethylene selectivity, a decrease may be explained by the high reactivity of C_2H_4 compared to higher α-olefins [55,78].

The hydrocarbon selectivity of CO_2-FT catalysts can be described by the suggested empirical equations 4–6 that depend on 4 parameters S_{CO}, α, γ, and δ. CO selectivity is usually known. The α parameter is the chain growth probability that defines the selectivity of CO_2-FT catalysts. The γ parameter describes the excess of CH_4 selectivity. The parameter δ defines a decrease of the ethylene selectivity. It was set to 0.1 to estimate α and γ values for cases where data were presented with only two degrees of freedom. It is worth mentioning, another important characteristic of the CO_2-FT catalysts that is olefin-paraffin ratio (or the portion of olefins in hydrocarbons) which was also included in the analysis. The rate of CO_2 conversion was used as a measure of catalyst activity. It was calculated by the following Equation:

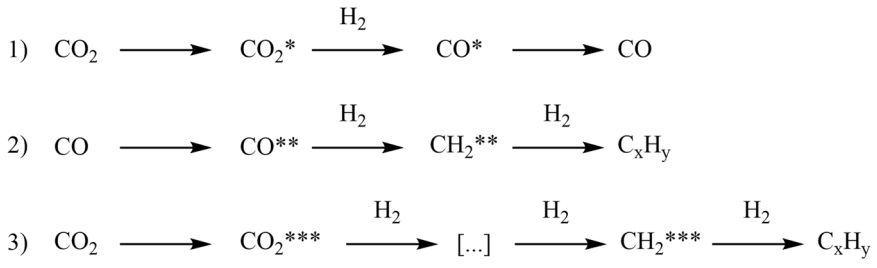

Fig. 5. Different pathways for CO_2/CO hydrogenation. * - surface intermediates.

$$r = \frac{f \bullet X_{CO_2}}{m_{cat}},$$

where m_{cat} – mass of catalyst; f – molar flow rate of CO_2 at reactor inlet; X_{CO_2} – CO_2 conversion.

For analyzing the alcohol production, alcohol content $w_{alc.}$ was calculated by the following equation:

$$w_{alc.} = \frac{\dot{n}_{alc.}}{\dot{n}_{alc.} + \dot{n}_{HC}} \bullet 100\%,$$

where $\dot{n}_{alc.}$ – molar flow of alcohol in the flow from reactor; $\dot{n}_{HC}$ – molar flow of hydrocarbons in the flow from reactor. We assumed that the main product of alcohols and oxygenates is methanol.

In the next sections of this work, the influence of reaction condition, catalyst composition, catalyst preparation and activation on the suggested parameters of CO_2-FT catalysts is analyzed.

4.2.1. *Influence of reaction condition*

The influence of reaction condition such as temperature, pressure, H_2:CO_2 ratio, and GHSV on catalyst performance has frequently been investigated in the literature [27,28,45,55,68,71,79–81]. Using this literature data, the suggested parameters for CO_2-FT catalysts such as α, γ, olefin content of CO_2-FT catalysts were calculated. The values of these parameters are shown in Fig. 6 as a function of the reaction conditions.

From Fig. 6 one can see that reaction parameters have a weak influence on the chain growth probability. It practically does not depend on GHSV and H_2:CO_2 ratio. There is a little decrease of α at pressures below 10 bar. It is worth noting various dependences between α and reaction temperature for different catalysts. Despite this, the values of α at different temperature are in a narrow range for each catalyst. For example, values of α are in a range 0.75–0.85 at temperatures between 260 and 340 °C for bulk K-Fe catalyst [80]. In the work of Shunwu Wang et al. [71], α are in a range 0.66–0.73 at 270–380 °C. In the case of olefins content, GHSV and temperature slightly influence it. One can see a decrease of the olefin content with rising pressure and H_2:CO_2 ratio. It relates to an increase hydrogen pressure resulting to acceleration of hydrogenation reactions. The excess of CH_4 selectivity γ also weakly depends on reaction condition. One may point at certain tendency that γ rises at high temperature which is observed for most catalysts.

The influence of reaction conditions on other catalyst parameters such as CO_2 conversion X_{CO_2}, CO selectivity, CH_4 selectivity, C_{2+} selectivity, and thermodynamic ratio is shown in the Supporting information (Fig. S6-S9). In the case of X_{CO_2}, there is a significant increase with rising temperature, pressure and H_2:CO_2 ratio and a decrease with space velocity that relates to a change of reaction rate. CO selectivity strongly decreases with rising pressure and H_2:CO_2 ratio resulting in an increase of C_{2+} selectivity. In the case of temperature influence on CO and C_{2+} selectivity, non-linear dependencies with an extremum are found for most catalysts.

In summary, the differences in terms of hydrocarbon distribution between catalysts are larger than the changes induced by varying the reaction conditions such as temperature, pressure, H_2:CO_2 ratio, and GHSV. Therefore, one can conclude that parameters such as catalyst composition, method of catalyst preparation, nature of active sites, and pretreatment conditions define α mainly.

The presented data also demonstrates an advantage of using the suggested parameters for describing CO_2-FT catalysts. For example, Fig. S6 shows the dependencies of the catalysts main parameters at different temperature for K-Fe catalysts from article [80] (green dots) and for Mn-Fe catalyst from [81] (purple dots). One can see that CH_4 selectivity is higher for the Mn-containing catalyst. For the latter the high CH4 selectivity is due to the lower chain growth probability. However, the higher value of excess of methane selectivity γ for K-containing catalyst clearly shows that an undesired (non-ASF) route for methane formation is a bigger problem for this catalyst than for the other (Mn-containing) one.

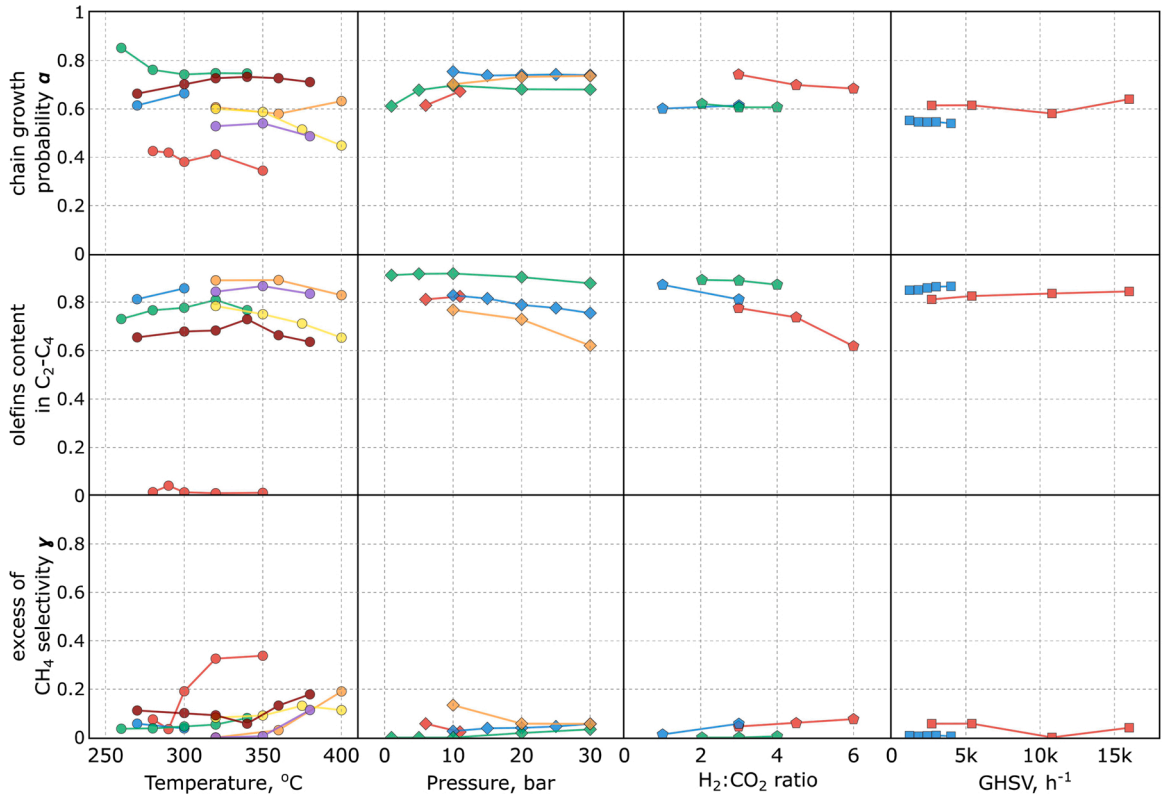

Fig. 6. The dependencies between the parameters of different CO_2-FT catalysts and reaction temperature, pressure, and H_2:CO_2 ratio [27,45,55,68,71,79–81]. The same color and shape mean one specific catalysts from one article.

Concerning the catalyst deactivation under CO_2-FT condition, there are only few works where it was investigated. Due to lack of data deactivation could not be analyzed in the same way as activity and selectivity. The reason of deactivation may be carbon deposit on catalyst surface which was reported for iron-based catalysts doped by alkali promoter (K, Rb, Cs) [82,83]. An oxidation-reduction treatment can regenerate the deactivated Fe-K/alumina catalyst [82]. Another reason of deactivation is phase transformation of FeC_x to FeO_x by oxidation with CO_2 and H_2O [32,84]. The dopants like Na and Zn were shown to be able to suppress the oxidation process [32]. It is also worth mentioning the growth of iron carbide crystallinity resulting in component separation as one of reason of catalyst deactivation that was found for Fe-Cu-K-Al catalyst in the work [85].

4.2.2. *Influence of catalyst composition*

This section addresses the influence of catalyst composition on the key parameters of CO_2-FT catalysts. Many different compositions of catalysts are reported in the literature. The dominating main component is Fe. In some works (for example this [69]) Co-based catalysts were investigated. The most popular dopants are alkali metals like K and Na. Fig. 7 shows distribution of elements in CO_2-FT catalysts from our database plotted on the periodic table. Mn, Co, and Cu are found to be the most employed dopants except for alkali metals. Wherein 70% of all the doped catalysts consist of these ones. Less popular are Zn, B, Mo, Zr, and La.

Fig. 8 shows values of the chain growth probability, olefins content, and an excess of CH_4 selectivity for catalysts with different alkali dopants and tested under the same reaction condition. One can see that K-doped catalysts are optimal due to providing highest values of α and ω, and a low value of γ. This is in line with prior work which reported potassium as the preferable alkali dopant [24]. Doping by alkali metals results in a rise of CO_2 conversion and a decrease of CO selectivity, and, therefore, in an increase of hydrocarbons production. More detailed results on the influence of K can be found in the Supporting information (Fig. S10). It is worth mentioning that doping by Li increased the chain growth probability and olefins content for some authors [24,86] although the opposite was reported in [7]. However, the positive effect of doping by Li is weaker than for other alkali metals.

The influence of K or Na content on the characteristic CO_2-FT parameters is presented in Fig. 9. One can see that adding alkali metals greatly increases the catalysts' selectivity to olefins and hydrocarbons with high carbon number. Simultaneously they reduce the loss of CO_2 via additional methane formation (see the decrease of excess of CH_4 selectivity γ in Figs. 8 and 9). Moreover, doping Fe-based catalysts by alkali metals increases CO_2 conversion (see Fig. S10–13), thus, improve catalysts performance. It is interesting that doping by K can increase catalyst performance even for CO_2-FT catalysts based on Fe-containing industrial waste that was demonstrated by Artem Russkikh et al. [25]. It emphasizes the general effectivity of using alkali dopants. It was also found that doping by alkaline metals increases the alcohol production of CO_2-FT catalysts. So, the mean value of alcohol content $w_{alc.}$ for alkaline doped catalysts calculated from the obtained database is around 18.5% and higher than the value for alkaline-free catalysts (4.3%). It can be clearly seen in the dependency between alcohol content and CO_2 conversion (see Fig. S20).

There are series of work where the effect of alkali dopants was investigated and analyzed. Numpilai Thanapha et al. [8] explained the effect of K by the enhanced bonding strength of adsorbed CO_2 and H_2 leading to a decrease of the hydrogenation activity of K-containing catalyst. This concept was proven by in situ XPS and DFT calculation in [87] and DFT calculation in [89]. Besides affecting adsorption, alkali metals promote formation and stability of Fe_5C_2. This was reported for alkali-modified catalysts where activity directly correlated with alkali content and amount of iron carbide [26,90]. It is noteworthy that Fe_5C_2 can be transformed to FeO_x with a loss of CO_2-FT activity under reaction condition [27] which further confirms the key role of alkali metals. But on the other hand, there are other works about active CO_2-FT catalysts that do not require doping by alkali metals [34,62]. Andrey Skrypnik et al. reported around 60 wt% of Fe_2C_5 for a catalyst obtained from iron (II) oxalate [62]. This indicates on an important role of preparation methods and catalyst pretreatment in the synthesis of highly-active and selective CO_2-FT catalysts.

Concerning other dopants, the most popular transitional metals like Mn, Co, and Cu were analyzed in more detail (see Fig. S14-S19). It was

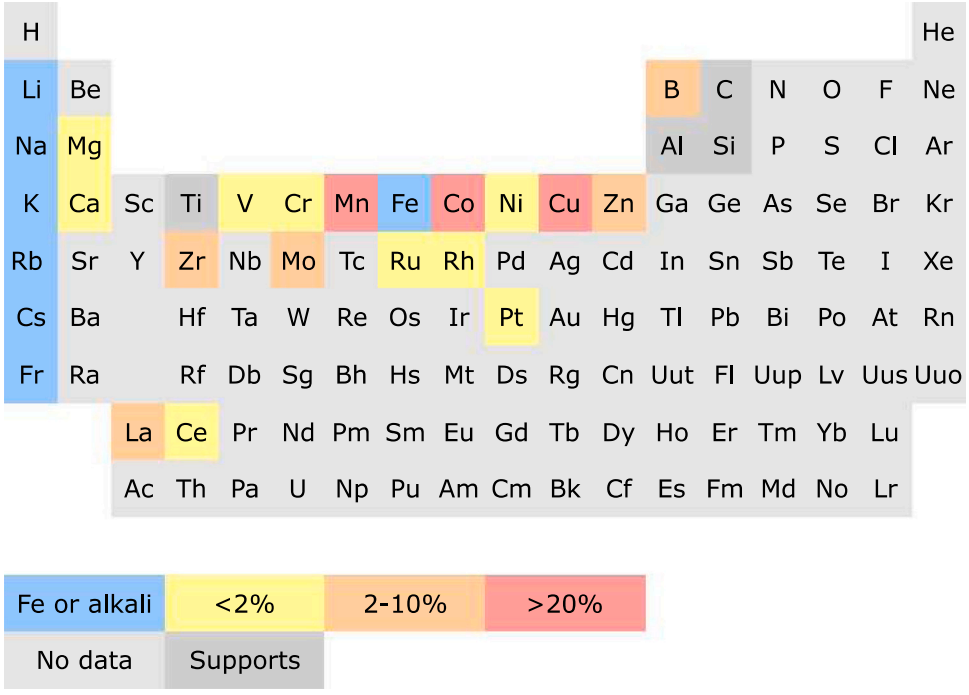

Fig. 7. Distribution of elements used for preparation of CO_2-FT catalysts plotted in the periodical table. % means a portion of catalysts with this element in the obtained database. The catalysts doped by alkali metals present separately and are labeled by blue color.

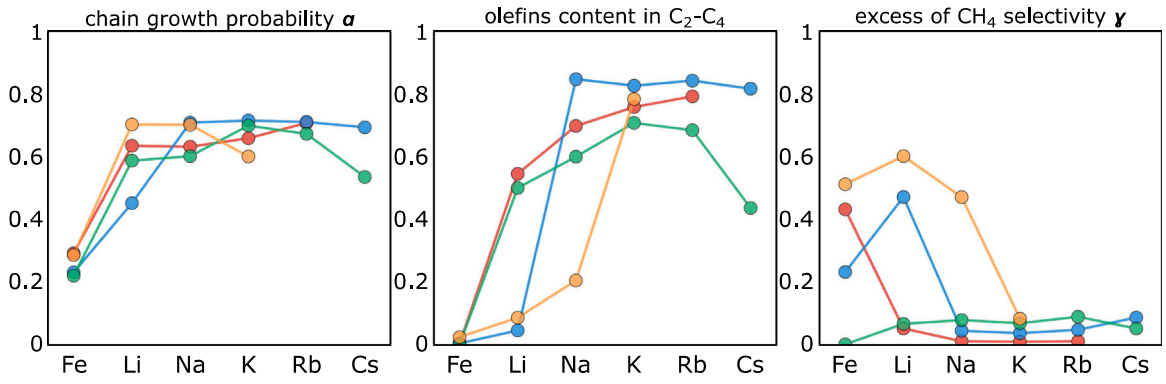

Fig. 8. Values of the chain growth probability, olefins content, and an excess of CH_4 selectivity for the catalysts with different alkali dopants [7,24,45,86]. Fe means a catalyst without alkali dopants. The same color means one specific catalysts from one article.

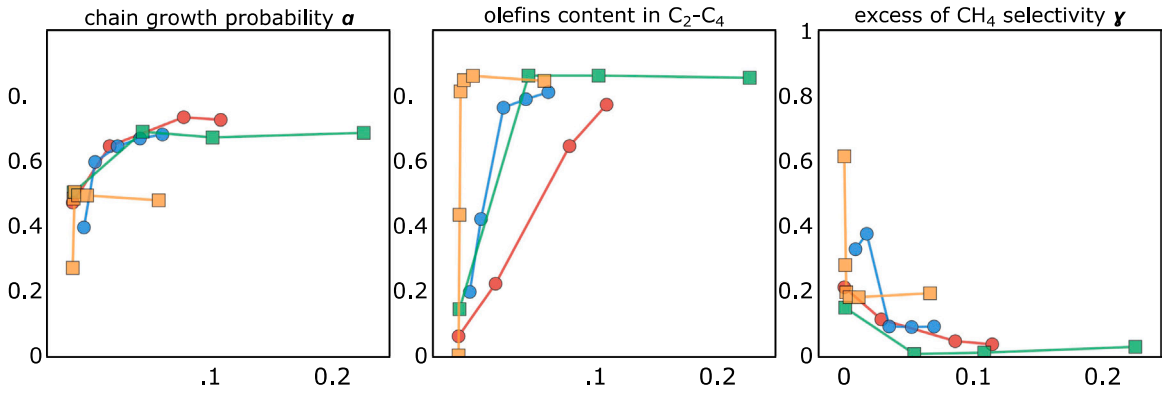

Fig. 9. Values of the chain growth probability, olefins content, and an "extra" increase of CH_4 selectivity for the catalysts with different molar ratio Me/Fe (where Me is K (circle) and Na (square)) [29,45,87,88]. The same color means one specific catalysts from one article.

shown that Mn can increase olefin content even without alkali dopants. In the cases of Cu and Co, a reduced olefins production was observed with and without alkali dopants. For Co-containing catalysts, the high value of the excess of methane parameter relates to their high hydrogenation ability. In conclusion, the most promising dopant for improving activity and selectivity CO_2-FT catalysts is K based on our data analysis is potassium. Due to its beneficial effects, it is in frequent use for CO_2-FT catalysts.

4.3. Descriptor importance analysis

For analyzing the influence of reaction condition, composition, and

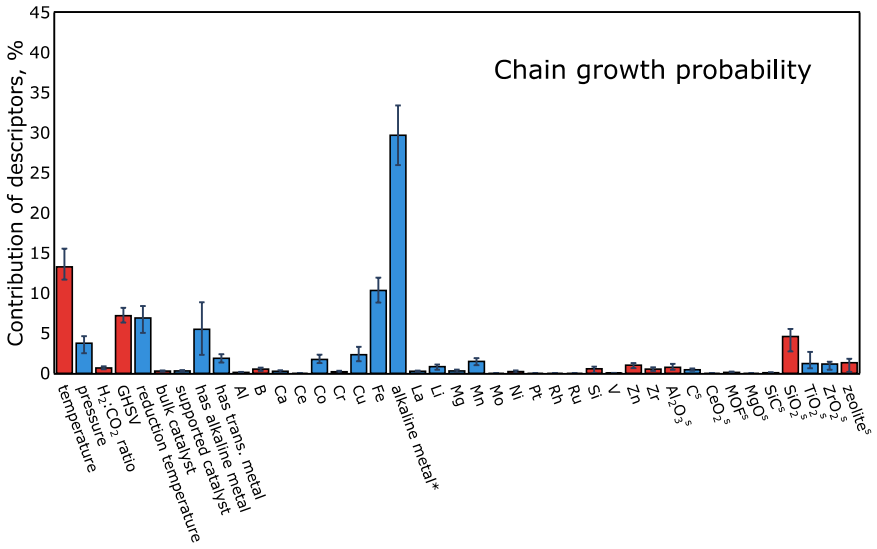

Fig. 10. The histogram of descriptors importance for chain growth probability calculated using random forest regression model. Blue bars are positive correlations, red bars – negative correlations. * except for Li, ^{s} type of supports.

other parameters of catalysts (type of support, reduction temperature etc.) in common, descriptor-importance (or feather-importance) analysis based on random forest regression model was used in this work. Fig. 10 presents the descriptor contributions of a random forest regression model for the prediction of the chain growth probability. The analogue analyses for the other catalytic parameters can be found in the Supporting information (Fig. S23-S25). The alkali content shows a significant positive correlation with the chain growth probability (Fig. 10). This means that an increase of potassium amount in the catalyst is accompanied by an increase of the α value. For reaction temperature, there is a negative correlation.

The descriptor-importance analysis indicates that the most important descriptor defining the chain growth probability is the alkaline metal content. The next-important descriptors are the reaction temperature and Fe content. The slight influence of the reaction temperature on α was discussed before. Alkali dopants also are the most dominant descriptor for olefin production (see Fig. S24, bottom). This key importance of presence and content of alkali metal for the selectivity of CO_2-FT catalyst proves the conclusions made before. In, the descriptor-importance analysis confirms that alkaline metal content is more important than other descriptors such as a type of support, doping by transitional metals, reduction temperature, supported or bulk catalysts etc.

In the case of reaction rate, supports based on carbon (active carbon, carbon nanotubes etc.) were found to be the most promising one for achieving high rates of CO_2 conversion (see Fig. S23, top). The next-important parameters are iron content, reaction temperature. Importance of carbon supports can be proved by calculating mean values of CO_2 conversion rate for different type of catalysts. So, the mean CO_2 conversion rate for the catalysts supported on carbon is around 1070 $ml \cdot h^{-1} \cdot g^{-1}$. In the case of bulk catalysts, the mean value is 500 $ml \cdot h^{-1} \cdot g^{-1}$. For catalysts supported on Al_2O_3 the one is – 370 $ml \cdot h^{-1} \cdot g^{-1}$. It allows one to conclude that carbon supports are promising ones for CO_2-FT catalysts.

It is worth mentioning that transition metals slightly influence on parameters of CO_2-FT catalysts except for Co metal (see Fig. S24 and S25). The last one relates to high hydrogenation activity and methane formation that try to be avoided and reduced in the CO_2-FT process. It explains a large contribution of Co content for prediction of CH_4 selectivity and excess CH_4 selectivity.

The model's performance for predicting the chain growth probability is presented in Fig. 11. The performance of other models can see in the Supplementary information (see Fig. S24 and S25). Fig. 11 shows that the generalization of the obtained random forest regression model is mediocre. Several reasons may be responsible for this. One of them is the experimental errors in the literature data because the catalytic data were obtained in various scientific groups using different laboratory equipment. Another reason is the likely existence of hidden parameters influencing the catalytic performance. Catalysis is defined by many factors including structure of active site, their number, the presence of additional sites for CO_2/H_2 adsorption, catalyst stability etc. These factors can be determined not only by parameters used here as descriptors (catalyst composition, reaction condition, support type etc.) but also by other catalyst preparation parameters, nature of supports, purity of reagents etc. Because the information about catalyst in literature is often incomplete, such parameters were not included into the models.

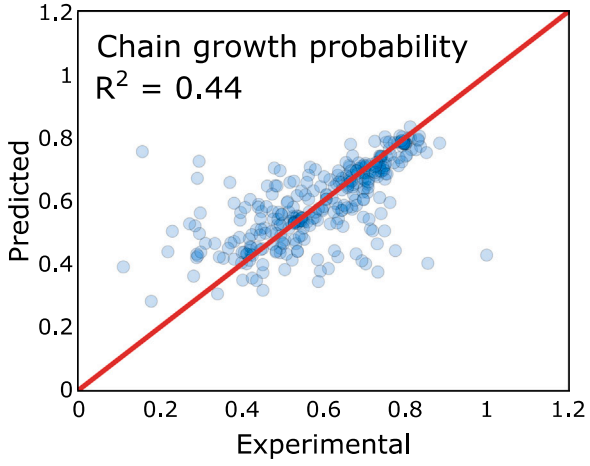

Fig. 11. Performance of random forest regression model for prediction of the chain growth probability. The dependence between experimental values of alpha and predicted values for test set on 10-fold cross validation.

5. Conclusions

The analysis of hydrocarbons distribution showed that their selectivity corresponds to the ASF distribution except for CH_4 and C_2H_4. Our proposed model based on ASF distribution modified by two additional parameters was demonstrated to describe hydrocarbons of CO_2-FT catalysts. The increase of methane selectivity reported for some catalysts may relate to direct hydrogenation CO_2 to CH_4 or splitting α-olefins. A decrease of ethylene selectivity may be connected with its high reactivity compared to other α-olefins. A lesson learned from this literature data analysis, is that the chain growth probability should be calculated from the hydrocarbon distribution C_{3+}; C_1 and C_2 should not be included but reported separately.

The analysis of RWGS reaction carrying out in the CO_2-FT process with different catalysts points to the existence of different pathways of CO_2 hydrogenation. The direct CO_2 converting to hydrocarbons via FT mechanism seems to play a role at least for some catalyst systems. Validation of this pathway by detailed kinetic modeling and further experiments would be of great interest. It was also found that the equilibrium of RWGS reaction is not established for most CO_2-FT catalysts. Therefore, the rates of RWGS and FTS are similar in magnitude.

The data analysis allowed us to conclude that reaction parameters such as temperature, pressure, H_2:CO_2 ratio slightly influence the chain growth probability, olefine content, and excess of CH_4 selectivity. These key performance parameters of CO_2-FT catalysts are predominantly defined by catalyst composition, method of catalyst preparation, nature of active sites and pretreatment conditions.

With respect to the catalyst composition, it was shown that doping catalysts by alkali metals like K or Na is the most effective measure to improve catalyst performance. It increases the chain growth probability as well as the olefins content and reduces the excess of CH_4 selectivity. Other factors that influence catalyst selectivity but to a smaller extend are type of support, doping by transitional metals, reduction temperature, and reaction conditions.

Funding

Financial support from Federal Ministry of Education and Research (BMBF) in project InnoSyn (FKZ: 03SF0616B) and Deutsche Forschungsgemeinschaft (DFG, German Research Foundation) in project NFDI4Cat (number 670389-NFDI 2/1) is gratefully acknowledged.

CRediT authorship contribution statement

Aleksandr Fedorov: Conceptualization, Methodology, Formal analysis, Investigation, Software, Data curation, Writing – original draft, Visualization. **David Linke**: Conceptualization, Supervision, Project administration, Writing – review & editing.

Declaration of Competing Interest

The authors declare that they have no known competing financial

interests or personal relationships that could have appeared to influence the work reported in this paper.

Appendix A. Supporting information

Supplementary data associated with this article can be found in the online version at doi:10.1016/j.jcou.2022.102034.

References

[1] M. Hermesmann, K. Grübel, L. Scherotzki, T.E. Müller, Promising pathways: The geographic and energetic potential of power-to-x technologies based on regeneratively obtained hydrogen, Renew. Sustain. Energy Rev. 138 (2021), 110644.

[2] D.Y.C. Leung, G. Caramanna, M.M. Maroto-Valer, An overview of current status of carbon dioxide capture and storage technologies, Renew. Sustain. Energy Rev. 39 (2014) 426–443.

[3] M.D. Garba, M. Usman, S. Khan, F. Shehzad, A. Galadima, M.F. Ehsan, A. S. Ghanem, M. Humayun, CO_2 towards fuels: a review of catalytic conversion of carbon dioxide to hydrocarbons, J. Environ. Chem. Eng. 9 (2) (2021), 104756.

[4] R. Guil-López, N. Mota, J. Llorente, E. Millán, B. Pawelec, J.L.G. Fierro, R. M. Navarro, Methanol synthesis from CO_2: a review of the latest developments in heterogeneous catalysis, Materials 12 (23) (2019) 3902.

[5] C. Panzone, R. Philippe, A. Chappaz, P. Fongarland, A. Bengaouer, Power-to-Liquid catalytic CO_2 valorization into fuels and chemicals: focus on the Fischer-Tropsch route, J. CO2 Util. 38 (2020) 314–347.

[6] M.V. Landau, N. Meiri, N. Utsis, R. Vidruk Nehemya, M. Herskowitz, Conversion of CO_2, CO, and H_2 in CO_2 hydrogenation to fungible liquid fuels on Fe-based catalysts, Ind. Eng. Chem. Res. 56 (45) (2017) 13334–13355.

[7] J. Wang, Z. You, Q. Zhang, W. Deng, Y. Wang, Synthesis of lower olefins by hydrogenation of carbon dioxide over supported iron catalysts, Catal. Today 215 (2013) 186–193.

[8] T. Numpilai, N. Chanlek, Y. Poo-Arporn, C.K. Cheng, N. Siri-Nguan, T. Sornchamni, M. Chareonpanich, P. Kongkachuichay, N. Yigit, G. Rupprechter, J. Limtrakul, T. Witoon, Tuning interactions of surface-adsorbed species over $Fe-Co/K-Al_2O_3$ catalyst by different K contents: selective CO_2 hydrogenation to light olefins, ChemCatChem 12 (12) (2020) 3306–3320.

[9] B. Yao, T. Xiao, O.A. Makgae, X. Jie, S. Gonzalez-Cortes, S. Guan, A.I. Kirkland, J. R. Dilworth, H.A. Al-Megren, S.M. Alshihri, P.J. Dobson, G.P. Owen, J.M. Thomas, P.P. Edwards, Transforming carbon dioxide into jet fuel using an organic combustion-synthesized Fe-Mn-K catalyst, Nat. Commun. 11 (1) (2020) 6395.

[10] U. Rodemerck, M. Holeňa, E. Wagner, Q. Smejkal, A. Barkschat, M. Baerns, Catalyst development for CO_2 hydrogenation to fuels, ChemCatChem 5 (7) (2013) 1948–1955.

[11] A. Ramirez, A. Dutta Chowdhury, A. Dokania, P. Cnudde, M. Caglayan, I. Yarulina, E. Abou-Hamad, L. Gevers, S. Ould-Chikh, K. De Wispelaere, V. van Speybroeck, J. Gascon, Effect of zeolite topology and reactor configuration on the direct conversion of CO_2 to light olefins and aromatics, ACS Catal. 9 (7) (2019) 6320–6334.

[12] J. Wei, R. Yao, Q. Ge, Z. Wen, X. Ji, C. Fang, J. Zhang, H. Xu, J. Sun, Catalytic hydrogenation of CO_2 to isoparaffins over Fe-Based multifunctional catalysts, ACS Catal. 8 (11) (2018) 9958–9967.

[13] P. Gao, S. Li, X. Bu, S. Dang, Z. Liu, H. Wang, L. Zhong, M. Qiu, C. Yang, J. Cai, W. Wei, Y. Sun, Direct conversion of CO_2 into liquid fuels with high selectivity over a bifunctional catalyst, Nat. Chem. 9 (10) (2017) 1019–1024.

[14] T. Riedel, G. Schaub, K.-W. Jun, K.-W. Lee, Kinetics of CO_2 hydrogenation on a K-promoted Fe catalyst, Ind. Eng. Chem. Res. 40 (5) (2001) 1355–1363.

[15] R.E. Owen, D. Mattia, P. Plucinski, M.D. Jones, Kinetics of CO_2 hydrogenation to hydrocarbons over iron–silica catalysts, ChemPhysChem 18 (22) (2017) 3211–3218.

[16] R. Satthawong, N. Koizumi, C. Song, P. Prasassarakich, Light olefin synthesis from CO_2 hydrogenation over K-promoted Fe–Co bimetallic catalysts, Catal. Today 251 (2015) 34–40.

[17] J. Zhang, S. Lu, X. Su, S. Fan, Q. Ma, T. Zhao, Selective formation of light olefins from CO_2 hydrogenation over Fe–Zn–K catalysts, J. CO2 Util. 12 (2015) 95–100.

[18] G.V. Schulz, Über die Beziehung zwischen Reaktionsgeschwindigkeit und Zusammensetzung des Reaktionsproduktes bei Makropolymerisationsvorgängen, Z. für Phys. Chem. 30B (1) (1935) 379–398.

[19] P.J. Flory, Molecular size distribution in linear condensation polymers1, J. Am. Chem. Soc. 58 (10) (1936) 1877–1885.

[20] R.B. Anderson, R.A. Friedel, H.H. Storch, Fischer-Tropsch reaction mechanism involving stepwise growth of carbon Chain, J. Chem. Phys. 19 (3) (1951) 313–319.

[21] G. Henrici-Olivé, S. Olivé, The Fischer-Tropsch synthesis: molecular weight distribution of primary products and reaction mechanism, Angew. Chem. Int. Ed. Engl. 15 (3) (1976) 136–141.

[22] E.S. Lox, G.F. Froment, Kinetics of the Fischer-Tropsch reaction on a precipitated promoted iron catalyst. 2. Kinetic modeling, Ind. Eng. Chem. Res. 32 (1) (1993) 71–82.

[23] F.A.N. Fernandes, Polymerization kinetics of Fischer-Tropsch reaction on iron based catalysts and product grade optimization, Chem. Eng. Technol. 28 (8) (2005) 930–938.

[24] Z. You, W. Deng, Q. Zhang, Y. Wang, Hydrogenation of carbon dioxide to light olefins over non-supported iron catalyst, Chin. J. Catal. 34 (5) (2013) 956–963.

[25] A. Russkikh, G. Shterk, B.H. Al-Solami, B.A. Fadhel, A. Ramirez, J. Gascon, Turning waste into value: potassium-promoted red mud as an effective catalyst for the hydrogenation of CO_2, ChemSusChem 13 (11) (2020) 2981–2987.

[26] B. Liang, H. Duan, T. Sun, J. Ma, X. Liu, J. Xu, X. Su, Y. Huang, T. Zhang, Effect of Na promoter on Fe-based catalyst for CO_2 hydrogenation to alkenes, ACS Sustain. Chem. Eng. 7 (1) (2019) 925–932.

[27] J. Liu, A. Zhang, X. Jiang, M. Liu, J. Zhu, C. Song, X. Guo, Direct transformation of carbon dioxide to value-added hydrocarbons by physical mixtures of Fe_5C_2 and K-Modified Al_2O_3, Ind. Eng. Chem. Res. 57 (28) (2018) 9120–9126.

[28] B. Liang, T. Sun, J. Ma, H. Duan, L. Li, X. Yang, Y. Zhang, X. Su, Y. Huang, T. Zhang, Mn decorated Na/Fe catalysts for CO_2 hydrogenation to light olefins, Catal. Sci. Technol. 9 (2) (2019) 456–464.

[29] S.-R. Yan, K.-W. Jun, J.-S. Hong, M.-J. Choi, K.-W. Lee, Promotion effect of Fe–Cu catalyst for the hydrogenation of CO_2 and application to slurry reactor, Appl. Catal. A: Gen. 194–195 (2000) 63–70.

[30] A. Aitbekova, E.D. Goodman, L. Wu, A. Boubnov, A.S. Hoffman, A. Genc, H. Cheng, L. Casalena, S.R. Bare, M. Cargnello, Engineering of ruthenium–iron oxide colloidal heterostructures: improved yields in CO_2 hydrogenation to hydrocarbons, Angew. Chem. Int. Ed. 58 (48) (2019) 17451–17457.

[31] S.-C. Lee, J.-H. Jang, B.-Y. Lee, J.-S. Kim, M. Kang, S.-B. Lee, M.-J. Choi, S.-J. Choung, Promotion of hydrocarbon selectivity in CO_2 hydrogenation by Ru component, J. Mol. Catal. A Chem. 210 (1) (2004) 131–141.

[32] C. Zhang, C. Cao, Y. Zhang, X. Liu, J. Xu, M. Zhu, W. Tu, Y.-F. Han, Unraveling the role of zinc on bimetallic Fe_5C_2–ZnO catalysts for highly selective carbon dioxide hydrogenation to high carbon α-Olefins, ACS Catal. 11 (4) (2021) 2121–2133.

[33] Y. Xu, P. Zhai, Y. Deng, J. Xie, X. Liu, S. Wang, D. Ma, Highly selective olefin production from CO_2 hydrogenation on iron catalysts: a subtle synergy between manganese and sodium additives, Angew. Chem. Int. Ed. 59 (48) (2020) 21736–21744.

[34] M. Albrecht, U. Rodemerck, M. Schneider, M. Bröring, D. Baabe, E.V. Kondratenko, Unexpectedly efficient CO_2 hydrogenation to higher hydrocarbons over non-doped Fe2O3, Appl. Catal. B Environ. 204 (2017) 119–126.

[35] R.W. Dorner, D.R. Hardy, F.W. Williams, H.D. Willauer, K and Mn doped iron-based CO_2 hydrogenation catalysts: detection of $KAlH_4$ as part of the catalyst's active phase, Appl. Catal. A: Gen. 373 (1) (2010) 112–121.

[36] R.W. Dorner, D.R. Hardy, F.W. Williams, H.D. Willauer, C_2-C_{5+} olefin production from CO_2 hydrogenation using ceria modified Fe/Mn/K catalysts, Catal. Commun. 15 (1) (2011) 88–92.

[37] T. Toyao, Z. Maeno, S. Takakusagi, T. Kamachi, I. Takigawa, K.-i Shimizu, Machine learning for catalysis informatics: recent applications and prospects, ACS Catal. 10 (3) (2020) 2260–2297.

[38] V. Tshitoyan, J. Dagdelen, L. Weston, A. Dunn, Z. Rong, O. Kononova, K.A. Persson, G. Ceder, A. Jain, Unsupervised word embeddings capture latent knowledge from materials science literature, Nature 571 (7763) (2019) 95–98.

[39] A. Smith, A. Keane, J.A. Dumesic, G.W. Huber, V.M. Zavala, A machine learning framework for the analysis and prediction of catalytic activity from experimental data, Appl. Catal. B Environ. 263 (2020), 118257.

[40] K. Suzuki, T. Toyao, Z. Maeno, S. Takakusagi, K.-i Shimizu, I. Takigawa, Statistical analysis and discovery of heterogeneous catalysts based on machine learning from diverse published data, ChemCatChem 11 (18) (2019) 4537–4547.

[41] U. Zavyalova, M. Holena, R. Schlögl, M. Baerns, Statistical analysis of past catalytic data on oxidative methane coupling for new insights into the composition of high-performance catalysts, ChemCatChem 3 (12) (2011) 1935–1947.

[42] E.V. Kondratenko, M. Schlüter, M. Baerns, D. Linke, M. Holena, Developing catalytic materials for the oxidative coupling of methane through statistical analysis of literature data, Catal. Sci. Technol. 5 (3) (2015) 1668–1677.

[43] Q. Yang, A. Skrypnik, A. Matvienko, H. Lund, M. Holena, E.V. Kondratenko, Revealing property-performance relationships for efficient CO_2 hydrogenation to higher hydrocarbons over Fe-based catalysts: Statistical analysis of literature data and its experimental validation, Appl. Catal. B Environ. 282 (2021), 119554.

[44] T. Herranz, S. Rojas, F.J. Pérez-Alonso, M. Ojeda, P. Terreros, J.L.G. Fierro, Hydrogenation of carbon oxides over promoted Fe-Mn catalysts prepared by the microemulsion methodology, Appl. Catal. A Gen. 311 (2006) 66–75.

[45] A. Ramirez, L. Gevers, A. Bavykina, S. Ould-Chikh, J. Gascon, Metal organic framework-derived iron catalysts for the direct hydrogenation of CO_2 to short chain Olefins, ACS Catal. 8 (10) (2018) 9174–9182.

[46] M. Owens, The definitive guide to SQLite, Apress.

[47] R.D. Hipp, SQLite.

[48] G. Van Rossum, F.L. Drake, Python 3 Reference Manual, CreateSpace.

[49] M. Bayer, SQLAlchemy, in: A. Brown, G. Wilson (Eds.), The Architecture of Open Source Applications Volume II: Structure, Sca le, and a Few More Fearless Hacks, aosabook.org, 2012.

[50] P. Virtanen, R. Gommers, T.E. Oliphant, M. Haberland, T. Reddy, D. Cournapeau, E. Burovski, P. Peterson, W. Weckesser, J. Bright, S.J. van der Walt, M. Brett, J. Wilson, K.J. Millman, N. Mayorov, A.R.J. Nelson, E. Jones, R. Kern, E. Larson, C. J. Carey, İ. Polat, Y. Feng, E.W. Moore, J. VanderPlas, D. Laxalde, J. Perktold, R. Cimrman, I. Henriksen, E.A. Quintero, C.R. Harris, A.M. Archibald, A.H. Ribeiro, F. Pedregosa, P. van Mulbregt, A. Vijaykumar, A.P. Bardelli, A. Rothberg, A. Hilboll, A. Kloeckner, A. Scopatz, A. Lee, A. Rokem, C.N. Woods, C. Fulton, C. Masson, C. Häggström, C. Fitzgerald, D.A. Nicholson, D.R. Hagen, D. V. Pasechnik, E. Olivetti, E. Martin, E. Wieser, F. Silva, F. Lenders, F. Wilhelm, G. Young, G.A. Price, G.-L. Ingold, G.E. Allen, G.R. Lee, H. Audren, I. Probst, J. P. Dietrich, J. Silterra, J.T. Webber, J. Slavič, J. Nothman, J. Buchner, J. Kulick, J. L. Schönberger, J.V. de Miranda Cardoso, J. Reimer, J. Harrington, J.L. C. Rodríguez, J. Nunez-Iglesias, J. Kuczynski, K. Tritz, M. Thoma, M. Newville, M. Kümmerer, M. Bolingbroke, M. Tartre, M. Pak, N.J. Smith, N. Nowaczyk,

N. Shebanov, O. Pavlyk, P.A. Brodtkorb, P. Lee, R.T. McGibbon, R. Feldbauer, S. Lewis, S. Tygier, S. Sievert, S. Vigna, S. Peterson, S. More, T. Pudlik, T. Oshima, T.J. Pingel, T.P. Robitaille, T. Spura, T.R. Jones, T. Cera, T. Leslie, T. Zito, T. Krauss, U. Upadhyay, Y.O. Halchenko, Y. Vázquez-Baeza, C. SciPy, SciPy 1.0: fundamental algorithms for scientific computing in Python, Nat. Methods 17 (3) (2020) 261–272.

[51] C.R. Harris, K.J. Millman, S.J. van der Walt, R. Gommers, P. Virtanen, D. Cournapeau, E. Wieser, J. Taylor, S. Berg, N.J. Smith, R. Kern, M. Picus, S. Hoyer, M.H. van Kerkwijk, M. Brett, A. Haldane, J.F. del Río, M. Wiebe, P. Peterson, P. Gérard-Marchant, K. Sheppard, T. Reddy, W. Weckesser, H. Abbasi, C. Gohlke, T.E. Oliphant, Array programming with NumPy, Nature 585 (7825) (2020) 357–362.

[52] W. McKinney, others, Data structures for statistical computing in python, Austin, TX, pp. 51–56.

[53] F. Pedregosa, G. Varoquaux, A. Gramfort, V. Michel, B. Thirion, O. Grisel, M. Blondel, P. Prettenhofer, R. Weiss, V. Dubourg, J. Vanderplas, A. Passos, D. Cournapeau, M. Brucher, M. Perrot, E. Duchesnay, Scikit-learn: Machine Learning in Python, Journal of Machine Learning Research 12 2825–2830.

[54] P.T. Inc, Collaborative data science, ⟨https://plot.ly⟩.

[55] C.G. Visconti, M. Martinelli, L. Falbo, A. Infantes-Molina, L. Lietti, P. Forzatti, G. Iaquaniello, E. Palo, B. Picutti, F. Brignoli, CO_2 hydrogenation to lower olefins on a high surface area K-promoted bulk Fe-catalyst, Appl. Catal. B Environ. 200 (2017) 530–542.

[56] S. Krishnamoorthy, A. Li, E. Iglesia, Pathways for CO_2 formation and conversion during fischer–tropsch synthesis on iron-based catalysts, Catal. Lett. 80 (1) (2002) 77–86.

[57] J.M. Moe, Design of water-gas shift reactors, Chem. Eng. Prog. 58 (1962) 3.

[58] J. Nocedal, S. Wright, Numerical Optimization, Springer, New York, 2006.

[59] T. Hastie, R. Tibshirani, J. Friedman, The Elements of Statistical Learning, Springer New York.

[60] V. Svetnik, A. Liaw, C. Tong, J.C. Culberson, R.P. Sheridan, B.P. Feuston, Random forest: a classification and regression tool for compound classification and QSAR modeling, J. Chem. Inf. Comput. Sci. 43 (6) (2003) 1947–1958.

[61] R.A. Fisher, On the interpretation of χ^2 from contingency tables, and the calculation of P, J. R. Stat. Soc. 85 (1) (1922) 87–94.

[62] A.S. Skrypnik, Q. Yang, A.A. Matvienko, V.Y. Bychkov, Y.P. Tulenin, H. Lund, S. A. Petrov, R. Kraehnert, A. Arinchtein, J. Weiss, A. Brueckner, E.V. Kondratenko, Understanding reaction-induced restructuring of well-defined $Fe_xO_yC_z$ compositions and its effect on CO_2 hydrogenation, Appl. Catal. B Environ. 291 (2021), 120121.

[63] J. Zhu, G. Zhang, W. Li, X. Zhang, F. Ding, C. Song, X. Guo, Deconvolution of the particle size effect on CO_2 hydrogenation over iron-based catalysts, ACS Catal. 10 (13) (2020) 7424–7433.

[64] J. Liu, G. Zhang, X. Jiang, J. Wang, C. Song, X. Guo, Insight into the role of Fe_5C_2 in CO_2 catalytic hydrogenation to hydrocarbons, Catal. Today 371 (2021) 162–170.

[65] S. Daniel, NIST Standard Reference Simulation Website - SRD 173, National Institute of Standards.

[66] J. Hunt, A. Ferrari, A. Lita, M. Crosswhite, B. Ashley, A.E. Stiegman, Microwave-specific enhancement of the carbon–carbon dioxide (Boudouard) reaction, J. Phys. Chem. C 117 (51) (2013) 26871–26880.

[67] X. Cui, P. Gao, S. Li, C. Yang, Z. Liu, H. Wang, L. Zhong, Y. Sun, Selective production of aromatics directly from carbon dioxide hydrogenation, ACS Catal. 9 (5) (2019) 3866–3876.

[68] S. Geng, F. Jiang, Y. Xu, X. Liu, Iron-based Fischer–Tropsch synthesis for the efficient conversion of carbon dioxide into isoparaffins, ChemCatChem 8 (7) (2016) 1303–1307.

[69] R.E. Owen, P. Plucinski, D. Mattia, L. Torrente-Murciano, V.P. Ting, M.D. Jones, Effect of support of Co-Na-Mo catalysts on the direct conversion of CO_2 to hydrocarbons, J. CO2 Util. 16 (2016) 97–103.

[70] D.L. Williamson, C. Herdes, L. Torrente-Murciano, M.D. Jones, D. Mattia, N-Doped Fe@CNT for combined RWGS/FT CO_2 hydrogenation, ACS Sustain. Chem. Eng. 7 (7) (2019) 7395–7402.

[71] S. Wang, T. Wu, J. Lin, Y. Ji, S. Yan, Y. Pei, S. Xie, B. Zong, M. Qiao, Iron–potassium on single-walled carbon nanotubes as efficient catalyst for CO_2 hydrogenation to heavy olefins, ACS Catal. 10 (11) (2020) 6389–6401.

[72] Z. He, M. Cui, Q. Qian, J. Zhang, H. Liu, B. Han, Synthesis of liquid fuel via direct hydrogenation of CO_2, Proc. Natl. Acad. Sci. 116 (26) (2019) 12654–12659.

[73] X. Su, J. Zhang, S. Fan, Q. Ma, T.-S. Zhao, Effect of preparation of Fe–Zr–K catalyst on the product distribution of CO_2 hydrogenation, RSC Adv. 5 (98) (2015) 80196–80202.

[74] R. Satthawong, N. Koizumi, C. Song, P. Prasassarakich, Bimetallic Fe–Co catalysts for CO_2 hydrogenation to higher hydrocarbons, J. CO2 Util. 3–4 (2013) 102–106.

[75] N. Boreriboon, X. Jiang, C. Song, P. Prasassarakich, Fe-based bimetallic catalysts supported on TiO_2 for selective CO_2 hydrogenation to hydrocarbons, J. CO2 Util. 25 (2018) 330–337.

[76] L. Guo, J. Sun, X. Ji, J. Wei, Z. Wen, R. Yao, H. Xu, Q. Ge, Directly converting carbon dioxide to linear α-olefins on bio-promoted catalysts, Commun. Chem. 1 (1) (2018) 11.

[77] M.J. Bradley, R. Ananth, H.D. Willauer, J.W. Baldwin, D.R. Hardy, F.W. Williams, The effect of copper addition on the activity and stability of iron-based CO_2 hydrogenation catalysts, Molecules 22 (9) (2017) 1579.

[78] T. Riedel, H. Schulz, G. Schaub, K.-W. Jun, J.-S. Hwang, K.-W. Lee, Fischer–Tropsch on Iron with H_2/CO and H_2/CO_2 as synthesis gases: the episodes of formation of the Fischer–Tropsch regime and construction of the catalyst, Top. Catal. 26 (1) (2003) 41–54.

[79] S. Hu, M. Liu, F. Ding, C. Song, G. Zhang, X. Guo, Hydrothermally stable MOFs for CO_2 hydrogenation over iron-based catalyst to light olefins, J. CO2 Util. 15 (2016) 89–95.

[80] F. Jiang, B. Liu, S. Geng, Y. Xu, X. Liu, Hydrogenation of CO_2 into hydrocarbons: enhanced catalytic activity over Fe-based Fischer–Tropsch catalysts, Catal. Sci. Technol. 8 (16) (2018) 4097–4107.

[81] J. Jiang, C. Wen, Z. Tian, Y. Wang, Y. Zhai, L. Chen, Y. Li, Q. Liu, C. Wang, L. Ma, Manganese-promoted Fe_3O_4 microsphere for efficient conversion of CO_2 to light olefins, Ind. Eng. Chem. Res. 59 (5) (2020) 2155–2162.

[82] J.S. Hwang, K.-W. Jun, K.-W. Lee, Deactivation and regeneration of Fe-K/alumina catalyst in CO_2 hydrogenation, Appl. Catal. A Gen. 208 (1) (2001) 217–222.

[83] W.D. Shafer, G. Jacobs, U.M. Graham, H.H. Hamdeh, B.H. Davis, Increased CO_2 hydrogenation to liquid products using promoted iron catalysts, J. Catal. 369 (2019) 239–248.

[84] Y. Zhang, C. Cao, C. Zhang, Z. Zhang, X. Liu, Z. Yang, M. Zhu, B. Meng, J. Xu, Y.-F. Han, The study of structure-performance relationship of iron catalyst during a full life cycle for CO_2 hydrogenation, J. Catal. 378 (2019) 51–62.

[85] J.-S. Hong, J.S. Hwang, K.-W. Jun, J.C. Sur, K.-W. Lee, Deactivation study on a coprecipitated Fe-Cu-K-Al catalyst in CO_2 hydrogenation, Appl. Catal. A: Gen. 218 (1) (2001) 53–59.

[86] T. Riedel, M. Claeys, H. Schulz, G. Schaub, S.-S. Nam, K.-W. Jun, M.-J. Choi, G. Kishan, K.-W. Lee, Comparative study of Fischer–Tropsch synthesis with H_2/CO and H_2/CO_2 syngas using Fe- and Co-based catalysts, Appl. Catal. A Gen. 186 (1) (1999) 201–213.

[87] B. Liu, S. Geng, J. Zheng, X. Jia, F. Jiang, X. Liu, Unravelling the new roles of Na and Mn promoter in CO_2 hydrogenation over Fe_3O_4-based catalysts for enhanced selectivity to light α-Olefins, ChemCatChem 10 (20) (2018) 4718–4732.

[88] J. Wei, J. Sun, Z. Wen, C. Fang, Q. Ge, H. Xu, New insights into the effect of sodium on Fe_3O_4-based nanocatalysts for CO_2 hydrogenation to light olefins, Catal. Sci. Technol. 6 (13) (2016) 4786–4793.

[89] X. Liu, C. Zhang, P. Tian, M. Xu, C. Cao, Z. Yang, M. Zhu, J. Xu, Revealing the effect of sodium on iron-based catalysts for CO_2 hydrogenation: insights from calculation and experiment, J. Phys. Chem. C 125 (14) (2021) 7637–7646.

[90] N. Fischer, R. Henkel, B. Hettel, M. Iglesias, G. Schaub, M. Claeys, Hydrocarbons via CO_2 hydrogenation over iron catalysts: the effect of potassium on structure and performance, Catal. Lett. 146 (2) (2016) 509–517.

The supporting information

Data Analysis of CO_2 Hydrogenation Catalysts for Hydrocarbon Production

Aleksandr Fedorov, David Linke

Leibniz-Institut für Katalyse e.V., Albert-Einstein-Str. 29a, 18059 Rostock, Germany

Calculation of thermodynamic ratio

For calculation of thermodynamic ratio, the following system of chemical reaction were considered:

S.1. $CO_2 + H_2 = CO + H_2O$

S.2. $CO_2 + 4H_2 = CH_4 + 2H_2O$

S.3. $CO_2 + 3H_2 = -(CH_2) - +2H_2O$

S.4. $CO_2 + 3H_2 = CH_3OH + H_2O$

S.5. $C_nH_{2n} + H_2 = C_nH_{2n+2}$

Thermodynamic ratio can be calculated by the following system of equations:

S.6. $n_{co_2} = n^o_{CO_2}(1 - X_{CO_2})$

S.7. $n_{CO} = n^o_{CO_2} X_{CO_2} S_{CO}$

S.8. $n_{H_2O} = n^o_{CO_2} X_{CO_2} S_{CO} + n^o_{CO_2} X_{CO_2} S_{CH_3OH} + 2n^o_{CO_2} X_{CO_2}(1 - S_{CO} - S_{CH_3OH})$

S.9. $n_{C_{2+}} = n^o_{CO_2} X_{CO_2} \sum_{i=2}^{\infty} \frac{S_i}{i}$

S.10. $\overline{w} = \frac{\sum_{i=2}^{\infty} n_{C_i} w_i}{\sum_{i=2}^{\infty} n_{C_i}}$

S.11. $n_{H_2} = n^o_{H_2} - n^o_{CO_2} X_{CO_2} S_{CO} - 4n^o_{CO_2} X_{CO_2} S_{CH_4} - -3n^o_{CO_2} X_{CO_2}(1 - S_{CO} - S_{CH_4}) - (1 - \overline{w}) n_{C_{2+}}$

S.12. $\Pi = \frac{p_{CO} p_{H_2O}}{p_{CO_2} p_{H_2}} = \frac{n_{CO} n_{H_2O}}{n_{co_2} n_{H_2}}$

S.13. $\eta = \Pi / K$

where n_i – molar flow of component i from the reactor, n_i^o – initial molar flow of component i to the reactor, X_{CO2} – CO_2 conversion, S_{CO} – CO selectivity, S_{CH4} – methane selectivity, S_{CH3OH} – methanol selectivity, Si – selectivity of hydrocarbons with carbon number, w_i – olefins content in hydrocarbons with carbon number i, p_i – pressure of i-component from the reactor, K – the equilibrium constant, η – thermodynamic ratio. In the case of known hydrocarbon distribution, olefins content in hydrocarbons was estimated by the following expression:

S.14. $\overline{w} = \frac{\sum_{i=2}^{n} n_{C_i} w_i}{\sum_{i=2}^{n} n_{C_i}}$

In general, researchers limit presenting only olefins content in C_2-C_4 fraction (w_{24}). The value of olefins content in all hydrocarbons was estimated by the linear equation:

S.15. $\overline{w} = k w_{24} + b,$

The values of coefficients k and b were calculated from the literature data having the information about hydrocarbon distribution that allows one to calculate w_{24} and $\overline{w}$ directly.

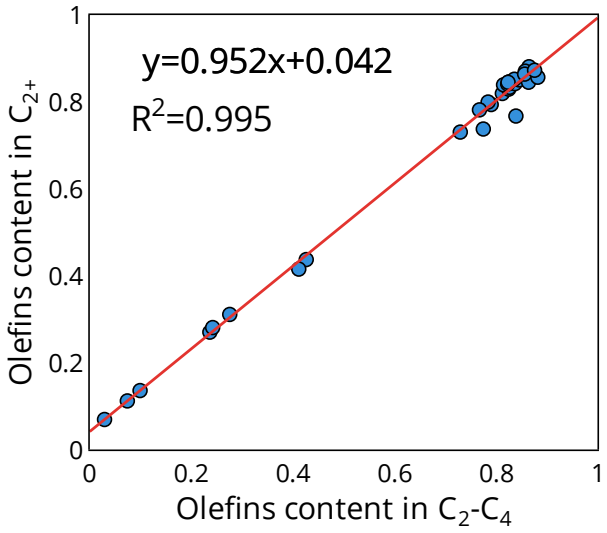

Figure S1. The dependence between olefins content in C_2-C_4 range and olefins in the products of CO_2-FTS.

Figure S1 shows the dependence between olefins content in C_2-C_4 range and olefins in all hydrocarbons. The value of R^2 is close to 1. Thus, this allows one to use this approximation for calculation of thermodynamic ration. The procedure was similar in the case of range C_2-C_6.

ASF distribution

For comparison of hydrocarbon distributions from different experiments the data was converted to the one line with fixed parameters using linear transformation. The first stage is to calculate the parameters k and b of linear regression for hydrocarbon distribution in ASF coordinates by the following equation:

S.16. $$y = \log\frac{S_n}{n} = kn + b$$

where S_n – selectivity of hydrocarbon with carbon number n. At the selected parameters k_s and b_s arbitrarily, the following linear transformation was carried out:

S.17. $$y_{new} = ay + b\,;\; a = \frac{k_s}{k}, b = -\frac{bk_s}{k} + b_s$$

The idea of the linear transformation is shown in the Figure S2. Figure S3 presents the hydrocarbon distribution data for different catalysts before and after linear transformation. The obtained data (see Figure S3 (B)) was used for calculation of the mean value and the

confidence interval for each carbon number (see Figure 2). The similar procedure was carried out for olefins and paraffins distributions.

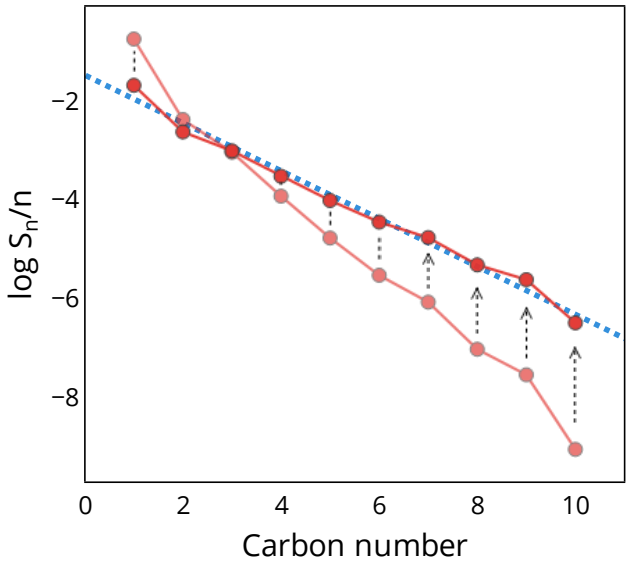

Figure S2 The linear transformation of the hydrocarbon distribution data plotted in ASF coordinates

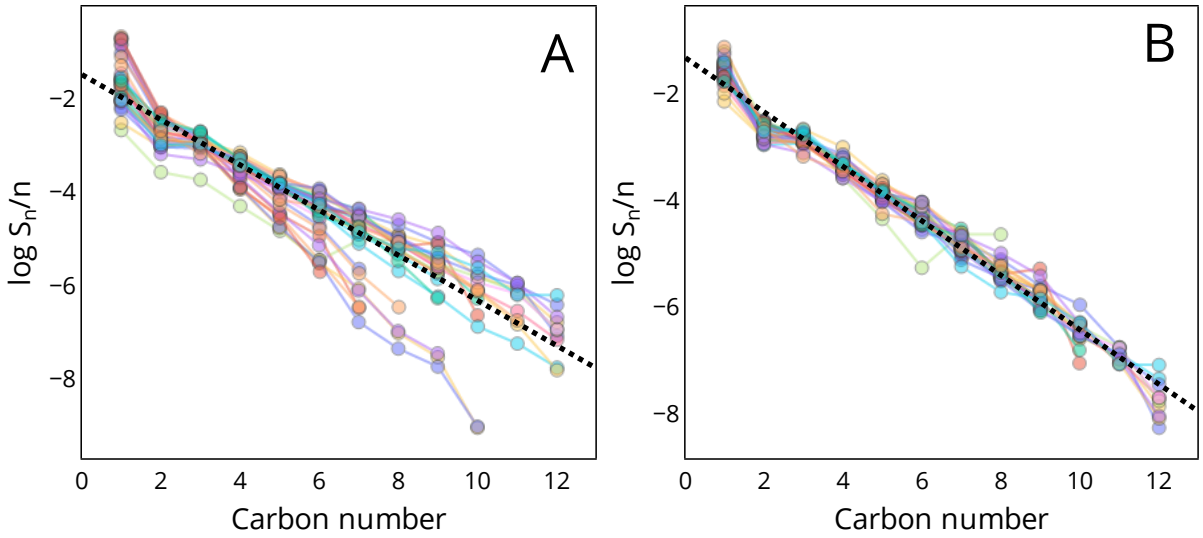

Figure S3. The hydrocarbon distribution data plotted in ASF coordinates before (A) and after (B) the linear transformation.

The parameters of Equations 6-8 can be calculated by minimization of the cost function 9. The chain growth probability can be got from the slope of a curve describing hydrocarbon distribution for C3+ in corresponding ASF coordinates. Figure S2 presents the dependence between the values of the chain growth probability calculated using different approaches. One can see good linear correlation that allows one to use both approaches for estimation.

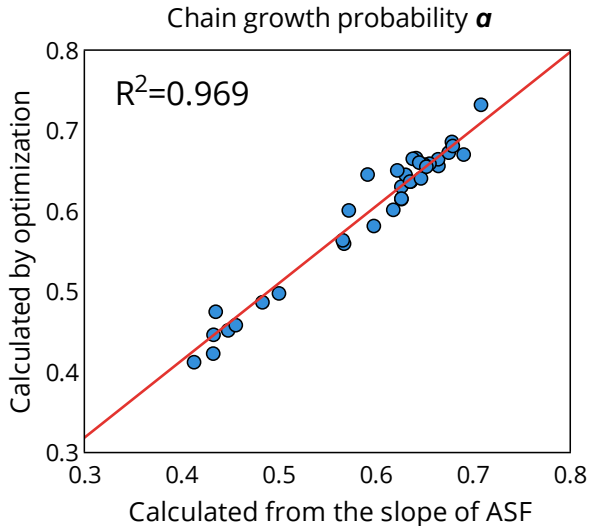

Figure S4. The dependence between the values of chain growth probability calculated from the slope and by the optimization using hydrocarbon distribution.

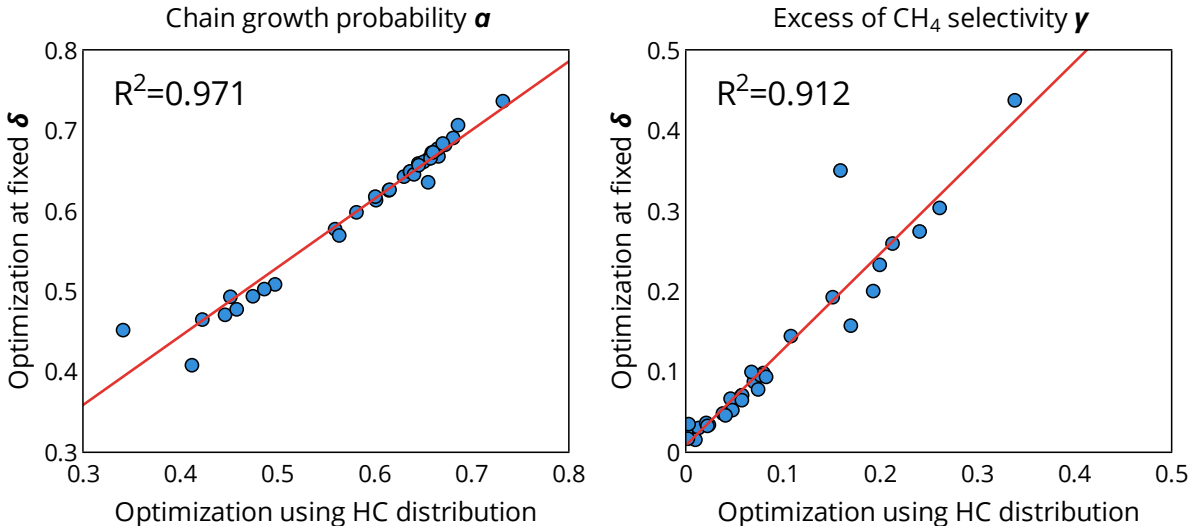

Figure S5. The dependencies between the values of chain growth probability and the 'extra' increase of methane selectivity calculated by the optimization using hydrocarbon distribution data and the range data at fixed δ.

Empirically, the hydrocarbon selectivity can be described by Equations 6-8. The majority information about hydrocarbons presents like C_1, C_{2-4} and C_{5+} selectivity (see Figure 2). However, it was found that a decrease of C_2 selectivity is around 10 % (the δ parameter) for the most catalysts. Setting δ to 0.1 the α and γ parameters can be calculated from the data having only a two degree of freedom. The dependencies between the values of chain growth probability and an 'extra' increase of methane selectivity calculated by the optimization using

hydrocarbon distribution data and the range data at fixed δ are presented in Figure S5. One can see a good linear correlation for both parameters using different methods for estimation.

Table S1. The activity of CO2-FT catalysts with the thermodynamic ratio > 1.5.

Ref.	Name	Pressure, bar	Temperature, °C	CO_2 conversion, %	Selectivity, %				Olefins in C_2-C_4	α	η	γ
					CO	CH_4	C_2-C_4	C_{5+}				
Co-based catalysts												
[1]	15Co/SiO_2	25	300	52.2	4.2	92.4	1.3	2.1	0.00	0.72	1.85	0.96
[2]	20-Co-1-Na-1-Mo/SiO_2	1	200	30.0	24.5	43.1	23.0	9.4	0.01	0.52	5.55	0.44
	20-Co-1-Na-1-Mo/SiO_2	1	200	15.6	59.0	17.3	16.1	7.7	-	0.55	1.88	0.27
	20-Co-1-Na-1-Mo/CeO_2	1	200	15.1	70.2	6.6	13.9	9.3	-	0.59	1.87	0.06
	20-Co-1-Na-1-Mo/Al_2O_3	1	200	15.4	57.3	12.5	19.0	11.2	-	0.58	1.79	0.13
	20-Co-1-Na-1-Mo/ZSM-5	1	200	29.1	20.6	76.0	3.3	0.2	-	0.27	4.58	0.90
	20-Co-1-Na-1-Mo/0.25-SiO_2-0.75-TiO_2	1	200	24.8	42.9	30.7	20.0	6.4	0.02	0.49	4.87	0.37
	20-Co-1-Na-1-Mo/0.50-SiO_2-0.50-TiO_2	1	200	26.9	41.2	23.5	19.3	16.0	0.02	0.63	5.83	0.30
	20-Co-1-Na-1-Mo/0.75-SiO_2-0.25-TiO_2	1	200	18.0	40.0	19.1	26.2	14.6	0.07	0.57	2.08	0.16
	20-Co-1-Na-1-Mo/0.90-SiO_2-0.10-TiO_2	1	200	13.8	70.8	9.3	12.4	7.4	0.19	0.58	1.53	0.17
Fe-based catalysts supported on nanotubes												
[3]	Fe/CNT	15	370	48.0	52.0	16.3	30.0	1.7	0.50	0.44	2.84	0.00
	Fe/NCNT	15	370	60.3	8.6	48.4	42.6	0.4	0.09	0.29	2.70	0.00
	Na-Fe/NCNT	15	370	48.0	24.8	20.7	39.5	15.0	0.33	0.51	1.90	0.04
[4]	FeK/SWNT	20	340	52.7	9.6	11.7	27.0	51.7	0.73	0.73	1.72	0.06
	FeK/MWNT	20	340	43.6	23.4	20.7	29.5	26.4	0.77	0.66	1.79	0.17
	FeK/SWNT	20	270	41.3	16.7	17.8	31.4	34.2	0.65	0.66	2.98	0.11
	FeK/SWNT	20	300	47.8	11.0	16.2	29.6	43.2	0.68	0.70	2.26	0.10
	FeK/SWNT	20	320	51.8	10.5	14.4	27.1	48.0	0.68	0.73	2.24	0.09
	FeK/SWNT	20	360	53.2	16.1	16.6	24.3	43.0	0.66	0.73	2.22	0.13
	FeK/SWNT	20	380	53.5	19.6	19.9	23.6	36.9	0.64	0.71	2.16	0.18
	FeK/SWNT	30	340	54.0	8.7	11.2	27.5	52.6	0.62	0.74	1.76	0.06
Fe-based catalysts doped by K												
[5]	Fe-K/Al_2O_3	10	300	36.0	30.0	11.2	27.9	30.9	0.84	0.66	1.92	0.05
[6]	Fe-K	5	320	53.9	5.5	29.0	53.7	11.8	0.88	0.45	1.58	0.00
	1Fe-3Zn-K	5	320	50.5	7.1	34.6	55.8	2.5	0.87	0.41	1.52	0.00

	1Fe-1Zn-K	5	320	54.0	6.3	29.2	53.1	11.4	0.89	0.45	1.79	0.00
[7]	K-Fe	6	270	40.1	13.2	17.6	37.7	31.4	0.81	0.62	2.20	0.06
	K-Fe	6	300	45.1	12.2	13.2	34.3	40.3	0.86	0.66	1.95	0.04
	K-Fe	1	270	24.5	93.0	2.4	3.3	1.3	0.79	0.52	1.76	0.14
	K-Fe	11	270	46.4	10.0	11.9	34.7	43.4	0.82	0.67	2.80	0.02
	K-Fe	6	270	40.2	14.5	17.3	37.1	31.1	0.83	0.62	2.39	0.06
	K-Fe	6	270	34.8	20.4	14.9	38.3	26.4	0.84	0.58	2.02	0.00
	K-Fe	6	270	30.2	29.3	11.8	30.1	28.8	0.85	0.64	1.77	0.04
	K-Fe	6	270	24.8	25.5	13.2	34.8	26.6	0.87	0.60	6.38	0.01
[8]	Fe_2O_3/KO_2	30	350	48.1	15.9	15.2	32.4	36.5	0.86	0.67	1.64	0.07

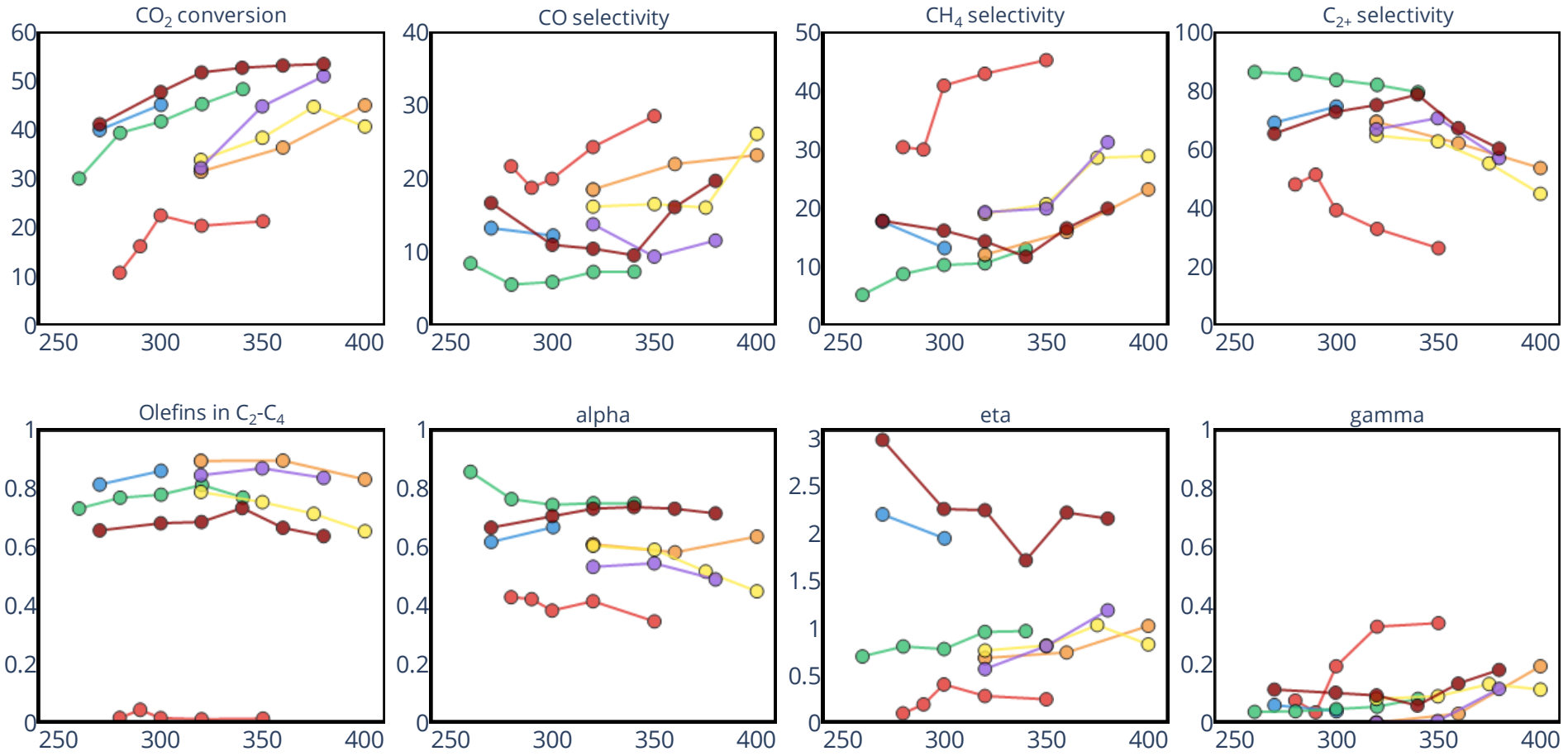

Figure S6. The dependencies between the parameters of different CO_2-FT catalysts and reaction temperature in ºC. The same color means one specific catalysts from one article.

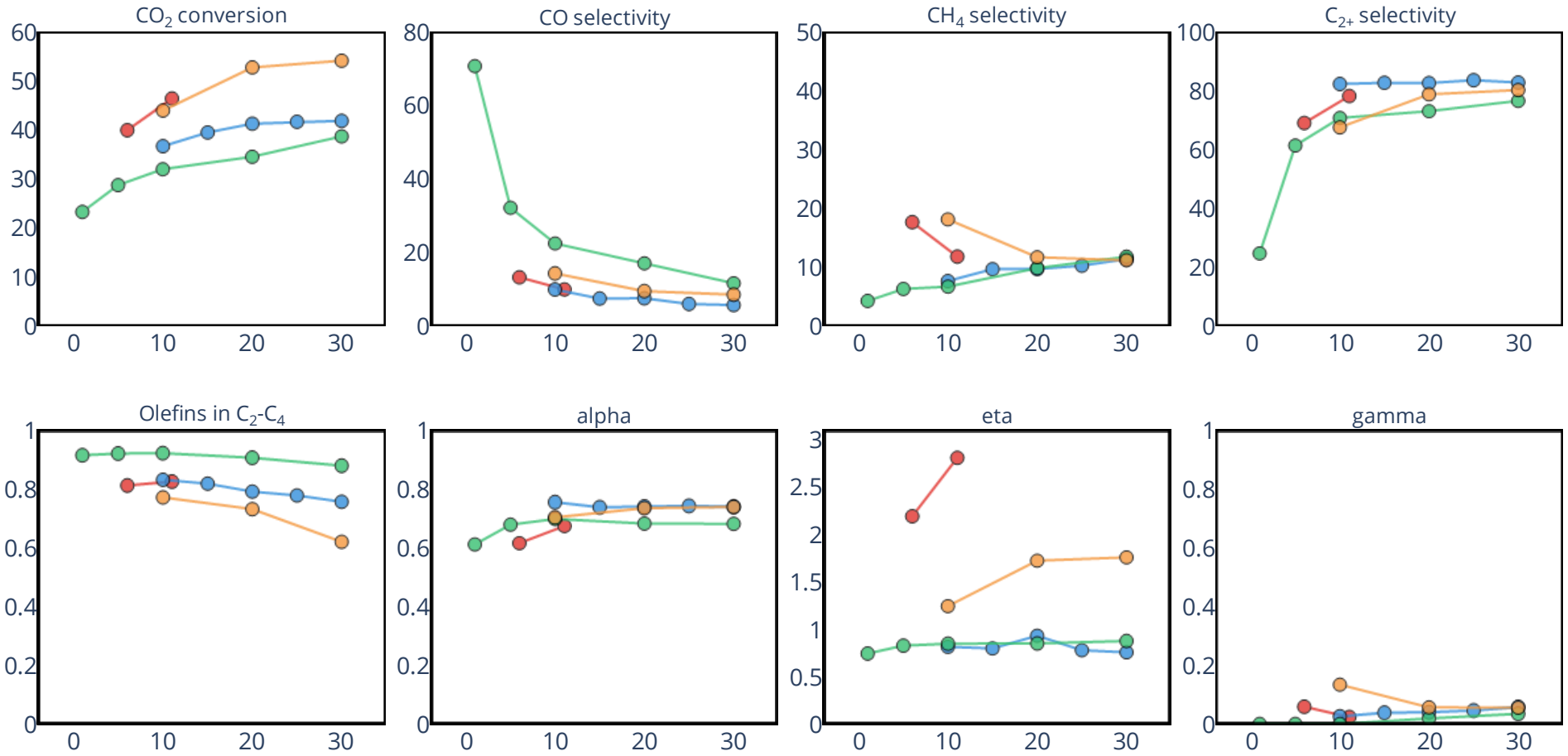

Figure S7. The dependencies between the parameters of different CO_2-FT catalysts and reaction pressure in bar. The same color means one specific catalysts from one article.

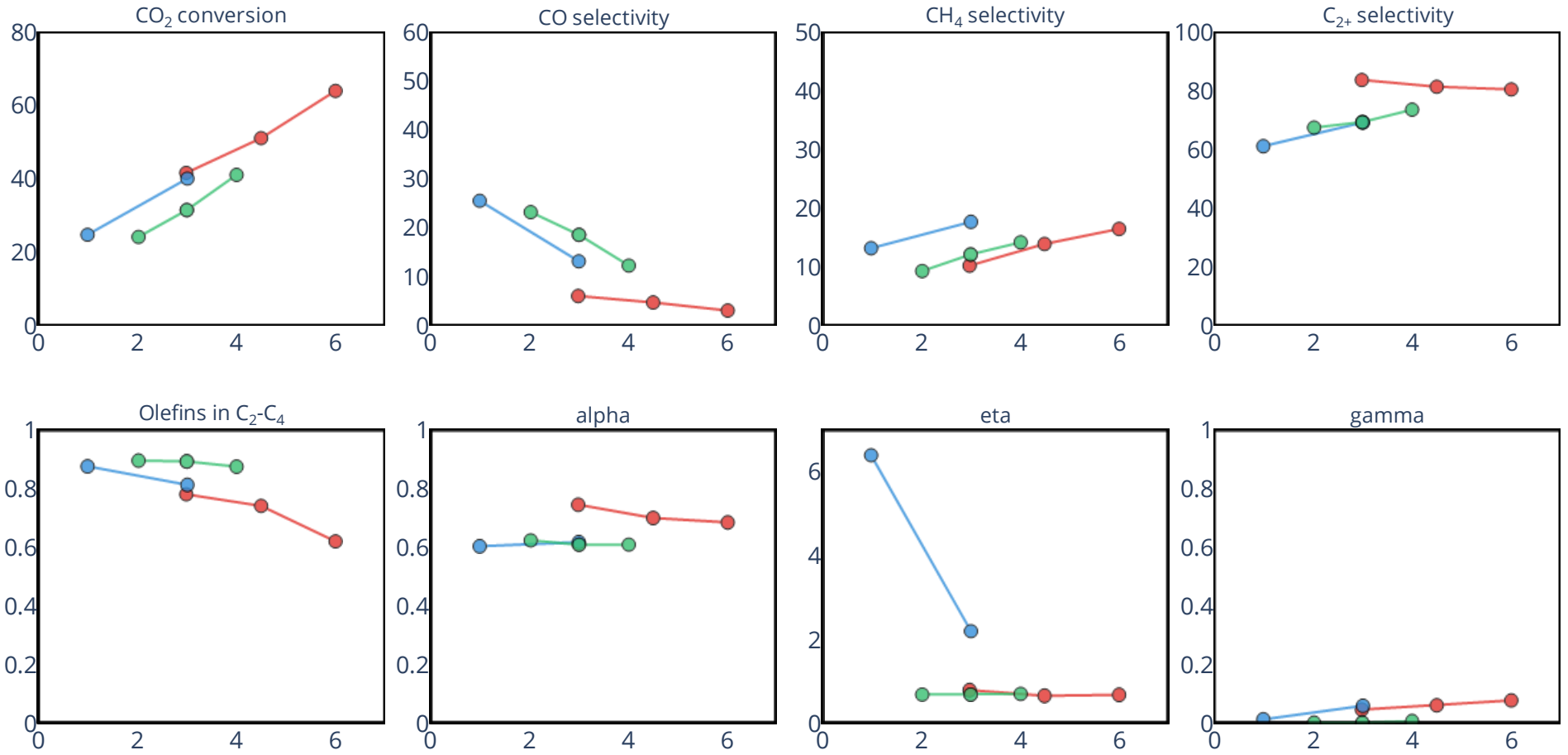

Figure S8. The dependencies between the parameters of different CO_2-FT catalysts and H_2:CO_2 molar ratio. The same color means one specific catalysts from one article.

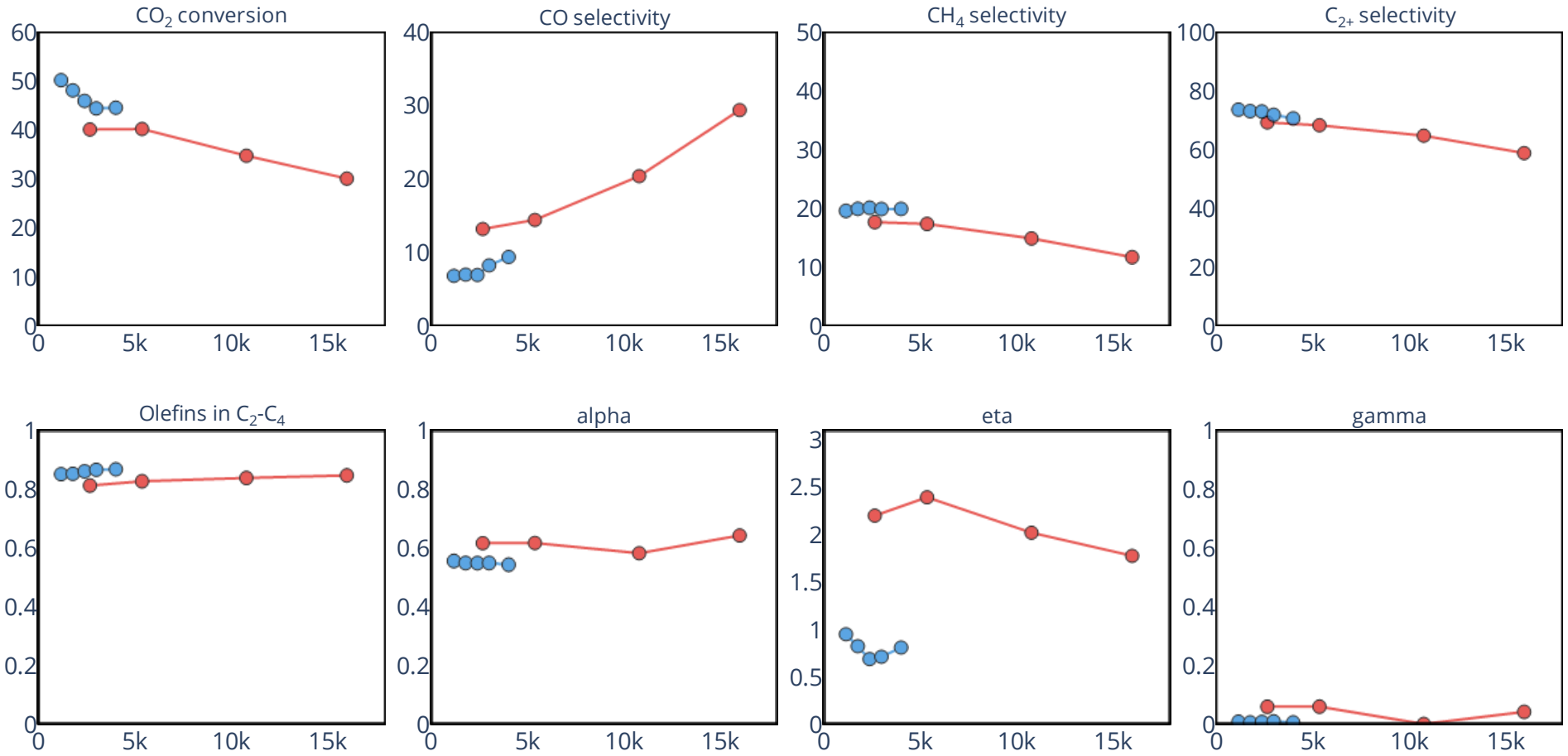

Figure S9. The dependencies between the parameters of different CO_2-FT catalysts and GHSV in $ml \cdot h^{-1} \cdot g^{-1}$. The same color means one specific catalysts from one article.

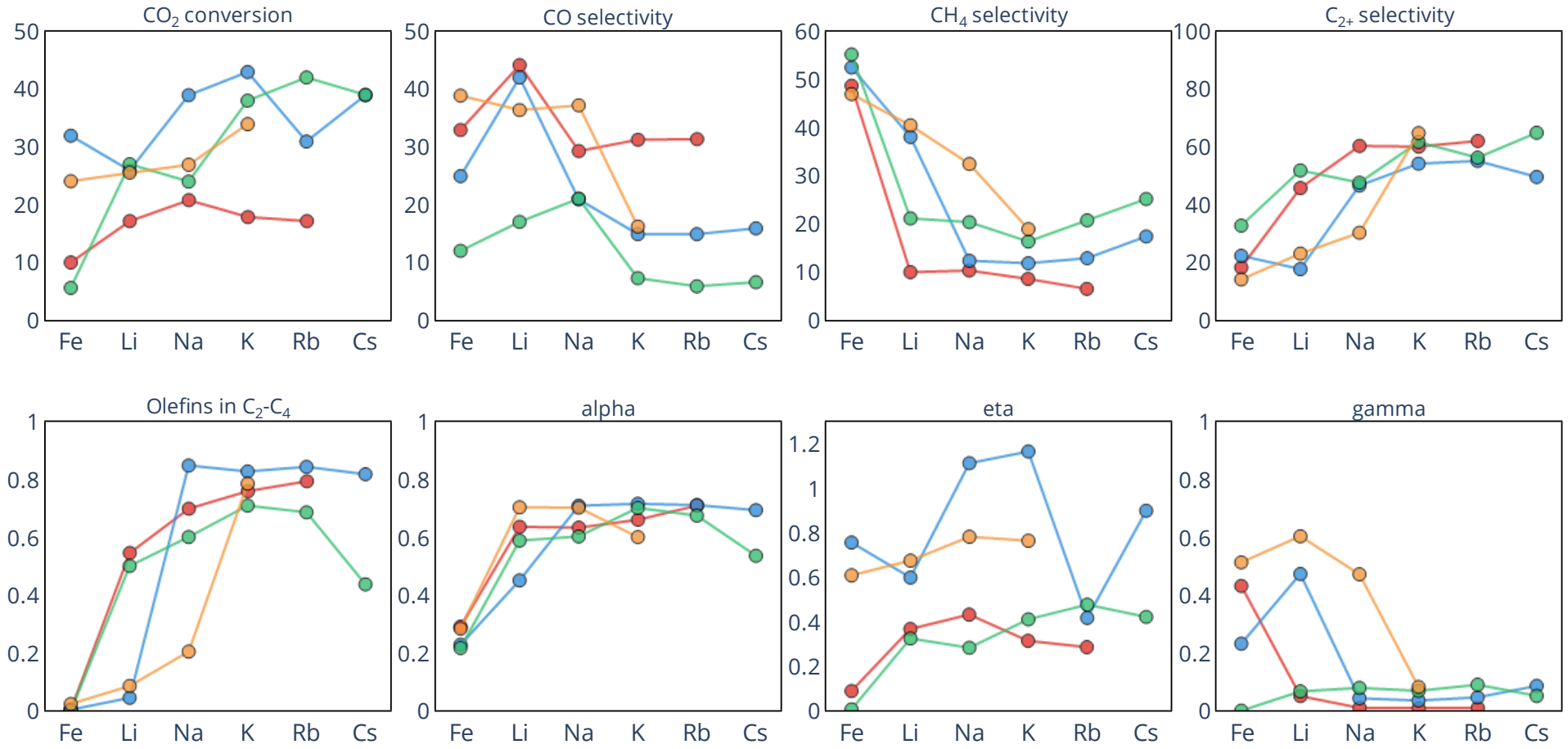

Figure S10. The parameters of different CO_2-FT catalysts with various alkali dopant. Fe means a catalyst without alkali dopants. The same color means one specific catalysts from one article.

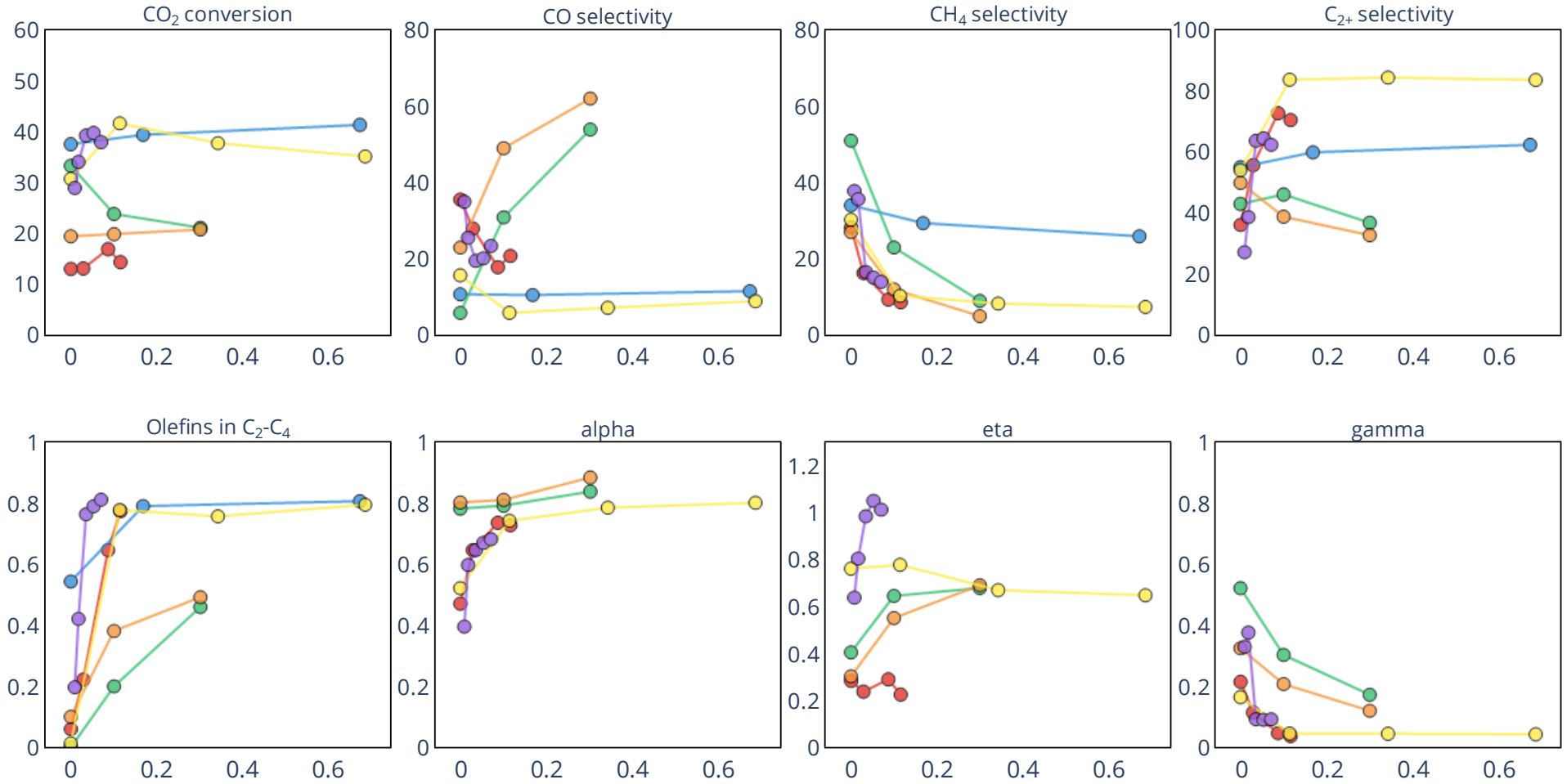

Figure S11. The dependencies between the parameters of different CO_2-FT catalysts and molar ratio K/Fe. Part I. The same color means one specific catalysts from one article.

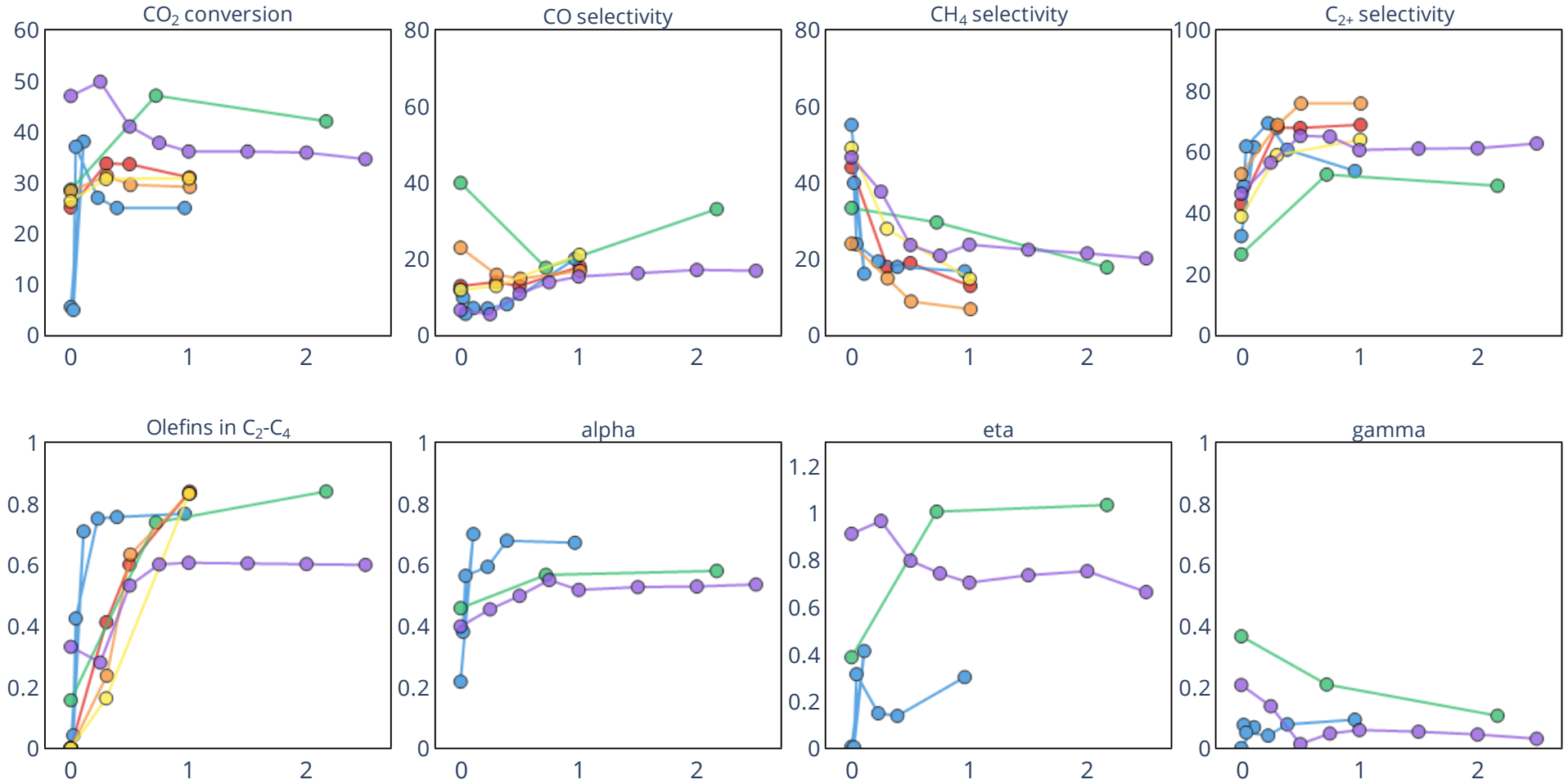

Figure S12. The dependencies between the parameters of different CO_2-FT catalysts and molar ratio K/Fe. Part II. The same color means one specific catalysts from one article.

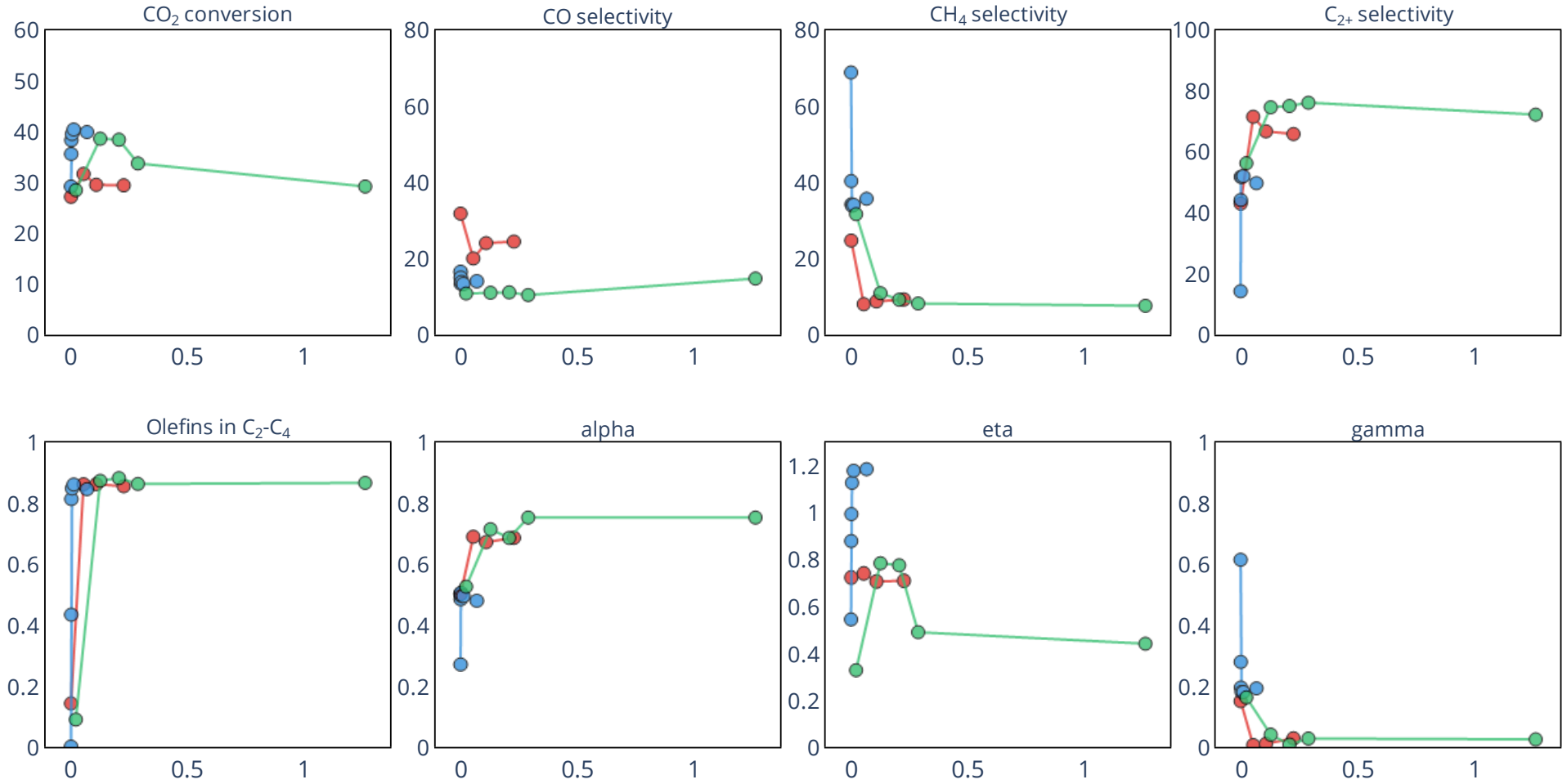

Figure S13. The dependencies between the parameters of different CO_2-FT catalysts and molar ratio Na/Fe. The same color means one specific catalysts from one article.

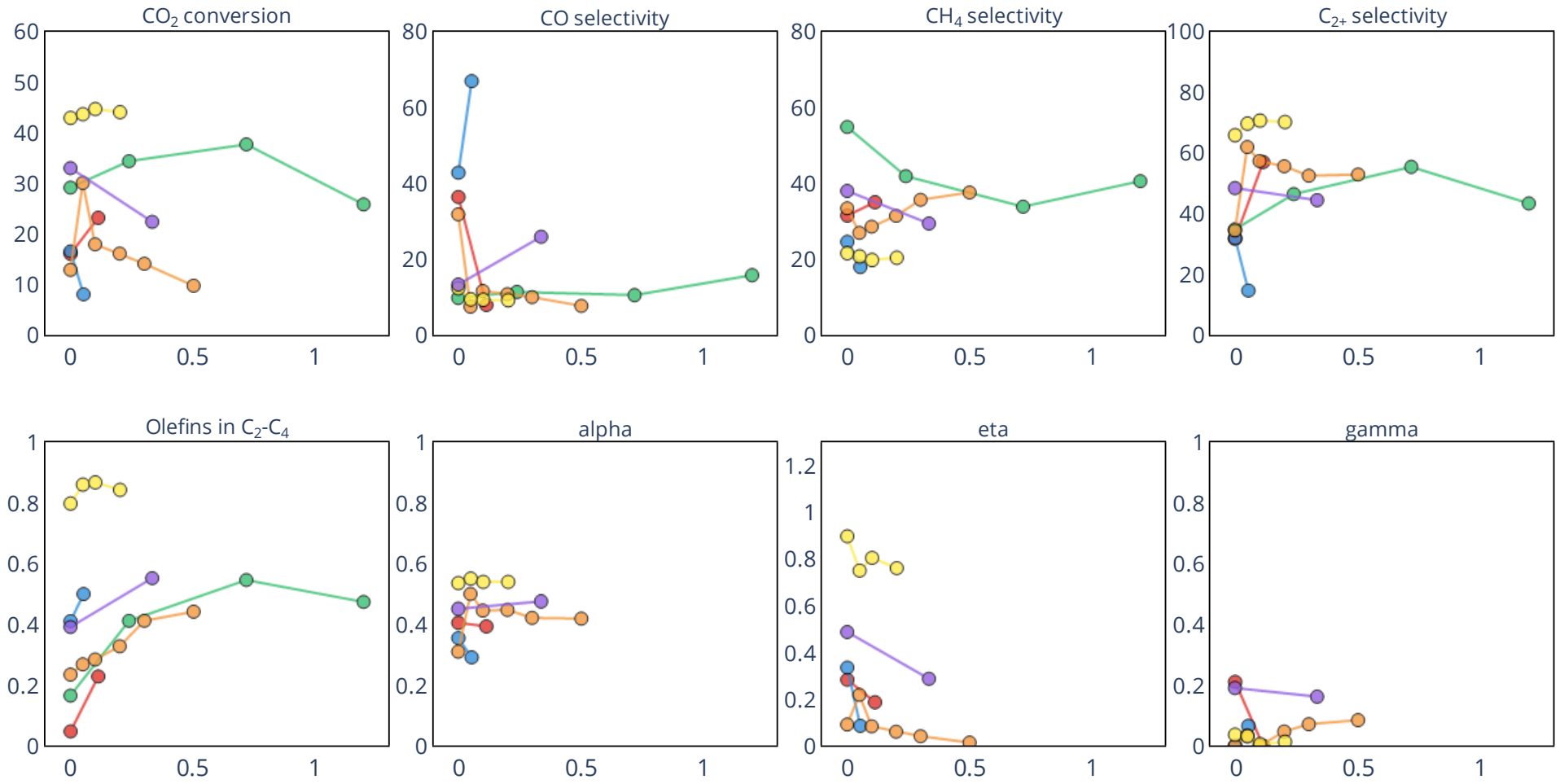

Figure S14. The dependencies between the parameters of different CO_2-FT catalysts and molar ratio Mn/Fe without alkali dopants. The same color means one specific catalysts from one article.

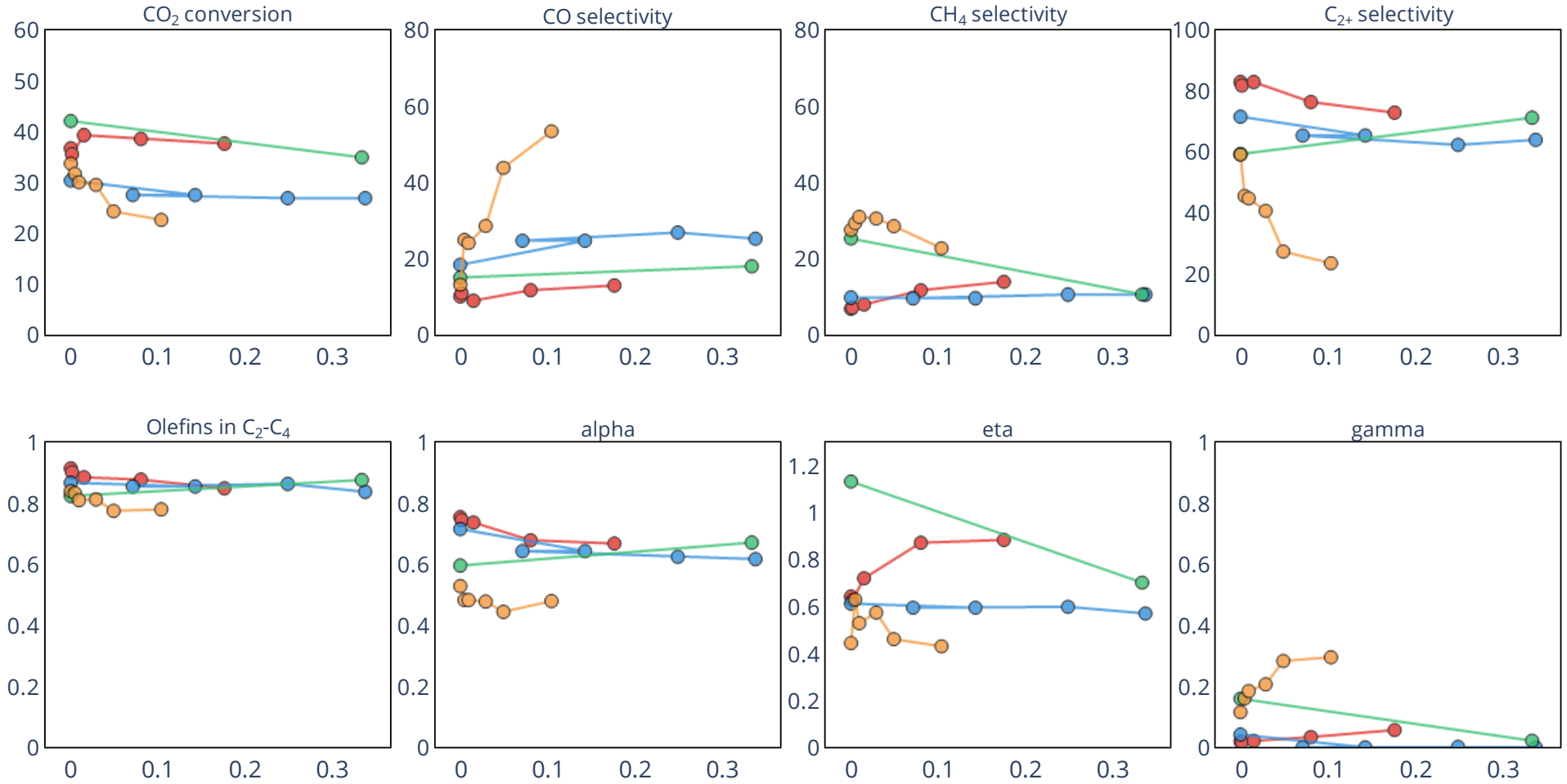

Figure S15. The dependencies between the parameters of different CO_2-FT catalysts and molar ratio Mn/Fe with alkali dopants. The same color means one specific catalysts from one article.

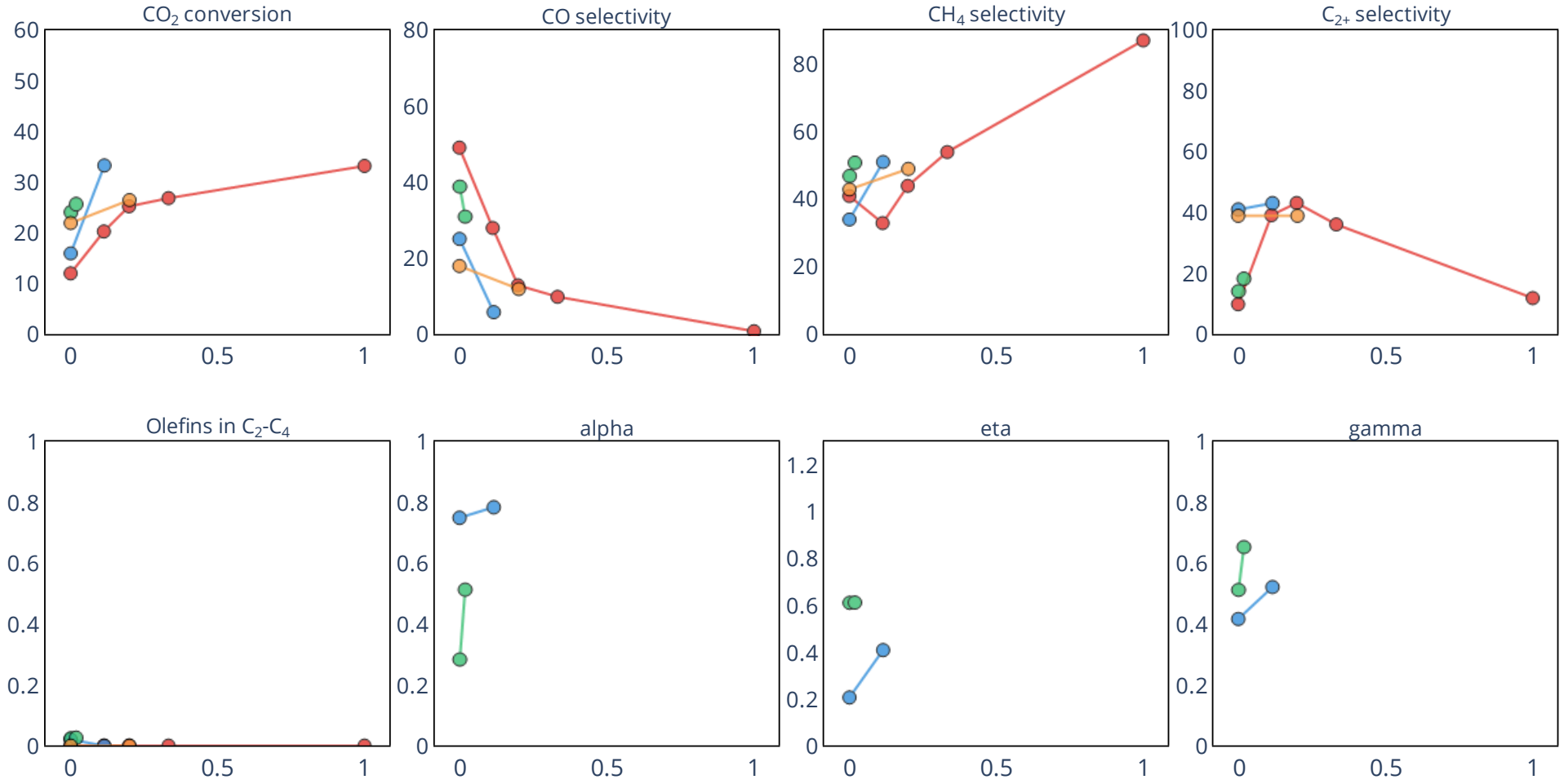

Figure S16. The dependencies between the parameters of different CO_2-FT catalysts and molar ratio Co/Fe without alkali dopants. The same color means one specific catalysts from one article.

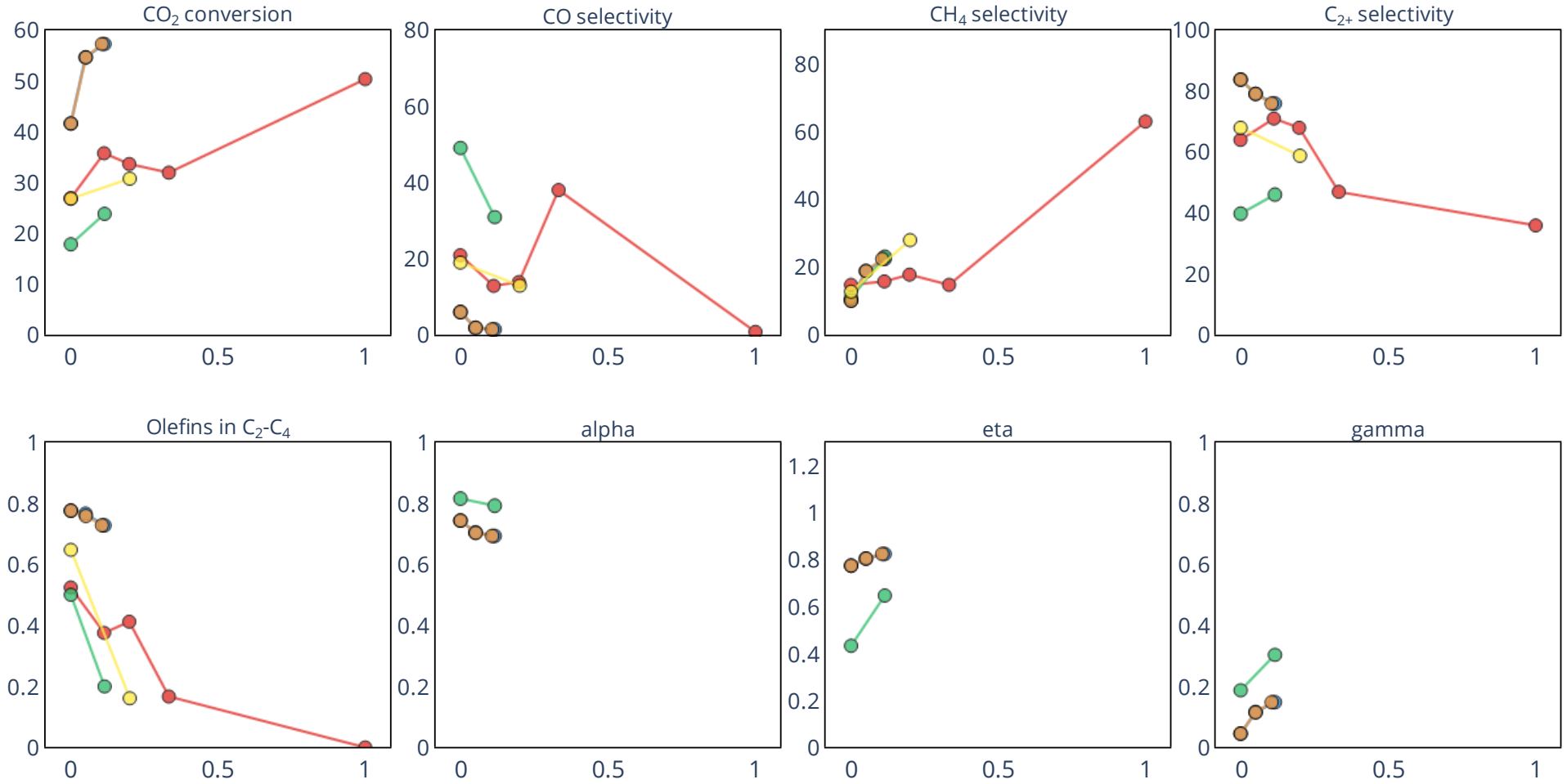

Figure S17. The dependencies between the parameters of different CO_2-FT catalysts and molar ratio Co/Fe with alkali dopants. The same color means one specific catalysts from one article.

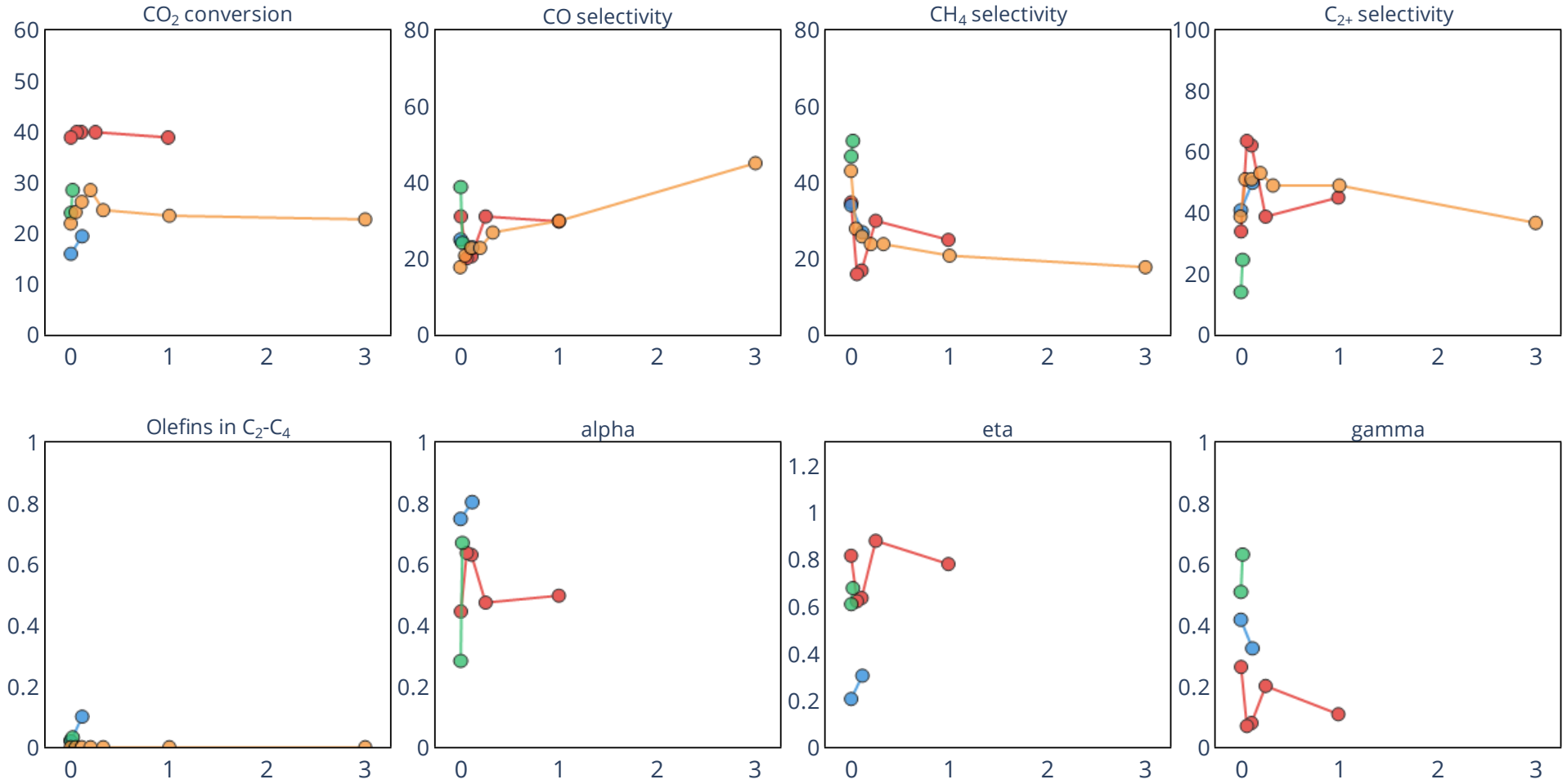

Figure S18. The dependencies between the parameters of different CO_2-FT catalysts and molar ratio Cu/Fe without alkali dopants. The same color means one specific catalysts from one article.

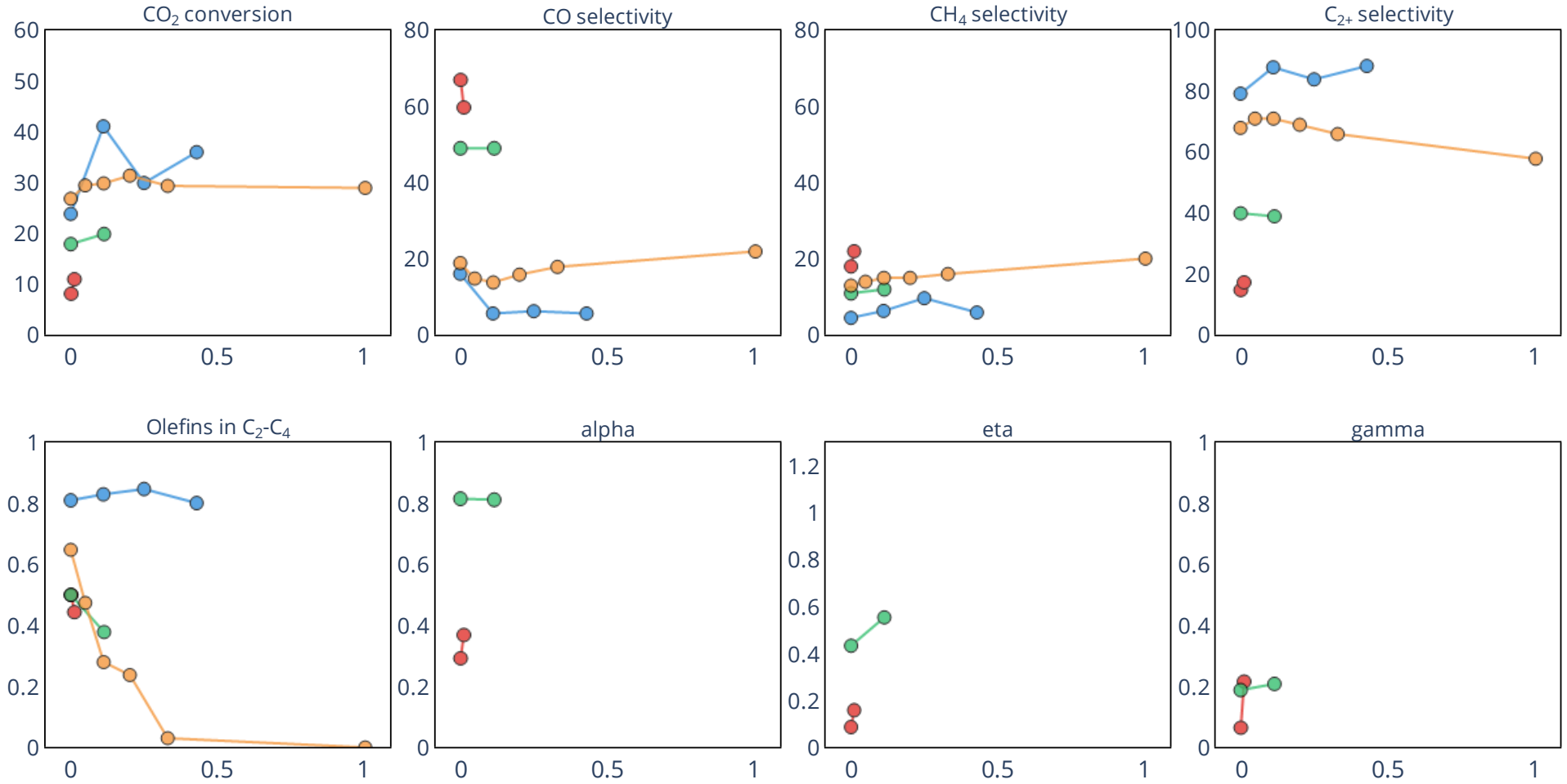

Figure S19. The dependencies between the parameters of different CO_2-FT catalysts and molar ratio Cu/Fe with alkali dopants. The same color means one specific catalysts from one article.

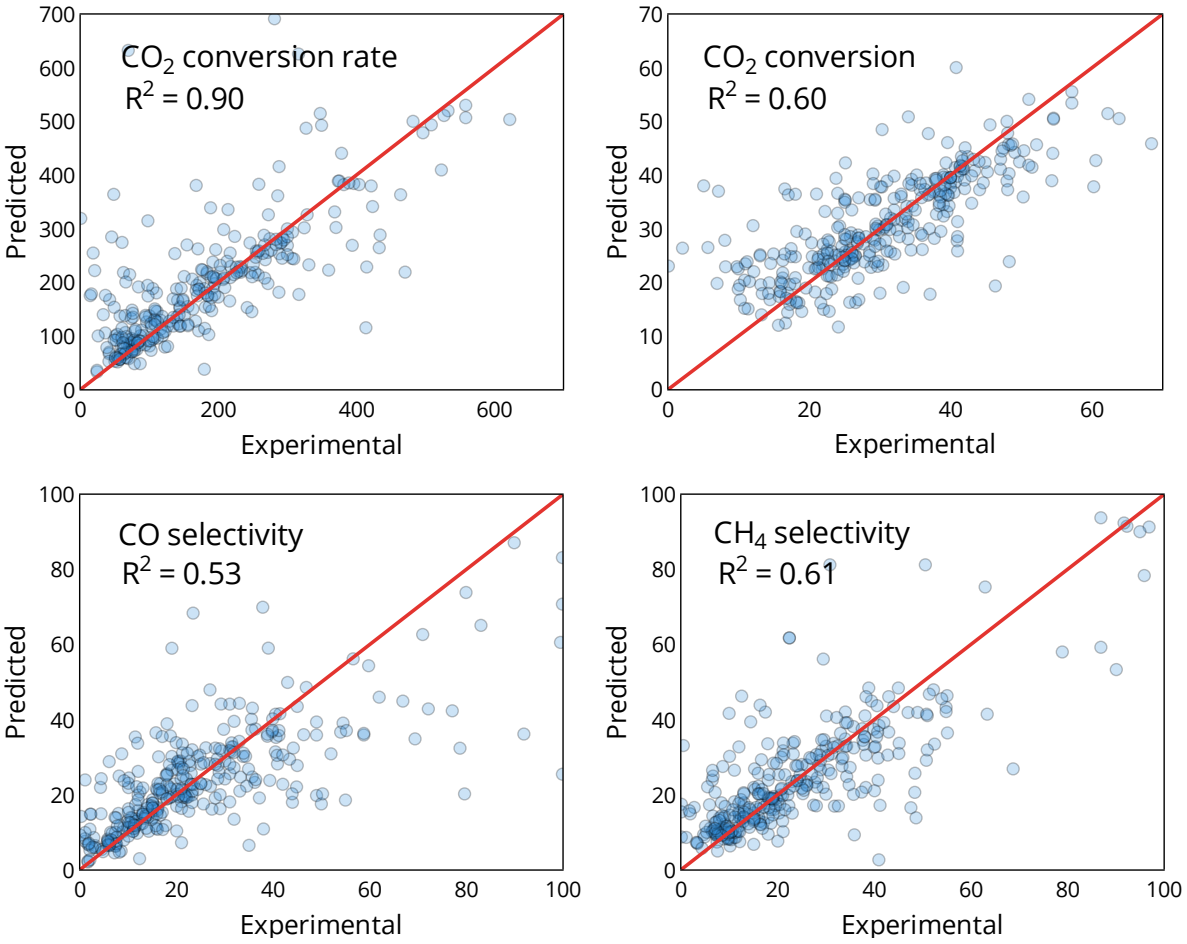

Figure S20. Performance of random forest regression model for prediction of catalytic parameters of CO_2-FT catalysts. The dependence between experimental and predicted values for test set on 10-fold cross validation.

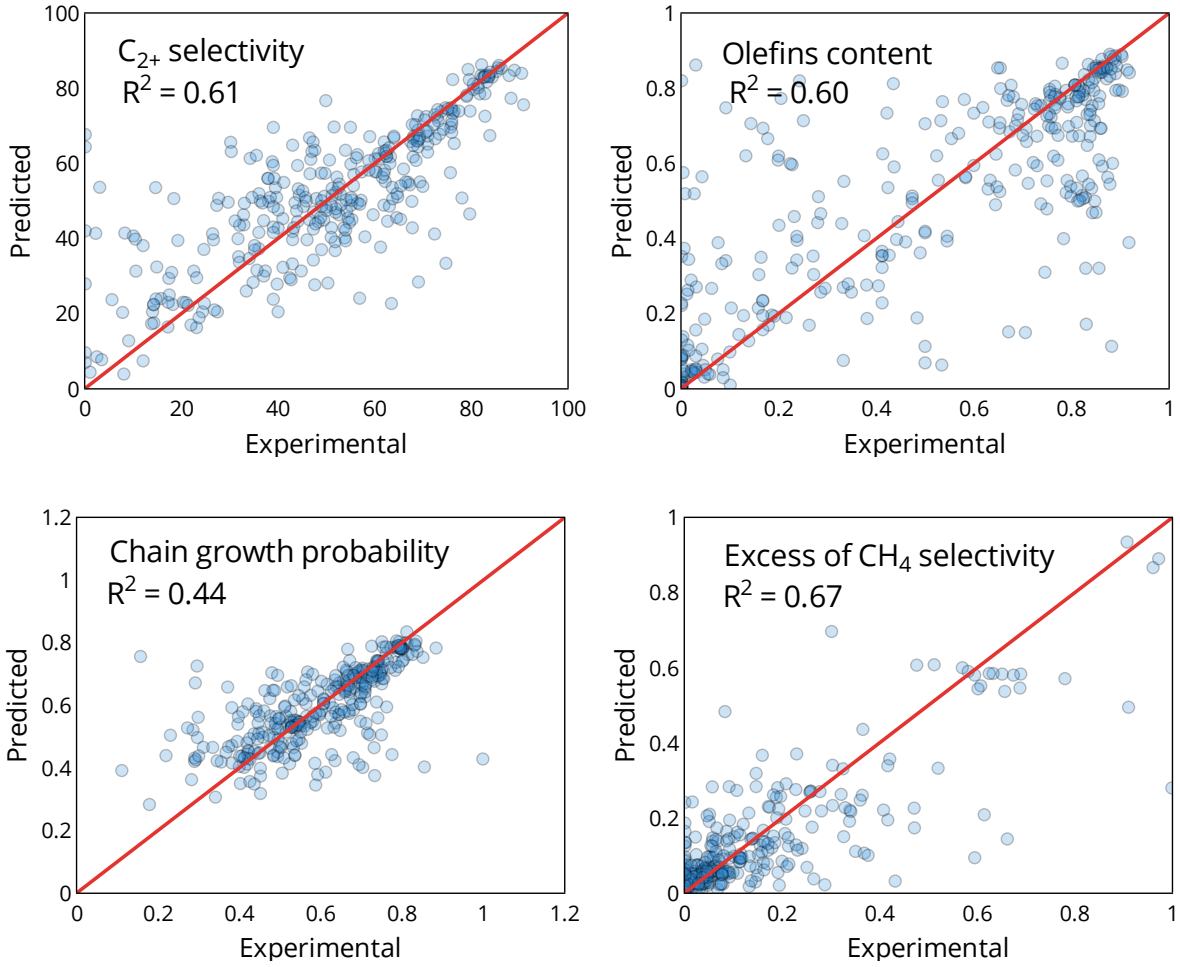

Figure S21. Performance of random forest regression model for prediction of catalytic parameters of CO_2-FT catalysts. The dependence between experimental and predicted values for test set on 10-fold cross validation.

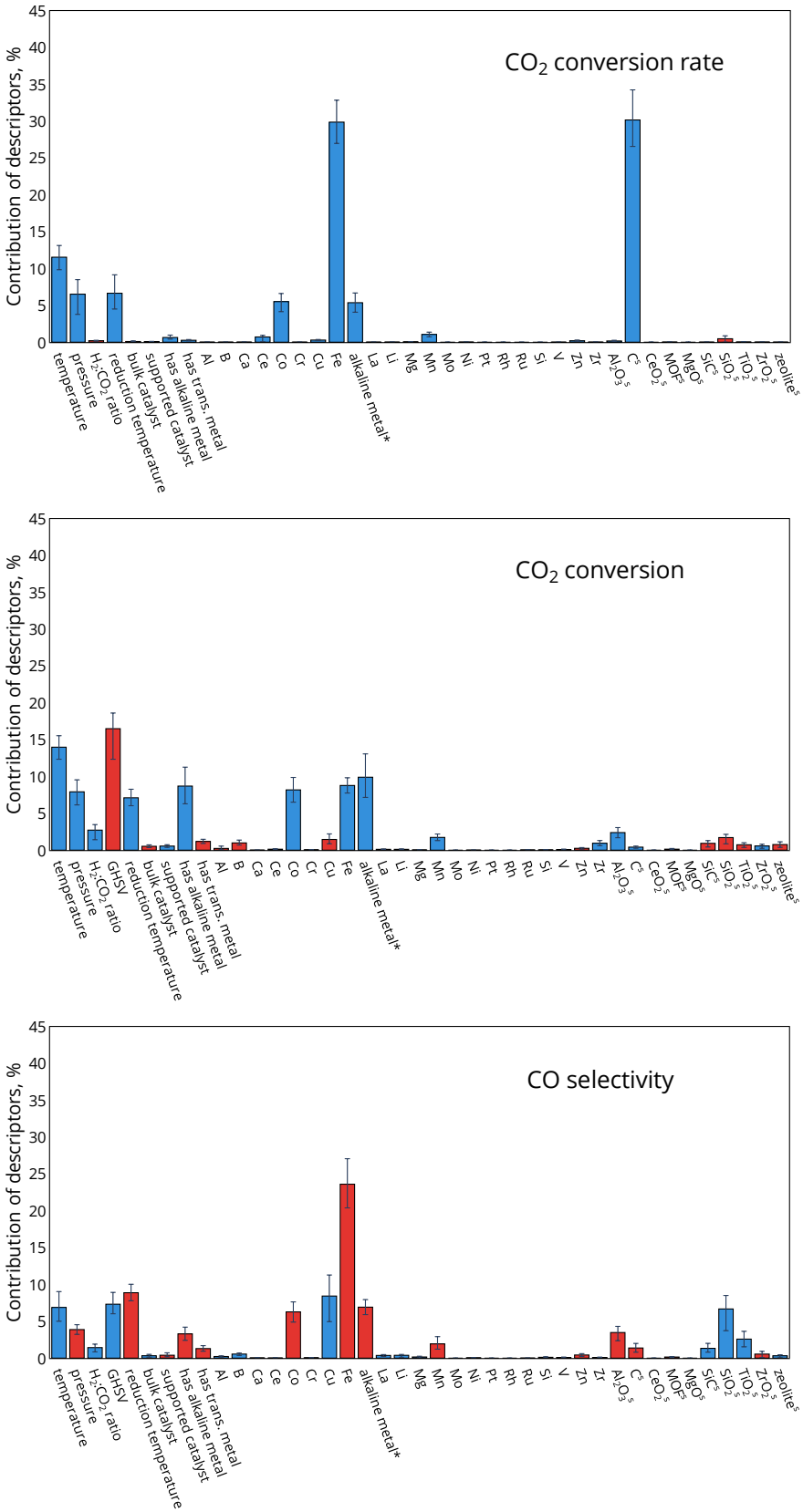

Figure S22. The histogram of descriptors importance calculated by using random forest regression model for CO_2 conversion rate, CO_2 conversion and CO selectivity. Blue bars are positive correlations, red bars – negative correlations.

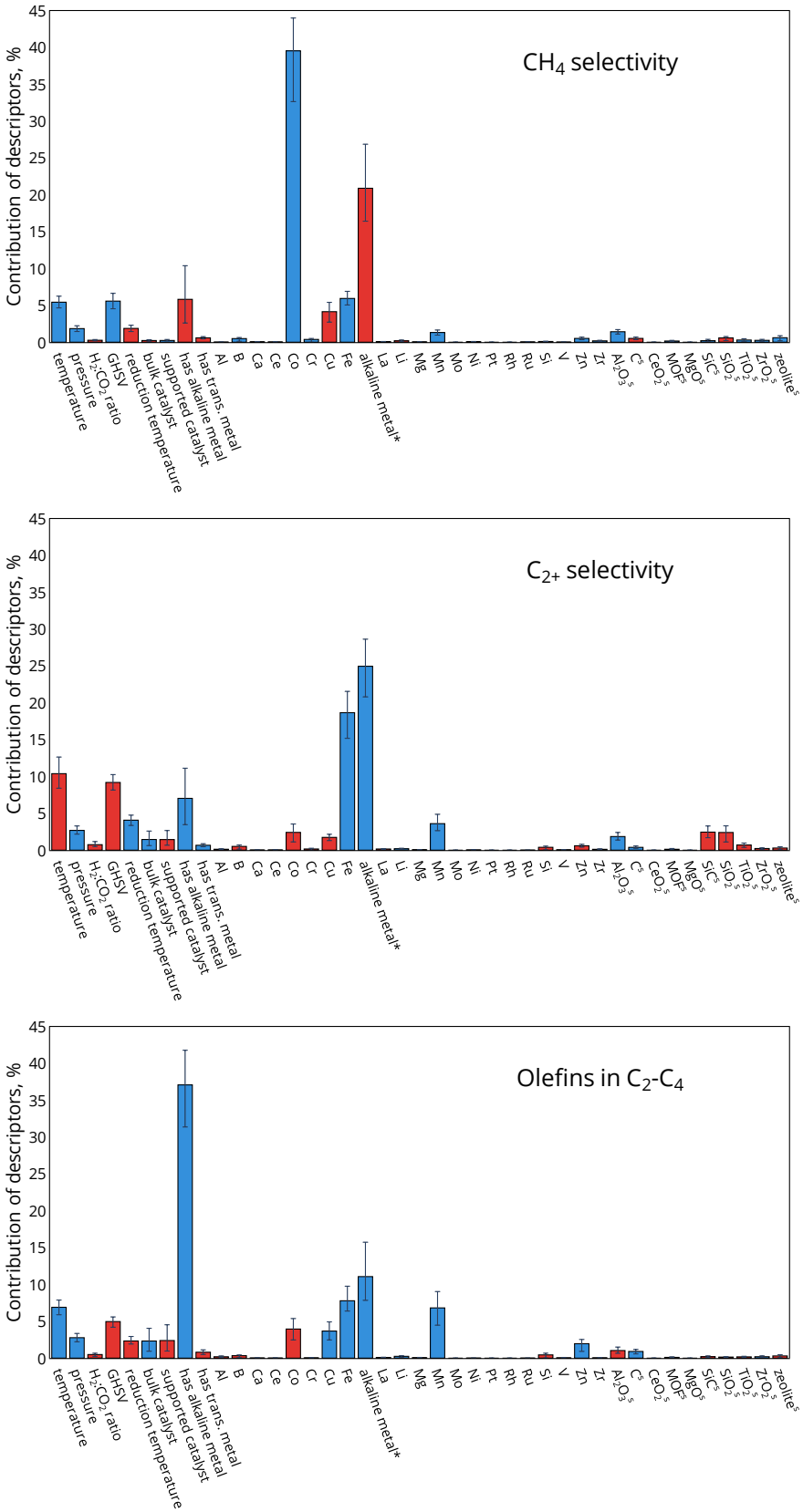

Figure S23. The histogram of descriptors importance calculated by using random forest regression model for CH_4, C_{2+} selectivity and olefin content in C_2-C_4. Blue bars are positive correlations, red bars – negative correlations.

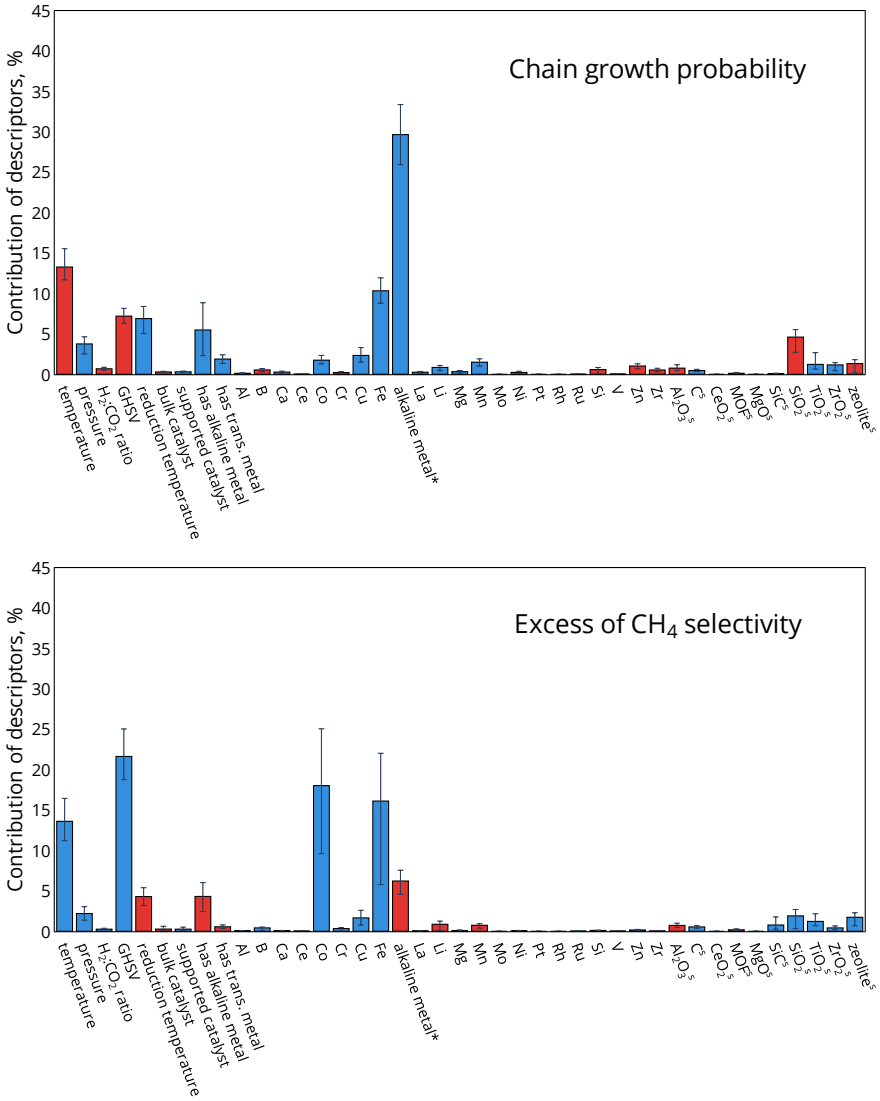

Figure S24. The histogram of descriptors importance calculated by using random forest regression model for α and γ. Blue bars are positive correlations, red bars – negative correlations.

Literature

[1] S. Geng, F. Jiang, Y. Xu, X. Liu, Iron-Based Fischer–Tropsch Synthesis for the Efficient Conversion of Carbon Dioxide into Isoparaffins, ChemCatChem, 8 (2016) 1303-1307.

[2] R.E. Owen, P. Plucinski, D. Mattia, L. Torrente-Murciano, V.P. Ting, M.D. Jones, Effect of support of Co-Na-Mo catalysts on the direct conversion of CO_2 to hydrocarbons, Journal of CO_2 Utilization, 16 (2016) 97-103.

[3] D.L. Williamson, C. Herdes, L. Torrente-Murciano, M.D. Jones, D. Mattia, N-Doped Fe@CNT for Combined RWGS/FT CO_2 Hydrogenation, ACS Sustainable Chemistry & Engineering, 7 (2019) 7395-7402.

[4] S. Wang, T. Wu, J. Lin, Y. Ji, S. Yan, Y. Pei, S. Xie, B. Zong, M. Qiao, Iron–Potassium on Single-Walled Carbon Nanotubes as Efficient Catalyst for CO_2 Hydrogenation to Heavy Olefins, ACS Catalysis, 10 (2020) 6389-6401.

[5] S.-C. Lee, J.-H. Jang, B.-Y. Lee, J.-S. Kim, M. Kang, S.-B. Lee, M.-J. Choi, S.-J. Choung, Promotion of hydrocarbon selectivity in CO_2 hydrogenation by Ru component, Journal of Molecular Catalysis A: Chemical, 210 (2004) 131-141.

[6] J. Zhang, S. Lu, X. Su, S. Fan, Q. Ma, T. Zhao, Selective formation of light olefins from CO2 hydrogenation over Fe–Zn–K catalysts, Journal of CO_2 Utilization, 12 (2015) 95-100.

[7] C.G. Visconti, M. Martinelli, L. Falbo, A. Infantes-Molina, L. Lietti, P. Forzatti, G. Iaquaniello, E. Palo, B. Picutti, F. Brignoli, CO_2 hydrogenation to lower olefins on a high surface area K-promoted bulk Fe-catalyst, Applied Catalysis B: Environmental, 200 (2017) 530-542.

[8] A. Ramirez, A. Dutta Chowdhury, A. Dokania, P. Cnudde, M. Caglayan, I. Yarulina, E. Abou-Hamad, L. Gevers, S. Ould-Chikh, K. De Wispelaere, V. van Speybroeck, J. Gascon, Effect of Zeolite Topology and Reactor Configuration on the Direct Conversion of CO_2 to Light Olefins and Aromatics, ACS Catalysis, 9 (2019) 6320-6334.

Applied Catalysis B: Environmental 328 (2023) 122505

Contents lists available at ScienceDirect

Applied Catalysis B: Environmental

journal homepage: www.elsevier.com/locate/apcatb

Elucidating reaction pathways occurring in CO_2 hydrogenation over Fe-based catalysts

Aleksandr Fedorov *, Henrik Lund, Vita A. Kondratenko, Evgenii V. Kondratenko, David Linke *

Leibniz-Institut für Katalyse e.V., Albert-Einstein-Str. 29a, 18059 Rostock, Germany

ARTICLE INFO

Keywords:
CO_2 hydrogenation
Segmental rates
Reaction pathways
Anderson-Schulz-Flory distribution

ABSTRACT

A detailed experimental analysis of reaction pathways proceeding in CO_2 hydrogenation over Fe-based catalysts was performed. The catalytic activity was measured at different degrees of conversion and used to analyze the production/consumption rates of reagents and products along the catalyst bed. It was demonstrated that except for the reverse water gas shift reaction and the subsequent hydrogenation of CO via Fischer-Tropsch (FT) mechanism, additional routes of hydrocarbon formation from CO_2 exist in the CO_2 hydrogenation. One of them is the methanation reaction which takes place over all studied catalysts. Another one is a direct pathway of C_{2+} hydrocarbon formation from CO_2 that plays a significant role at least for some catalysts. In this route, iron carbides may be responsible for hydrogenating CO_2 into C_{2+} hydrocarbons. Based on these results, the concept of requiring iron oxides as an essential active component for catalyzing the RWGS reaction in CO_2-FT should be reviewed.

1. Introduction

The increase in energy production and commodity products results in dramatic rise in emissions of carbon dioxide in the atmosphere. CO_2 is well-known to be the main reason of greenhouse effect, and thus, it motivates to develop new approaches and methods for reducing and controlling its emissions [1]. The capture of carbon dioxide and its chemical transformation to valuable organic compounds are considered as a perspective strategy for the development of clean and sustainable energy technologies [2–4]. They can be based on direct catalytic CO_2 hydrogenation with H_2 to higher hydrocarbons (CO_2-Fischer-Tropsch (CO_2-FT)) that is the one of a potential solution for the CO_2 emission problem [4–6].

It is generally accepted [7,8] that CO_2-FT synthesis proceeds through two stages: the endothermic reverse water gas shift reaction (RWGS, $CO_2 + H_2 \rightleftarrows CO + H_2O$) followed by the exothermic CO hydrogenation according to classical FT reaction (CO-FT, $CO + 2\ H_2 \rightarrow -(CH_2)- + H_2O$). The RWGS reaction has a thermodynamic limitation. The FT reaction has a kinetic limitation, wherein the fraction of hydrocarbons can be described by the Anderson-Schulz-Flory (ASF) distribution [9–11]:

$$W_n = n\cdot(1-\alpha)^2\cdot\alpha^{n-1}, \quad (1)$$

where n – carbon number; W_n – mass fraction of hydrocarbon with carbon number n; α – the chain growth probability that is defined as a ratio between the rate of the chain prolongation per the sum of the chain prolongation and termination rates [12,13].

Iron-based catalysts are usually applied for CO_2-FT, because they can catalyze both reactions [14–16]. It is considered that the RWGS reaction occurs on Fe_3O_4, while iron carbides (Fe_5C_2, Fe_3C etc.) formed in situ under reaction conditions are responsible for the CO-FT reaction [7]. Unpromoted Fe-based catalysts produce a lot of methane. To suppress this undesired reaction and to improve the performance of Fe-based catalysts to C_{2+} hydrocarbon production, various promoters are typically applied during catalyst preparation [17–24]. The most effective promoters are alkali metals (K, Na). They decrease CH_4 formation and increase the rate of CO_2 consumption and of C_{2+} hydrocarbon production. This positive effect is explained by an enhanced bonding strength of adsorbed CO_2 leading to a decrease in catalyst hydrogenation ability [18,25,26]. Moreover, alkali metals are able to accelerate the formation of Fe_5C_2 [27,28].

Kinetic modeling of CO_2 hydrogenation over Fe-containing catalysts is usually based on empirical Langmuir-Hinshelwood-Hougen-Watson (LHHW) models [14,29–31]. However, recently Carlotta Panzone et al. [32] proposed a detailed microkinetic model for CO_2 hydrogenation over a Fe-K/Al_2O_3 catalyst. All these models have been developed according to a two-stages mechanism of CO_2-FT, where the RWGS and

* Corresponding authors.
E-mail addresses: aleksandr.fedorov@catalysis.de (A. Fedorov), david.linke@catalysis.de (D. Linke).

https://doi.org/10.1016/j.apcatb.2023.122505
Received 19 December 2022; Received in revised form 13 February 2023; Accepted 20 February 2023
Available online 24 February 2023

FT reactions proceed over different active sites. The direct pathway of CO_2 hydrogenation to hydrocarbons via FT reaction was to our knowledge only considered in the paper published by Riedel et al. [14]. However, an experimental proof of the presence of direct route was not given. Besides, the data analysis of CO_2 hydrogenation catalysts performed by our group indicates the presence of the direct pathway for some catalytic systems [33]. Moreover, an additional pathway of direct CO_2 hydrogenation to methane, also known as the Sabatier reaction, was suggested and discussed in the works [15,34,35]. However, the reaction was not taken into account in kinetic modeling. Recently, Skrypnik et al. [3] performed the analysis of the spatial profiles of C_{2+} formation rates and composition distribution along the catalyst bed for CO_2-FT. It was demonstrated that the highest formation rate of C_{2+} hydrocarbons was observed at the front part of the bed, wherein, Fe was present in the form of Fe_5C_2 at this part of bed but not as iron oxide which is supposed to catalyze the RWGS reaction. From this we concluded that the two-stage mechanism may be a too simple model and Fe_5C_2 could possibly also catalyze the RWGS reaction. It should be also noted that the analysis of pathways was usually performed for CO, CH_4, and C_{2+} hydrocarbons; the individual analysis of the formation of each hydrocarbon has not been considered. Wherein, the ASF analysis of rates of hydrocarbon formation and especially the deviation from ASF distribution can give additional information about the mechanism of CO_2 hydrogenation.

Reviewing the literature on the CO_2-FT synthesis revealed that different pathways of CO_2 hydrogenation were suggested and considered. Despite a number of studies, there are still fundamental questions open regarding the mechanism and reaction pathways occurring in CO_2 hydrogenation into hydrocarbons. Thus, the present work is devoted to investigating and analyzing reaction pathways proceeding in the process of CO_2 hydrogenation to hydrocarbons using typical Fe-based catalysts. For this, the iron-based catalysts with/without different dopants (K, K and Mn, K and Al) were synthesized by using an organic-combustion method that is effective for the preparation of highly active and selective catalysts in direct CO_2 hydrogenation to hydrocarbons [7]. K was chosen as dopant because it is the most effective and preferable promoter for improving the performance of Fe-based catalysts [33,36–39]. Mn is the most effective transitional metal as a dopant for Fe-based catalysts according to statistical analysis [17,40]. Moreover, a synergic effect between Mn and K metals was reported in work [41]. Al dopant was chosen as a textural promoter [14]. The obtained catalysts were tested in CO_2 hydrogenation. By varying the residence time, we obtained data on product selectivity in a wide range of CO_2 conversion from 2.5 % to 30 % in small increments of CO_2 conversion which allowed estimating rates of reagents consumption and products formation along the catalyst bed using simple arithmetic operations and analyze the mechanism of CO_2 hydrogenation without kinetic modeling. The ASF distribution was used for analyzing the rates of hydrocarbon formation.

2. Experimental part

2.1. Catalyst synthesis

In this study, the catalysts were obtained by an organic-combustion method. The solutions of nitrates and citric acid (CA) were prepared by mixing iron (III) nitrate nonahydrate (99.0 %, Merck), potassium nitrate (99.7 %, Fischer Chemical), aluminum nitrate nonahydrate (98 %, ChemPure), manganese (II) nitrate hydrate (97 %, Sigma Aldrich), and citric acid monohydrate (99.5 %, ChemSolute), in distilled water. The obtained solutions (the solution volume is around 100 cm^3 for the preparation of ~ 3.5 g of catalyst, the concentrations of compounds in the solutions are presented in the Table 1) were heated in air up to 200 °C (the heating rate was 1 K/min) in an electrically oven and hold at this temperature up to combustion of the mixtures.

The obtained deposits were removed from the oven and crushed in a mortar. Resulting powders were heated in air up to 600 °C (ramp 10 K/min) and finally calcined at 600 °C for 4 h in an electrically oven. The samples were marked as Fe, Fe-K, Fe-K-Al, and Fe-K-Mn. The molar ratio of Fe:K and Fe:(Al or Mn) was 10:1 in the promoted catalysts. Molar ratios of citric acid (CA) to precursor metal ion were CA:Fe = 5:6, CA:K = 5:18, CA:Al = 5:6, and CA:Mn = 1:2 which corresponds to the stoichiometric amount required for the combustion reaction between metal nitrate and citric acid. As an example, the reaction between iron nitrate and citric acid can be written as:

$$6Fe(NO_3)_3{\cdot}9H_2O + 5C_6H_8O_7{\cdot}H_2O \rightarrow 3Fe_2O_3 + 9N_2 + 30CO_2 + 79H_2O \quad (2)$$

The mass ratio water:(citric acid + precursor) was 5.0.

Table 1
The concentrations of compounds in the solutions used for the catalyst preparation.

The sample	Concentration, M				
	$Fe(NO_3)_3$	KNO_3	$Al(NO_3)_3$	$Mn(NO_3)_2$	$C_6H_8O_7$
Fe	2.0	–	–	–	1.67
Fe-K	2.0	0.2	–	–	1.72
Fe-K-Al	2.0	0.2	0.2	–	1.89
Fe-K-Mn	2.0	0.2	–	0.2	1.82

2.2. Catalyst characterization

To determine the surface area of the catalysts, low-temperature nitrogen adsorption-desorption isotherms were obtained at − 196 °C using BELSORP-max II (BEL Japan, Inc.) instrument. Before the measurements, the samples were heated in vacuum at 250 °C for 2 h. The initial branch of N_2 adsorption isotherm in the range of P/P_0 (0.05–0.25) was used to calculate the BET surface area.

The mass fraction of Fe, K, Al, and Mn in the catalysts was determined by inductively coupled plasma optical emission spectroscopy (ICP-OES) on Varian 715-ES ICP-Emission-Spectrometer. 10 mg of each sample was mixed with 8 ml of aqua regia. The sample preparation system “Multiwave PRO” from Anton Paar was used at 220 °C and 50 bar for the sample digestion with a microwave-assisted method. The digested solution was filled up to 100 ml and measured with ICP-OES. The data analysis was performed on the Varian 715-ES software “ICP Expert”.

The tests of temperature-programmed reduction with hydrogen (TPR-H_2) were performed in an in-house build set-up equipped with 8 quartz tubular reactors connected to an on-line mass spectrometer (Pfeiffer OmniStar GSD 300 01) for analysing the outlet gas flow. Before the tests, the samples were placed inside the reactor and heated up to 300 °C in a flow of Ar (20 ml/min) for 4 h. After cooling down to room temperature, a flow (5 % H_2 in Ar) was fed (20 ml/min) to the reactors followed by heating up to 900 °C with a constant heating rate 10°/min. The atomic mass units 2 (H_2) and Ar (40) were used to determine the H_2 concentration.

XRD powder patterns were recorded on a Stoe Stadi P transmission diffractometer equipped with a DECTRIS Mythen2 1 K detector applying Ge (111) monochromatized Mo Kα1 radiation (50 kV, 40 mA, 0.70930 Å). The samples were ground to a fine powder and placed between two acetate foils before the measurement. Data acquisition was done with 0.01 s^{-1}. Peak positions and profiles were fitted with Pseudo-Voigt function using the HighScore Plus software package (Panalytical). Phase identification was done by using the PDF-2 database of the International Center of Diffraction Data (ICDD). To estimate content of Fe-containing phases in the samples, the reference intensity ratio (RIR) method [42] was used; n-paraffin and $MnCO_3$ phases were neglected when estimating the fraction of carbidic and oxidic iron phases in the obtained catalysts. It is worth noting that we tried to apply the Rietveld method for determination of phase composition but due to the complexity of phase composition of the studied samples we were not able to obtain reliable results.

2.3. Transient experiments and their kinetic evaluation

Mechanistic and kinetic aspects of CO_2 and H_2 adsorption over the catalysts tested in CO_2 hydrogenation (the spent catalysts) were studied in the temporal analysis of the product reactor (TAP-2) system, which was described in detail in Refs. [43–45]. In a typical experiment, each catalyst (14 mg, 250–350 μm fraction) was placed in a home-made quartz-tube reactor within its isothermal zone between two layers of quartz particles of the same size. Previous to pulse experiments, the catalyst was heated in H_2-CO_2 mixture (H_2 flow rate was 4.50 $cm^3 \cdot min^{-1}$; CO_2 flow rate was 1.94 $cm^3 \cdot min^{-1}$) from room temperature to 300 °C and held at this temperature for 2 h. After that the reactor was evacuated to ca. 10^{-5} Pa.

Transient experiments with CO_2/Ar = 1:1 or H_2/D_2/Ar = 1:1:1 mixtures were performed at 300 °C in the single pulse mode. The mixtures were prepared using H_2 (Air Liquide, 5.0), D_2 (CK Special Gases Limited, 2.8), CO_2 (Air Liquide, 4.5) and Ar (Air Liquide, 5.0) without additional purification. In experiments with CO_2 the pulse size was below 10^{15} molecules per pulse to ensure Knudsen diffusion regime. The composition of the gases leaving the reactor was quantitatively analyzed by a quadrupole mass spectrometer (HAL RC 301 Hiden Analytical). The following atomic mass units (AMUs) were used for mass-spectrometric identification of different compounds: 44 (CO_2), 32 (O_2), 28 (CO_2, CO), 4 (D_2), 3 (HD), (H_2) and 40 (Ar). Pulses were repeated 10 times for each AMU and averaged to improve the signal-to-noise ratio. The concentration of each gaseous component was calculated from the ratio of the area of signal recorded at the respective AMU to the area of Ar. The fragmentation patterns and sensitivity factors required for the calculations were determined separately by pulsing the same mixtures in the reactor filled only with quartz particles. Using a model-free approach developed for this technique, [46] the experimental responses of CO_2 and Ar were transformed into the dimensionless form according to Eqs. (3) and (4). Such transformation allows to unambiguously determine the type of interactions (diffusion, reversible, or irreversible adsorption) of feed components with catalysts.

$$Dimensionless\ flow = \frac{flux(CO_2\ or\ Ar)\cdot reactor\ length^2}{N(CO_2\ or\ Ar)\cdot D^{eff}_{Knudsen}(CO_2\ or\ Ar)} \tag{3}$$

$$Dimensionless\ time = \frac{t\cdot D^{eff}_{Knudsen}(CO_2\ or\ Ar)}{reactor\ length^2} \tag{4}$$

$$Flux(CO_2\ or\ Ar) = I(CO_2\ or\ Ar)\frac{N(CO_2\ or\ Ar)}{\int_0^t I(CO_2\ or\ Ar)dt} \tag{5}$$

where $I(CO_2\ or Ar)$, $N(CO_2\ or\ Ar)$, and $D^{eff}_{Knudsen}(CO_2\ or\ Ar)$ are the experimental mass spectroscopic signal intensity, the number of molecules per pulse, and the diffusion coefficient, respectively. To determine the diffusion coefficient of CO_2, the diffusion coefficient of Ar was initially derived through fitting the experimental response of this gas to the Knudsen diffusion model, as described in [45,47]. Eq. (6) was used to obtain the required coefficient:

$$D^{eff}_{Knudsen}(CO_2) = D^{eff}_{Knudsen}(Ar)\sqrt{\frac{M(Ar)}{M(CO_2)}} \tag{6}$$

To obtain the kinetic parameters of CO_2 interaction with spent catalysts, transient responses of CO_2 were fitted to a model considering non-dissociative reversible adsorption of CO_2, as described in Refs. [45, 47]. The TAP reactor was considered as a one pseudo-homogeneous system and divided into three different zones: upstream inert zone, catalyst zone and downstream inert zone. The mass balances for gas-phase and surface species outside the catalyst layer can be described using Eqs. (7) and (8), respectively:

$$\frac{\partial C_i}{\partial t} = D^{eff}_{Knudsen}\frac{\partial^2 C_i}{\partial x^2} \tag{7}$$

$$\theta_i = 0 \tag{8}$$

where C_i – the concentration of CO_2 or Ar, t – the time, and x – the coordinate along the reactor. In the catalyst zone, the reaction term was included in the mass balances for gas-phase (Eq. (9)) and surface species (Eq. (10)):

$$\frac{\partial C_{CO_2}}{\partial t} = D^{eff}_{Knudsen}\frac{\partial^2 C_{CO_2}}{\partial x^2} - N_{total}\cdot(k_+\cdot C_{CO_2}\cdot(1-\theta_{CO_2}) - k_-\cdot\theta_{CO_2}) \tag{9}$$

$$\frac{\partial \theta_{CO_2}}{\partial t} = k_+\cdot C_{CO_2}\cdot(1-\theta_{CO_2}) - k_-\cdot\theta_{CO_2} \tag{10}$$

where N_{total} is the total concentration of surface species and $\theta_{CO_2} = \frac{N_{CO_2}}{N_{total}}$, where N_{CO_2} stands for the concentration of adsorbed CO_2.

The following boundary conditions are applied for solving these partial differential equations:

$$C_i = 0,\ \text{for all species at outlet of the reactor} \tag{11}$$

$$\frac{\partial C_i}{\partial x} = 0,\ t \geq t_{open},\ \text{at the inlet of the reactor} \tag{12}$$

$$\frac{\partial C_{in}}{\partial x} = \left.\frac{\partial C_{in}}{\partial x}\right|_{t=0}\left(1-\frac{t}{t_{open}}\right),\ at\ t < t_{open}, \text{at the inlet of the reactor} \tag{13}$$

where t_{open} – opening time of pulse valve. The condition 12 describes high vacuum conditions at reactor outlet. The second condition (Eq. (13)) considers the fact that the gradient of the gas concentrations at the inlet is zero since the reactor is closed at each time after introduction of the reactant gas. The inlet pulse of reactant is described as gradient for a certain interval, which is dropped linearly up to zero at $t = t_{open}$ (t_{open} is ca. 10 ms) [45].

The resulting system of partial differential equations was solved using a FORTRAN-program applying the numerical routine PDEONE [48]. The search for kinetic parameters was performed in a wide range of possible values (10^{-4}–10^8) using first a genetic algorithm to find good starting values and then the Nelder-Mead simplex algorithms [49]. The quality of fit was characterized by an objective function defined as the sum of squares of the shortest deviation between the respective points of the experimental and simulated data.

2.4. Catalytic tests

Catalytic tests were carried out in an in-house developed setup containing 16-continuous-flow fixed bed stainless-steel tube reactors. The reactors are grouped in sets of 4. Each of these reactor sets has its own heating; the heating design assures high heat-transfer rates between furnace and reactor tube in order to maintain the set temperature even for more exothermic reactions. The outer and inner diameters of reactors are 9.5 and 7.0 mm, respectively. CO_2, H_2, N_2, and He gases were dosed by electronic mass flow controllers (Brooks 5850s). The total flow of feed gases was equally distributed among all the reactors and a bypass channel. The outlet lines from reactors are split at 150 °C into a main flow and a sample portion where the sample portion is connected to a 16-channels automatic valve to select and direct one stream to a gas chromatograph through a heated line (its temperature is 180 °C). A flow of He (3 ml min^{-1} per reactor) is additionally added to this sample stream to prevent condensation of long-chain hydrocarbons. The main flows are led through hot traps where a wax phase is condensed (at 150 °C). The remaining gas streams are combined and passed through a cold trap where H_2O is condensed before they reach the electronic pressure controller (Brooks 5866s).

The catalysts (100 mg, 0.25–0.45 mm) were diluted by SiC (ESK-SiC,

F54, 0.2–0.5 mm fraction) to carry out tests at isothermal condition. The weight fraction of SiC to catalyst was 3:1. Regardless of the mixture of the catalyst and SiC, an additional layer of SiC (800 mg, ESK-SiC, F54, 0.2–0.5 mm fraction) was added on the top to ensure plug flow and to preheat the reaction feed.

The feed components (bypass channel) and the reaction products were analyzed by on-line Agilent 7890A gas chromatograph equipped with a thermal conductivity detector (TCD) and two flame ionization detectors (FID). HP Plot/Q (for CO_2) and MolSieve 5A (for H_2, O_2, N_2, and CO) columns were connected to TCD. For separating hydrocarbons and alcohols, PONA (for C_5-C_{16} hydrocarbons) and HP Plot/Q (for C_1-C_4) columns connected to FIDs were used.

Before catalytic testing the as-prepared catalysts were heated up to 300 °C (the heating rate was 5°/min) in N_2 flow at 1.5 bar (abs.) and after that were reduced in-situ. The hydrogen concentration was increased stepwise, starting with 10 % H_2 in N_2 flow for 10 min, then 30 % H_2 in N_2 flow for 10 min, 50 % H_2 in N_2 flow for 10 min, and finally undiluted CO-H_2 mixture (CO:H_2 was 1:2) for 240 min. During these steps the temperature was kept at 300 °C, pressure at 1.5 bar (abs.) and the residence time was 136 kg s m^{-3}. After the reduction, the catalysts were tested under CO_2-FT conditions (CO_2:H_2:N_2 ratio was 1:3:1) at 15 bar, 300 °C, and at a modified residence time of 328 kg s m^{-3} for 25 h to achieve a steady-state condition. After this, the residence time was varied in a range of 8–328 kg s m^{-3} by adjusting the feed flow rate in a range of 1097–45,000 ml h^{-1}. The time on stream for each condition was 10 h.

The CO_2 conversion (X) and products selectivity were calculated by the following equations:

$$X = 1 - \frac{\dot{n}_{CO_2}^{out}}{\dot{n}_{CO_2}^{in}}, \tag{14}$$

$$S_i = \frac{a_i \cdot \dot{n}_i^{out}}{\sum_{j=1}^{n} a_j \cdot \dot{n}_j^{out}}, \tag{15}$$

where $\dot{n}_{CO_2}^{in}$ – the molar flow of CO_2 in the inlet flow; $\dot{n}_{CO_2}^{out}$ – the molar flow of CO_2 in the outlet flow; S_i – the selectivity of i-product; a_i – the carbon number of i-product; $\dot{n}_i^{out}$ – the molar flow of i-product in the outlet flow. Carbon balance was established to be higher than 98 %.

2.5. The data evaluation

The catalyst activity was determined at different values of the modified residence time τ_{mod} that can be defined as:

$$\tau_{mod} = \frac{m_{cat}}{F}, \tag{16}$$

where m_{cat} – the mass of the catalyst; F – the feed flow. Let M_f be a set of the flows as (F_0, F_1, F_2 … F_n), wherein the set is sorted in ascending order. Thus, F_0 and F_n are 1097 and 45,000 ml h^{-1}, respectively. It can be presented as the set of (F_0, $\gamma_1 F_0$, $\gamma_2 F_0$ … $\gamma_n F_0$), where γ_i – dimensionless constants. Thus, the data with the different modified residence times obtained by varying the feed flow can be presented as data with the fixed flow F_0 and different catalysts mass as (m_{cat}, m_{cat}/γ_1, m_{cat}/γ_2 … m_{cat}/γ_n). In this context, the catalyst bed can be presented as a list of catalyst segments that are graphically shown in Fig. 1.

Where the catalyst mass m_i in segment i can be calculated as:

$$m_i = m_{cat} \Big/ \gamma_{n-i+1} - \sum_{j=1}^{i-1} m_{cat} / \gamma_{n-j+1}, \tag{17}$$

It allows one to calculate the compound formation rates in i-segment according to the following formula:

$$r_j^i = \frac{\dot{n}_j^i - \dot{n}_j^{i-1}}{m_i}, \tag{18}$$

where r_j^i – the rate of the formation of j-compound in the segment i (mol g^{-1} s^{-1}); $\dot{n}_j^i$ and $\dot{n}_j^{i-1}$ – molar flows of j-compound in segments of i and i-1, respectively (mol s^{-1}). The example of the calculation of the segmental rates is presented in the supplementary material (pages 3–4).

The AFS distribution was used for the analysis of the formation rates of hydrocarbons. Let r_n be the formation rate of hydrocarbon with carbon number n. Assuming the absence of the deviations from the ASF distribution, one can show that:

$$\begin{aligned} &\frac{r_n}{r_{n-1}} = \frac{\alpha^{n-1}}{\alpha^{n-2}} \\ &r_n = r_1 \cdot \alpha^{n-1} \\ &\log r_n = n \cdot \log \alpha + \log \frac{r_1}{\alpha} \end{aligned} \tag{19}$$

where α is the chain growth probability. The α and r_1 parameters were calculated by linear fitting in the corresponding coordinates $(n, \log r_n)$ using the data of the hydrocarbon rates calculated by Eq. (18) (see Fig. S1). To calculate the parameters of $\log\alpha$ and $\log r_1$, the rates of C_{3+} hydrocarbons formation were used because it is known that the deviations from the ASF distribution are usually observed for C_1 and C_2 hydrocarbons [33]. The relative 'rates' r^{rel} of hydrocarbons formation were defined as:

$$r_n^{rel} = \frac{r_n^{\exp}}{r_n^{ASF}} \cdot 100\%, \tag{20}$$

where $r_n^{\exp}$ – the formation rate of hydrocarbon with carbon number n calculated by the Eq. (18); r_n^{ASF} – the rate of the formation of hydrocarbon with carbon number n calculated by the equation 19 using α and r_1 parameters. Python programming language (version 3.8.10) [50] and a scientific library NumPy (version 1.20.3) [51] were used for the calculations. Plotly (version 5.1.0) [52] was used to visualize the results.

3. Results and discussion

3.1. Catalyst characterization

Elemental composition and textural characteristics of as-prepared catalysts are summarized in Table S1. The content of dopants in the obtained catalysts measured by ICP corresponds to the theoretical content. It is worth mentioning that the samples are characterized by low values of specific surface area. Wherein, the highest value of 30 m^2 g^{-1} is observed for Fe-K-Al catalyst that was doped by aluminum. Al is known to be a textural promoter that can lead to an increase in surface area [53].

To investigate the reducibility of the obtained catalysts, TPR-H_2 tests were performed. The profiles of TPR-H_2 curves for the as-prepared catalysts are presented in Fig. S3. In the case of the unpromoted Fe

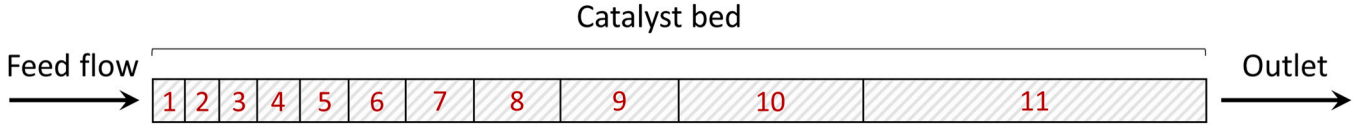

Fig. 1. The derived segments of the catalyst bed.

catalyst, one can see three broad peaks of hydrogen consumption with the maxima at 425, 630, and 780 °C respectively. They relate to three stages process of the reduction of iron oxide ($Fe_2O_3 \rightarrow Fe_3O_4 \rightarrow FeO \rightarrow Fe$) [54]. The profiles of TPR-H_2 curves for the promoted catalysts are similar. However, slight changes in the TPR-H_2 profiles such as shift and broadening of the first peak is observed. The shift of the maximum of the first peak to higher temperature is related to the presence of K, Al and/or Mn in the catalysts as shown in the works [34,53]. Moreover, for the Fe-K-Mn catalyst an additional peak in the temperature range 270–370 °C is observed that may be related to reduction of Mn-containing phases [55].

To identify phase composition of the obtained catalysts, the samples were characterized by XRD. Besides as-prepared catalysts, the catalysts after reduction in CO:H_2 mixture (the ratio was 1:2) (reduced catalysts) and after testing in CO_2 hydrogenation (spent catalysts) were investigated. XRD patterns are presented in Figs. S4-S6. The information about phase composition of the samples are summarized in Table 2. According to the obtained results, the unpromoted Fe catalyst contains only α-Fe_2O_3 hematite phase that is indicated by an existence of corresponding reflexes (PDF 01–087–1164). The phase composition of promoted Fe-K, Fe-K-Al, and Fe-K-Mn catalysts are complex mixtures of different oxides. Besides α-Fe_2O_3 and Fe_3O_4 the K-containing phase $KFe_{11}O_{17}$ was found for all K-doped catalysts. Moreover, the additional phase of Mn_2O_3 was identified in the case of Fe-K-Mn catalyst. No Al-containing phases were detected in the Fe-K-Al catalyst.

After reduction in CO:H_2 mixture, the presence of Fe_5C_2, α-Fe_2O_3, Fe_3O_4 and Fe phases was found for the pure Fe catalyst. Thus, iron carbide was formed after CO:H_2 treatment. The formation of iron carbides from Fe_2O_3 under CO-H_2 mixture is known to proceed via $FeO_x \rightarrow Fe \rightarrow FeC_x$ reactions [56]. It explains the presence of Fe and Fe_3O_4 phases in the reduced catalysts. The iron carbides were also found for reduced Fe-K, Fe-K-Al, and Fe-K-Mn catalysts. Moreover, the reflexes at 10° and 12° at 2θ indicate the presence of n-paraffin in the reduced Fe-K and Fe-K-Mn catalysts. Thus, the formation of hydrocarbons via FT reaction takes place under treatment in CO-H_2 mixture for these catalysts. In the case of the reduced Fe-K-Mn catalyst, Mn was found to be in the form of mixed oxide $Fe_xMn_{1-x}O$ of cubic structure (F*m-3 m* symmetry).

The spent Fe catalyst consists of iron carbides (Fe_5C_2, Fe_7C_3) and Fe_3O_4 phases. The mixture of iron carbides and oxides were also found for the spent K-promoted catalysts. In addition, XRD data indicate the presence of n-paraffin in the Fe-K, Fe-K-Al, Fe-K-Mn catalysts. The phase of $MnCO_3$ was detected for the Fe-K-Mn catalyst. Thus, iron in the spent catalysts is presented in the form of iron carbides and oxides. The content of Fe-containing phases in the spent samples was estimated with the reference intensity ratio (RIR) method. The content of iron carbides are 40, 96, 66, and 93 wt% for the spent Fe, Fe-K, Fe-K-Al, and Fe-K-Mn catalysts, respectively. Thereby, doping by K of Fe-based catalyst stabilizes the formation of iron carbides that is agreed with conclusions made in the works [28]. One can suppose that doping by alumina counteracts the formation of iron carbides under CO/CO_2-H_2 conditions. Al as a textural promoter reduces the formation of carbides from iron oxides during the reduction in CO-H_2. This was also observed in work [57].

Table 2
Phase composition of as-prepared, reduced, and spent catalysts.

Sample	As-prepared	Reduced	Spent
Fe	α-Fe_2O_3	Fe_5C_2, α-Fe_2O_3, Fe_3O_4, Fe	Fe_5C_2 (28)*, Fe_7C_3 (12) Fe_3O_4 (60)
Fe-K	α-Fe_2O_3, Fe_3O_4, $KFe_{11}O_{17}$	Fe_5C_2, Fe_3O_4, n-Paraffin	Fe_5C_2 (96), Fe_3O_4 (4), FeO (<1), n-Paraffin
Fe-K-Al	α-Fe_2O_3, Fe_3O_4, $KFe_{11}O_{17}$	Fe_5C_2, Fe_3O_4, Fe	Fe_5C_2 (48), Fe_7C_3 (18), Fe_3O_4, (34) n-Paraffin
Fe-K-Mn	α-Fe_2O_3, Fe_3O_4, $KFe_{11}O_{17}$, Mn_2O_3	Fe_5C_2, Fe_7C_3, α-Fe_2O_3, Fe_3O_4, $Fe_xMn_{1-x}O$, Fe, n-Paraffin	Fe_5C_2 (93), Fe_3O_4 (7), FeO (<1), $MnCO_3$, n-Paraffin

* Numbers in brackets mean the amount of phase estimated by RIR method (only Fe-containing phases were used for estimation).

3.2. Catalyst activity of the obtained catalysts

To analyze reaction pathways of CO_2 hydrogenation for the obtained samples, catalytic tests were carried out at different CO_2 conversion by varying the total flow rate. Time on stream profiles of CO_2 conversion and product selectivity in CO_2 hydrogenation over the obtained catalysts are presented in Fig. S7. Fig. 2 presents the dependencies of CO, CH_4, alcohols, C_{2+} hydrocarbon selectivity on CO_2 conversion. For all catalysts we observe a decrease in CO selectivity and an increase in hydrocarbon selectivity with rising CO_2 conversion. It is explained by a two-stages mechanism of CO_2-FT where CO is formed as an intermediate compound via RWGS reaction [14,58] that is then subsequently hydrogenated to form hydrocarbons. In the case of unpromoted Fe catalyst, methane selectivity was found to be high reaching 41 % at 30 % CO_2 conversion. The catalysts promoted by K show significant lower values of CH_4 selectivity which are less than 10 % over the whole range of conversion studied which agrees with works [27,59,60]. More detailed information on products distribution and olefins content for the studied catalysts is given in Table S2.

When examining the selectivity-conversion relationships in Fig. 2 closer, different curves are observed for the different catalysts which indicate different kinetics of CO_2/CO hydrogenation over the catalysts. Because values of product selectivity were also obtained at low CO_2 conversion, it allows one to estimate the selectivity of hydrogenation products at zero CO_2 conversion by extrapolation (the calculation procedure can be found in the supplementary material, page 7). In the context of the two-stages mechanism of carbon dioxide hydrogenation where CO is an intermediate compound for hydrocarbons formation, one can expect 100 % of CO selectivity and 0 % of hydrocarbons selectivity at zero CO_2 conversion (see supplementary material, pages 5–6).

In the case of unpromoted Fe catalyst, CO, CH_4 and C_{2+} hydrocarbon selectivity at zero CO_2 conversion were around 76.3 %, 18.5 % and 4.4 % respectively. The high value of methane selectivity indicates a direct route of carbon dioxide hydrogenation to CH_4. This route was discussed in the works [15,35,61] and attributed to the methanation reaction ($CO_2 + 4\ H_2 \rightarrow CH_4 + 2\ H_2O$). It may occur not via FT reaction but as direct hydrogenation on active sites different from the ones responsible for chain growth. Interestingly, a larger-than-zero value of selectivity at zero CO_2 conversion was estimated also for C_{2+} hydrocarbon selectivity. For the unpromoted Fe catalyst it is less clear if a direct route of C_{2+} hydrocarbons formation via FT reaction from CO_2 exists. The non-zero value of C_{2+} selectivity may be related to an error of the data extrapolation due to missing information about selectivity in the range of extremely low CO_2 conversion and a non-linear dependency of C_{2+} selectivity on CO_2 conversion. To check this assumption, Monte Carlo simulations were performed to estimate an error for C_{2+} selectivity at zero conversion for the Fe catalysts (see Fig. S1, the supplementary material). The simulation showed that the value of C_{2+} hydrocarbon selectivity is in a range of 0–10 % which indicates that, based on these data alone, the direct route may not exist and non-zero C_{2+} selectivity at zero conversion could be related to an extrapolation error. A similar selectivity-conversion-dependency was reported for unpromoted Fe_5C_2 catalyst by Junhui Liu et al. [61] where non-zero value of C_{2+} hydrocarbons selectivity at zero CO_2 conversion was claimed but not statistically proven. Nevertheless, they concluded that the direct route of C_{2+} hydrocarbons formation via the FT reaction occurs over this catalyst. However, since the conversion-selectivity curves for the Fe_5C_2 catalyst

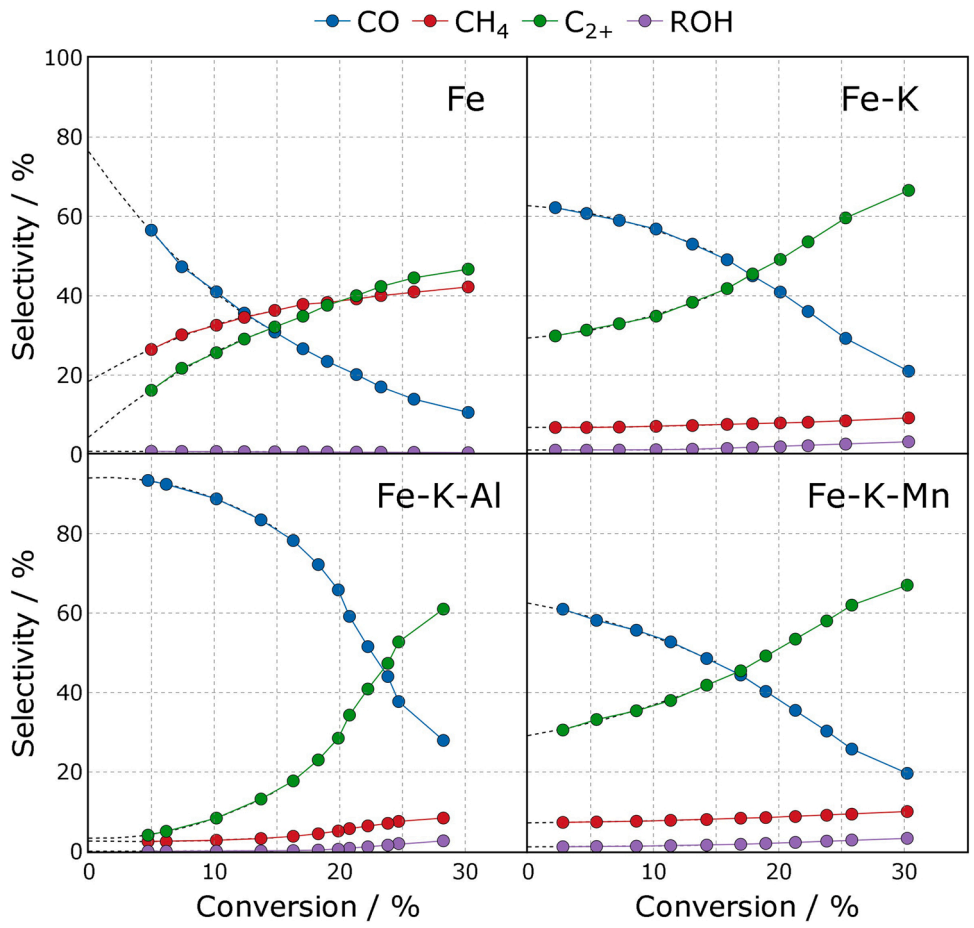

Fig. 2. Selectivity-conversion relationship obtained for different catalysts. Reaction condition: pressure – 15 bar; temperature – 300 °C; CO_2:H_2:N_2 – 1:3:1.

[61] and for the Fe catalyst investigated in the present work are similar and both may be explained by an error of data extrapolation.

For the Fe-K-Al catalyst CO selectivity is around 94 % that is close to 100 % at zero conversion. Wherein the values of methane and C_{2+} hydrocarbons selectivity are less than 4 % and close to zero. The difference form 0 %/100 % is not statistically significantly. Therefore, the data on this catalyst correspond to the conception of two-stage mechanism of CO_2-FT.

For the Fe-K catalyst, the estimated selectivities at zero CO_2 conversion are 62.7 % for CO, 29.4 % for C_{2+} hydrocarbons and 6.8 % for methane. Similar values were obtained for the Fe-K-Mn catalyst (see Table S3, the supplementary material). It is also worth noting that CH_4 selectivity is approximately constant over a wide range of conversion for both Fe-K and Fe-K-Mn catalysts. Non-zero values of CH_4 selectivity at zero CO_2 conversion for these catalysts means that methane is a primary product in CO_2 conversion and, as in the case of the Fe catalyst, the direct formation of methane from CO_2 takes place over these catalysts. Moreover, high values of C_{2+} hydrocarbons selectivity at zero CO_2 conversion are observed for these catalysts. This indicates the presence of direct route of CO_2 hydrogenation to C_{2+} hydrocarbons via FT reaction. It can be explained by a concept that active sites (or ensembles of closely neighbored sites) responsible for chain growth (i.e., hydrocarbon formation via FT) can also activate and hydrogenate CO_2 to CO with hydrogen. Fig. 3 shows different routes of hydrocarbon formation via FT mechanism (excluding the methanation reaction). Direct CO_2-FT means that the active sites responsible for FT reaction are also able to hydrogenate CO_2. Although, active sites for CO and CO_2 hydrogenation to C_{2+} hydrocarbons via FT reaction may also be different leading to a sequential reaction path to hydrocarbons via CO as gas-phase intermediate (see Fig. 3, blue & green route).

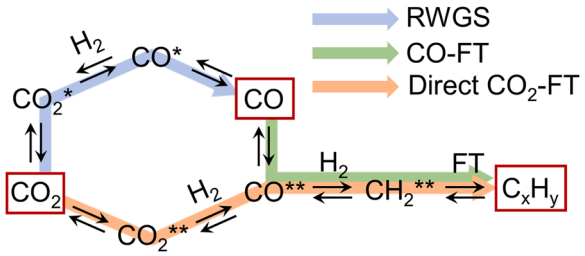

Fig. 3. Different pathways for CO_2/CO hydrogenation via FT. * and ** stand for different surface sites.

Because iron carbides are known to be the active component for CO hydrogenation to form hydrocarbons via FT reaction [7,8], it can be postulated that iron carbides are able to hydrogenate CO_2 to hydrocarbons via FT reaction. In fact, the conversion-selectivity data presented in the Fig. 2 is an experimental proof of the presence of the direct route of CO_2 hydrogenation to C_{2+} hydrocarbons over iron carbides in CO_2-FT. It agrees with the results of first-principles microkinetic modeling performed by Seung Ju Han et al. [62]. They demonstrated that unpromoted iron carbides can catalyze the RWGS reaction. However, it was shown that unpromoted Fe_3O_4 is more active in the RWGS compared to iron carbides.

From the presented results (Fig. 2) one can see that the Fe-K and Fe-K-Mn catalysts show very similar behavior. According to XRD data, the phase composition of both catalysts is similar except for the existence of a Mn-containing phase in the form of $MnCO_3$ in the case of the spent Fe-K-Mn sample. Given the similar performance for Fe-K and Fe-K-Mn, one

can suppose that the Mn in the spent Fe-K-Mn catalyst is preferably in the form of $MnCO_3$ and does not take a part in CO_2 hydrogenation. It is also worth mentioning the difference in activity of the Fe-K and Fe-K-Al catalysts (see Fig. 2) which have complex and differing phase composition according to the XRD data. The fraction of iron oxides in the spent Fe-K-Al catalyst is around 34 wt% and higher than in the spent Fe-K catalyst with just 4 wt%. Thus, the differing amounts of iron oxides may define the difference in the selectivity-conversion relationships of these catalysts.

The analysis of selectivity-conversion relationships allows one to make the following conclusions. The direct CH_4 formation from CO_2 takes place in addition to the RWGS reaction and CO hydrogenation via FT reaction over the Fe, Fe-K, and Fe-K-Mn catalysts. The direct CO_2 hydrogenation to C_{2+} hydrocarbons via FT reaction plays a significant role for at least the Fe-K and Fe-K-Mn catalysts.

3.3. Hydrocarbon distribution analysis

To analyze the hydrocarbon distribution observed over the different catalysts, the ASF distribution was used. Fig. 4 shows the distribution of the hydrocarbons formed in CO_2 hydrogenation over Fe and Fe-K catalysts in corresponding ASF coordinates. The hydrocarbon distribution for Fe-K-Al and Fe-K-Mn catalysts are presented in Fig. S8 (see the supplementary material).

For all catalysts the distributions of the sum of paraffins and olefins corresponds to ASF except for C_1 and C_2 which is typical for products of CO_2 hydrogenation over Fe-based catalysts [33]. The value of the chain growth probability for unpromoted Fe catalyst is around 0.50 and clearly lower than the values for K-doped catalysts which have α in a range 0.65–0.68. The higher chain growth probability for K-doped catalysts correlates with the lower CH_4 selectivity compared to the unpromoted Fe catalyst. Moreover, the low value of α for the Fe catalyst explains why wax was not detected by XRD on the surface of the spent Fe catalyst.

Paraffins and olefins distributions are also presented in Fig. 4 and S7 in the corresponding ASF coordinates. A linear relationship in ASF coordinates is observed in the case of paraffins and olefins distributions for K-promoted catalyst except for ethylene and methane selectivity. Wherein, the values of α for these catalysts is a little higher for paraffins than for olefins (see Fig. 4 and Table S2, the supplementary material). The chain growth probability of the Fe-K catalyst is 0.71 in the case of paraffins distribution compared to α for olefins distribution being 0.66.

For the Fe catalyst, deviation from ASF distribution related to non-linear dependence of hydrocarbon selectivity in the corresponding coordinates is observed for the paraffin distribution. Thus, the chain growth probability depends on the carbon number. In this case, the calculated values of α are 0.18 and 0.68 for carbon number ranges of C_1-C_3 and C_8-C_{10}, respectively.

The reasons of deviations from ASF distribution have been already analyzed and described [63]. An increase in CH_4 selectivity may be related to additional routes of methane formation. One of them is the methanation reaction from CO_2 not via FT reaction [15,35] that agrees with the analysis of conversion-selectivity plots. The other reason may be a double-bond split of α-olefines with higher carbon number leading to additional methane production [21]. Yet another possible explanation was put forward by Wojciechowski and Sarup discussed [64,65] who proposed that the excess of methane selectivity may alternatively be described with a separate parameter of the termination probability. According to their idea, the methane termination probability parameter (the rate constant) is 10 times higher than the one of other hydrocarbons (C_2H_6, C_3H_8 etc.).

The observed decrease in C_2 selectivity compared to the ASF distribution is due to high reactivity of C_2H_4 or surface C_2-intermediates participating in the chain growth compared to olefins with a higher carbon number [66,67]. Our data also confirm that the decrease in C_2 selectivity is only observed in the olefin distribution. The decrease in ethylene selectivity is higher for unpromoted Fe catalyst compared to the catalysts doped by K (see Fig. 4, right) which correlates with the higher activity of unselective hydrogenation to CH_4. It should be also noted that the chain growth probability for the catalysts doped by alkaline metal is higher than for the unpromoted Fe catalyst (see Table S2). It indicates the difference in hydrogenation ability of the obtained catalysts. It is known that unpromoted Fe-based catalysts have higher hydrogenation ability that can be reduced by the promotion of alkali metals leading to enhanced bonding strength of adsorbed CO_2 [18].

The difference in the values of the chain growth probability for olefin and paraffin distributions can be presented as an exponential decrease in olefin-paraffin ratio with the chain length in the form $O_n/P_n \propto \exp(-Cn)$, where $C-$ the natural logarithm of the ratio of α calculated by paraffin and olefin distributions. In the work [63] Van der Laan and Beenackers concluded that the secondary reactions of olefins on Fe-based catalysts are responsible for the observed decrease in olefin-paraffin ratio with increasing carbon number. Wherein, the most

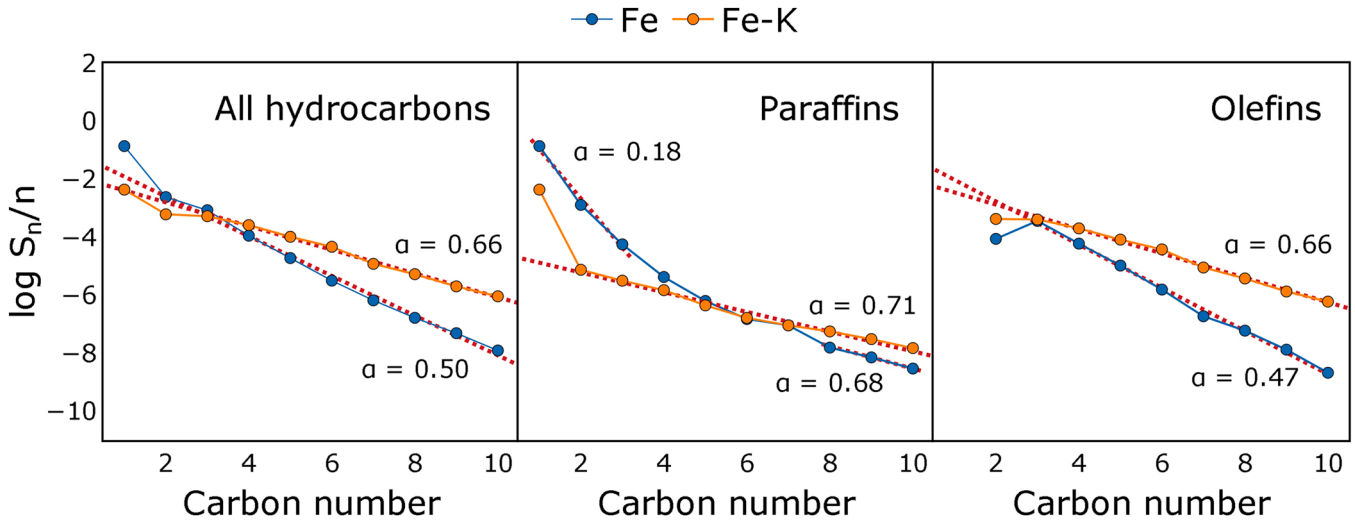

Fig. 4. The hydrocarbons distribution in products of CO_2 hydrogenation over Fe and Fe-K catalysts in ASF coordinates. The C_3-C_{10} range of hydrocarbons was used for fitting the data except for paraffin distribution in the case of Fe catalyst where C_1-C_3 and C_8-C_{10} ranges were used. Reaction condition: pressure – 15 bar; temperature – 300 °C; CO_2:H_2:N_2 – 1:3:1; GHSV – 10,970 ml h^{-1} g^{-1}; time on stream – 25 h.

important secondary reaction is re-adsorption of olefins resulting in initiation of chain growth processes. On the other hand, it may alternatively be explained by the presence of carbon number dependence for olefin desorption. By using an exponential dependence of olefin desorption rate constant, Branislav Todic et al. [68] developed a kinetic model of CO-FT that was able to describe such behavior in olefin and paraffin distributions.

The non-linear relationship of paraffin distribution over carbon number for the Fe catalyst may be related to the presence of two different types of active sites taking part in the molecular processes of the chain growth mechanism as discussed in the work [69]. In this case, the hydrocarbon distribution can be described as:

$$W_n = X{\cdot}n{\cdot}(1-\alpha_1)^2\alpha_1^{n-1} + (1-X){\cdot}n{\cdot}(1-\alpha_2)^2\alpha_2^{n-1}, \quad (21)$$

where X and $1-X$ are the fraction of hydrocarbon products having molecular weight distribution parameters α_1 and α_2 respectively; W_n – weight fraction of an alkane with carbon number n in paraffins. The calculated parameters X, α_1 and α_2 for paraffin distribution in the case of the Fe catalyst are 0.86, 0.15, 0.63 respectively. It implies the presence of 'low-selective' active sites responsible for chain growth via FTS with the chain growth probability of around 0.15. The fraction of hydrocarbons formed by these 'low-selective' sites is predominant and accounts for around 86 % of all hydrocarbons. The existence of the 'low-selective' sites could be one of main the reason for high selectivity of the Fe catalyst to CH_4.

Because catalysts were tested at different CO_2 conversion, we could estimate the chain growth probability α at various CO_2 conversion, see Fig. S9. One can see that the chain growth probability as the key parameter of catalyst selectivity slightly depends on CO_2 conversion which agrees with the data analysis of CO_2 hydrogenation catalysts [33]. However, it is worth mentioning the decrease in α at low CO_2 conversion for the Fe-K-Al catalyst.

3.4. Segmental rates analysis

For a more detailed analysis of the processes occurring in the CO_2 hydrogenation over the obtained catalysts, the segmental rates of CO_2 consumption, CH_4, CO, and C_{2+} formations along the catalyst bed were calculated and are shown in Fig. 5. The overall CO_2 consumption rate decreases along the catalyst bed for all the samples. It is obviously related to a decrease in the concentration of CO_2 and H_2 transforming into products of reactions. Wherein, a sharper decrease in CO_2 consumption is observed for Fe and Fe-K-Al catalysts compared to Fe-K and Fe-K-Mn ones. Already within the front part of the catalyst bed (extending to around 20 % of the bed length for the Fe catalyst and 30 % for Fe-K and Fe-K-Mn catalysts), the rate of CO production decreases to nearly zero where it stays for the remaining part of the bed. A sharper decrease in the CO formation rate is also observed for the initial 20 % bed-part in the case of the Fe-K-Al catalyst. For this catalyst, CO formation rates become negative for the remaining part. It means that the rate of CO-FT becomes higher than the rate of the RWGS reaction.

The rate of methane formation is high at the beginning part and decreases along the catalyst bed for the Fe catalyst. Since CO_2 and H_2 are the main compounds in the gas flow at the beginning of the catalyst bed, carbon dioxide (not carbon monoxide) seems to be responsible for the high rate of CH_4 production at the beginning of the bed. If this catalyst is compared to the ones doped by K, a strong reduction of CH_4 formation is obvious. The initial rate of methane formation for the unpromoted Fe catalyst is around 6 times higher than the rates of the K-doped catalysts.

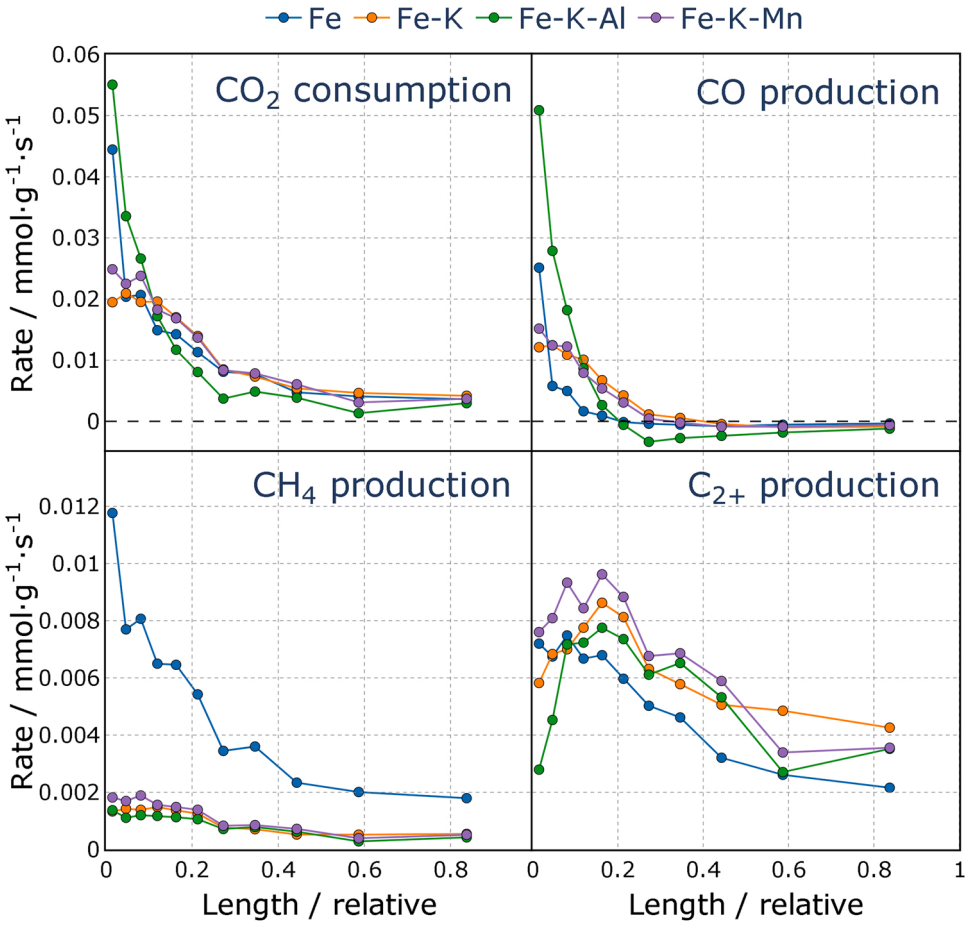

Fig. 5. The segmental rates of CO_2 consumption, CH_4, CO, and C_{2+} formation over the obtained catalysts.

For the rate of formation of C_{2+} hydrocarbons, volcano-like curves are observed along the catalyst bed. However, no maximum is observed in the case of the Fe catalyst. It is worth noting that rates of C_{2+} hydrocarbon production are similar along the catalyst bed for all the catalysts. There is only slightly difference in the front part of the catalyst bed (~ 10 % of length). A slight decrease of C_{2+} hydrocarbon formation rate is seen for the unpromoted Fe catalyst along the whole length. Compared to other catalysts, the Fe-K-Al catalyst is showing a lower C_{2+} formation rate at the initial part of the bed. In conclusion, the rates of hydrocarbon formation over K-doped catalysts do not significantly differ.

The difference in selectivity-conversion relationships (Fig. 2) for the Fe-K-Al catalyst compared to Fe-K and Fe-K-Mn catalysts is rather related to their different activity in the RWGS reaction. As shown above, according to XRD data, the Fe-K-Al catalyst contains 36 wt% iron oxides which is higher than in the Fe-K and Fe-K-Mn catalysts which contain only 4 and 7 wt%, respectively. Since iron oxide is known to be active in the RWGS reaction and to play a key role in CO formation from CO_2 [8], the difference in the content of iron oxide may explain the different activities of the K-promoted catalysts in the RWGS reaction. Indeed, the Fe-K-Al catalyst with the highest iron oxides content was more active in the RWGS reaction than the Fe-K and Fe-K-Mn catalysts. Moreover, the higher amount of iron oxides in the Fe-K-Al catalyst compared to the Fe-K and Fe-K-Mn catalysts could explain the fact that the direct route of CO_2 hydrogenation to C_{2+} hydrocarbons is not observed in the case of the Fe-K-Al catalyst. This may be related to higher activity of iron oxides to catalyze the RWGS reaction compared to direct CO_2-FT route, and, thus, the contribution of the direct route is much lower than the RWGS reaction in CO_2 hydrogenation over the Fe-K-Al catalyst.

The presence of a maximum for hydrocarbon production rate (Figure 5, C_{2+} production) agrees with the concept of the two-stage mechanism of CO_2 hydrogenation where CO is an intermediate compound for hydrocarbons production. In addition, the maximum in the rates of C_{2+} hydrocarbon formation is shifted compared to the maximum of CO concentration (it corresponds to the rate of zero CO production because the rate is the derivative of concentration) along the catalyst bed. This shift might also indicate an additional pathway of hydrocarbon formation from CO_2. On the other hand, it could also be correlated with the increase in H_2O concentration along the bed that may reduce the rate of FT e.g. by competitive adsorption on active sites.

Because the rates of hydrocarbon formation should follow the ASF distribution for an ideal FT, a comparison of the experimental rates and the ones calculated from ASF distribution may give additional information about differences in the mechanism of CO_2 hydrogenation over the 4 catalysts. Fig. 6 presents how the ratio between the observed rates of C_1-C_6 hydrocarbon formation, and the rates predicted via ASF changes along the catalyst bed.

From the presented data one can see that the rates of C_{3+} hydrocarbons formation correspond to the ASF distribution for all the catalysts because of the relative rates being close to one. A slight decrease in the relative rate of C_2 formation with increasing length of the catalyst bed is observed. In the case of CH_4, the formation rates are higher than 1 at the front and decrease along the first part of catalyst bed (around 30 %) and become constant for the rest of the bed (close to 1 for K-promoted catalysts and around 1.5–1.7 for the Fe catalyst). The initial decrease indicates the presence of an additional pathway of methane formation not via FT mechanism which may be the direct methanation reaction discussed above. The rate of CH_4 formation for the unpromoted Fe catalyst decreases also over the first part of the bed, but it remains 1.5–1.7 times

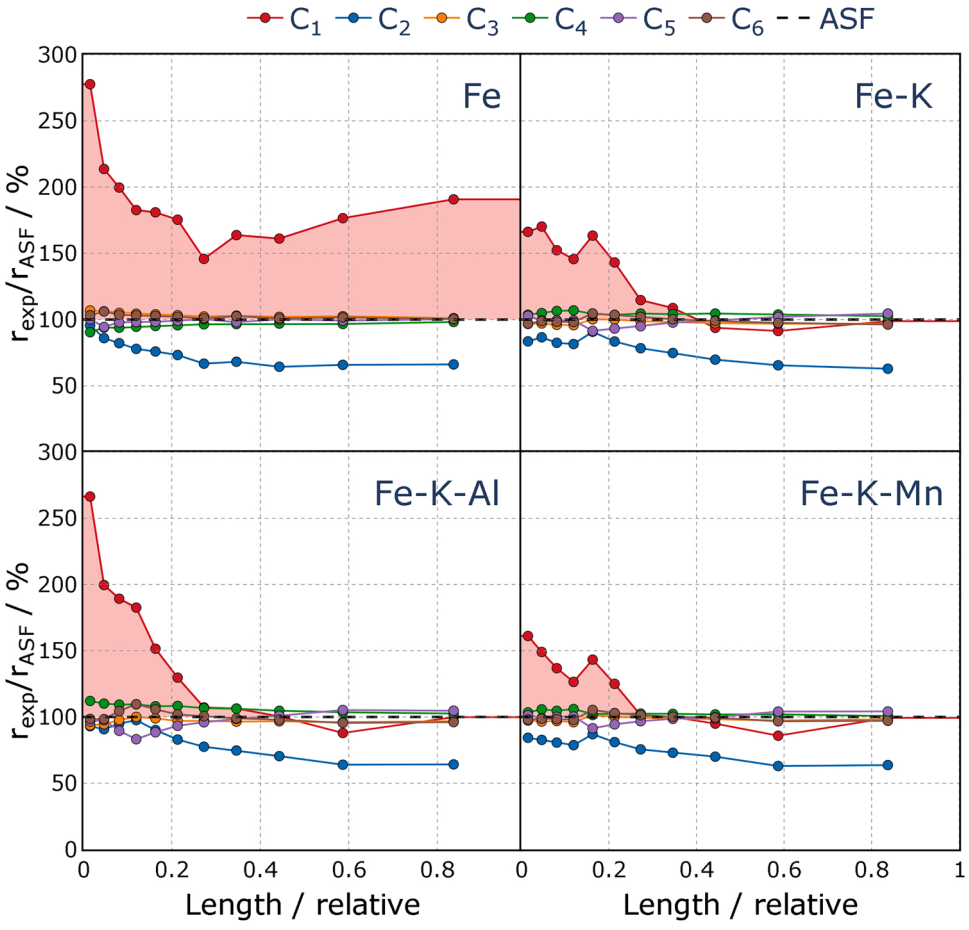

Fig. 6. The relative segmental rates of C_1-C_6 hydrocarbon formation. The "red" shaded region visualizes the excess-methane formation compared to the values calculated by ASF distribution.

higher than the rate calculated by the ASF distribution for the remaining part of the catalyst bed. This deviation from ASF distribution for the remaining part of the bed (>30 % of the bed) could be connected to the existence of low-selective active sites (chain growth probability around 0.18) responsible for hydrocarbons formation only on the Fe catalyst.

3.5. Temporal analysis of CO_2 and H_2 interaction with spent catalysts

The interaction between CO_2 and spent catalysts was studied by pulsing of a CO_2:Ar mixture at 300 °C. A comparison of transient responses of CO_2 and Ar transformed to dimensionless form according to [46] showed that the modified CO_2 response crosses the Ar response (Figs. S10). Such intersection is a fingerprint of reversible adsorption of CO_2 [46]. To derive kinetic parameters of this interaction, the experimental CO_2 responses were fitted to a simple micro-kinetic model, which assumes reversible non-dissociative CO_2 adsorption:

$$\begin{aligned} CO_2 + * &\xrightarrow{k_+} CO_2^* \\ CO_2^* &\xrightarrow{k_-} CO_2 + * \end{aligned} \quad (22)$$

The experimental and simulated responses are compared in Fig. S11. The residual values illustrating the goodness of fit, results of sensitivity and correlation analyses are shown in Table S4 and S5. The values of the parameters resulting from the fitting procedure are summarized in Table 3. Due to a correlation between the total concentration of active sites N_0 and the constant of CO_2 adsorption k_+, only their product $N_0 \cdot k_+ = k_+^{eff}$, further called an effective constant, could be determined. It is worth mentioning that such a correlation is frequently found in kinetic modeling of TAP experiments [70]. For better comparison of the adsorptive properties of spent catalysts the ratio k_+^{eff}/k_- being an efficient equilibrium constant of CO_2 adsorption (K_{eq}^{eff}) is provided in logarithmic form. According to the values in Table 3, doping of Fe with K led to an increase in k_+^{eff} accompanied by the decrease in k_-. Thus, the presence of K increases the equilibrium constant of CO_2 adsorption. The addition of Al led a further increase in this constant. It is worth mentioning that the CO_2 adsorption ability for Fe-K and Fe-K-Mn catalysts are similar in TAP which agrees with the catalytic data where Fe-K and Fe-K-Mn catalysts demonstrated similar activity.

The ability of spent catalysts to activate gas-phase hydrogen was investigated by H/D exchange tests at 300 °C using a H_2:D_2:Ar mixture. Due to negligible amounts of HD formed in these experiments, a quantitative evaluation was not possible. Nevertheless, some relevant information can be obtained from analyzing the shape and the order of appearance of D_2, HD, H_2 and Ar recorded in these experiments (Fig. S12). For the spent Fe and Fe-K-Al catalysts, the HD response is broader than that of D_2 and H_2 and its maximum is situated after those of D_2 and H_2. This is a clear sign of HD formation, i.e., these catalysts are able to break H-H and D-D bonds and to form new H-D bonds. Since the broadening of HD response is more marked over the Fe catalyst, it can be assumed that this catalyst possesses higher activity towards HD formation. No significant difference between the HD and D_2 responses was observed for the Fe-K catalyst versus the Fe-K-Mn one. Both catalysts show lower activity towards HD formation in comparison to the spent Fe and Fe-K-Al catalysts. Therefore, addition of K reduces the ability of Fe-based catalysts to activate gas-phase hydrogen. Using Al as promoter diminishes this effect, whereas the presence of Mn does not have an influence. Considering the phase composition of the spent Fe-K and Fe-K-Mn catalysts, which consist of predominantly iron carbides, and the spent Fe and Fe-K-Al catalysts, which consist of a mixture of iron oxides and carbides phases, one can assume that H_2-D_2 exchange occurs over the surface of iron oxide phase at the condition of TAP experiment.

Table 3
Kinetic parameters of CO_2 adsorption over spent catalysts.

Sample	k_+^{eff}, s^{-1}	k_-, s^{-1}	$\log K_{eq}^{eff}$
Fe	19.4	1.13	2.85
Fe-K	128	0.15	6.75
Fe-K-Al	8190	0.08	11.5
Fe-K-Mn	341	0.28	7.11

3.6. The proposed reaction scheme of CO_2 hydrogenation

Based on the obtained results, we can suggest the reaction pathways occurring at CO_2 hydrogenation over Fe-based catalysts. The scheme of main routes of CO and hydrocarbons formation is presented in Fig. 7.

Besides the previously established routes via RWGS with the formation of CO as intermediate followed by hydrogenation to C_{2+} hydrocarbons via FT reaction, the direct routes of hydrocarbon formation may not be neglected for some catalysts. Methane can be formed as a product of CO_2/CO hydrogenation via FT reaction as well as via an additional direct CO_2 hydrogenation (methanation reaction). The route of direct methanation was shown to occur over all obtained catalysts but to a different extent. The direct route of CO_2 hydrogenation to C_{2+} hydrocarbons via FT reaction plays a role at least for Fe-K and Fe-K-Mn catalysts. The difference in activity of the Fe-K-Al catalyst compared to the Fe-K and Fe-K-Mn catalysts is related to their different ability to catalyze the RWGS reaction. The higher activity of Al-promoted catalyst in RWGS reaction may be explained by the higher content of iron oxide according to XRD data (see Table 2). Thus, in the case of the Fe-K-Al catalyst, the lower contribution (approximately zero) of direct route of CO_2 hydrogenation to C_{2+} hydrocarbons compared to the Fe-K and Fe-K-Mn catalysts may be related to higher activity in RWGS reaction. In the case of the unpromoted Fe catalyst, high CH_4 selectivity compared to K-promoted catalysts was observed that can be caused by the two reasons. The first one is the methanation reaction. The other one is the presence of low-selective active sites with the low chain growth probability (α is around 0.18).

4. Conclusions

The analysis of reaction pathways occurring over Fe-based catalysts demonstrated that except for the RWGS reaction and CO hydrogenation via FT reaction, additional routes of hydrocarbon formation from CO_2 can be important in the carbon dioxide hydrogenation. One of them is the methanation reaction which occurs over all four catalysts. The direct pathway of C_{2+} hydrocarbon formation via FT reaction plays a significant role at least for the Fe-K and Fe-K-Mn catalysts. In the case of the Fe-K catalyst, the spent sample consist of predominantly Fe_5C_2 phase. From this we conclude that certain iron carbides are able to hydrogenate CO_2 directly to C_{2+} hydrocarbons. Accordingly, the concept of requiring iron oxides as an essential active component for catalyzing the RWGS reaction in CO_2-FTS need to be revised.

The ASF analysis of hydrocarbon distribution in the products of CO_2 hydrogenation over the unpromoted Fe catalyst indicates the presence of two types of active sites responsible for hydrocarbon formation via FT reaction. Wherein, low-selective active sites with a chain growth probability of around 0.18 are responsible for high CH_4 selectivity as well as for an additional direct pathway of CO_2 hydrogenation to methane.

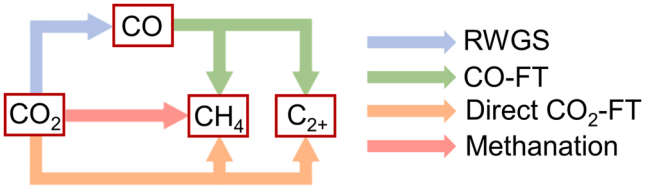

Fig. 7. Scheme including all observed reaction pathways for CO_2 hydrogenation over Fe-based catalysts. The difference between CO-FT and CO_2-FT pathways is presented in Fig. 3.

These sites explain the low selectivity of unpromoted Fe-based catalysts and also the necessity of suppressing their formation by doping with alkaline metals.

The obtained results expand the knowledge about reactions pathway occurring in CO_2 hydrogenation over Fe-based catalysts and are important for accurate kinetic modeling of the process of CO_2-FT synthesis. Moreover, further elucidating the role of iron carbide in the direct pathway of CO_2 hydrogenation to hydrocarbons may help in preparing new catalytic systems with improved performance and high selectivity to the desired products.

Funding

Financial support from Federal Ministry of Education and Research (BMBF) in project InnoSyn (FKZ: 03SF0616B) is gratefully acknowledged. The authors thank Anja Simmula for ICP measurements.

CRediT authorship contribution statement

Aleksandr Fedorov: Conceptualization, Investigation, Methodology, Data curation, Writing – original draft, Writing – review & editing. **Henrik Lund:** Investigation, Writing – review & editing. **Vita A. Kondratenko:** Investigation, Writing – review & editing. **Evgenii V. Kondratenko:** Investigation, Methodology, Writing – review & editing. **David Linke:** Conceptualization, Supervision, Project administration, Funding acquisition, Methodology, Writing – review & editing.

Declaration of Competing Interest

The authors declare that they have no known competing financial interests or personal relationships that could have appeared to influence the work reported in this paper.

Data Availability

The data that has been used is confidential.

Appendix A. Supporting information

Supplementary data associated with this article can be found in the online version at doi:10.1016/j.apcatb.2023.122505.

References

[1] Z.A. Manan, W.N.R. Mohd Nawi, S.R. Wan Alwi, J.J. Klemeš, Advances in process integration research for CO_2 emission reduction – a review, J. Clean. Prod. 167 (2017) 1–13.
[2] F. Marques Mota, D.H. Kim, From CO_2 methanation to ambitious long-chain hydrocarbons: alternative fuels paving the path to sustainability, Chem. Soc. Rev. 48 (2019) 205–259.
[3] W. Wang, S. Wang, X. Ma, J. Gong, Recent advances in catalytic hydrogenation of carbon dioxide, Chem. Soc. Rev. 40 (2011) 3703–3727.
[4] M.D. Garba, M. Usman, S. Khan, F. Shehzad, A. Galadima, M.F. Ehsan, A. S. Ghanem, M. Humayun, CO_2 towards fuels: a review of catalytic conversion of carbon dioxide to hydrocarbons, J. Environ. Chem. Eng. 9 (2021), 104756.
[5] M.V. Landau, N. Meiri, N. Utsis, R. Vidruk Nehemya, M. Herskowitz, Conversion of CO_2, CO, and H_2 in CO_2 hydrogenation to fungible liquid fuels on fe-based catalysts, Ind. Eng. Chem. Res. 56 (2017) 13334–13355.
[6] L. Guo, J. Sun, Q. Ge, N. Tsubaki, Recent advances in direct catalytic hydrogenation of carbon dioxide to valuable C2+ hydrocarbons, J. Mater. Chem. A 6 (2018) 23244–23262.
[7] B. Yao, T. Xiao, O.A. Makgae, X. Jie, S. Gonzalez-Cortes, S. Guan, A.I. Kirkland, J. R. Dilworth, H.A. Al-Megren, S.M. Alshihri, P.J. Dobson, G.P. Owen, J.M. Thomas, P.P. Edwards, Transforming carbon dioxide into jet fuel using an organic combustion-synthesized Fe-Mn-K catalyst, Nat. Commun. 11 (2020) 6395.
[8] J. Wei, Q. Ge, R. Yao, Z. Wen, C. Fang, L. Guo, H. Xu, J. Sun, Directly converting CO_2 into a gasoline fuel, Nat. Commun. 8 (2017) 15174.
[9] G.V. Schulz, Über die Beziehung zwischen Reaktionsgeschwindigkeit und Zusammensetzung des Reaktionsproduktes bei Makropolymerisationsvorgängen, Z. für Phys. Chem. 30B (1935) 379–398.
[10] P.J. Flory, Molecular size distribution in linear condensation polymers1, J. Am. Chem. Soc. 58 (1936) 1877–1885.
[11] R.B. Anderson, R.A. Friedel, H.H. Storch, Fischer-Tropsch reaction mechanism involving stepwise growth of carbon chain, J. Chem. Phys. 19 (1951) 313–319.
[12] G. Henrici-Olivé, S. Olivé, The Fischer-Tropsch synthesis: molecular weight distribution of primary products and reaction mechanism, Angew. Chem. Int. Ed. Engl. 15 (1976) 136–141.
[13] E.S. Lox, G.F. Froment, Kinetics of the Fischer-Tropsch reaction on a precipitated promoted iron catalyst. 2. Kinetic modeling, Ind. Eng. Chem. Res. 32 (1993) 71–82.
[14] T. Riedel, G. Schaub, K.-W. Jun, K.-W. Lee, Kinetics of CO_2 hydrogenation on a K-promoted Fe catalyst, Ind. Eng. Chem. Res. 40 (2001) 1355–1363.
[15] M. Albrecht, U. Rodemerck, M. Schneider, M. Bröring, D. Baabe, E.V. Kondratenko, Unexpectedly efficient CO_2 hydrogenation to higher hydrocarbons over non-doped Fe_2O_3, Appl. Catal. B: Environ. 204 (2017) 119–126.
[16] T. Herranz, S. Rojas, F.J. Pérez-Alonso, M. Ojeda, P. Terreros, J.L.G. Fierro, Hydrogenation of carbon oxides over promoted Fe-Mn catalysts prepared by the microemulsion methodology, Appl. Catal. A: Gen. 311 (2006) 66–75.
[17] B. Liang, T. Sun, J. Ma, H. Duan, L. Li, X. Yang, Y. Zhang, X. Su, Y. Huang, T. Zhang, Mn decorated Na/Fe catalysts for CO_2 hydrogenation to light olefins, Catal. Sci. Technol. 9 (2019) 456–464.
[18] T. Numpilai, N. Chanlek, Y. Poo-Arporn, C.K. Cheng, N. Siri-Nguan, T. Sornchamni, M. Chareonpanich, P. Kongkachuichay, N. Yigit, G. Rupprechter, J. Limtrakul, T. Witoon, Tuning interactions of surface-adsorbed species over Fe−Co/K−Al_2O_3 catalyst by different K contents: selective CO_2 hydrogenation to light olefins, ChemCatChem 12 (2020) 3306–3320.
[19] S.-R. Yan, K.-W. Jun, J.-S. Hong, M.-J. Choi, K.-W. Lee, Promotion effect of Fe–Cu catalyst for the hydrogenation of CO_2 and application to slurry reactor, Appl. Catal. A: Gen. 194–195 (2000) 63–70.
[20] A. Aitbekova, E.D. Goodman, L. Wu, A. Boubnov, A.S. Hoffman, A. Genc, H. Cheng, L. Casalena, S.R. Bare, M. Cargnello, Engineering of ruthenium–iron oxide colloidal heterostructures: improved yields in CO_2 hydrogenation to hydrocarbons, Angew. Chem. Int. Ed. 58 (2019) 17451–17457.
[21] S.-C. Lee, J.-H. Jang, B.-Y. Lee, J.-S. Kim, M. Kang, S.-B. Lee, M.-J. Choi, S.-J. Choung, Promotion of hydrocarbon selectivity in CO_2 hydrogenation by Ru component, J. Mol. Catal. A: Chem. 210 (2004) 131–141.
[22] C. Zhang, C. Cao, Y. Zhang, X. Liu, J. Xu, M. Zhu, W. Tu, Y.-F. Han, Unraveling the role of zinc on bimetallic Fe_5C_2–ZnO catalysts for highly selective carbon dioxide hydrogenation to high carbon α-Olefins, ACS Catal. 11 (2021) 2121–2133.
[23] N. Chaipraditgul, T. Numpilai, C. Kui Cheng, N. Siri-Nguan, T. Sornchamni, C. Wattanakit, J. Limtrakul, T. Witoon, Tuning interaction of surface-adsorbed species over Fe/K-Al_2O_3 modified with transition metals (Cu, Mn, V, Zn or Co) on light olefins production from CO_2 hydrogenation, Fuel 283 (2021), 119248.
[24] T. Witoon, V. Lapkeatseree, T. Numpilai, C. Kui Cheng, J. Limtrakul, CO_2 hydrogenation to light olefins over mixed Fe-Co-K-Al oxides catalysts prepared via precipitation and reduction methods, Chem. Eng. J. 428 (2022), 131389.
[25] B. Liu, S. Geng, J. Zheng, X. Jia, F. Jiang, X. Liu, Unravelling the new roles of Na and Mn promoter in CO_2 hydrogenation over Fe_3O_4-based catalysts for enhanced selectivity to light α-Olefins, ChemCatChem 10 (2018) 4718–4732.
[26] X. Liu, C. Zhang, P. Tian, M. Xu, C. Cao, Z. Yang, M. Zhu, J. Xu, Revealing the effect of sodium on iron-based catalysts for CO_2 hydrogenation: insights from calculation and experiment, J. Phys. Chem. C 125 (2021) 7637–7646.
[27] B. Liang, H. Duan, T. Sun, J. Ma, X. Liu, J. Xu, X. Su, Y. Huang, T. Zhang, Effect of Na promoter on Fe-based catalyst for CO_2 hydrogenation to alkenes, ACS Sustain. Chem. Eng. 7 (2019) 925–932.
[28] N. Fischer, R. Henkel, B. Hettel, M. Iglesias, G. Schaub, M. Claeys, Hydrocarbons via CO_2 hydrogenation over iron catalysts: the effect of potassium on structure and performance, Catal. Lett. 146 (2016) 509–517.
[29] L. Brübach, D. Hodonj, P. Pfeifer, Kinetic analysis of CO_2 hydrogenation to long-chain hydrocarbons on a supported iron catalyst, Ind. Eng. Chem. Res. 61 (2022) 1644–1654.
[30] C. Panzone, R. Philippe, C. Nikitine, L. Vanoye, A. Bengaouer, A. Chappaz, P. Fongarland, Catalytic and kinetic study of the CO_2 hydrogenation reaction over a Fe–K/Al_2O_3 catalyst toward liquid and gaseous hydrocarbon production, Ind. Eng. Chem. Res. 60 (2021) 16635–16652.
[31] S. Saeidi, S. Najari, F. Fazlollahi, M.K. Nikoo, F. Sefidkon, J.J. Klemeš, L.L. Baxter, Mechanisms and kinetics of CO_2 hydrogenation to value-added products: a detailed review on current status and future trends, Renew. Sustain. Energy Rev. 80 (2017) 1292–1311.
[32] C. Panzone, R. Philippe, C. Nikitine, A. Bengaouer, A. Chappaz, P. Fongarland, Development and validation of a detailed microkinetic model for the CO_2 hydrogenation reaction toward hydrocarbons over an Fe–K/Al_2O_3 catalyst, Ind. Eng. Chem. Res. 61 (2022) 4514–4533.
[33] A. Fedorov, D. Linke, Data analysis of CO_2 hydrogenation catalysts for hydrocarbon production, J. CO_2 Util. 61 (2022), 102034.
[34] A.S. Skrypnik, Q. Yang, A.A. Matvienko, V.Y. Bychkov, Y.P. Tulenin, H. Lund, S. A. Petrov, R. Kraehnert, A. Arinchtein, J. Weiss, A. Brueckner, E.V. Kondratenko, Understanding reaction-induced restructuring of well-defined $Fe_xO_yC_z$ compositions and its effect on CO_2 hydrogenation, Appl. Catal. B: Environ. 291 (2021), 120121.
[35] J. Zhu, G. Zhang, W. Li, X. Zhang, F. Ding, C. Song, X. Guo, Deconvolution of the particle size effect on CO_2 hydrogenation over iron-based catalysts, ACS Catal. 10 (2020) 7424–7433.
[36] T. Riedel, M. Claeys, H. Schulz, G. Schaub, S.-S. Nam, K.-W. Jun, M.-J. Choi, G. Kishan, K.-W. Lee, Comparative study of Fischer–Tropsch synthesis with H_2/CO and H_2/CO_2 syngas using Fe- and Co-based catalysts, Appl. Catal. A: Gen. 186 (1999) 201–213.

[37] J. Wang, Z. You, Q. Zhang, W. Deng, Y. Wang, Synthesis of lower olefins by hydrogenation of carbon dioxide over supported iron catalysts, Catal. Today 215 (2013) 186–193.
[38] Z. You, W. Deng, Q. Zhang, Y. Wang, Hydrogenation of carbon dioxide to light olefins over non-supported iron catalyst, Chin. J. Catal. 34 (2013) 956–963.
[39] A. Ramirez, L. Gevers, A. Bavykina, S. Ould-Chikh, J. Gascon, Metal organic framework-derived iron catalysts for the direct hydrogenation of CO_2 to short chain olefins, ACS Catal. 8 (2018) 9174–9182.
[40] Q. Yang, A. Skrypnik, A. Matvienko, H. Lund, M. Holena, E.V. Kondratenko, Revealing property-performance relationships for efficient CO_2 hydrogenation to higher hydrocarbons over Fe-based catalysts: Statistical analysis of literature data and its experimental validation, Appl. Catal. B: Environ. 282 (2021), 119554.
[41] Y. Xu, P. Zhai, Y. Deng, J. Xie, X. Liu, S. Wang, D. Ma, Highly selective olefin production from CO_2 hydrogenation on iron catalysts: a subtle synergy between manganese and sodium additives, Angew. Chem. Int. Ed. 59 (2020) 21736–21744.
[42] C.R. Hubbard, R.L. Snyder, RIR - measurement and use in quantitative XRD, Powder Diffr. 3 (1988) 74–77.
[43] J. Pérez-Ramírez, E.V. Kondratenko, Evolution, achievements, and perspectives of the TAP technique, Catal. Today 121 (2007) 160–169.
[44] K. Morgan, N. Maguire, R. Fushimi, J.T. Gleaves, A. Goguet, M.P. Harold, E. V. Kondratenko, U. Menon, Y. Schuurman, G.S. Yablonsky, Forty years of temporal analysis of products, Catal. Sci. Technol. 7 (2017) 2416–2439.
[45] M. Soick, D. Wolf, M. Baerns, Determination of kinetic parameters for complex heterogeneous catalytic reactions by numerical evaluation of TAP experiments, Chem. Eng. Sci. 55 (2000) 2875–2882.
[46] J.T. Gleaves, G.S. Yablonskii, P. Phanawadee, Y. Schuurman, TAP-2: an interrogative kinetics approach, Appl. Catal. A: Gen. 160 (1997) 55–88.
[47] M. Rothaemel, M. Baerns, Modeling and simulation of transient adsorption and reaction in vacuum using the temporal analysis of products reactor, Ind. Eng. Chem. Res. 35 (1996) 1556–1565.
[48] R.F. Sincovec, N.K. Madsen, Software for nonlinear partial differential equations, ACM Trans. Math. Softw. 1 (1975) 232–260.
[49] F. Gao, L. Han, Implementing the Nelder-Mead simplex algorithm with adaptive parameters, Comput. Optim. Appl. 51 (2012) 259–277.
[50] Python Software Foundation. Python Language Reference, version 3.8. Available at http://www.python.org.
[51] C.R. Harris, K.J. Millman, S.J. van der Walt, R. Gommers, P. Virtanen, D. Cournapeau, E. Wieser, J. Taylor, S. Berg, N.J. Smith, R. Kern, M. Picus, S. Hoyer, M.H. van Kerkwijk, M. Brett, A. Haldane, J.F. del Río, M. Wiebe, P. Peterson, P. Gérard-Marchant, K. Sheppard, T. Reddy, W. Weckesser, H. Abbasi, C. Gohlke, T.E. Oliphant, Array programming with NumPy, Nature 585 (2020) 357–362.
[52] Plotly Technologies Inc, Collaborative data science (2015). https://plotly.com.
[53] O.A. Bulavchenko, A.A. Pochtar', E.Y. Gerasimov, A.V. Fedorov, Y.A. Chesalov, A. A. Saraev, V.A. Yakovlev, V.V. Kaichev, Chemical and texture promoters in Cu-Fe-Al oxide nanocomposite catalysts for combustion of solid fuel gasification products, Appl. Catal. A: Gen. 590 (2020), 117364.
[54] J. Zieliński, I. Zglinicka, L. Znak, Z. Kaszkur, Reduction of Fe_2O_3 with hydrogen, Appl. Catal. A: Gen. 381 (2010) 191–196.
[55] Y. Li, Y. Wan, Y. Li, S. Zhan, Q. Guan, Y. Tian, Low-temperature selective catalytic reduction of NO with NH_3 over Mn_2O_3-doped Fe_2O_3 hexagonal microsheets, ACS Appl. Mater. Interfaces 8 (2016) 5224–5233.
[56] A. Arinchtein, M.-Y. Ye, M. Geske, M. Frisch, R. Kraehnert, Influence of phase composition and pretreatment on the conversion of iron oxides into iron carbides in syngas atmospheres, Catalysts 11 (2021).
[57] M. Xu, X. Liu, G. Song, Y. Cai, B. Shi, Y. Liu, X. Ding, Z. Yang, P. Tian, C. Cao, J. Xu, Regulating iron species compositions by Fe-Al interaction in CO_2 hydrogenation, J. Catal. 413 (2022) 331–341.
[58] R.E. Owen, D. Mattia, P. Plucinski, M.D. Jones, Kinetics of CO_2 hydrogenation to hydrocarbons over iron–silica catalysts, ChemPhysChem 18 (2017) 3211–3218.
[59] A. Russkikh, G. Shterk, B.H. Al-Solami, B.A. Fadhel, A. Ramirez, J. Gascon, Turning waste into value: potassium-promoted red mud as an effective catalyst for the hydrogenation of CO_2, ChemSusChem 13 (2020) 2981–2987.
[60] J. Liu, A. Zhang, X. Jiang, M. Liu, J. Zhu, C. Song, X. Guo, Direct transformation of carbon dioxide to value-added hydrocarbons by physical mixtures of Fe_5C_2 and K-modified Al_2O_3, Ind. Eng. Chem. Res. 57 (2018) 9120–9126.
[61] J. Liu, G. Zhang, X. Jiang, J. Wang, C. Song, X. Guo, Insight into the role of Fe_5C_2 in CO_2 catalytic hydrogenation to hydrocarbons, Catal. Today 371 (2021) 162–170.
[62] S.J. Han, S.-M. Hwang, H.-G. Park, C. Zhang, K.-W. Jun, S.K. Kim, Identification of active sites for CO_2 hydrogenation in Fe catalysts by first-principles microkinetic modelling, J. Mater. Chem. A 8 (2020) 13014–13023.
[63] G.P. Van Der Laan, A.A.C.M. Beenackers, Kinetics and selectivity of the Fischer–Tropsch synthesis: a literature review, Catal. Rev. 41 (1999) 255–318.
[64] B.W. Wojciechowski, The kinetics of the Fischer-Tropsch synthesis, Catal. Rev. 30 (1988) 629–702.
[65] B. Sarup, B.W. Wojciechowski, Studies of the fischer-tropsch synthesis on a cobalt catalyst i. evaluation of product distribution parameters from experimental data, Can. J. Chem. Eng. 66 (1988) 831–842.
[66] C.G. Visconti, M. Martinelli, L. Falbo, A. Infantes-Molina, L. Lietti, P. Forzatti, G. Iaquaniello, E. Palo, B. Picutti, F. Brignoli, CO_2 hydrogenation to lower olefins on a high surface area K-promoted bulk Fe-catalyst, Appl. Catal. B: Environ. 200 (2017) 530–542.
[67] T. Riedel, H. Schulz, G. Schaub, K.-W. Jun, J.-S. Hwang, K.-W. Lee, Fischer–Tropsch on Iron with H_2/CO and H_2/CO_2 as synthesis gases: the episodes of formation of the fischer–tropsch regime and construction of the catalyst, Top. Catal. 26 (2003) 41–54.
[68] B. Todic, T. Bhatelia, G.F. Froment, W. Ma, G. Jacobs, B.H. Davis, D.B. Bukur, Kinetic model of fischer–tropsch synthesis in a slurry reactor on Co–Re/Al_2O_3 catalyst, Ind. Eng. Chem. Res. 52 (2013) 669–679.
[69] L.S. Glebov, G.A. Kliger, The molecular weight distribution of the products of the Fischer-Tropsch synthesis, Russ. Chem. Rev. 63 (1994) 185–195.
[70] Q. Yang, V.A. Kondratenko, S.A. Petrov, D.E. Doronkin, E. Saraçi, H. Lund, A. Arinchtein, R. Kraehnert, A.S. Skrypnik, A.A. Matvienko, E.V. Kondratenko, Identifying Performance Descriptors in CO_2 Hydrogenation over Iron-Based Catalysts Promoted with Alkali Metals, Angew. Chem. Int. Ed. 61 (2022), e202116517.

Supplementary material

Elucidating reaction pathways occurring in CO_2 hydrogenation over Fe-based catalysts

Aleksandr Fedorov, Henrik Lund, Vita A. Kondratenko,

Evgenii V. Kondratenko, David Linke

Leibniz-Institut für Katalyse e.V., Albert-Einstein-Str. 29a, 18059 Rostock, Germany

Table of contents

Calculation of the segmental rates

In this part, the procedure of the calculation of the segmental rates is described. As an example, the rates of CO formation and CO_2 consumption are estimated in the case of the catalytic data of the Fe-K catalyst. The intermediate results and the calculated values of the rates are presented in the following table:

segment number i	1	2	3	4	5	6	7	8	9	10	11
flow F_i, $cm^3 \cdot h^{-1}$	36000	17500	11000	7850	5890	4570	3600	2840	2200	1630	1097
CO_2 conversion, %	2.2	4.7	7.3	10.2	13.1	15.9	17.9	20.1	22.3	25.3	30.3
CO selectivity, %	62.2	60.7	59.0	56.8	53.0	49.1	45.0	40.9	36.1	29.3	21.0
γ_i	32.8	16.0	10.0	7.16	5.37	4.17	3.28	2.59	2.01	1.49	1.00
m_i^{cum}, g	0.0030	0.0063	0.0100	0.014	0.019	0.024	0.030	0.039	0.050	0.067	0.100
m_i, g	0.0030	0.0033	0.0037	0.004	0.0047	0.0054	0.0065	0.0082	0.011	0.017	0.033
$\dot{n}_i^{CO_2}$, $10^2 \cdot mmol \cdot s^{-1}$	0.2659	0.2591	0.2521	0.2442	0.2363	0.2287	0.2232	0.2173	0.2113	0.2031	0.1895
$\dot{n}_i^{CO}$, $10^2 \cdot mmol \cdot s^{-1}$	0.0037	0.0078	0.0117	0.0158	0.0189	0.0212	0.0219	0.0224	0.0219	0.0202	0.0173
$r_i^{CO_2}$, $mmol \cdot s^{-1} \cdot g^{-1}$	0.0199	0.0206	0.0191	0.0197	0.0168	0.0141	0.0084	0.0073	0.0054	0.0048	0.0041
r_i^{CO}, $mmol \cdot s^{-1} \cdot g^{-1}$	0.0124	0.0122	0.0107	0.0101	0.0066	0.0043	0.0010	0.0006	-0.0004	-0.0010	-0.0009

Dimensionless parameter γ_i is estimated according to the following formula:

$$\gamma_i = \frac{F_i}{\min(\{F_i\})},$$

where $\min(\{F_i\})$ is 1097 $cm^3 \cdot h^{-1}$ in our case.

The values of dimensionless parameter γ_i are used for calculating of the catalyst weight for each segments according to the following formulas:

$$m_i^{cum} = \sum_{j=1}^{i} m_j = \frac{m_{cat}}{\gamma_i},$$

$$m_i = m_i^{cum} - m_{i-1}^{cum},$$

where m_{cat} is the overall catalyst weight (in our case $m_{cat} = 0.100$ g). It is worth noting that m_0^{cum} is equal to 0. The molar flow of CO_2 and CO were calculated according to the following formulas:

$$\dot{n}_i^{CO_2} = C_{CO_2} \cdot \min(\{F_i\}) \cdot \left(1 - X_{CO_2}\right),$$

$$\dot{n}_i^{CO} = C_{CO_2} \cdot \min(\{F_i\}) \cdot X_{CO_2} \cdot S_{CO},$$

where C_{CO_2} is molar concentration of CO_2 in inlet of the reactor (in our case the one is equal to 0.2). Thus, the rates of CO_2 consumption and CO formation can be calculated:

$$r_i^{CO_2} = \frac{\dot{n}_{i-1}^{CO_2} - \dot{n}_i^{CO_2}}{m_i}$$

$$r_i^{CO} = \frac{\dot{n}_i^{CO} - \dot{n}_{i-1}^{CO}}{m_i}$$

Reaction pathways analysis

It is known that the conversion-selectivity plots are usually used for the analysis of the reaction pathways occurring over the catalysts. Let's consider two-stages mechanism of hydrocarbon formation via the following reactions:

1. $CO_2 + H_2 \rightleftarrows CO + H_2O$ (RWGS)
2. $CO + 2H_2 \rightleftarrows -(CH_2) - + H_2O$ (CO-FT)

Let r_{RWGS} and r_{CO-FT} be the rates of the reactions 1 and 2, respectively. Selectivity for i-compound S_i can be defined as:

3. $S_i = \frac{r_i}{\sum_{j=1}^{n} r_j}$,

where r_i – the rate of the formation of i-product, n – the number of products. Then, CO and hydrocarbon selectivity can be presented as:

4. $S_{CO} = \frac{r_{CO}}{r_{CO} + r_{CH_2}} = \frac{r_{RWGS} - r_{CO-FT}}{r_{RWGS} - r_{CO-FT} + r_{CO-FT}} = \frac{r_{RWGS} - r_{CO-FT}}{r_{RWGS}} = 1 - \frac{r_{CO-FT}}{r_{RWGS}}$
5. $S_{CH_2} = \frac{r_{CH_2}}{r_{CO} + r_{CH_2}} = \frac{r_{CO-FT}}{r_{RWGS} - r_{CO-FT} + r_{CO-FT}} = \frac{r_{CO-FT}}{r_{RWGS}}$

Because at zero CO_2 conversion the CO concentration is equal to 0 (there are only CO_2 and H_2 in the gas feed) we have that:

6. $\lim_{X_{CO_2} \to 0} r_{CO-FT} = 0$

Thus, by combining expression 6 with 4 and 5 we can see that in the case of the two-stages mechanism the CO and hydrocarbons selectivities are 100 and 0 %, respectively, at zero CO_2 conversion. In the case of the mechanism including direct route of hydrocarbons formation from CO_2:

1. $CO_2 + H_2 \rightleftarrows CO + H_2O$ (RWGS)
2. $CO + 2H_2 \rightleftarrows -(CH_2) - + H_2O$ (CO-FT)
1. $CO_2 + 3H_2 \rightleftarrows -(CH_2) - + 2H_2O$ (CO_2-FT)

CO and hydrocarbon selectivities can be presented as:

1. $S_{CO} = \frac{r_{CO}}{r_{CO} + r_{CH_2}} = \frac{r_{RWGS} - r_{CO-FT}}{r_{RWGS} - r_{CO-FT} + r_{CO-FT} + r_{CO_2-FT}} = \frac{r_{RWGS} - r_{CO-FT}}{r_{RWGS} + r_{CO_2-FT}}$
2. $S_{CH_2} = \frac{r_{CH_2}}{r_{CO} + r_{CH_2}} = \frac{r_{CO-FT} + r_{CO_2-FT}}{r_{RWGS} - r_{CO-FT} + r_{CO-FT} + r_{CO_2-FT}} = \frac{r_{CO-FT} + r_{CO_2-FT}}{r_{RWGS} + r_{CO_2-FT}}$

And selectivity to CO and hydrocarbons at zero CO_2 conversion are:

1. $\lim_{X_{CO_2} \to 0} S_{CO} = \frac{r_{RWGS}}{r_{RWGS} + r_{CO_2-FT}} = 1 - \frac{r_{CO_2-FT}}{r_{RWGS} + r_{CO_2-FT}}$
2. $\lim_{X_{CO_2} \to 0} S_{CH_2} = \frac{r_{CO_2-FT}}{r_{RWGS} + r_{CO_2-FT}} = 1 - \frac{r_{RWGS}}{r_{RWGS} + r_{CO_2-FT}}$

One can see that selectivity of hydrocarbons are not equal to 0 % at zero CO_2 conversion and defined by the rates of RWGS and CO_2-FT reactions.

Product selectivity calculation at zero CO_2 conversion

To estimate the values of product selectivity at zero CO_2 conversion, the data about conversion-selectivity-relationship was approximated by 2-order polynomial function which was used for calculating product selectivity at zero CO_2 conversion:

$$S_i = A \cdot X_{CO_2}^2 + B \cdot X_{CO_2} + C,$$

where S_i – selectivity of i-product; X_{CO_2} – CO_2 conversion; A, B, C – coefficients of the polynomial function. The first 5 points closest to zero CO_2 conversion were used for determining polynomial coefficients.

In the case of unpromoted Fe catalyst, C_{2+} hydrocarbon selectivity at zero conversion was around 4.4%. Because this value is a little higher than zero, we performed Monte Carlo simulation for estimating an error in determination of this value. For this, we added Gauss noise (with $\sigma = 0.0167 \cdot x_i$ and mean = 0; where x_i – C_{2+} selectivity or CO_2 conversion) to the current data and created 500 sets of noised conversion-selectivity-relationship data. For each set of conversion-selectivity-relationship points, the polynomial coefficients were calculated and used for estimating C_{2+} selectivity at zero CO_2 conversion. The result of Monte Carlo simulation is presented in the Figure S2. One can see that the obtained values of C_{2+} selectivity are in a range of 0-10%. An obtained big error is related to an absent of the information about selectivity in a range of extremely low CO_2 conversion and non-linear behavior of C_{2+} selectivity and conversion relationship.

Figures

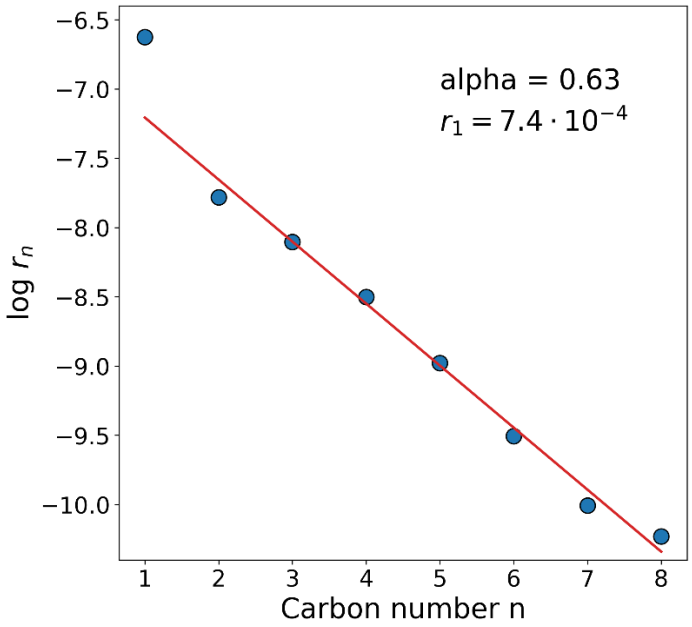

Figure S1. The distribution of hydrocarbon rates in ASF coordinates (equation 19).

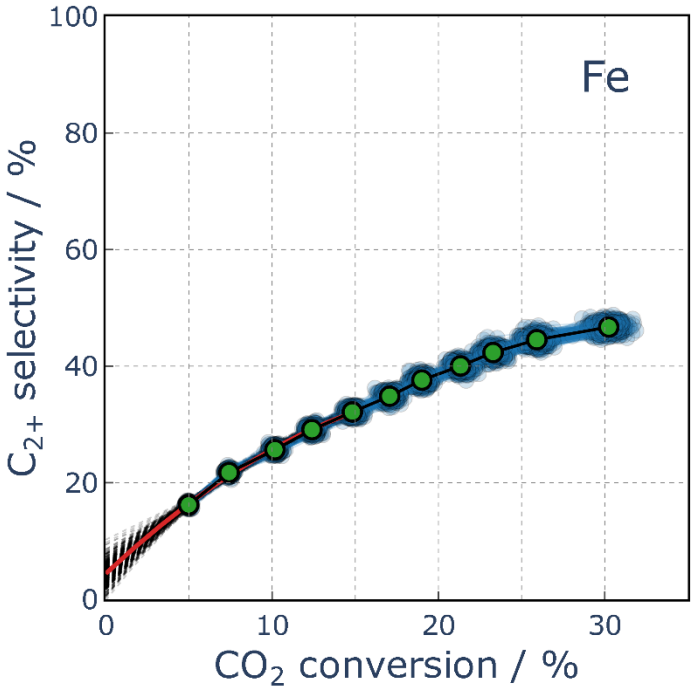

Figure S2. The result of Monte Carlo simulation for estimating C_{2+} selectivity at zero CO_2 conversion. Green dots – experimental data. Blue dots – simulated data. The red solid line – experimental data approximation using 2-order polynomial function. Black dash lines – simulated data approximation using 2-order polynomial function.

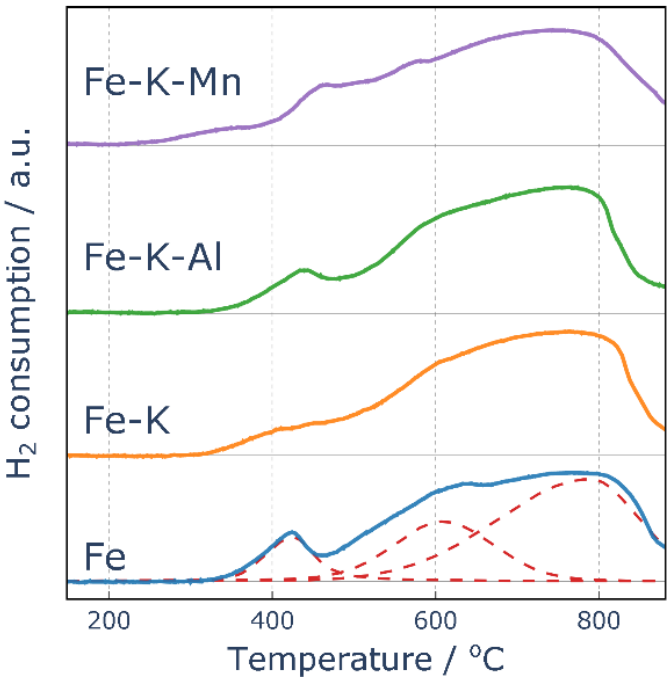

Figure S3. TPR-H_2 curves of fresh catalysts.

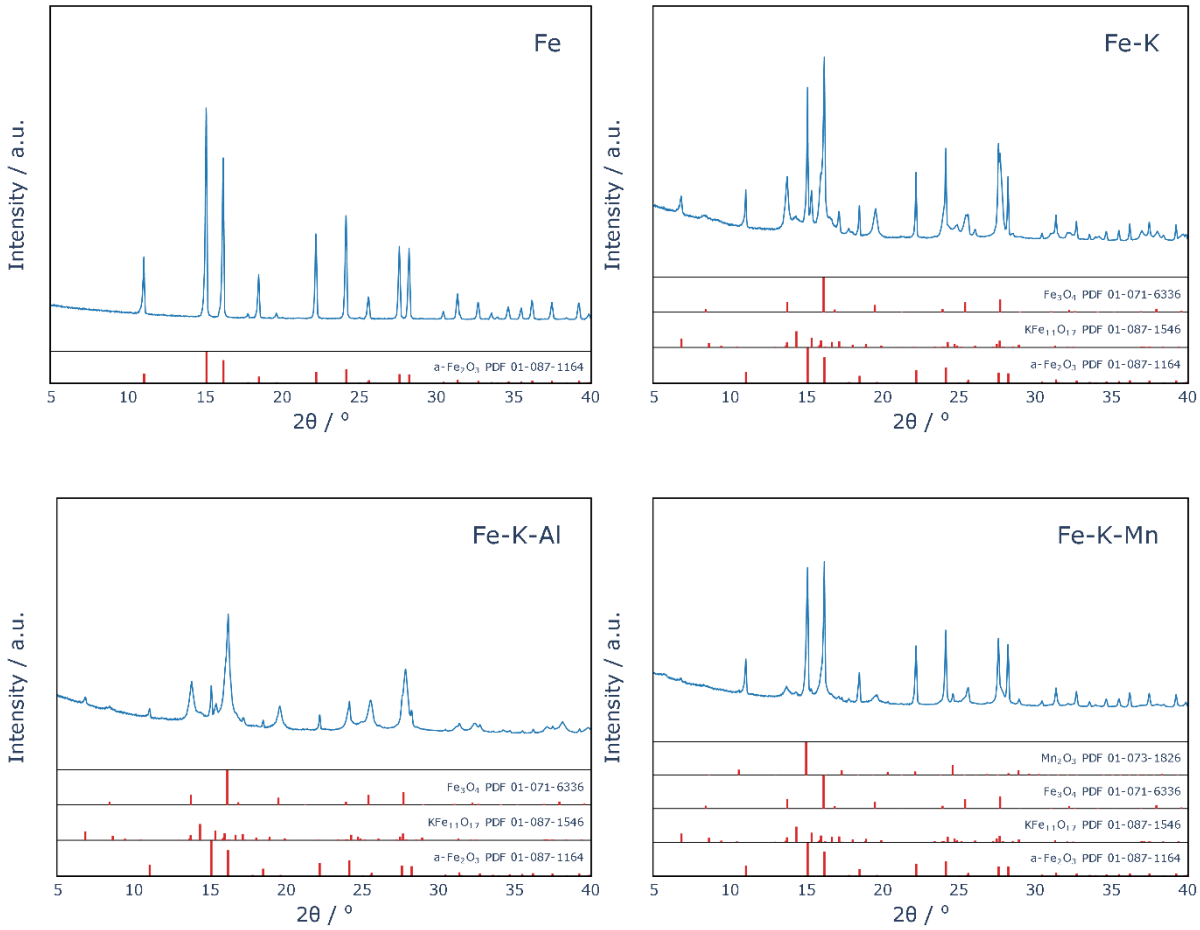

Figure S4. XRD patterns of as-prepared catalysts. $\lambda = 0.7093$ Å (Mo-K-α_1)

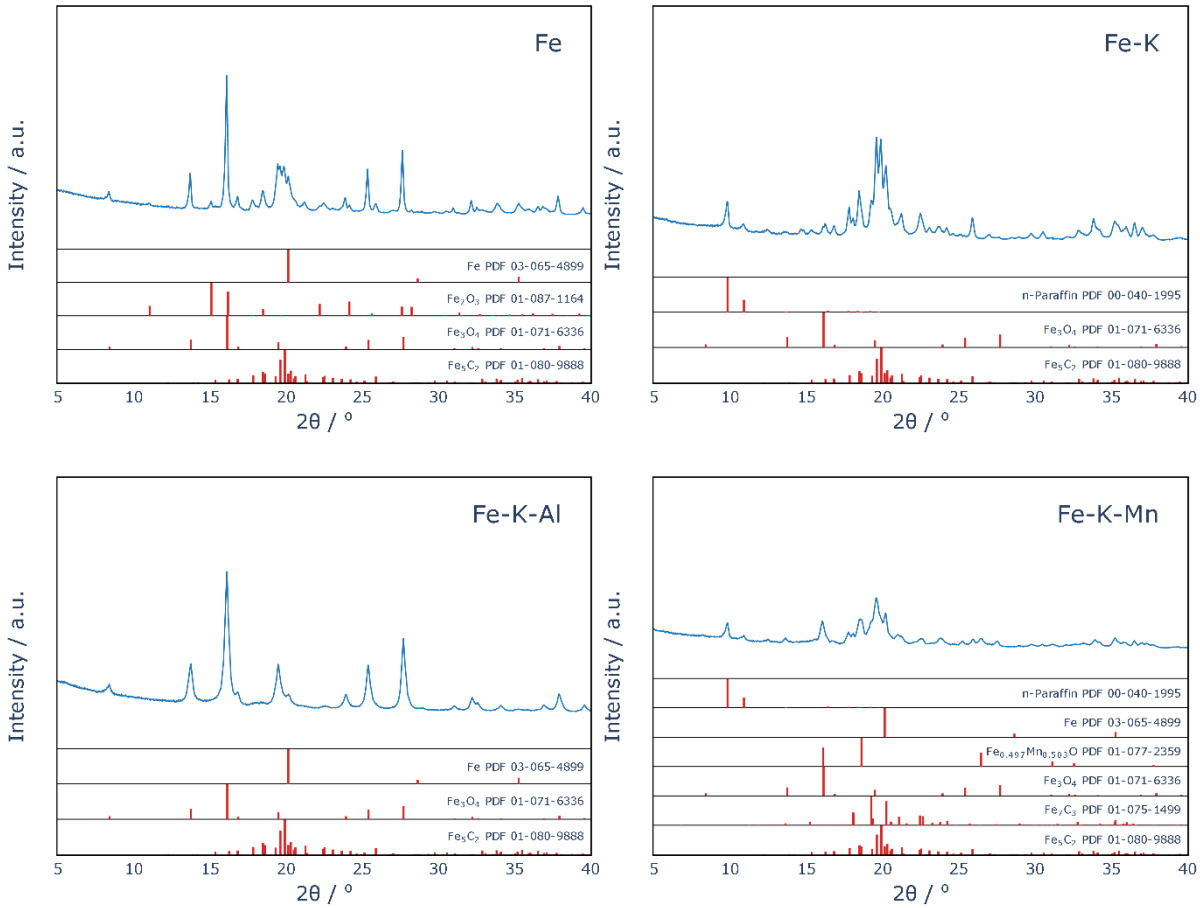

Figure S5. XRD patterns of reduced catalysts. $\lambda = 0.7093$ Å (Mo-K-α_1)

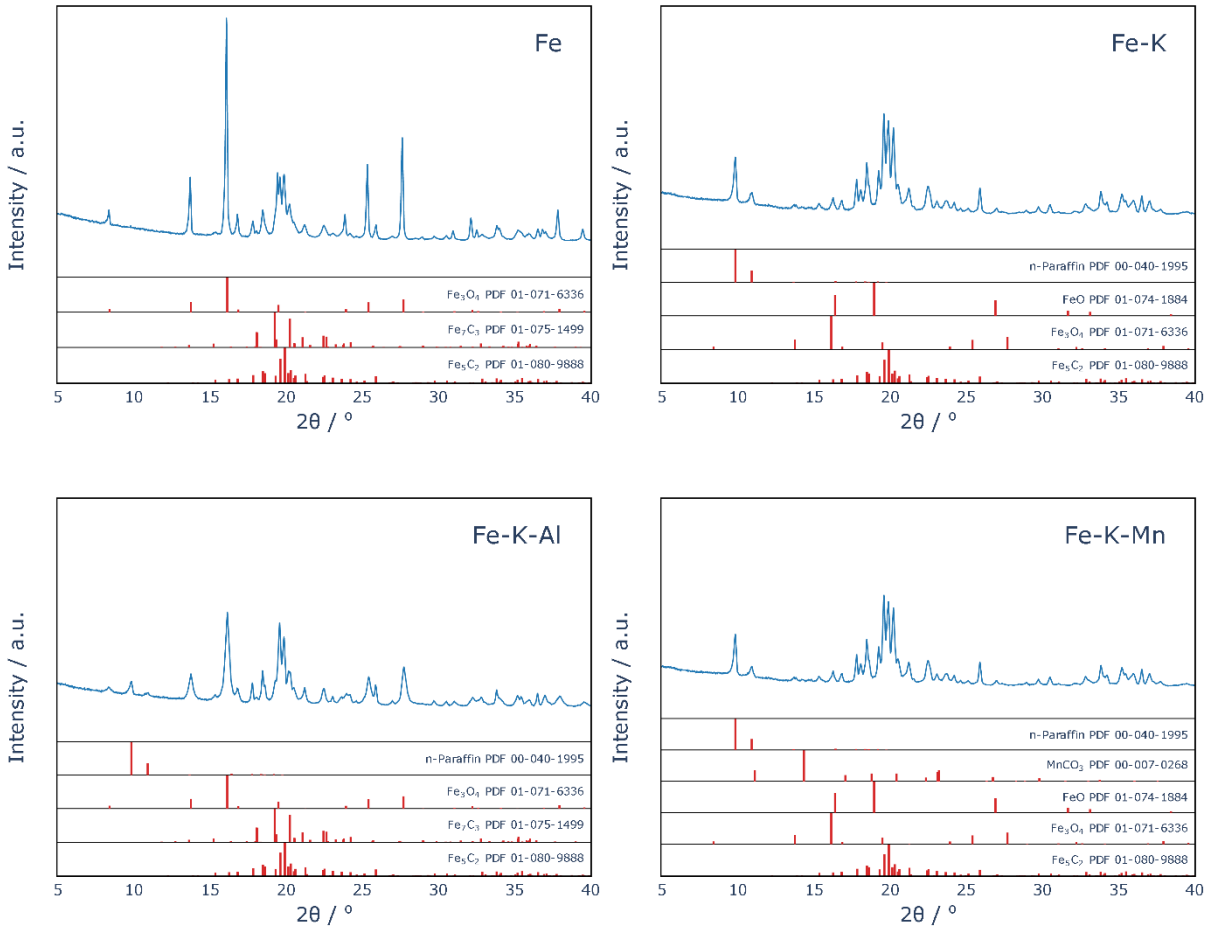

Figure S6. XRD patterns of spent catalysts. $\lambda = 0.7093$ Å (Mo-K-α_1)

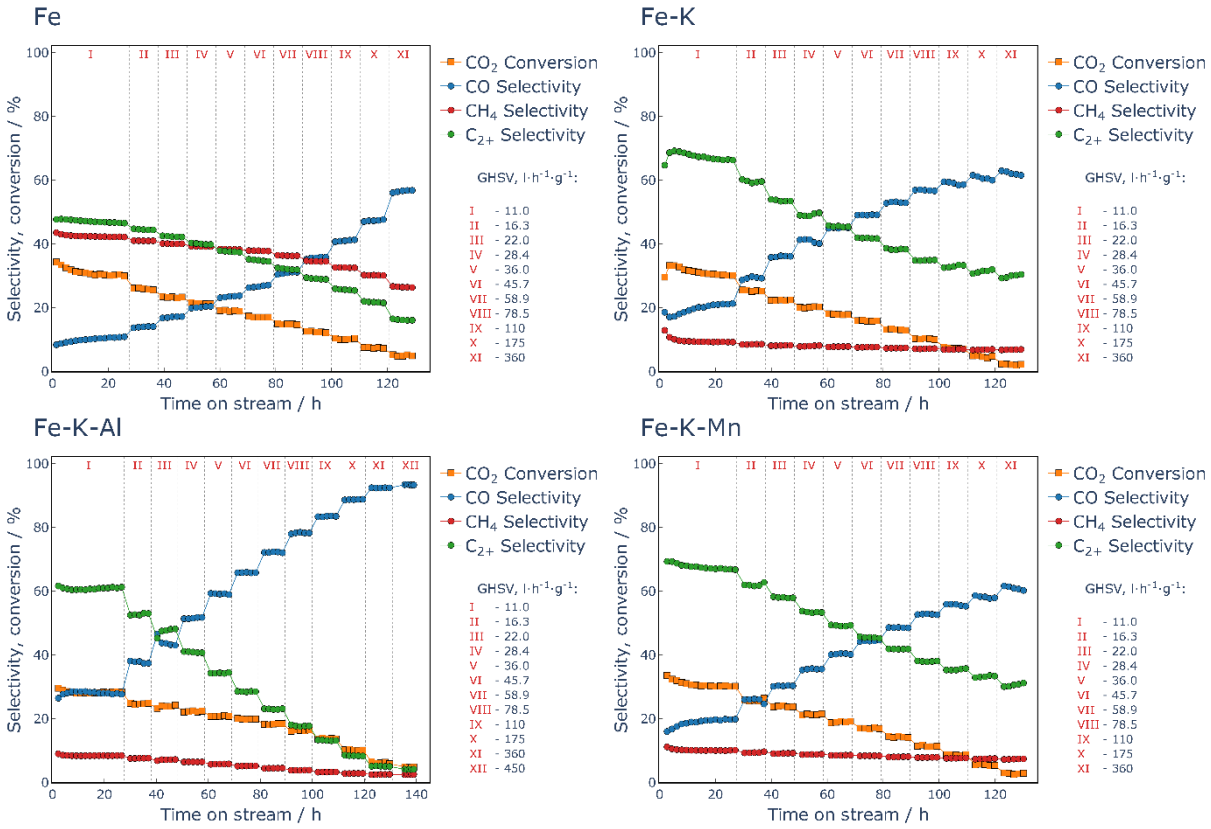

Figure S7. Time on stream profiles of CO_2 conversion and product selectivity in CO_2 hydrogenation over the obtained catalysts. Reaction condition: pressure – 15 bar; temperature – 300 °C; CO_2:H_2:N_2 – 1:3:1.

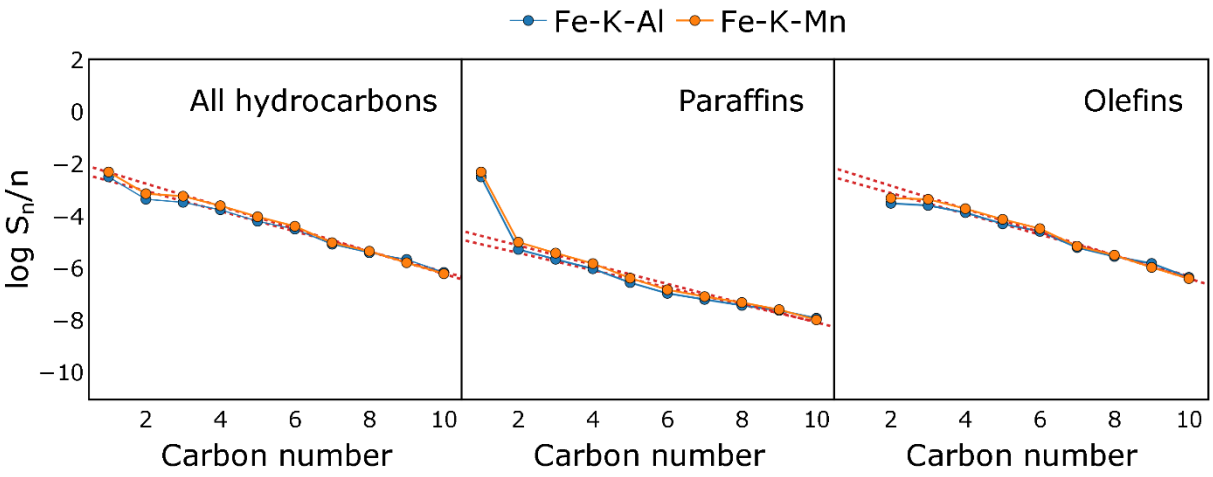

Figure S8. The hydrocarbons distribution in products of CO_2 hydrogenation over Fe-K-Al and Fe-K-Mn catalysts in corresponding ASF coordinates. Reaction condition: pressure – 15 bar; temperature – 300 °C; CO_2:H_2:N_2 – 1:3:1; GHSV – 10 970 ml· h^{-1}·g^{-1}; time on stream – 25 h.

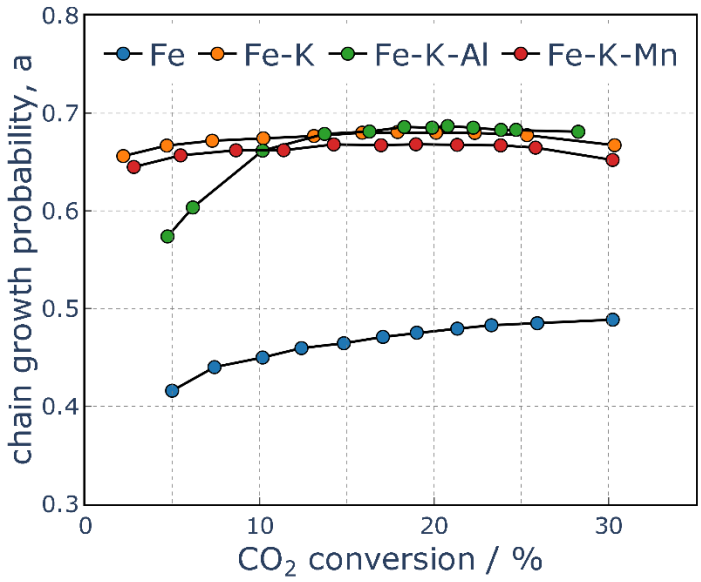

Figure S9. The dependencies between the chain growth probability α and CO_2 conversion for the obtained catalysts. C_3-C_{10} range of hydrocarbons was used for fitting the data. Reaction condition: pressure – 15 bar; temperature – 300 °C; CO_2:H_2:N_2 – 1:3:1.

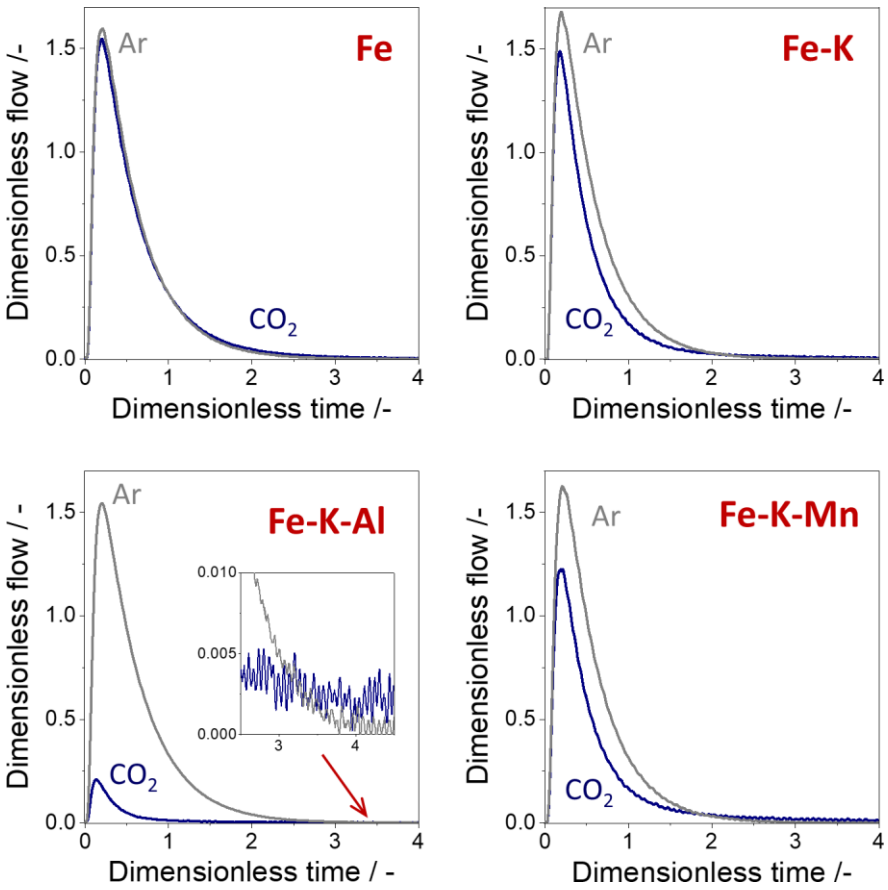

Figure S10. Dimensionless responses of Ar and CO_2 obtained after pulsing of CO_2:Ar = 1:1 at 300 °C over spent catalysts.

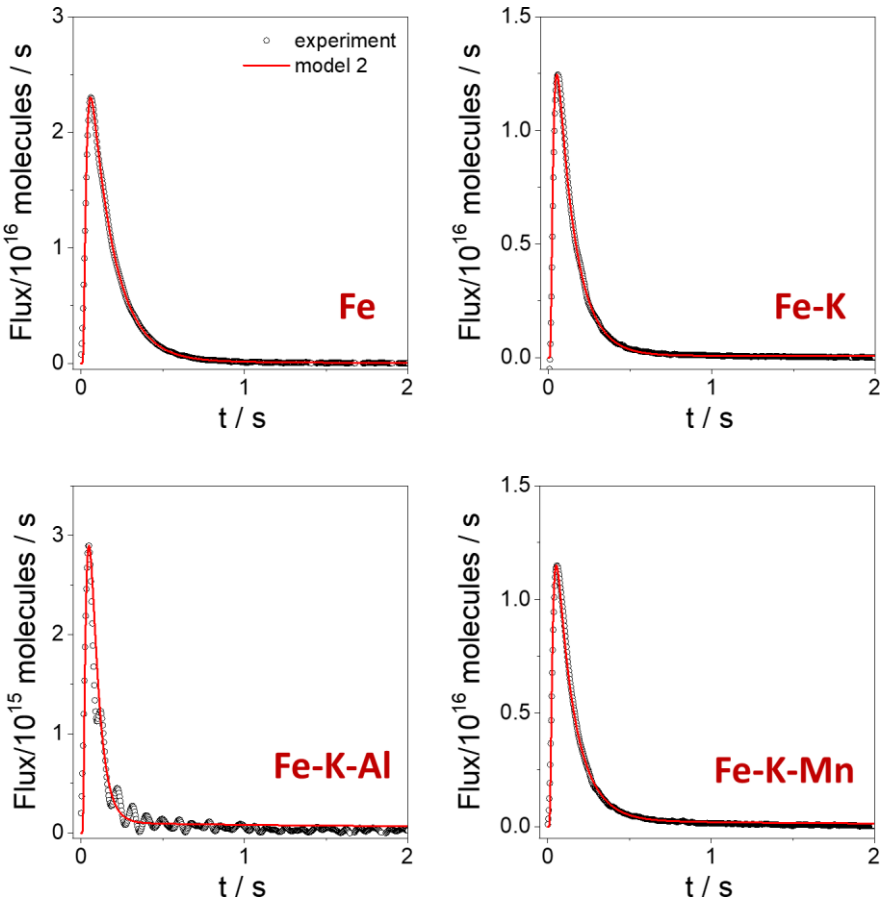

Figure S11. Comparison of simulated responses obtained with kinetic model with the experimental CO_2 responses over spent catalysts.

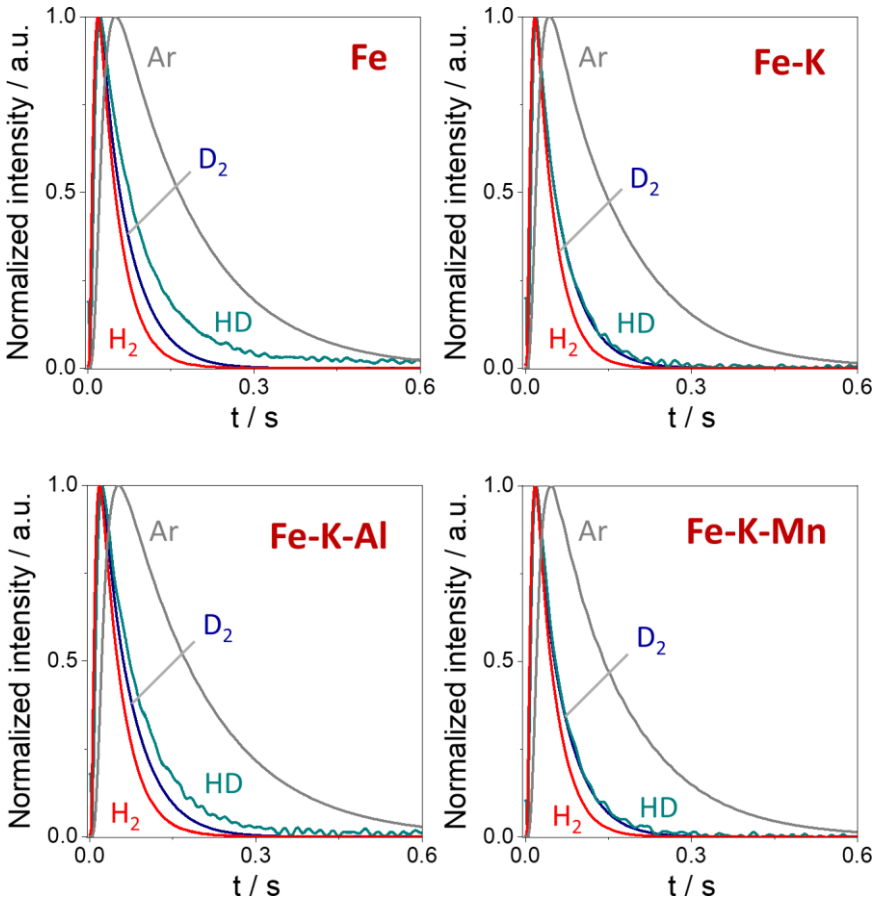

Figure S12. Height-normalized responses of Ar, H_2, D_2 and HD obtained after pulsing of $H_2/D_2/Ar$ = 1:1:1 at 300 °C over spent catalysts.

Tables

Table S1. Elemental composition and textural characteristics of as-prepared catalysts.

Catalyst	Composition, wt. %			Specific surface area, $m^2 \cdot g^{-1}$	Pore volume, $cm_3 \cdot g^{-1}$	Pore size, nm
	K	Mn	Al			
Fe	-	-	-	4	0.08	45
Fe-K	4.42 (4.62)*	-	-	13	0.12	40
Fe-K-Al	4.11 (4.36)*	-	2.94 (3.01)*	30	0.13	17
Fe-K-Mn	4.06 (4.23)*	5.99 (5.94)*	-	26	0.12	20

* theoretical content

Table S2. The catalytic performances of the obtained catalysts. C_3-C_{10} range of hydrocarbons was used for calculating the chain growth probability by fitting the data in corresponding ASF coordinates. Reaction condition: pressure – 15 bar; temperature – 300 °C; CO_2:H_2:N_2 – 1:3:1; GHSV – 10 970 $cm^3 \cdot h^{-1} \cdot g^{-1}$; time on stream – 25 h.

sample	CO_2 conversion, %	Selectivity, %					Olefins content in C_2-C_4, %	chain growth probability		
		CO	CH_4	C_2-C_4	C_{5+}	alcohols		all hydrocarbons	paraffins	olefins
Fe	30.2	10.6	42.2	35.9	10.8	0.5	46.4	0.50	0.18-0.68*	0.47
Fe-K	30.3	21.0	9.2	29.2	37.3	3.2	87.7	0.66	0.71	0.66
Fe-K-Al	28.3	27.9	8.4	25.9	35.1	2.7	87.8	0.68	0.72	0.67
Fe-K-Mn	30.2	19.6	10.0	31.1	35.9	3.3	87.2	0.65	0.69	0.64

* Because α depends on the carbon number, carbon number ranges of C_1-C_3 and C_8-C_{10} were used for calculating α. See Figure 3.

Table S3. The product selectivity at zero CO_2 conversion in carbon dioxide hydrogenation over Fe-based catalysts.

sample	Selectivity, %			
	CO	CH_4	C_{2+}	alcohols
Fe	76.3	18.5	4.4	0.8
Fe-K	62.7	6.8	29.4	1.1
Fe-K-Al	94.0	3.3	2.6	0.1
Fe-K-Mn	62.4	7.2	29.3	1.1

Table S4. Kinetic parameters of CO_2 adsorption over spent catalysts. The confidence interval for each parameter is listed in the parenthesis below the parameter.

Catalysts	k_+^{eff}, s^{-1}	k_-, s^{-1}	residual
Fe	$1.94 \cdot 10^{1}$ $(1.84 \cdot 10^{1} – 2.04 \cdot 10^{1})$	$1.13 \cdot 10^{0}$ $(5.69 \cdot 10^{-1} - 1.88 \cdot 10^{0})$	$8.64 \cdot 10^{-4}$
Fe-K	$1.28 \cdot 10^{2}$ $(1.27 \cdot 10^{2}-1.29 \cdot 10^{2})$	$1.50 \cdot 10^{-1}$ $(8.53 \cdot 10^{-2} - 2.12 \cdot 10^{-1})$	$1.16 \cdot 10^{-3}$
Fe-K-Al	$8.19 \cdot 10^{3}$ $(8.17 \cdot 10^{3} - 8.21 \cdot 10^{3})$	$8.29 \cdot 10^{-2}$ $(8.13 \cdot 10^{-2} - 8.41 \cdot 10^{-2})$	$2.95 \cdot 10^{-3}$
Fe-K-Mn	$3.41 \cdot 10^{2}$ $(3.39 \cdot 10^{2} - 3.43 \cdot 10^{2})$	$2.77 \cdot 10^{-1}$ $(2.45 \cdot 10^{-1} - 3.08 \cdot 10^{-1})$	$1.54 \cdot 10^{-3}$

Table S5. Correlation matrix of kinetic parameters obtained from modelling procedure for CO_2 adsorption over spent catalysts.

Catalysts	N_0 and k_+	N_0 and k_-	k_+ and k_-
Fe	-0.9699	0.3131	0.2988
Fe-K	-0.9722	0.2175	0.1618
Fe-K-Al	-0.7893	0.4130	-0.1079
Fe-K-Mn	-0.9673	0.1290	0.0617

Chemical Engineering Journal 477 (2023) 146869

Contents lists available at ScienceDirect

Chemical Engineering Journal

journal homepage: www.elsevier.com/locate/cej

Kinetics-constrained neural ordinary differential equations: Artificial neural network models tailored for small data to boost kinetic model development

Aleksandr Fedorov *, Anna Perechodjuk, David Linke *

Leibniz-Institut für Katalyse e.V., Albert-Einstein-Str. 29a, 18059 Rostock, Germany

ARTICLE INFO

Keywords:
Kinetic modelling
Machine learning
Artificial neural networks
CO_2 hydrogenation
Neural ordinary differential equations

ABSTRACT

Artificial neural networks (ANNs) are powerful tools for solving a wide range of tasks in fundamental and applied science. However, training and building reliable ANN models requires a lot of data which so far hinders their wider application in kinetic modelling where typically only small (experimental) datasets are available. In the present work we propose a method to design ANN models for kinetic modelling that can be trained even with small data sets as are typically available. The key idea is to constrain the architecture of the ANN models by integrating kinetic and thermodynamic knowledge leading to what we call Kinetics-Constrained Neural Ordinary Differential Equations (KCNODE). The feasibility and effectiveness of the approach is first demonstrated in a numerical experiment using the catalytic hydrogenation of CO_2 to methane as example. Next, we demonstrate the approach for real experimental data of a more complex reaction, the hydrogenation of CO_2 to higher hydrocarbons (CO_2-FT). Finally, the ANN trained for CO_2-FT is used to derive an improved mechanistic model for the reverse water gas shift reaction which is a key reaction in the CO_2-FT reaction network. This last step exemplifies how the opportunity to obtain reliable ANN models from small data opens new ways to approach kinetic model development.

1. Introduction

The use of ordinary differential equations (ODEs) for describing dynamic systems plays a key role in different fields of applied science and engineering. One of these fields is kinetic modelling of heterogeneous catalytic reactions. Another is the development of reliable models for describing catalytic process for scale-up or optimizing industrial plants in chemical engineering [1]. Traditionally, the development of such models builds upon a microkinetic analysis that requires a deep knowledge about the reaction mechanism. Postulating rate-determining steps and equilibrium stages or a most abundant reaction intermediate are general approaches to simplify the model resulting in Langmuir-Hinshelwood-Hougen-Watson (LHHW) expressions [2]. Moreover, the parameter estimation from experimental data is still an untrivial calculation problem [3].

In recent years, there has been a rapid rise in the use of machine learning (ML) and data science methods for solving many complex tasks in the different fields of science, industry, and business. These methods were successfully applied for smart discovery of high-performance and functional materials [4], revealing the latent knowledge from the material science literature [5], modelling complex physicochemical processes [6,7] etc. [8–12]. The modern approaches of ML are also applied for accelerating the development of kinetic models [13,14].

Artificial neural networks (ANNs) as universal approximators [15] are a frequently applied machine learning instrument. Their popularity is related to their flexibility to be used in various types of ANN architectures [16–20]. In the field of dynamic system modelling, Maziar Raissi et al. [7] introduced physics informed neural networks (PINN) as a kind of neural networks for solving forward and inverse problems involving nonlinear partial differential equations. They embed the knowledge about physical laws into the loss function and, thus, the trained ANN models satisfy the experimental data as well as the governing equations. Weiqi Ji et al. successfully applied PINN for solving stiff chemical problem [21]. Gabriel S.Gusmão et al. [22] generalized PINN for any chemical kinetics that was called kinetics-informed neural networks. Despite of the effectivity of the suggested approach, it still requires knowledge about the reaction mechanism and reaction rate expressions.

In 2018, Ricky T. Q. Chen et al. introduced a new family of deep neural network models that are Neural ODEs [23]. They suggested

* Corresponding authors.
E-mail addresses: aleksandr.fedorov@catalysis.de (A. Fedorov), david.linke@catalysis.de (D. Linke).

https://doi.org/10.1016/j.cej.2023.146869
Received 19 May 2023; Received in revised form 13 July 2023; Accepted 21 October 2023
Available online 25 October 2023

parametrizing the derivative of the hidden state using a neural network:

$$\frac{dx}{dt} = ANN(x, t, \theta) \tag{1}$$

The application of neural ODEs is an attractive approach for data-driven modelling of dynamic systems including kinetic models [24,25]. In fact, ANN can be used for approximating reaction rate expressions that are usually unknown. Weiqi Ji and Sili Deng [26] suggested a new type of neural ODE – chemical reaction neural network (CRNN) for autonomous identifying reaction pathways. The architecture of CRNN is based on the law of mass action and the Arrhenius law. Despite of successfully demonstration for numerical examples [26], in the case of complex dynamic system of biomass pyrolysis [27], it is difficult to interpret the developed CRNN model. This is caused by the fact that many chemical processes including heterogeneous and catalytic reactions cannot be described by simple power-law-like equations.

In summary, ANNs are a powerful instrument of ML for developing quantitative regression models and can be applied for solving a lot of tasks. The main advantage is that only data are required for building models, and, thus, in the case of kinetic modelling, it obviates the need to suggest (guess) reaction mechanism, rate-determining stage etc. However, one of the known disadvantages in applying neural networks is the requirement of a lot of data for training [28]. This so far limits the usage of ANNs in the case of small data sets which are typically available for experiment-driven development of kinetic models. Therefore, a methodology to obtain reliable ANN-based models from small data sets would be extremely valuable because it could significantly expand the scope of applying ANN models. In the present work we investigated new approaches to apply neural ODEs for kinetic modelling based on small data sets. The hydrogenation of CO_2 to hydrocarbons served as an example. To solve the small data problem and to improve the predicting ability of the models, the architecture of ANN was constrained by integrating the kinetic and thermodynamic knowledge. The novelty of the current study is that we introduce a new approach for kinetic modeling based on neural ODE that can be applied even for small noisy data. The efficiency of these new ANN models was validated by carrying out numerical experiments using a recent LHHW-type model of CO_2 hydrogenation to methane from literature [2]. The suggested approach was finally applied to a more challenging problem, the kinetics of CO_2 hydrogenation into hydrocarbons, which was modelled based on real measured experimental data.

2. Methodology

In this part the approach for kinetic modelling of catalytic reactions using neural ODE is presented. Two neural ODE models are described: the baseline neural ODE used as a reference as well as an improved neural ODE whose architecture was constrained with general information about kinetics and thermodynamics. As an example, the architecture of the neural ODE models for kinetic modelling of CO_2 hydrogenation to methane is presented. The following set of the chemical reactions was used:

$$CO_2 + H_2 \rightleftarrows CO + H_2O \quad \text{(RWGS)} \tag{2}$$

$$CO + 4H_2 \rightleftarrows CH_4 + H_2O \quad \text{(CO-FT)} \tag{3}$$

As a basic model, the following neural ODE model was used in the numerical experiment:

$$\frac{dF}{dV} = ANN(\bar{p}, T, \theta), \tag{4}$$

where F are molar flows of compounds, V – the catalyst volume, the reaction temperature T, and the vector of the partial pressure $\bar{p}$, θ – learnable parameters of ANN. In such notation the inputs of neural network have partial pressure of components, and, thus, the partial pressure was calculated by the following formula:

$$p_i = \frac{F_i \cdot P_\Sigma}{\sum F_j}, \tag{5}$$

where P_Σ is the total pressure. It is worth mentioning that there are parameters like T or P_Σ which are independent of V and should be constant along the reactor length. Parameterized neural ODE (PNODE) [29] suggested by Kookjin Lee and Eric J.Parish is an extension of neural ODE and was developed for cases when such independent parameters have to be taken into account. The main idea is to use additional encoder-decoder neural layers. Despite of authors demonstrated the effectiveness of PNODEs on benchmark problems from computational physics, the suggested approach still has a disadvantage. It is related to the complication of the architecture of neural ODEs and an increase in number of learnable parameters that require more data for model training. In our work we suggest a simpler approach for the problem of independent parameters that does not require to use additional ANN learnable variables. Our approach is to return zeros values as outputs of the ANN implementation for such constant parameters (their derivatives are zero). This makes them to be constant and independent of V.

In the case of improved neural ODE model, the following modifications were applied. Firstly, instead of using ANN for approximating molar flows of each component as in the baseline model, we suggest using ANN for approximating the reaction rates which are the feature of most interest to reaction engineers but also the basis for a detailed, mechanism-based kinetic modelling. In the case of the CO_2 hydrogenation to methane, the considered reactions are RWGS and CO-FT. It is worth mentioning that reactions pathways can be obtained by analyzing selectivity-conversion dependencies for any reaction networks [30–33]. So, the rates of formation/consumption of each compound can be calculated by using the stoichiometric matrix M_ν of the corresponding reactions:

$$\bar{r}_c = M_\nu \bar{r}_R, \tag{6}$$

where $\bar{r}_c$ and $\bar{r}_R$ are the vectors of the compound and reaction rates. Secondly, the ANN model of the rate expression is split into two parts. The first part is a feedforward neural network where inputs are partial pressure of components, and the second one is the Arrhenius-type expression for temperature dependence of rates. The second part represents a neural network layer with exponential activation function that is applied in the CRNN [26]. 'Arrhenius' temperature T_m as input for this layer was used and is defined as:

$$T_m = \frac{1}{R}\left(\frac{1}{T} - \frac{1}{T_{ref}}\right) \tag{7}$$

where R – the gas constant, T – temperature, T_{ref} = 573.15 K. Thus, weights and biases for this layer represent the activation energies and the logarithm of rate constants, respectively. The next step is to integrate the information about thermodynamic of the RWGS reaction. At equilibrium of partial pressure of components, the rate of RWGS reaction must be equal to 0 and if the reaction product Π is more than K_{eq} the rate must be negative. Finally, the trivial information that the rates must be equal to 0 at the absence of reagents is added (the rates should be zero if the partial pressure of involved reagents is zero). As summary, the rates can be presented as:

$$r_{RWGS} = k^{ref}_{RWGS} exp\left(-\frac{E^{RWGS}_a}{R}\left(\frac{1}{T} - \frac{1}{T_{ref}}\right)\right) \cdot p_{CO_2} p_{H_2}\left(1 - \frac{\Pi}{K_{eq}}\right) ANN(\bar{p}, \theta) \tag{8}$$

$$r_{FT} = k^{ref}_{FT} exp\left(-\frac{E^{FT}_a}{R}\left(\frac{1}{T} - \frac{1}{T_{ref}}\right)\right) \cdot p_{CO} p_{H_2} ANN(\bar{p}, \theta) \tag{9}$$

Π – the reaction product of the RWGS that can be defined as:

$$\Pi = \frac{p_{CO} p_{H_2O}}{p_{CO_2} p_{H_2}} \tag{10}$$

We refer to such type of neural ODE a 'Kinetics-Constrained Neural ODE' (KCNODE). The general idea and the architecture of KCNODE for kinetic modelling of CO_2 hydrogenation to methane are presented in the Fig. 1.

It is important to emphasize that for any values of neural network parameters the following constraints are met:

- Material balance.
- The rate of RWGS reaction is 0 at equilibrium. At $\Pi < K_{eq}$ the rate > 0.
- Arrhenius dependency of the rates on temperature.
- The rates are equal to 0 in absence of reagents.

It is worth also noting the key difference between our approach and PINN models. In PINN, the knowledge about physical laws is embedded at training of ANN by using corresponding loss functions. In our case, the architecture of ANN is already intrinsically constrained by kinetic and thermodynamic knowledge.

3. Experimental part

3.1. Numerical data generation

To train and validate the ANN models, the data from a typical fixed bed reactor are needed. Since one of the tasks in the present study is to develop a kinetic model of CO_2 hydrogenation to higher hydrocarbons (CO_2 Fischer-Tropsch synthesis (CO_2-FTS)) using ANNs, for the numerical experiment we have selected the kinetic model recently published by Lucas Brübach et al. [2]. The authors demonstrated that the suggested kinetic model describes the CO_2-FTS well. This model is based on two reactions: the RWGS and CO-FT reaction. Based on elementary reaction steps, the authors suggested the following empirical LHHW expressions for describing the rates r_i of the RWGS and CO-FT reactions:

$$r_{RWGS} = \frac{k_{RWGS}\left(p_{CO_2}\sqrt{p_{H_2}} - \frac{p_{CO}p_{H_2O}}{K_{eq}\sqrt{p_{H_2}}}\right)}{\left(1 + a_{RWGS}\frac{p_{H_2O}}{p_{H_2}}\right)^2} \tag{11}$$

$$r_{FT} = \frac{k_{FT} p_{CO} p_{H_2}}{\left(1 + a_{FT}\frac{p_{H_2O}}{p_{H_2}} + b_{FT} p_{CO}\right)^2} \tag{12}$$

To simplify the numerical experiment, we did not model the hydrocarbons distribution in full detail but considered methane to be the only product of CO-hydrogenation reaction (r_{FT} was used as rate of methane formation).

The temperature dependency of the rate constants is given by re-parameterized Arrhenius equation:

$$k_i = k_{i,ref}\exp\left(-\frac{E_{a,i}}{R}\left(\frac{1}{T} - \frac{1}{T_{ref}}\right)\right) \tag{13}$$

For calculation of the equilibrium constant K_{eq} of the RWGS reaction at different temperature the following expression was used:

$$\log K_{eq} = 3.933 - \frac{4076}{T/K - 39.64} \tag{14}$$

The values of all parameters used in the simulations can be found in the Table S1. As reactor model, we selected the steady-state ideal plug-flow reactor model. It was assumed that temperature and total pressure are constant along the reactor length; axial dispersion and wall effect are negligible; internal and external mass transfer limitations are also negligible. Based on this, the data was generated by the solving the following system of ordinary differential equations:

$$\frac{dF_j}{dV} = \rho_c \sum_i \nu_{i,j} r_i, \tag{15}$$

For solving this stiff system of ordinary differential equations, the numerical Adams/BDF method with automatic stiffness detection and switching was used [34]. The developed reactor model was used for generating training and test data sets. A small training data set mimicking a typical set of catalytic experiments that could be used for

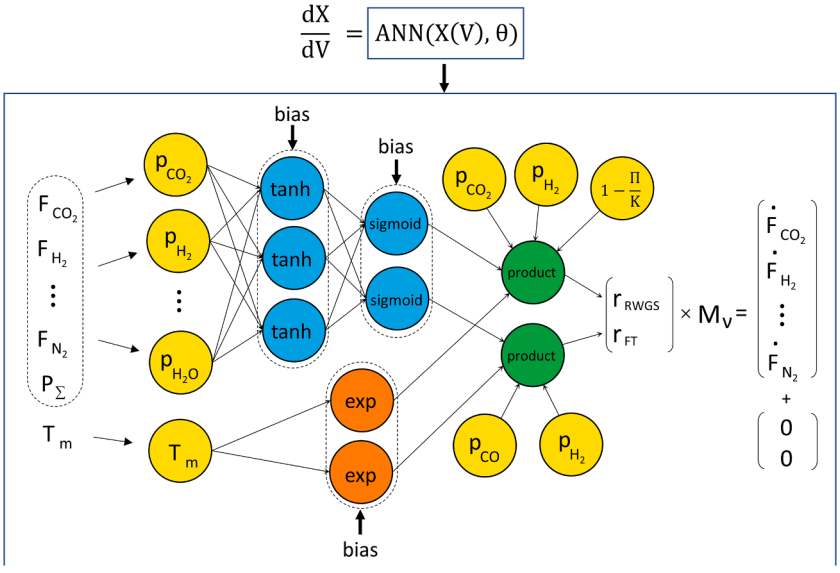

Fig. 1. Topology of kinetics-constrained neural ordinary differential equation. *tanh*, *sigmoid* and *exp* are neural layers with hyperbolic tangent, sigmoid and exponential activation functions, respectively; *product* is a layer which returns the multiplication of all the inputs; the sign ' × ' expresses matrix multiplication and the sign ' + ' is the concatenation. F_i – molar flow of i-compound; P_Σ – the total pressure; P_i – the partial pressure of i-compound; Π – the reaction product; K – the equilibrium constant.

creating the kinetic models in conventional way was used for training ANN models. The reaction conditions used for generating the training data set are presented in the Table 1. The catalyst volume V was varied in a range from 10^{-4} to 10^{-1} cm^{-3}. For each reaction conditions, the 7 points of V were uniformly spaced in a logarithmic scale across the chosen range. In the case of training the baseline model (see the baseline model), the data with zero molar flows of CO_2 + CO or zero flow of H_2 were additionally added. In these cases, the molar flows are constant along the reactor length and equal to the molar flows at the reactor inlet.

To investigate the influence of data size on the generalization of neural ODE models, training datasets with different amount of datapoints were generated (see Table 2).

To make the modelling task more realistic, we added Gauss noise to the data to imitate an experimental error. Training sets with 0.0, 2.5 %, 5.0 %, and 10 % noise were generated. To validate the performance of the obtained neural ODE models, another larger test data set was generated by a full factorial design [35] using the following reaction conditions:

- Temperature: 255, 285, 315, 345 °C.
- Pressure: 12, 14, 16, 18 bar.
- CO_2 molar flow: 0.0, 0.5, 1.2 mol·s^{-1}.
- H_2 molar flow: 2.5, 4.0, 5.5 mol·s^{-1}.
- CO molar flow: 0.0, 0.3 mol·s^{-1}.
- CH_4 molar flow: 0.0, 0.3 mol·s^{-1}.
- H_2O molar flow: 0.0, 0.3 mol·s^{-1}.

The molar flow of N_2 was set to 1.0 mol·s^{-1}. Thus, the total amount of different reaction conditions was 1152 (compared to 8 in the training data set, Table 1). The catalyst volume V was varied in a range from 10^{-4} to 1 cm^{-3}. For each reaction conditions, the 20 points of V were uniformly spaced in a logarithmic scale across the chosen range.

3.2. The architecture of the baseline neural ODE

The neural network consists of 3 layers with 8, 8, and 5 nodes per layer, and with activation functions: hyperbolic tangent, exponential and linear, respectively. The first layer consists of 6 inputs: partial pressure of compounds (for CO_2, CO, H_2, H_2O, CH_4) and temperature. The output of the linear layer is expanded by concatenating with 3-dimensional zeros vector (for temperature, total pressure and N_2 molar flow). Before training, the value of total pressure and temperature were scaled by dividing by the maximum values.

3.3. The architecture of the kinetics-constrained neural ODE

3.3.1. CO_2 hydrogenation to methane

The detailed architecture of the KCNODE for modelling of CO_2 hydrogenation to methane was described in the methodology. The hidden layer of the neural network with a hyperbolic tangent activation function consists of 8 nodes. The first layer consists of 6 inputs: partial pressure of compounds (for CO_2, CO, H_2, H_2O, CH_4) and temperature. To investigate the performance of KCNODE models, an analogue model with 20 nodes in the hidden layer was also constructed. Before training the values of pressure was scaled by dividing by the maximum total pressure.

Table 1
Reaction conditions for generating the training data set.

#	Temperature, °C	Pressure, bar	Molar flow, mol·s^{-1}			
			CO_2	CO	H_2	N_2
1	250	10	1.0	0	3.0	1.0
2	300	10	1.0	0	3.0	1.0
3	350	10	1.0	0	3.0	1.0
4	300	15	1.0	0	3.0	1.0
5	300	20	1.0	0	3.0	1.0
6	300	10	1.0	0	2.0	1.0
7	300	10	1.0	0	6.0	1.0
8	300	10	0.5	0.5	3.0	1.0

Table 2
Reaction conditions for generating the training datasets with different size.

#	Number of experimental data points[a]	Used reaction conditions [b]	Values of V, cm^{-3}
1	112	1–8	10^{-4}, $3.2{\cdot}10^{-4}$, 10^{-3}, $3.2{\cdot}10^{-3}$, 10^{-2}, $3.2{\cdot}10^{-2}$, 10^{-1}
2	80	1–8	10^{-4}, $5.6{\cdot}10^{-4}$, $3.2{\cdot}10^{-3}$, $1.8{\cdot}10^{-2}$, 10^{-1}
3	48	1–8	10^{-4}, $3.2{\cdot}10^{-3}$, 10^{-1}
4	20	2, 3, 5, 7, 8	10^{-2}, 10^{-1}

[a] number of experimental data points = number of reaction conditions × number of points of V × number of reactions;
[b] reaction condition used for the data generation from Table 1.

3.3.2. CO_2 hydrogenation to hydrocarbons

The suggested approach was applied for kinetic modeling of the process of CO_2 hydrogenation into hydrocarbons using real experimental data. It is generally accepted [36,37] that the process of CO_2-FT synthesis proceeds in two stages: the RWGS reaction followed by CO hydrogenation via FT mechanism. Besides, an additional pathway of direct CO_2 hydrogenation to methane, also known as the Sabatier reaction, occurs over Fe-based catalysts that was suggested in the works [30,33,38,39]. Thus, the following reaction set was used for building the model:

$$CO_2 + H_2 \rightleftarrows CO + H_2O \tag{16}$$

$$CO + \left(2 + {}^{1}/_{n}\right)H_2 \rightarrow {}^{1}/_{n}C_nH_{2n+2} + H_2O \tag{17}$$

$$CO + 2H_2 \rightarrow {}^{1}/_{n}C_nH_{2n} + H_2O \tag{18}$$

$$CO + 2H_2 \rightarrow \frac{1}{n}C_nH_{2n+1}OH + \left(1 - \frac{1}{n}\right)H_2O \tag{19}$$

$$CO_2 + 4H_2 \rightarrow CH_4 + 2H_2O \tag{20}$$

The reaction of CO hydrogenation via FT mechanism has a kinetic limitation. The mass fraction W_n(n – carbon number) of hydrocarbons (or alcohols) in the products can be described by the Anderson-Schulz-Flory (ASF) distribution [40–42]:

$$W_n = n(1-\alpha)^2\alpha^{n-1} \tag{21}$$

where n is carbon number, α is the chain growth probability that is defined as ratio between the rate of the chain prolongation per the sum of the chain prolongation and termination rates [43]. The equation allows describing the formation of each product observed using only a few parameters. Thus, assuming the validity of the ASF the formation rate of compound with carbon number n can be defined as:

$$r_n = n\alpha^{n-1}r_1 \tag{22}$$

The expression (22) was also used to describe the formation of olefins and alcohols because they correspond to ASF except for CH_3OH and C_2H_4 (see Fig. 3, D and E). To consider these deviations from ASF, additional dimensionless empirical coefficients (δ_{en} and δ_{OH}) were used and the rates of methanol and ethylene formation are defined as:

$$r_{C_2H_4} = 2{\cdot}\delta_{en}{\cdot}\alpha_{en}{\cdot}r_1^{en} \tag{23}$$

$$r_{CH_3OH} = \delta_{OH}{\cdot}r_1^{OH} \tag{24}$$

Here, it is worth mentioning that r_1^{en} means the rate of formation of

'hypothetical' alkene with carbon number 1 which are not considered as a product of CO_2 hydrogenation but used only to calculate the rates of alkene formation. The deviation from ASF distribution in C_2 could be due to high reactivity of ethylene or C_2-intermediates participating in the chain growth compared to other olefins [44–46]. A decrease in methanol selectivity compared to ideal ASF distribution could be explained by a separate parameter of the termination probability. So, Panzone et al. found that the methanol termination probability parameter (the rate constant) is 3.5 lower than the one of other alcohols [47]. In the case of paraffins, a non-linear dependence of hydrocarbon distribution in the corresponding ASF coordinates is observed (see Fig. 3, C). Such non-linear behavior can be related to the presence of the two different types of active sites taking part in processes of the chain growth that was discussed in the works [46,48]. Thus, the rate of paraffin formation with carbon number n can be described as:

$$r_n = \mu \cdot n \cdot \alpha_{an_1}^{n-1} \cdot r_1^{an} + (1-\mu) \cdot n \cdot \alpha_{an_2}^{n-1} \cdot r_1^{an}, \tag{25}$$

where μ and $1-\mu$ are the fraction of paraffin products having molecular weight distribution parameters α_{an_1} and α_{an_2} respectively. It is worth noting that the suggested parameters like the chain growth probability α_{an_1}, α_{an_2}, α_{en}, and α_{OH}; empirical coefficients δ_{en} and δ_{OH}; fraction μ also depend on reaction conditions (partial pressure of compounds, temperature), and that the ANN model was used for predicting the values of these parameters.

The inputs for the hidden layer of ANN in the case of modeling of the CO_2-FT process are partial pressure of compounds (CO_2, CO, H_2, H_2O), temperature, and time on stream. Time on stream was used because an activation-deactivation process was observed (see Fig. S9) during the measurement of the catalyst activity in CO_2 hydrogenation. The ANN was used for predicting the reaction rates (16)–(20) as well as the suggested parameters (α_{an_1}, α_{an_2}, α_{en}, α_{OH}, δ_{en}, δ_{OH}, and μ). Thus, the number of outputs for each a node of the hidden layer was 12. For the hidden layer of the ANN with a hyperbolic tangent activation function 8 nodes were used. The model takes into consideration the formation of alkanes and alkenes (up to 15 carbon number), and alcohols (up to 7). Before training the value of total pressure was scaled by dividing by the maximum total pressure and time-on-stream was scaled by dividing by the maximum value of time-on-stream in the experimental data set.

3.4. Training neural network models

The Runge-Kutta 3/8 Method (*RK4*) and Runge-Kutta of order 5 of Dormand-Prince-Shampine method (*DOPRI5*) method were used for the integration of neural ODE [49]. Training neural network models was carried out by minimization of the loss functions using ADAM [50] optimizer with a learning rate of 0.005. The training ended when the loss function flatlined. In the case of the numerical experiment, the following loss function was used:

$$loss = MSE(F^{exp}, F^{pred}), \tag{26}$$

where MSE is the mean squared error.

In the case of training KCNODE using experimental data the following loss function was used:

$$\begin{aligned} loss \quad = {} & 5 \cdot MSE_{i=(CO_2,CO,CH_4)}\left(\frac{F_i^{exp}}{F_i^{scale}}, \frac{F_i^{pred}}{F_i^{scale}}\right) + \\ & \frac{1}{3} MSE_{i=alkene}\left(\frac{F_i^{exp}}{F_i^{scale}}, \frac{F_i^{pred}}{F_i^{scale}}\right) + \\ & \frac{1}{3} MSE_{i=alkane}\left(\frac{F_i^{exp}}{F_i^{scale}}, \frac{F_i^{pred}}{F_i^{scale}}\right) + \\ & \frac{1}{3} MSE_{i=alcohol}\left(\frac{F_i^{exp}}{F_i^{scale}}, \frac{F_i^{pred}}{F_i^{scale}}\right) \end{aligned} \tag{27}$$

where F_i^{scale} – a characteristic scale for compound i that was calculated as a maximum value for the molar flow of i-compound in the dataset. In the work [51] Suyong Kim et al. suggested using such the scaling (dividing by F_i^{scale} in the expression (27)) to mitigate stiffness of ODE. Another, reason for splitting the loss function in this way is to make the contribution of each hydrocarbon (or alcohol) in the loss function smaller than the contribution of CO_2, CO, and CH_4. This is related to the point that only few parameters (α_{an_1}, α_{an_2} etc.) are needed to describe hydrocarbon (and alcohol) distribution (36 measured compounds: 15 paraffins + 14 olefins + 7 alcohols). L_2-regularization was used for mitigating stiffness of neural ODE at training. The parameter of the regularization was set to 10^{-6}.

3.5. Catalyst preparation, characterization, and testing

For measuring data for kinetic modeling of CO_2 hydrogenation to hydrocarbons, a typical Fe-based catalyst doped by K and Cu was prepared by incipient wetness impregnation method using Al_2O_3 support. The full description of preparation method and catalyst characterization can be found in the supplementary material. The catalysts were tested in CO_2-FT reaction at the following reaction conditions:

- Temperature in a range 250–310 °C.
- Pressure in a range 10–20 bar.
- Modified residence time in a range 52.4–5327 kg·s·m^{-3}.
- CO_2:H_2 ratio in a range 1.5–6.0.
- CO:CO_2 ratio in a range 0.0–0.52.

Time on stream was at least 14 h for each reaction condition. The detailed description of catalytic experiments and experimental setup can be found in the supplementary material. The absence of any external heat transfer, external diffusion limitations, the wall effect, and axial dispersion were checked by applying Mears and Weisz-Prater criteria [52,53] (see supplementary material). It is worth noting that the catalysts were periodically tested at the same condition (baseline) during catalytic measurements. This allowed to follow activation-deactivation processes occurring under CO_2 reaction conditions (see Fig. S9).

3.6. Software and hardware specifications

Python programming language (version 3.9.12-64bit, Windows 10 Pro) was used for calculation [54]. Scientific libraries NumPy [55] (version 1.23.0), SciPy [56] (version 1.8.1), Pandas [57] (version 1.23.0), Scikit-learn [58] (version 1.1.1) were used for data analysis and evaluation. Pytorch [59] (version 1.12.0) and Torchdyn [49] (version 1.0.3) were used for building and training neural networks models. Plotly [60] (version 5.9.0) was used to visualize the results. All calculations were performed by using 11th Gen Intel Core i-7 11700F (no GPU was used). All the code is openly available on GitHub at https://github.com/LIKAT-Rostock/kcnode-paper.

4. Results

4.1. Numerical experiment

In this part we investigated the generalization of the neural ODE models trained by using the small, simulated data set. The process of training the neural ODE models represented as dependency between loss function and epoch number is summarized in the Fig. S1. The generalization of the obtained models in predicting training and test data sets are presented in Fig. 2.

One can see that the baseline model fits the training data correctly which corresponds to the low value of loss function (see Table 2). However, this model performs poorly when it was used for predicting and describing data outside of the training range. This is clearly visible

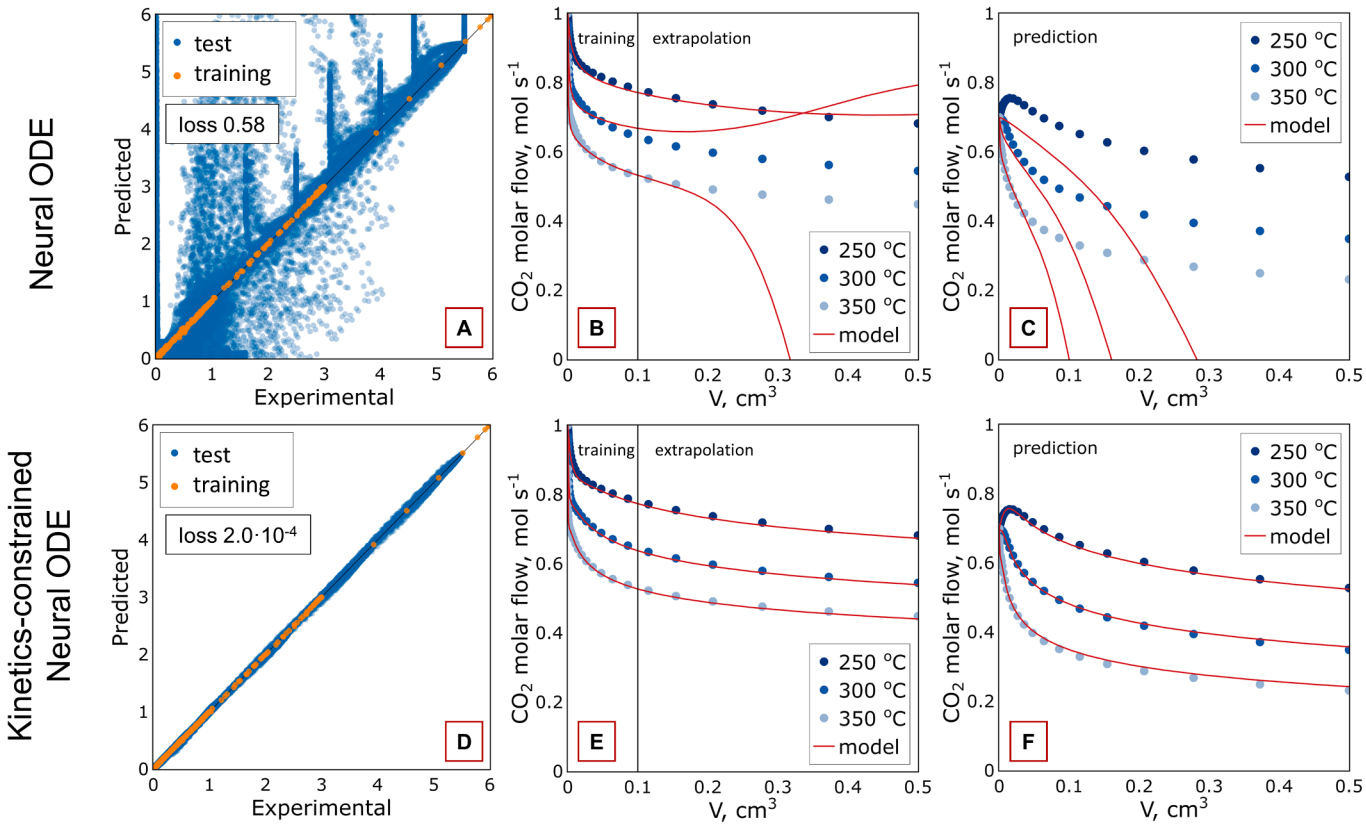

Fig. 2. Comparison of the generalization capability between baseline neural ODE (top) and kinetics-constrained neural ODE (bottom) models. **A** and **D**: Parity plots for molar flows of reagents and products. **B** and **E**: Observed (dots) and fitting (line) data of dependencies between the molar flow of CO_2 and the catalyst volume V for training data and their extrapolation (reaction condition: CO_2:H_2:N_2 – 1:3:1, pressure – 10 bar). **C** and **F**: Observed (dots) and fitting (line) data of dependencies between the molar flow of CO_2 and the catalyst volume V for selected test data (reaction condition: CO_2:CO:H_2:H_2O:N_2 – 0.7:0.3:4:0.2:0.5, pressure – 12 bar).

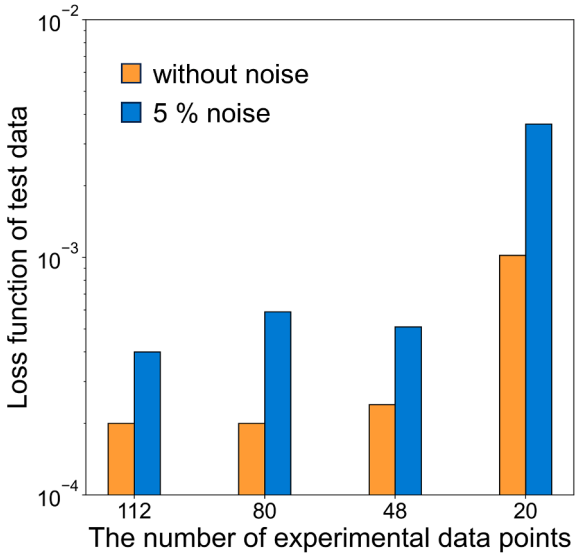

Fig. 3. The loss function of the test data for the obtained KCNODE models trained with different non-noisy and noisy training datasets having various number of experimental data points. The loss function was calculated by the expression (26).

in Fig. 2 (B-C) where the baseline model was used for extrapolating and fitting the test data set. Accordingly, a high value for the loss function was obtained for the test data test (Table 2). ANN models are known to require a lot of data for training, and the obtained result proves this. Therefore, we can conclude that the standard approach for chemical kinetics modelling using neural ODE cannot be applied when ANN models are trained based on small data set.

To improve the neural ODE models, the kinetic and thermodynamic information about CO_2 hydrogenation to methane was added into the architecture of neural ODE model. From the lower row of plots in Fig. 2 one can see that the suggested approach improves the predicting ability of ANN model significantly. With this model, the value of the loss function for the test data set has decreased around 2900 times compared to the baseline model (Table 3). Moreover, the KCNODE model can describe the data outside of the training range correctly that is seen from the presented results. It is also worth noting that the loss function for the training data set in the case of the KCNODE model is lower than in the case of the baseline model (see Table 3). Wherein, the numbers of learnable parameters for the baseline and KCNODE models are 177 and 70, respectively. Thus, an increased number of parameters of the baseline model is not enough to achieve the same low value of the loss

Table 3
Values of loss function of the obtained models for training and test data sets.

	Loss function	
	training data set	test data set
Baseline model	$5.2{\cdot}10^{-4}$	0.58
KCNODE 0 %	$0.4{\cdot}10^{-4}$	$2.0{\cdot}10^{-4}$
KCNODE 2.5 %	$1.6{\cdot}10^{-4}$	$4.6{\cdot}10^{-4}$
KCNODE 5.0 %	$3.1{\cdot}10^{-4}$	$4.0{\cdot}10^{-4}$
KCNODE 10 %	$1.6{\cdot}10^{-3}$	$1.1{\cdot}10^{-3}$
KCNODE 20 N*	$0.4{\cdot}10^{-4}$	$2.1{\cdot}10^{-4}$

% means the value of Gauss noise in the training data set; *Kinetics-constrained neural ODE model with 20 nodes in the hidden layer and was trained by 'no-noise' data. The loss function was calculated by the expression (26).

function for training data set as in the case of the KCNODE model.

It is well-known that real data has experimental errors that can influence the performance of ANN models. This can be especially critical in the case of small data sets. For investigating this influence, KCNODE models were obtained by using the training data sets with added Gauss noise (0–10 %). The loss function values for the models trained on data of various noise levels are presented in the Table 3 (training of the models in Fig. S2, parity plots can be found in Fig. S3). One can see an increase in the values of the loss function for training and test data sets with increasing noise in the training data, but the values of the loss function for test data have the same order of magnitude in the case of 0–5 % of Gauss noise. Thus, the generalization of KCNODE models trained with noisy data is still high. It is interesting to mention that the obtained KCNODE models are quite resistant to overfitting. This cannot at all be said about the baseline model. To investigate the resistance of KCNODE model to overfitting in more detail, the model with an increased number of learnable parameters (the number of nodes in the hidden layer was increased from 8 to 20) was trained by using the same training data set (see Table 3). The obtained model has also high predicting ability. Wherein, the number of parameters of the obtained ANN model is 166 and even higher than the number of independent experimental data points (the number of reaction conditions × the number of points of V × the number of reactions = 8·7·2 = 112 < 166).

Since the obtained results indicates that the KCNODE models are not prone to overfitting, we investigated in more detail how the training data size impacts the performance of KCNODE models. Fig. 3 shows the values of the loss function of the test data for the KCNODE models trained with different datasets of varying size. One can see that a decrease in the data size does not lead to significant change in the loss function for noisy and non-noisy training data sets. A large increase in the loss function is observed only for the smallest training data set with only 20 experimental data points.

Thus, we demonstrated that neural ODE models additionally constrained by adding kinetic and thermodynamic knowledge can be used to successfully model the kinetics of CO_2 hydrogenation to methane using a small data set even in the presence of noise in the data. They described experimental data correctly, wherein, the obtained models do not show a tendency for overfitting during the training. The presence of chemistry knowledge in the architecture of KCNODE model is the reason for the resistance to overfitting. The next part of work is devoted to applying this approach for kinetic modeling CO_2 hydrogenation to hydrocarbons using real experimental data.

4.2. *Modelling of CO_2 hydrogenation to hydrocarbons*

The KCNODE model was applied for kinetic modeling of CO_2 hydrogenation to hydrocarbons. To validate the generalization of KCNODE model, 10-fold cross validation was used. The training runs of the model are presented in Fig. S4. The absence of an increase in values of the loss function for the test data sets during the training indicates that the ANN models are not overfitting. The mean values of the loss function are $2.5{\cdot}10^{-3}$ and $1.6{\cdot}10^{-2}$ for training and test data sets, respectively. A parity plot comparing experimental and predicted values of molar flows in the test data is presented in Fig. 4A. The final KCNODE model was trained by using all the experimental data because the ANN model was shown to be not prone to overfitting.

As seen in Fig. 4, the obtained model correctly describes the conversion-selectivity profiles of CO_2 hydrogenation as well as the distribution of the reaction products (alkanes, alkenes, and alcohols). The profiles of the reaction products and reagents at other reaction conditions are also correctly described (see the supplementary material, Figs. S5–S8). Thus, the KCNODE was successfully applied for describing the kinetics of CO_2 hydrogenation to hydrocarbons over Fe-based catalysts and is able to predict reactant consumption and products formation

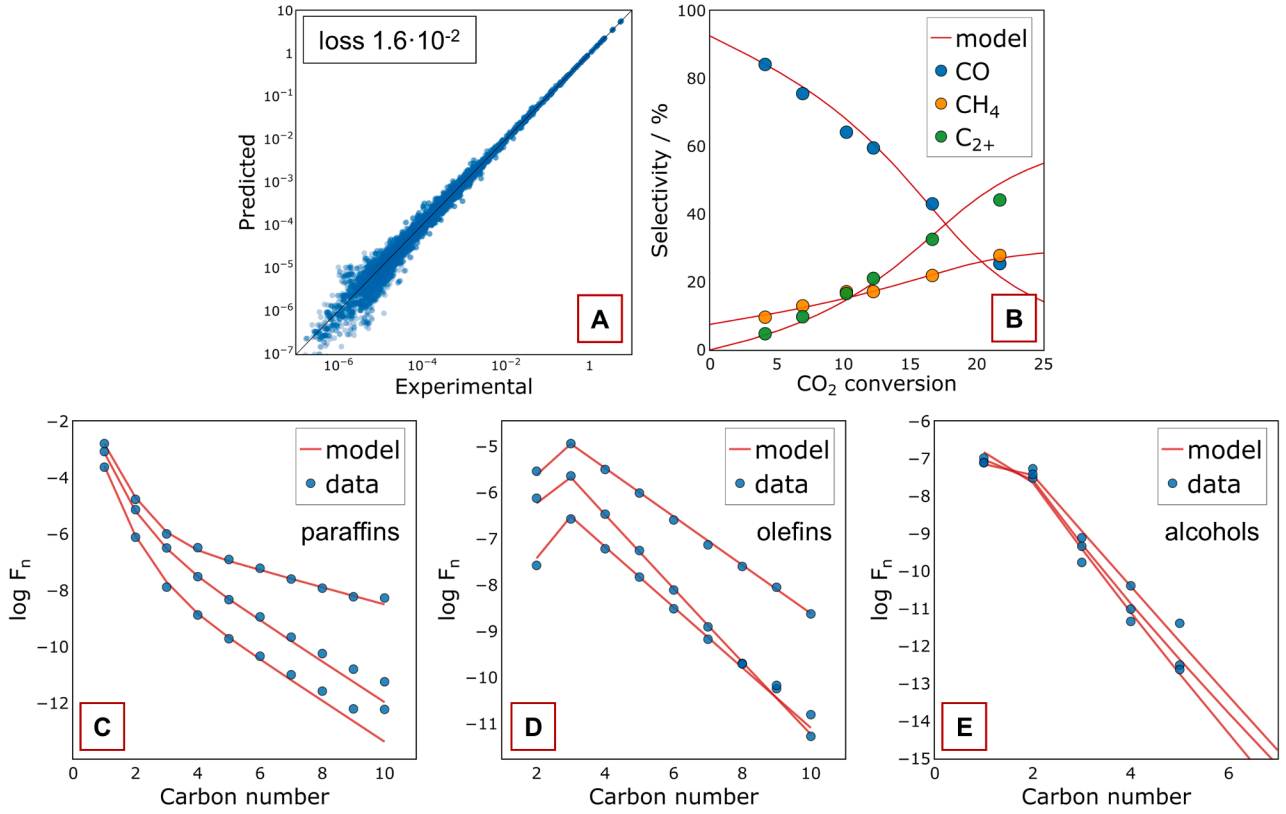

Fig. 4. **A**: Parity plot of the KCNODE model for describing CO_2 hydrogenation to hydrocarbons using 10-fold cross validation. **B**: Product selectivity versus CO_2 conversion at reaction condition: CO_2:H_2:N_2 – 1:3:1, pressure – 15 bar temperature – 270 °C. **C**, **D**, **E**: Experimental and fitting data representing products distribution for alkanes, alkenes, and alcohols, respectively.

as well as the hydrocarbon (and alcohol) distribution.

5. Discussion

Kinetic modeling of CO_2 hydrogenation over Fe-containing catalysts is usually based on empirical LHHW models. Riedel et al. [61] were the first who investigated the kinetics of CO_2 hydrogenation and suggested a LHHW model based on RWGS, CO-FT, and CO_2-FT reactions, where only propane was considered as a product of the FT synthesis. In the work [2], Brübach et al. suggested a new LHHW type kinetics expressions for modeling CO_2 hydrogenation, but they also considered only one organic compound (C_4) for describing reaction products. It is noted that the development of models predicting hydrocarbon distribution is a difficult task for kinetic modeling of CO_2 hydrogenation. Panzone et al. [62] developed a semiempirical macrokinetic model to describe products of CO_2 hydrogenation including hydrocarbon distribution using the ASF distribution. Recently, a microkinetic approach was applied that allowed obtaining the models successfully describing reagent consumption and products formation as well as hydrocarbon distribution of CO_2 hydrogenation that were demonstrated in works [47,63]. From the presented works one can see the complexity of kinetic modeling of CO_2 hydrogenation to hydrocarbons. In our work we demonstrated that KCNODE could be successfully applied for describing the kinetics of this complicated reaction.

It is worth mentioning that the calculational and time costs for building ANN models are significantly lower compared to the development of a kinetics model in the traditional way which requires deep knowledge about mechanism of reactions and great expertise in making appropriate simplifying assumptions, and for the solving inverse kinetic task (Fig. 5). In contrast, an easily obtained KCNODE model can already be used for further development, e.g. scale-up related modelling in chemical engineering. However, the KCNODE model can be also used for gaining insights into the underlying chemical processes by generating virtual data. It could be considered as an intermediate model helping to develop a kinetic model based on fundamental mechanistic principles and to elucidate the reaction mechanism.

To demonstrate this procedure of using the KCNODE as intermediate model, we screened the literature for kinetic models of the RWGS reaction to find the kinetic expression that is best matching the rates estimated by the developed KCNODE model and the one calculated by the LHHW expressions suggested in the literature (see the supplementary material). We also derived a new type of LHHW expression for describing the rate of the RWGS based on elementary reaction steps:

$$r_{RWGS} = \frac{k\left(p_{CO_2}p_{H_2} - \frac{p_{CO}p_{H_2O}}{K_{eq}}\right)}{\sqrt{p_{H_2}}\left(1 + a{\cdot}p_{CO} + b{\cdot}\frac{p_{H_2O}}{\sqrt{p_{H_2}}} + c{\cdot}p_{CO_2}\right)^2} \tag{28}$$

which is a composition of the models suggested in two publications [2,64]. We found that our model fits the data as well as the best literature model but has fewer parameters. Thus, the KCNODE model was useful as an intermediate model to identify a suitable rate equation for the RWGS reaction. In a similar way, the KCNODE model can be used to develop and test other rate equations that may then be based on fundamental principles. Applying this procedure for other parameters (like r_{FT}, α, etc.) as well as the analysis of the catalyst activation/deactivation of CO_2-FTS was out of scope for the current investigation but would be of great interest. It worth mentioning that the suggested approach can be easily expanded and applied in the kinetic modelling of continuous stirred-tank reactor.

6. Conclusions

In summary, we have introduced the KCNODE (Kinetics-Constrained Neural Ordinary Differential Equation) approach for describing kinetics of heterogeneous catalytic reactions. The approach is based on constraining the architecture of neural ODE by integrating general knowledge about kinetics and thermodynamics of a catalytic process. A numerical experiment demonstrated that KCNODE model can be used for kinetic modeling of CO_2 hydrogenation to methane using a small data set. The method does work even in presence of noise in the data. The developed approach could also be successfully applied for modeling the kinetics of CO_2 hydrogenation to hydrocarbons based on experimental data. The obtained KCNODE model was able to describe reagent consumption and product formation as well as their distribution correctly. Because the KCNODE models can be trained on small data sets and are resistant to overfitting, the approach can be recommended for the fast development of kinetic models of any catalytic reaction; the KCNODE model can also help in developing kinetic models based on fundamental principles and for elucidating reaction mechanism. An application of the KCNODE for other catalytic reactions in homogeneous and heterogeneous catalysis would be of great interest. Training ANN models on small data does not incur high computational costs which makes the development such ANN approachable for many researchers. The KCNODE significantly expands the scope of usage of neural ODE for describing, analyzing, and developing models based on ordinary differential equations.

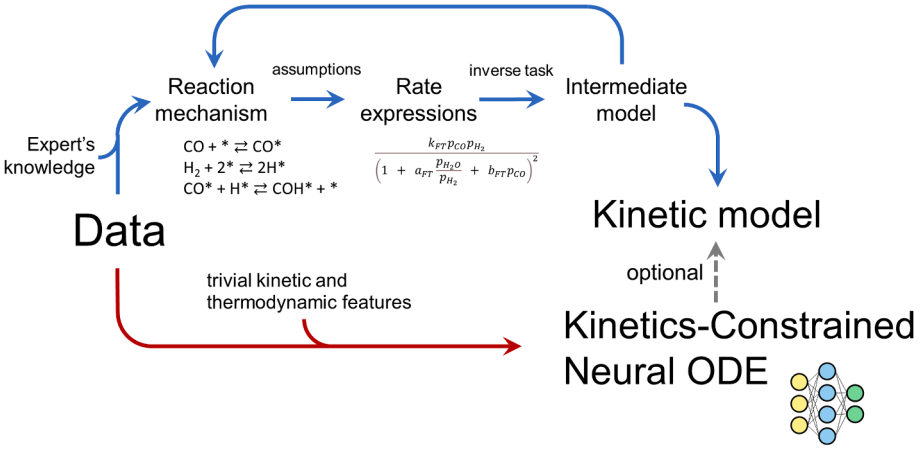

Fig. 5. Comparison of traditional and KCNODE-based kinetic modeling.

CRediT authorship contribution statement

Aleksandr Fedorov: Conceptualization, Investigation, Methodology, Data curation, Writing – original draft, Writing – review & editing. **Anna Perechodjuk:** Investigation. **David Linke:** Conceptualization, Supervision, Project administration, Funding acquisition, Writing – review & editing.

Declaration of Competing Interest

The authors declare that they have no known competing financial interests or personal relationships that could have appeared to influence the work reported in this paper.

Data availability

Data will be made available on request.

Acknowledgements

Financial support from German Federal Ministry of Education and Research (BMBF) through the project InnoSyn (FKZ: 03SF0616B) and from German Research Foundation (DFG) through the project NFDI4Cat (DFG no. 441926934) are gratefully acknowledged. The authors thank Dr. Henrik Lund and Dr. Armin Springer for the XRD analysis and recording SEM images as well as Anja Simmula for ICP-OES measurement. The authors also thank Reinhard Eckelt and Dr. Hanan Atia for BET and TPR-H_2 measurement.

Appendix A. Supplementary data

Supplementary data to this article can be found online at https://doi.org/10.1016/j.cej.2023.146869.

References

[1] G. Yablonsky, V. Bykov, A. Gorban, V. Elokhin, Kinetic Models of Catalytic Reactions, Elsevier, 1991.
[2] L. Brübach, D. Hodonj, P. Pfeifer, Kinetic analysis of CO_2 hydrogenation to long-chain hydrocarbons on a supported iron catalyst, Ind. Eng. Chem. Res. 61 (2022) 1644–1654.
[3] S. Matera, W.F. Schneider, A. Heyden, A. Savara, Progress in accurate chemical kinetic modeling, simulations, and parameter estimation for heterogeneous catalysis, ACS Catal. 9 (2019) 6624–6647.
[4] P. Priya, N.R. Aluru, Accelerated design and discovery of perovskites with high conductivity for energy applications through machine learning, npj Comput. Mater. 7 (2021) 90.
[5] V. Tshitoyan, J. Dagdelen, L. Weston, A. Dunn, Z. Rong, O. Kononova, K.A. Persson, G. Ceder, A. Jain, Unsupervised word embeddings capture latent knowledge from materials science literature, Nature 571 (2019) 95–98.
[6] G.E. Karniadakis, I.G. Kevrekidis, L. Lu, P. Perdikaris, S. Wang, L. Yang, Physics-informed machine learning, Nat. Rev. Phys. 3 (2021) 422–440.
[7] M. Raissi, P. Perdikaris, G.E. Karniadakis, Physics-informed neural networks: A deep learning framework for solving forward and inverse problems involving nonlinear partial differential equations, J. Comput. Phys. 378 (2019) 686–707.
[8] M. Bogojeski, L. Vogt-Maranto, M.E. Tuckerman, K.-R. Müller, K. Burke, Quantum chemical accuracy from density functional approximations via machine learning, Nat. Commun. 11 (2020) 5223.
[9] H. Gerdes, P. Casado, A. Dokal, M. Hijazi, N. Akhtar, R. Osuntola, V. Rajeeve, J. Fitzgibbon, J. Travers, D. Britton, S. Khorsandi, P.R. Cutillas, Drug ranking using machine learning systematically predicts the efficacy of anti-cancer drugs, Nat. Commun. 12 (2021) 1850.
[10] D. Silver, J. Schrittwieser, K. Simonyan, I. Antonoglou, A. Huang, A. Guez, T. Hubert, L. Baker, M. Lai, A. Bolton, Y. Chen, T. Lillicrap, F. Hui, L. Sifre, G. van den Driessche, T. Graepel, D. Hassabis, Mastering the game of Go without human knowledge, Nature 550 (2017) 354–359.
[11] F. Ashtiani, A.J. Geers, F. Aflatouni, An on-chip photonic deep neural network for image classification, Nature 606 (2022) 501–506.
[12] A.V. Fedorov, I.V. Shamanaev, Crystal Structure Representation for Neural Networks using Topological Approach, Mol. Inf. 36 (2017) 1600162.
[13] J. Burés, I. Larrosa, Organic reaction mechanism classification using machine learning, Nature 613 (2023) 689–695.
[14] J.T. Margraf, H. Jung, C. Scheurer, K. Reuter, Exploring catalytic reaction networks with machine learning, Nat. Catal. (2023).
[15] K. Hornik, M. Stinchcombe, H. White, Multilayer feedforward networks are universal approximators, Neural Netw. 2 (1989) 359–366.
[16] G. Bebis, M. Georgiopoulos, Feed-forward neural networks, IEEE Potentials 13 (1994) 27–31.
[17] W. Rawat, Z. Wang, Deep Convolutional Neural Networks for Image Classification: A Comprehensive Review, Neural Comput. 29 (2017) 2352–2449.
[18] S.M. Anwar, M. Majid, A. Qayyum, M. Awais, M. Alnowami, M.K. Khan, Medical Image Analysis using Convolutional Neural Networks: A Review, J. Med. Syst. 42 (2018) 226.
[19] J. Zhou, G. Cui, S. Hu, Z. Zhang, C. Yang, Z. Liu, L. Wang, C. Li, M. Sun, Graph neural networks: A review of methods and applications, AI Open 1 (2020) 57–81.
[20] Y. Yu, X. Si, C. Hu, J. Zhang, A Review of Recurrent Neural Networks: LSTM Cells and Network Architectures, Neural Comput. 31 (2019) 1235–1270.
[21] W. Ji, W. Qiu, Z. Shi, S. Pan, S. Deng, Stiff-PINN: Physics-Informed Neural Network for Stiff Chemical Kinetics, Chem. A Eur. J. 125 (2021) 8098–8106.
[22] G.S. Gusmão, A.P. Retnanto, S.C.d. Cunha, A.J. Medford, Kinetics-informed neural networks, Catalysis Today, (2022).
[23] R.T.Q. Chen, Y. Rubanova, J. Bettencourt, D. Duvenaud, Neural ordinary differential equations, (2018).
[24] S. Kim, W. Ji, S. Deng, Y. Ma, C. Rackauckas, Stiff neural ordinary differential equations, Chaos 31 (2021), 093122.
[25] O. Owoyele, P. Pal, ChemNODE: A neural ordinary differential equations framework for efficient chemical kinetic solvers, Energy AI 7 (2022), 100118.
[26] W. Ji, S. Deng, Autonomous Discovery of Unknown Reaction Pathways from Data by Chemical Reaction Neural Network, Chem. A Eur. J. 125 (2021) 1082–1092.
[27] W. Ji, F. Richter, M.J. Gollner, S. Deng, Autonomous kinetic modeling of biomass pyrolysis using chemical reaction neural networks, Combust. Flame 240 (2022), 111992.
[28] W. Yang, T.T. Fidelis, W.-H. Sun, Machine Learning in Catalysis, From Proposal to Practicing, ACS Omega 5 (2020) 83–88.
[29] K. Lee, E.J. Parish, Parameterized neural ordinary differential equations: applications to computational physics problems, Proc. Math. Phys. Eng. Sci. 477 (2021) 20210162.
[30] M. Albrecht, U. Rodemerck, M. Schneider, M. Bröring, D. Baabe, E.V. Kondratenko, Unexpectedly efficient CO_2 hydrogenation to higher hydrocarbons over non-doped Fe_2O_3, Appl. Catal. B 204 (2017) 119–126.
[31] F. Rahman, K.F. Loughlin, M.A. Al-Saleh, M.R. Saeed, N.M. Tukur, M.M. Hossain, K. Karim, A. Mamedov, Kinetics and mechanism of partial oxidation of ethane to ethylene and acetic acid over MoV type catalysts, Appl. Catal. A 375 (2010) 17–25.
[32] T.P. Otroshchenko, U. Rodemerck, D. Linke, E.V. Kondratenko, Synergy effect between Zr and Cr active sites in binary $CrZrO_x$ or supported $CrO_x/LaZrO_x$: Consequences for catalyst activity, selectivity and durability in non-oxidative propane dehydrogenation, J. Catal. 356 (2017) 197–205.
[33] A. Fedorov, H. Lund, V.A. Kondratenko, E.V. Kondratenko, D. Linke, Elucidating reaction pathways occurring in CO_2 hydrogenation over Fe-based catalysts, Applied Catalysis B: Environmental, (2023) 122505.
[34] L. Petzold, Automatic Selection of Methods for Solving Stiff and Nonstiff Systems of Ordinary Differential Equations, SIAM J. Sci. Stat. Comput. 4 (1983) 136–148.
[35] J. Antony, 6 - Full Factorial Designs, in: J. Antony (Ed.), Design of Experiments for Engineers and Scientists (second Edition), Elsevier, Oxford, 2014, pp. 63–85.
[36] B. Yao, T. Xiao, O.A. Makgae, X. Jie, S. Gonzalez-Cortes, S. Guan, A.I. Kirkland, J. R. Dilworth, H.A. Al-Megren, S.M. Alshihri, P.J. Dobson, G.P. Owen, J.M. Thomas, P.P. Edwards, Transforming carbon dioxide into jet fuel using an organic combustion-synthesized Fe-Mn-K catalyst, Nat. Commun. 11 (2020) 6395.
[37] J. Wei, Q. Ge, R. Yao, Z. Wen, C. Fang, L. Guo, H. Xu, J. Sun, Directly converting CO_2 into a gasoline fuel, Nat. Commun. 8 (2017) 15174.
[38] A.S. Skrypnik, Q. Yang, A.A. Matvienko, V.Y. Bychkov, Y.P. Tulenin, H. Lund, S. A. Petrov, R. Kraehnert, A. Arinchtein, J. Weiss, A. Brueckner, E.V. Kondratenko, Understanding reaction-induced restructuring of well-defined $Fe_xO_yC_z$ compositions and its effect on CO_2 hydrogenation, Appl. Catal. B 291 (2021), 120121.
[39] J. Zhu, G. Zhang, W. Li, X. Zhang, F. Ding, C. Song, X. Guo, Deconvolution of the Particle Size Effect on CO_2 Hydrogenation over Iron-Based Catalysts, ACS Catal. 10 (2020) 7424–7433.
[40] G.V. Schulz, Über die Beziehung zwischen Reaktionsgeschwindigkeit und Zusammensetzung des Reaktionsproduktes bei Makropolymerisationsvorgängen, Z. Phys. Chem. 30B (1935) 379–398.
[41] P.J. Flory, Molecular Size Distribution in Linear Condensation Polymers1, J. Am. Chem. Soc. 58 (1936) 1877–1885.
[42] R.B. Anderson, R.A. Friedel, H.H. Storch, Fischer-Tropsch Reaction Mechanism Involving Stepwise Growth of Carbon Chain, J. Chem. Phys. 19 (1951) 313–319.
[43] G. Henrici-Olivé, S. Olivé, The Fischer-Tropsch Synthesis: Molecular Weight Distribution of Primary Products and Reaction Mechanism, Angew. Chem. Int. Ed. Eng. 15 (1976) 136–141.
[44] C.G. Visconti, M. Martinelli, L. Falbo, A. Infantes-Molina, L. Lietti, P. Forzatti, G. Iaquaniello, E. Palo, B. Picutti, F. Brignoli, CO_2 hydrogenation to lower olefins on a high surface area K-promoted bulk Fe-catalyst, Appl. Catal. B 200 (2017) 530–542.
[45] T. Riedel, H. Schulz, G. Schaub, K.-W. Jun, J.-S. Hwang, K.-W. Lee, Fischer-Tropsch on Iron with H_2/CO and H_2/CO_2 as Synthesis Gases: The Episodes of Formation of the Fischer-Tropsch Regime and Construction of the Catalyst, Top. Catal. 26 (2003) 41–54.
[46] G.P. Van Der Laan, A.A.C.M. Beenackers, Kinetics and Selectivity of the Fischer-Tropsch Synthesis: A Literature Review, Catal. Rev. 41 (1999) 255–318.
[47] C. Panzone, R. Philippe, C. Nikitine, A. Bengaouer, A. Chappaz, P. Fongarland, Development and Validation of a Detailed Microkinetic Model for the CO_2

Hydrogenation Reaction toward Hydrocarbons over an Fe–K/Al_2O_3 Catalyst, Ind. Eng. Chem. Res. 61 (2022) 4514–4533.
[48] L.S. Glebov, G.A. Kliger, The molecular weight distribution of the products of the Fischer-Tropsch synthesis, Russ. Chem. Rev. 63 (1994) 185–195.
[49] M. Poli, S. Massaroli, A. Yamashita, H. Asama, J. Park, TorchDyn: A neural differential equations library, (2020).
[50] D.P. Kingma, J. Ba, Adam: A method for stochastic optimization, (2014).
[51] S. Kim, W. Ji, S. Deng, Y. Ma, C. Rackauckas, Stiff neural ordinary differential equations, Chaos: An Interdisciplinary, J. Nonlinear Sci. 31 (2021), 093122.
[52] D.E. Mears, Diagnostic criteria for heat transport limitations in fixed bed reactors, J. Catal. 20 (1971) 127–131.
[53] H.S. Fogler, Elements of chemical reaction engineering, 5 ed., Prentice Hall, Philadelphia, PA, 2016.
[54] G. Van Rossum, F.L. Drake, Python 3 Reference Manual, CreateSpace.
[55] C.R. Harris, K.J. Millman, S.J. van der Walt, R. Gommers, P. Virtanen, D. Cournapeau, E. Wieser, J. Taylor, S. Berg, N.J. Smith, R. Kern, M. Picus, S. Hoyer, M.H. van Kerkwijk, M. Brett, A. Haldane, J.F. del Río, M. Wiebe, P. Peterson, P. Gérard-Marchant, K. Sheppard, T. Reddy, W. Weckesser, H. Abbasi, C. Gohlke, T.E. Oliphant, Array programming with NumPy, Nature 585 (2020) 357–362.
[56] P. Virtanen, R. Gommers, T.E. Oliphant, M. Haberland, T. Reddy, D. Cournapeau, E. Burovski, P. Peterson, W. Weckesser, J. Bright, S.J. van der Walt, M. Brett, J. Wilson, K.J. Millman, N. Mayorov, A.R.J. Nelson, E. Jones, R. Kern, E. Larson, C. J. Carey, İ. Polat, Y. Feng, E.W. Moore, J. VanderPlas, D. Laxalde, J. Perktold, R. Cimrman, I. Henriksen, E.A. Quintero, C.R. Harris, A.M. Archibald, A.H. Ribeiro, F. Pedregosa, P. van Mulbregt, A. Vijaykumar, A.P. Bardelli, A. Rothberg, A. Hilboll, A. Kloeckner, A. Scopatz, A. Lee, A. Rokem, C.N. Woods, C. Fulton, C. Masson, C. Häggström, C. Fitzgerald, D.A. Nicholson, D.R. Hagen, D. V. Pasechnik, E. Olivetti, E. Martin, E. Wieser, F. Silva, F. Lenders, F. Wilhelm, G. Young, G.A. Price, G.-L. Ingold, G.E. Allen, G.R. Lee, H. Audren, I. Probst, J. P. Dietrich, J. Silterra, J.T. Webber, J. Slavič, J. Nothman, J. Buchner, J. Kulick, J. L. Schönberger, J.V. de Miranda Cardoso, J. Reimer, J. Harrington, J.L. C. Rodríguez, J. Nunez-Iglesias, J. Kuczynski, K. Tritz, M. Thoma, M. Newville, M. Kümmerer, M. Bolingbroke, M. Tartre, M. Pak, N.J. Smith, N. Nowaczyk, N. Shebanov, O. Pavlyk, P.A. Brodtkorb, P. Lee, R.T. McGibbon, R. Feldbauer, S. Lewis, S. Tygier, S. Sievert, S. Vigna, S. Peterson, S. More, T. Pudlik, T. Oshima, T.J. Pingel, T.P. Robitaille, T. Spura, T.R. Jones, T. Cera, T. Leslie, T. Zito, T. Krauss, U. Upadhyay, Y.O. Halchenko, Y. Vázquez-Baeza, C. SciPy, SciPy 1.0: fundamental algorithms for scientific computing in Python, Nat. Methods 17 (2020) 261–272.
[57] W. McKinney, others, Data structures for statistical computing in python, Austin, TX, pp. 51-56.
[58] F. Pedregosa, G. Varoquaux, A. Gramfort, V. Michel, B. Thirion, O. Grisel, M. Blondel, P. Prettenhofer, R. Weiss, V. Dubourg, J. Vanderplas, A. Passos, D. Cournapeau, M. Brucher, M. Perrot, E. Duchesnay, Scikit-learn: Machine Learning in Python, Journal of Machine Learning Research, 12 2825-2830.
[59] A. Paszke, S. Gross, F. Massa, A. Lerer, J. Bradbury, G. Chanan, T. Killeen, Z. Lin, N. Gimelshein, L. Antiga, A. Desmaison, A. Kopf, E. Yang, Z. DeVito, M. Raison, A. Tejani, S. Chilamkurthy, B. Steiner, L. Fang, J. Bai, S. Chintala, PyTorch: An Imperative Style, High-Performance Deep Learning Library, Advances in Neural Information Processing Systems 32, Curran Associates Inc.2019, pp. 8024–8035.
[60] P.T. Inc., Collaborative data science, (2015).
[61] T. Riedel, G. Schaub, K.-W. Jun, K.-W. Lee, Kinetics of CO_2 Hydrogenation on a K-Promoted Fe Catalyst, Ind. Eng. Chem. Res. 40 (2001) 1355–1363.
[62] C. Panzone, R. Philippe, C. Nikitine, L. Vanoye, A. Bengaouer, A. Chappaz, P. Fongarland, Catalytic and Kinetic Study of the CO_2 Hydrogenation Reaction over a Fe–K/Al_2O_3 Catalyst toward Liquid and Gaseous Hydrocarbon Production, Ind. Eng. Chem. Res. 60 (2021) 16635–16652.
[63] L. Brübach, D. Hodonj, L. Biffar, P. Pfeifer, Detailed kinetic modeling of CO_2-based Fischer-Tropsch synthesis, Catalysts 12 (2022) 630.
[64] A.A. Hakeem, M. Li, R.J. Berger, F. Kapteijn, M. Makkee, Kinetics of the high temperature water–gas shift over Fe_2O_3/ZrO_2, Rh/ZrO_2 and $Rh/Fe_2O_3/ZrO_2$, Chem. Eng. J. 263 (2015) 427–434.

Supplementary Information to

Kinetics-Constrained Neural Ordinary Differential Equations: Artificial Neural Network Models tailored for Small Data to boost Kinetic Model Development

Aleksandr Fedorov, Anna Perechodjuk, David Linke

Leibniz-Institut für Katalyse e.V., Albert-Einstein-Str. 29a, 18059 Rostock, Germany

Contents

Catalyst preparation, characterization, and testing

For kinetic modeling of CO_2 hydrogenation to hydrocarbons the Fe-K-Cu/γ-Al_2O_3 catalyst was prepared by wet impregnation method, characterized by X-ray diffraction (XRD), temperature-programmed reduction with H_2 (TPR-H_2), low-temperature N_2 adsorption, scanning electron microscopy (SEM). The elemental composition of the prepared catalyst was determined by inductively coupled plasma (ICP). This part of the work is devoted to describing catalyst preparation, characterization, and its testing in CO_2 hydrogenation.

Experimental part

Catalyst synthesis

Fe-K-Cu/γ-Al_2O_3 catalyst was prepared via incipient wetness impregnation. γ-Al_2O_3 (99%, Alfa Aesar, 32-63 micron, APS powder) was used as a support. Briefly, γ-Al_2O_3 was firstly impregnated with desired amount of an aqueous solution contains $Fe(NO_3)_3 \cdot 9H_2O$ (98+%, Thermo scientific), $Cu(NO_3)_2 \cdot 3H_2O$ (99+%, Fluka) and K_2CO_3 (99%, Merck) to obtain the Fe-K-Cu/γ-Al_2O_3 catalyst with content of Fe, K, Cu being to 10, 2.5, and 1 wt. %, respectively. After that, the slurry was dried at 70 °C for 12 h and calcined at 110 °C for 5 h and 400 °C for 5 h.

Catalyst characterization

XRD powder pattern was recorded on a Panalytical X'Pert θ/2θ -diffractometer equipped with Xcelerator detector using automatic divergence slits and Cu K*α1/α2* radiation (40 kV, 40 mA; λ= 1.54060 Å, 1.54443 Å). Cu beta-radiation was excluded using a nickel filter foil. The measurements were performed with 0.021° s^{-1} or 0.005° s^{-1}, respectively. Samples were mounted on silicon zero background holders. Obtained intensities were converted from automatic to fixed divergence slits (0.25°) for further analysis. Peak positions and profile were fitted with Pseudo-Voigt function using the HighScore Plus software package (Panalytical). Phase identification was done by using the PDF-2 database of the International Center of Diffraction Data (ICDD).

To determine the surface area of the catalysts, low-temperature nitrogen adsorption-desorption isotherms were obtained at -196 °C using Micromeritics ASAP 2010 setup. Before the measurements, the samples were heated in the vacuum at 300 °C for 2 hours. The initial

branch of N_2 adsorption isotherm in the range of P/P_0 (0.05-0.25) was used to calculate the BET surface area.

The metal loading in the catalyst was determined by inductively coupled plasma optical emission spectroscopy (ICP-OES) on Varian 715-ES ICP-Emission-Spectrometer. 10 mg of each sample was mixed with 8 ml of aqua regia. The sample preparation system "Multiwave PRO" from Anton Paar was used at 220 °C and 50 bar for the sample digestion with a microwave-assisted method. The digested solution was filled up to 100 ml and measured with ICP-OES. The data analysis was performed on the Varian 715-ES software "ICP Expert".

The tests of temperature-programmed reduction with hydrogen (TPR-H_2) were performed in a Micromeritics Autochem II 2920 instrument. Before the tests, 75 mg sample was loaded into the U-shaped quartz reactor and heated up to 250°C in the flow of Ar (50 $cm^3 \cdot min^{-1}$) for 30 min with heating rate of 20 °/min. After cooling down to room temperature, a flow (5% H_2 in Ar) was fed (50 $cm^3 \cdot min^{-1}$) to the reactor followed by heating to 750 °C with a constant heating rate 10 °/min. The hydrogen consumption was measured using a TCD detector.

The catalyst was analyzed by a field emission scanning electron microscope (SEM, MERLIN® VP Compact, Co. Zeiss, Oberkochen, Germany) equipped with an energy dispersive X-ray (EDX) detector (XFlash 6/30, Co. Bruker, Berlin, Germany). The sample was mounted on heavy metal-free Al-SEM-carrier (co. PLANO, Wetzlar, Germany) with adhesive conductive carbon tape (Spectro Tabs, TED PELLA INC, Redding, USA) and coated with carbon (5.0 nm thickness) under vacuum (CCU 010 HV-Coating Unit, Co. Safematic GmbH, Zizers, Switzerland). Representative areas of the sample were analyzed and mapped for elemental distribution on basis of the EDX-spectra data by QUANTAX ESPRIT Microanalysis software (version 2.0). SEM-images were taken from the selected regions (conditions like applied detector, accelerating voltage, working distance are given in the figures).

Catalytic tests

Catalytic tests were carried out in an in-house developed setup containing 16-continuos-flow fixed bed stainless-steel tube reactors. The reactors are grouped in sets of 4. Each of these reactor sets has its own heating; the heating design assures high heat-transfer rates between furnace and reactor tube in order to maintain the set temperature even for more exothermic reactions. The outer and inner diameters of reactors are 9.53 and 7.04 mm,

respectively. CO_2, H_2, N_2, and He gases were dosed by electronic mass flow controllers (Brooks 5850s). The total flow of feed gases was equally distributed among all the reactors and a bypass channel. The outlet lines from reactors are split at 150°C into a main flow and a sample portion where the sample portion is connected to a 16-channels automatic valve to select and direct one stream to a gas chromatograph through a heated line (the temperature is 180 °C). A flow of He (3 $ml \cdot min^{-1}$ per reactor) is additionally added to this sample stream to prevent condensation of long-chain hydrocarbons. The main flows are led through hot traps where a wax phase is condensed (at 150 °C). The remaining gas streams are combined and passed through a cold trap where H_2O is condensed before they reach the electronic pressure controller (Brooks 5866s).

The feed components (bypass channel) and the reaction products were analyzed by on-line Agilent 7890A gas chromatograph equipped with a thermal conductivity detector (TCD) and two flame ionization detectors (FID). HP Plot/Q (for CO_2) and MolSieve 5A (for H_2, O_2, N_2, and CO) columns were connected to TCD. For separating hydrocarbons and alcohols, PONA (for C_5-C_{16} hydrocarbons and C_2-C_7 alcohols) and HP Plot/Q (for C_1-C_4 hydrocarbons and CH_3OH) columns connected to FIDs were used.

The principal scheme of reactors and heating sets numeration is presented in Figure S10. The required amount of catalyst (size 0.08-0.20 mm) was diluted by SiC (ESK-SiC, F54, 0.2-0.5 mm fraction) to further minimize temperature gradients. The weight ratio of catalyst to SiC was to 1:2. Regardless of the mixture of the catalyst and SiC, an additional layer of SiC (800 mg, ESK-SiC, F54, 0.2-0.5 mm fraction) was added on the top of the bed to ensure plug flow and to preheat the reaction feed. In Table S2 the list of different catalyst loading, and reactor heating sets are presented.

Before catalytic testing the as-prepared catalyst was heated up to 300 °C (the heating rate was 5 °/min) in N_2 flow at 5.0 bar (abs.) and after that were reduced in-situ. The hydrogen concentration was increased stepwise, starting with 10 % H_2 in N_2 flow for 10 min, then 30 % H_2 in N_2 flow for 10 min, 50 % H_2 in N_2 flow for 10 min, and finally undiluted CO-H_2 mixture (CO:H_2 was 1:2) for 240 min. During these steps the temperature was kept at 300 °C, pressure at 5.0 bar (abs.) and gas hourly space velocity (GHSV) was 18 000 $cm^3 \cdot h^{-1} \cdot g^{-1}$. The catalytic setup construction allows one to feed two different gas flows through reactors. One of them was used for feeding treatment and reaction gas mixtures. Another one was used for feeding N_2 flow. Because of the different catalyst loading was used, the samples were pre-

treated in series to achieve the same GHSV for all reactor channels. Namely, while the catalysts with the same mass were reduced according to the above procedure, other catalyst samples were kept in the N_2 flow. After the reduction, the gas mixture (CO_2:H_2:N_2 ratio was 1:3:1) was supplied into reactors at pressure 15 bar, 300 °C, and at 45.8 $cm^3 \cdot min^{-1}$ flow per each channel for 20 hours to achieve steady-state condition. After this, the total flow was decreased up to 18.3 $cm^3 \cdot min^{-1}$ and reactor temperature was decreased/increased according to selected conditions (Table S2). After reaching the target temperature, the reactors were kept at the current flow for 15 min followed by catalytic measurements. In Table S3 different reaction conditions used for testing catalyst activity are presented. It is worth noting that the selected conditions were applied in series. Time on stream for each reaction condition was 15 hours. Conditions with number 2, 6, 9, and 12 are repetitions which allowed one to investigate the processes of activation/deactivation occurring under CO_2-FT condition.

The CO_2 conversion (X) and products selectivity were calculated by the following equations:

$$X = 1 - \frac{\dot{n}_{CO_2}^{out}}{\dot{n}_{CO_2}^{in}}$$

$$S_i = \frac{a_i \cdot \dot{n}_i^{out}}{\sum_{j=1}^{n} a_j \cdot \dot{n}_j^{out}}$$

where $\dot{n}_{CO_2}^{in}$ – the molar flow of CO_2 in the inlet flow; $\dot{n}_{CO_2}^{out}$ – the molar flow of CO_2 in the outlet flow; S_i – the selectivity of i-product; a_i – the carbon number of i-product; $\dot{n}_i^{out}$ – the molar flow of i-product in the outlet flow.

The absence of any external heat transfer, external diffusion limitations, the wall effect, and axial dispersion were checked by applying Mears and Weisz-Prater criteria [1, 2]. In the case of internal diffusion limitation, applying the corresponding criteria is not trivial task because liquid wax is formed under FT condition inside the catalyst pores. To check the influence of internal diffusion, catalysts of different particle size were tested under CO_2-FT condition (see Table S4). One can see that CO_2 conversion is similar in a range from 0.08-0.40 mm which allows to conclude that internal diffusion limitation can be neglected for the studied particle size range (0.08-0.20 mm).

The wall effect is negligible if $\frac{d_{reactor}}{2 \cdot R_{catalyst}} > 10$. The obtained value was 50.3 that is more than 10. External diffusion limitation is negligible if:

$$\frac{r_{obs} \cdot \rho_b \cdot R_{catalyst} \cdot n}{k_d \cdot C} < 0.15$$

External heat transfer limitation is negligible if:

$$\frac{r_{obs} \cdot \rho_b \cdot R_{catalyst} \cdot E_a \cdot \Delta H}{k_g \cdot R \cdot T^2} < 0.15$$

Axial dispersion is negligible if:

$$\frac{40 \cdot n \cdot R_{catalyst}}{Pe_{ax} \cdot L_{bed}} \ln\left(\frac{1}{1-X}\right) < 1$$

The following equations and parameters values were used for estimation:

a. $$Sh = \frac{2 \cdot k_d \cdot R_{catalyst}}{D} = 2 + 0.552 \cdot Re^{1/2} \cdot Sc^{1/3}$$

b. $$Re = \frac{2 \cdot u_{feed} \cdot R_{catalyst} \cdot \rho_{feed}}{\mu}$$

c. $$Sc = \frac{\mu}{\rho_{feed} \cdot D}$$

e. $$\frac{1}{Pe_{ax}} = \frac{0.3}{Re \cdot Sc} + \frac{0.5}{1 + \frac{3.8}{Re \cdot Sc}}$$

The values of the parameters used for calculation of corresponding criteria are listed in Table S5. Figure S11 shows the distributions of the values of corresponding criteria calculated for different reaction conditions. One can clearly see that external diffusion and external heat transfer limitations are not relevant. In the case of axial dispersion, some values are a little higher than 1. However, we assumed that axial dispersion can be also negligible to simplify the calculations.

Results and discussion

Elemental composition and textural characteristics of as-prepared catalyst and support are summarized in Table S6. The content of dopants in the obtained catalyst measured by ICP is slightly lower than the theoretical one. The small difference can be related to the preparation method. The values of specific surface area, pore volume, and pore size for the prepared catalyst are lower than for γ-Al_2O_3. It is obviously caused by the deposition of active component on the surface of alumina support.

To identify the phase composition of the obtained catalyst, XRD analysis was performed. In Figure S12 one can see XRD pattern of the Fe-K-Cu/γ-Al_2O_3 catalyst. According to the obtained results, the catalyst contains γ-Al_2O_3 (PDF 01-074-4629) and α-Fe_2O_3 (PDF 01-089-8104) phases that are indicated by the corresponding reflexes. No K- or Cu- containing phases were detected in the obtained catalyst.

A selected region of Fe-K-Cu/γ-Al_2O_3 catalyst was analyzed by SEM and the elemental distribution was determined on basis of the EDX-spectra (see Figure S13). One can that the distribution of Cu, Fe, and K in Fe-K-Cu/γ-Al_2O_3 is very homogeneous.

TPR-H_2 measurement was carried out to investigate the reducibility of the supported catalyst (see Figure S14). The reduction occurs in a broad temperature range from 200 to 750 °C. Maxima for H_2 consumption (T_{max}) were found at 312, 360 and 542 °C. According to the literature data, the process of the reduction of Fe_2O_3 occurs via three stages ($Fe_2O_3 \rightarrow Fe_3O_4 \rightarrow FeO \rightarrow Fe$) [3]. Moreover, it is known that copper oxide in mixed CuO-Fe_2O_3 catalysts is reduced at lower temperature compared to Fe_2O_3 [4]. Thus, the double signal at lower temperature (T_{max} = 312 °C and T_{max} = 360 °C) can be ascribed to the reduction of CuO to Cu and of Fe_2O_3 to Fe_3O_4. The reduction of Fe_3O_4 to FeO/Fe is responsible for a broad signal at higher temperature with T_{max}= 542 °C.

Elucidating LHHW expression for RWGS reaction

In this part we describe procedure of reconstructing the rate expression for the RWGS reaction. By screening the literature data, we tried to find Langmuir-Hinshelwood-Hougen-Watson (LHHW) expression which is the most suitability to RWGS rate obtained by the developed ANN model. First, we calculated the rates of RWGS using the developed KCNODE at the following conditions:

- CO_2 pressure: 1.5, 2.1, 3.3, 3.7 bar.
- CO pressure: 0.0, 0.12, 0.24, 0.36 bar.
- H_2 pressure: 7.0, 8.0, 9.0, 10 bar.
- H_2O pressure: 0.0, 0.5, 1.0, 1.5 bar.
- Temperature: 280 °C.
- Time on steam: 100 hours.

The data set was generated by the full factorial design [5]. The list of reaction rate expressions used is presented in Table S7. The search for the values of parameters of LHHW expressions were performed by minimizing the following loss function:

$$\frac{1}{N}\sum_{i=1}^{N}\left(r_i^{KCNODE} - r_i^{LHHW}\right)^2$$

where r_i^{KCNODE} – the value of RWGS reaction rate calculated by the developed KCNODE model at reaction condition i; r_i^{LHHW} – the value of RWGS reaction rate calculated by the LHHW model at reaction condition i. The Levenberg–Marquardt algorithm was used for minimization of the loss function [6]. The values of the loss function and coefficient of determination R^2 obtained for the different LHHW expressions suggested in the literature are summarized in Table S7.

After the analysis the obtained results (Table S7), we suggested the following reaction mechanism for describing the RWGS reaction:

1	$CO_2 + * \rightleftarrows CO_2*$	equilibrium
2	$H_2 + 2* \rightleftarrows 2H*$	equilibrium
3	$CO_2* + H* \rightleftarrows CO* + OH*$	RDS
4	$CO* \rightleftarrows CO + *$	equilibrium
5	$OH* + H* \rightleftarrows H_2O + 2*$	equilibrium
	$CO_2 + H_2 \rightleftarrows CO + H_2O$	

* - active site.

Assuming the elementary reaction step 3 is rate-determining, the rate of RWGS can be presented as:

S.1. $$r_{RWGS} = k_3\theta_{CO_2}\theta_H - k_{-3}\theta_{CO}\theta_{OH}$$

Assuming elementary reactions steps 1, 2, 4, and 5 are in quasi equilibrium, the surface concentrations of intermediates can be presented as:

S.2. $$\theta_{CO_2} = K_1 p_{CO_2}\theta$$

S.3. $$\theta_H = \sqrt{K_2 p_{H_2}}\theta$$

S.4. $$\theta_{CO} = \frac{1}{K_4} p_{CO}\theta$$

S.5. $$\theta_{OH} = \frac{1}{K_5}\frac{p_{H_2O}\theta^2}{\theta_H} = \frac{p_{H_2O}\theta}{K_5\sqrt{K_2 p_{H_2}}}$$

By incorporating eq. S.2-S.6 to S.1, the rate of RWGS becomes as:

S.6. $$r_{RWGS} = k_3 K_1\sqrt{K_2 p_{H_2}} p_{CO_2}\theta^2 - k_{-3}\frac{1}{K_4 K_5\sqrt{K_2}}\frac{p_{CO}p_{H_2O}}{\sqrt{p_{H_2}}}\theta^2$$

With the catalytic site balance and reactions 1, 2, 4, and 5 we can derive:

S.7. $$\theta = 1 - \theta_{CO_2} - \theta_H - \theta_{CO} - \theta_{OH}$$

S.8. $$\theta = \frac{1}{1 + K_1 p_{CO_2} + \sqrt{K_2 p_{H_2}} + \frac{1}{K_4} p_{CO} + \frac{p_{H_2O}}{K_5\sqrt{K_2 p_{H_2}}}}$$

Because CO_2, CO, H_2O are more strongly adsorbed than H_2 on the surface of iron carbides/oxides [7], the contribution of $\sqrt{K_2 p_{H_2}}$ in the denominator can be neglected, and thus, the following expression for the rate of RWGS reaction was obtained:

S.9. $$r_{RWGS} = \frac{k_3 K_1 \sqrt{K_2 p_{H_2}} p_{CO_2} - k_{-3} \frac{1}{K_4 K_5 \sqrt{K_2}} \frac{p_{CO} p_{H_2O}}{\sqrt{p_{H_2}}}}{\left(1 + K_1 p_{CO_2} + \frac{1}{K_4} p_{CO} + \frac{p_{H_2O}}{K_5 \sqrt{K_2 p_{H_2}}}\right)^2} =$$

$$\frac{k_3 K_1 \sqrt{K_2} \left(p_{CO_2} p_{H_2} - \frac{k_{-3} p_{CO} p_{H_2O}}{k_3 K_1 K_2 K_4 K_5}\right)}{p_{H_2}^{0.5} \left(1 + K_1 p_{CO_2} + \frac{1}{K_4} p_{CO} + \frac{p_{H_2O}}{K_5 \sqrt{K_2 p_{H_2}}}\right)^2} = \frac{k \left(p_{CO_2} p_{H_2} - \frac{p_{CO} p_{H_2O}}{K_{eq}}\right)}{p_{H_2}^{0.5} \left(1 + a \cdot p_{CO} + b \cdot \frac{p_{H_2O}}{p_{H_2}^{0.5}} + c \cdot p_{CO_2}\right)^2}$$

where $k = k_3 K_1 \sqrt{K_2}$; $\frac{k_{-3}}{k_3 K_1 K_2 K_4 K_5} = K_{eq}$ – equilibrium constant of the RWGS reaction; $a = \frac{1}{K_4}$; $b = \frac{1}{K_5 \sqrt{K_2}}$; $c = K_1$. Figure S15 shows the dependency between the values of the rates of the RWGS reaction estimated by the developed KCNODE model and by the LHHW model (expression 9).

Figures

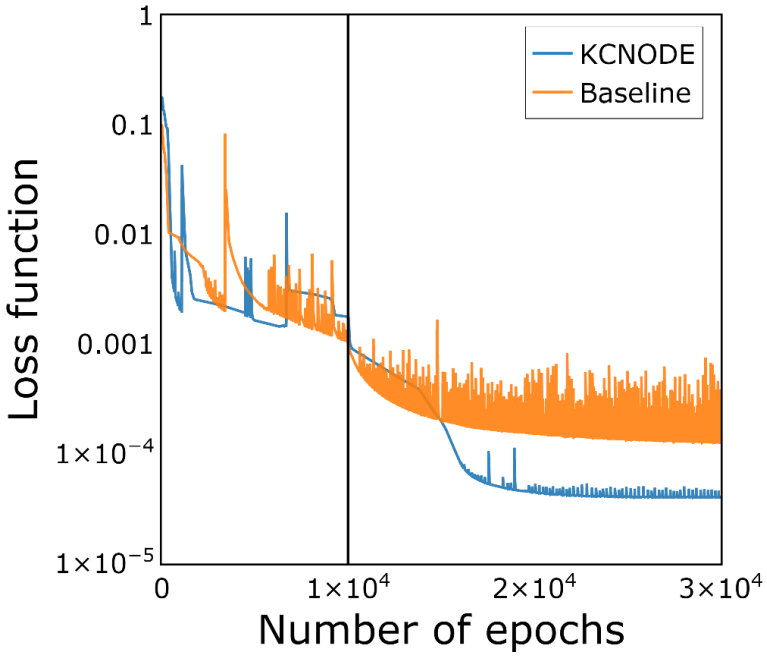

Figure S1. Dependency between loss function and number of epochs at training baseline and KCNODE models using simulated dataset of CO_2 methanation reaction. For the first 10^4 iterations the systems of ODE were integrated by Runge-Kutta method. After this, the solver was changed to more precise but slower Dormand-Prince-Shampine method.

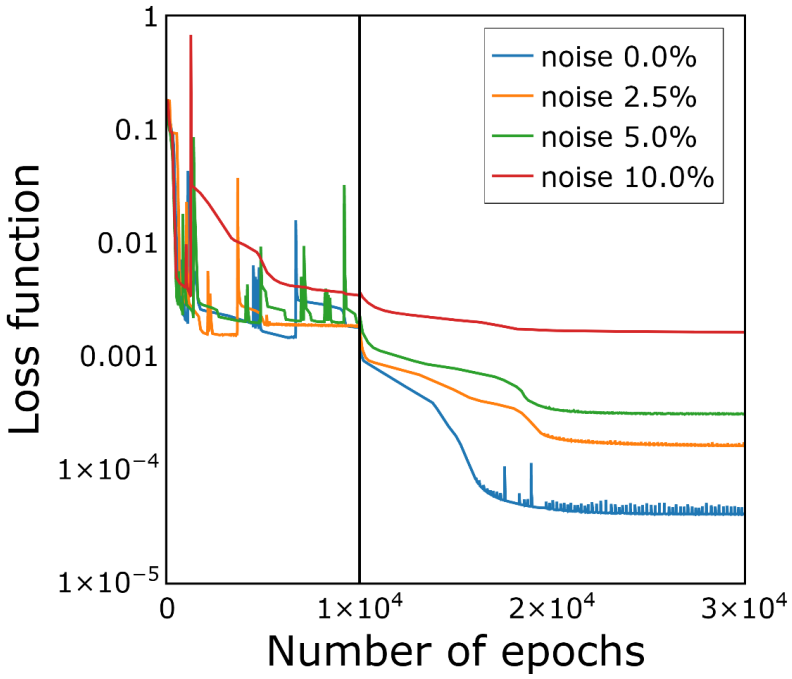

Figure S2. Dependency between loss function and number of epochs at training KCNODE models using simulated dataset of CO_2 methanation reaction with Gauss noise. For the first 10^4 iterations the systems of ODE were integrated by Runge-Kutta method. After this, the solver was changed to more precise but slower Dormand-Prince-Shampine method.

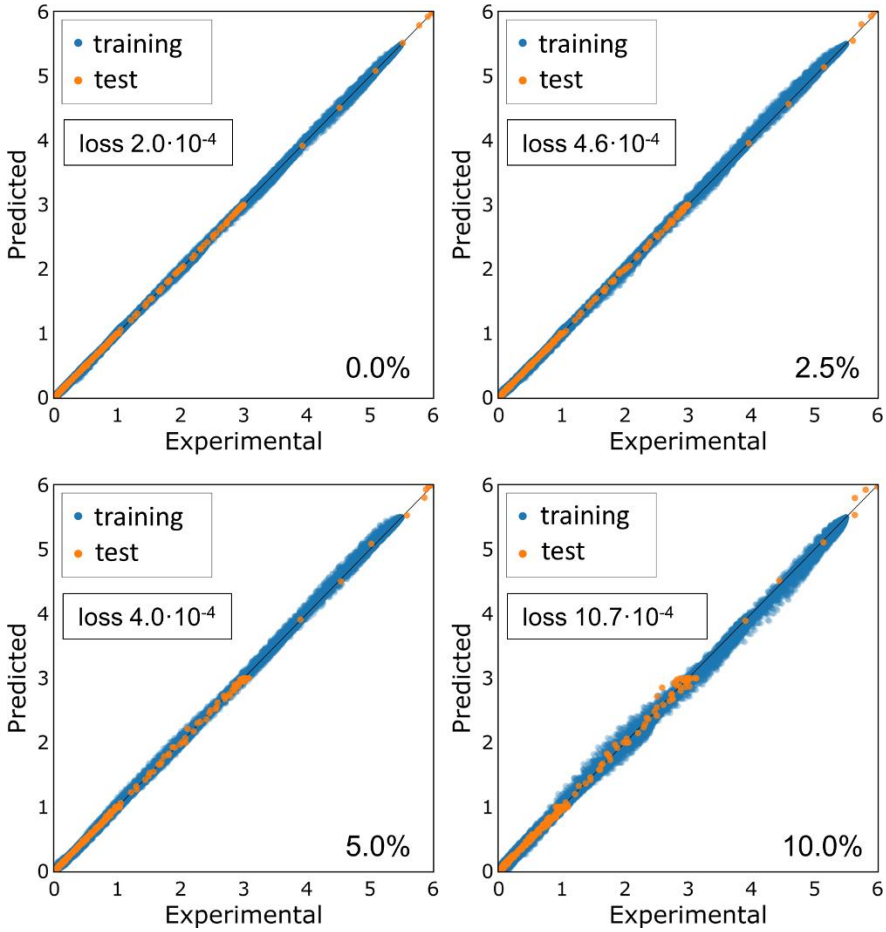

Figure S3. Parity plot of the obtained neural KCNODE models trained with noisy data.

Values in % in lower right corners expresses the amount of Gauss noise added.

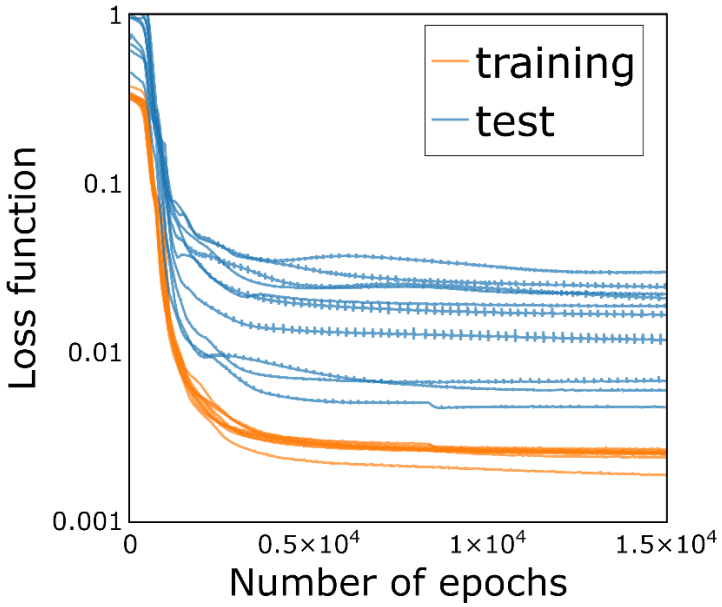

Figure S4. Dependency between loss functions (for training and test datasets) and epoch number during training the KCNODE model using 10-fold cross-validation.

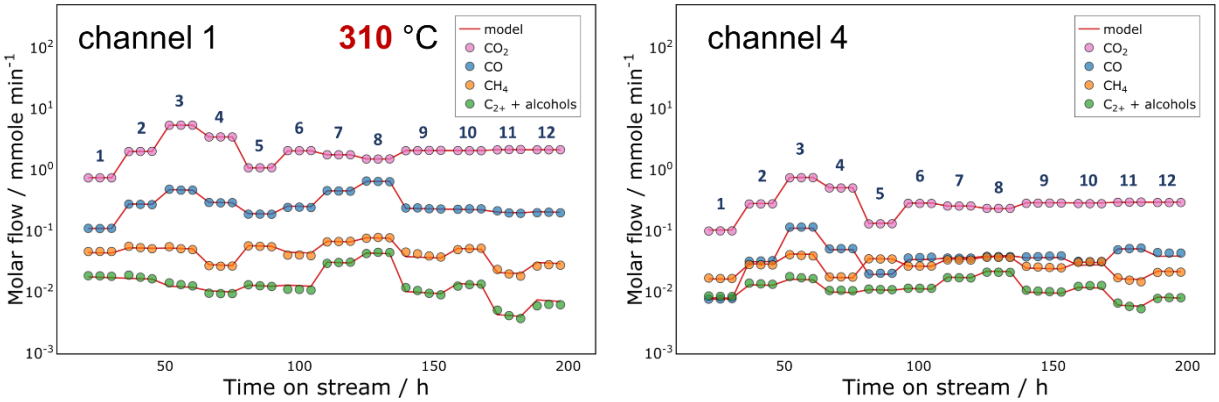

Figure S5. Outlet molar flows of reagents and products as a function of time-one-stream for reactor channels 1 and 4. Numbers from 1 to 12 stand for different reaction conditions (see Table S3).

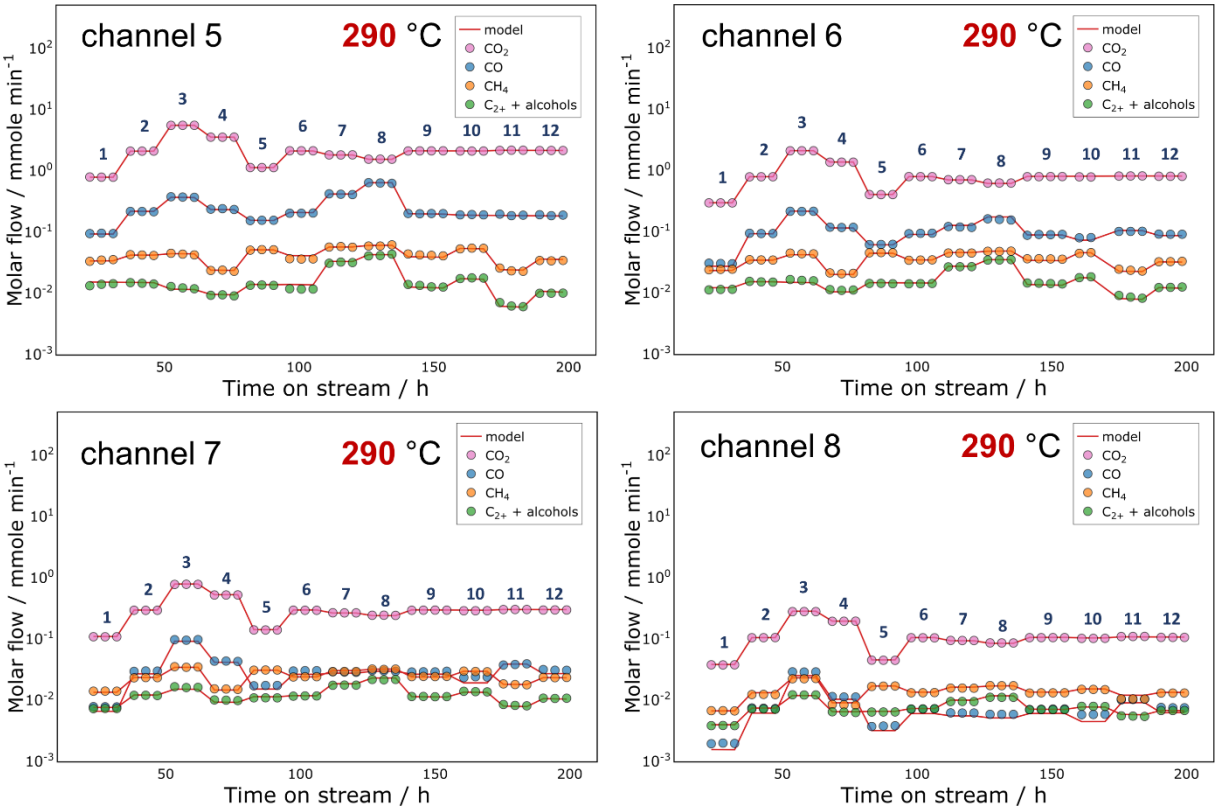

Figure S6. Outlet molar flows of reagents and products as a function of time-one-stream for reactor channels 5, 6, 7, and 8. Numbers from 1 to 12 stand for different reaction conditions (see Table S3).

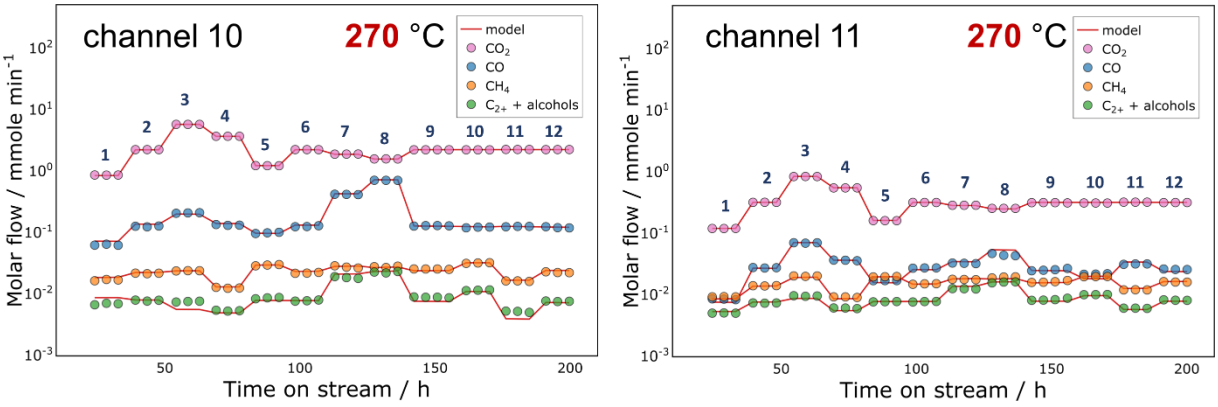

Figure S7. Outlet molar flows of reagents and products as a function of time-one-stream for reactor channels 10 and 11. Numbers from 1 to 12 stand for different reaction conditions (see Table S3).

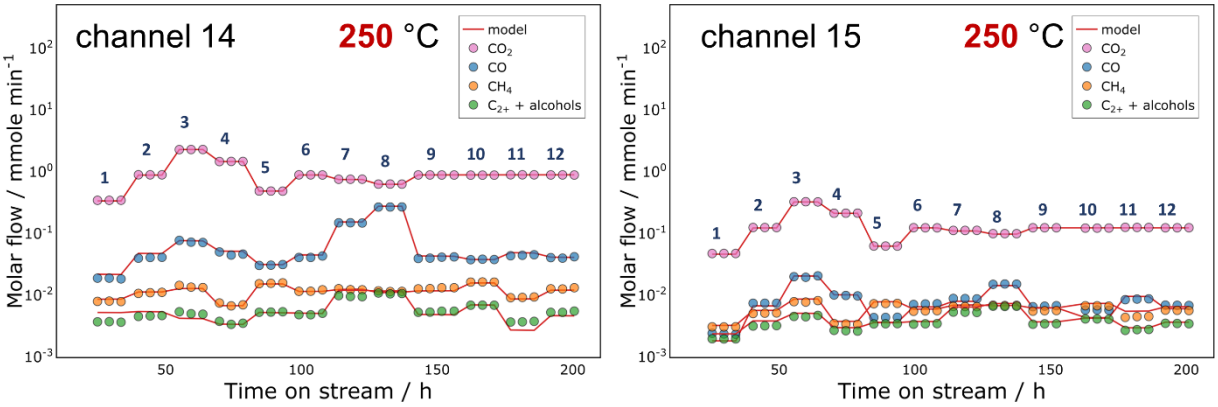

Figure S8. Outlet molar flows of reagents and products as a function of time-one-stream for reactor channels 14 and 15. Numbers from 1 to 12 stand for different reaction conditions (see Table S3).

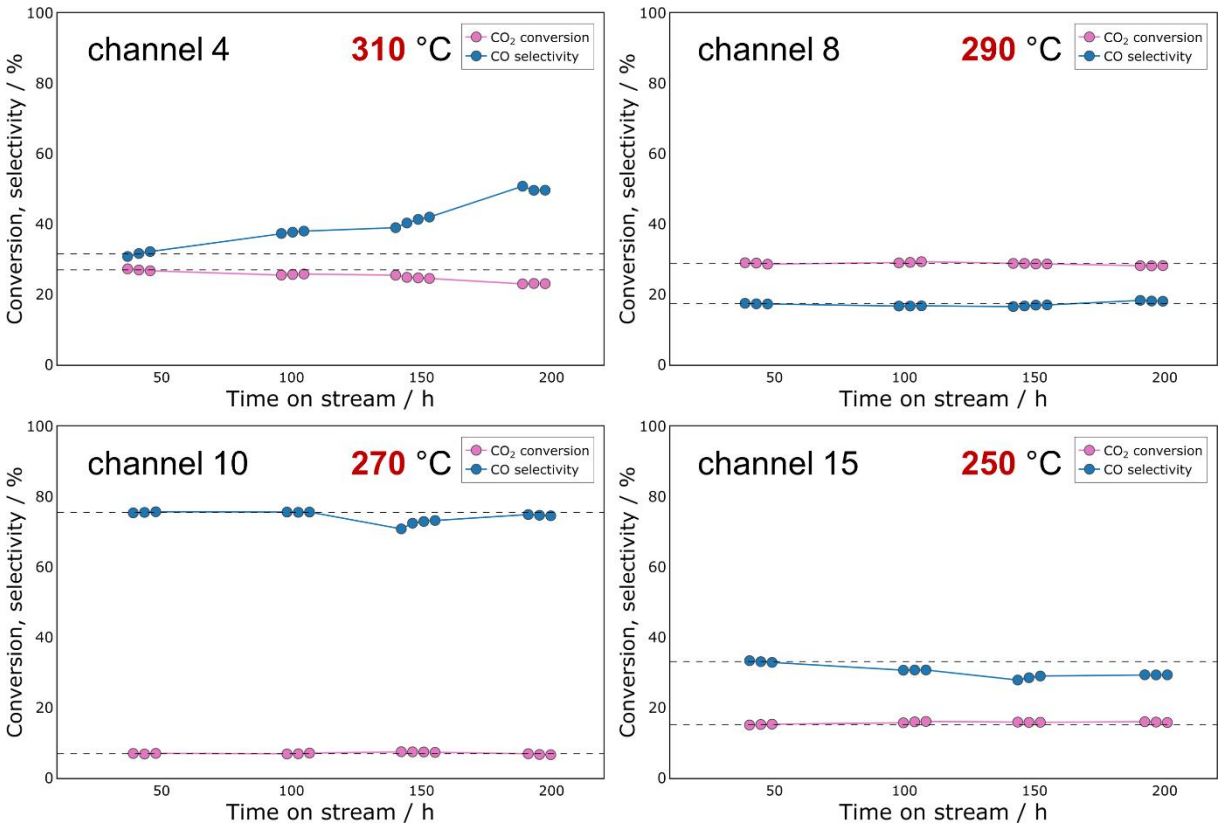

Figure S9. Change of CO_2 conversion/CO selectivity as a function of time-one-stream for catalyst repeatedly tested at the same reference reaction conditions (the condition numbers are 2, 6, 9, and 12) for the selected reactor channels 4, 8, 10, 15 (see Table S3).

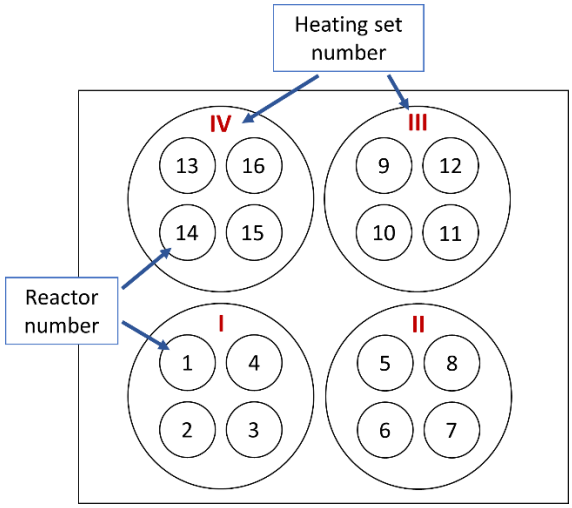

Figure S10. Scheme of the labelling of reactors and heating sets.

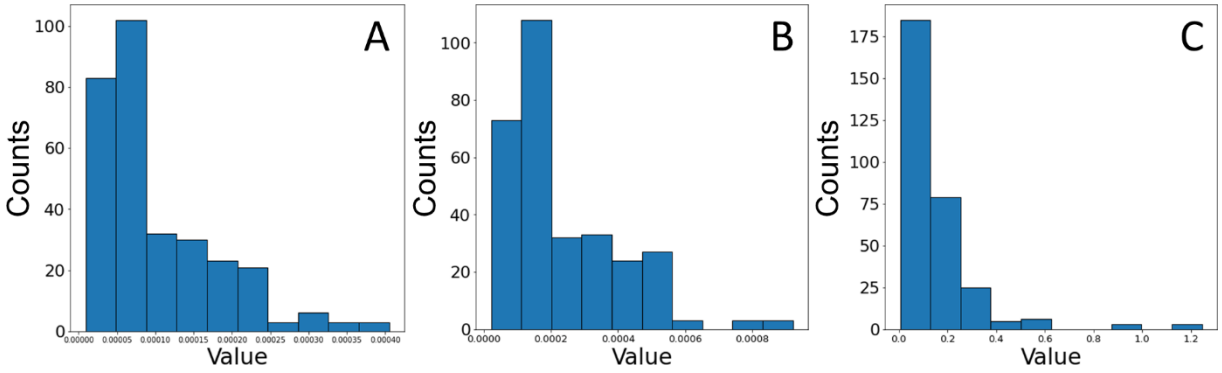

Figure S11. Distributions of the values for all reaction conditions for validation the influence of A - External diffusion; B - External heat transfer, C - Axial dispersion for all experimental conditions applied.

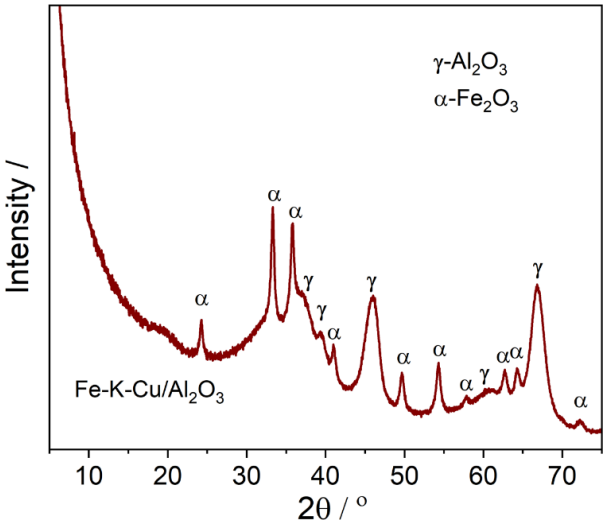

Figure S12. XRD pattern Fe-K-Cu/γ-Al_2O_3 catalyst.

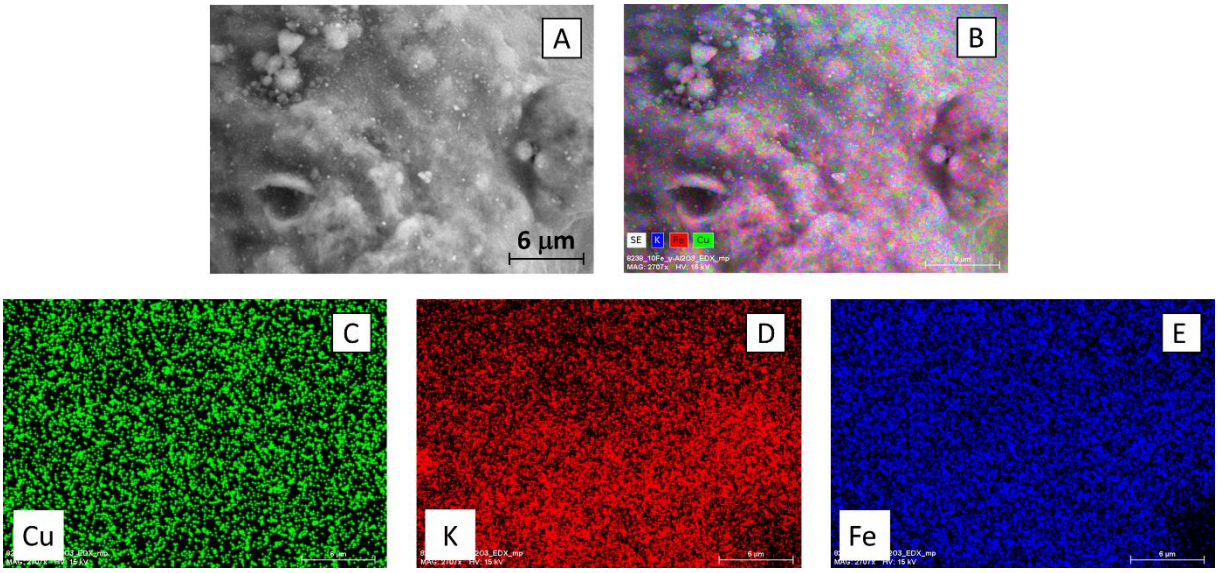

Figure S13. SEM picture (A) and the distribution of elements (B)-(E) based on EDX spectra.

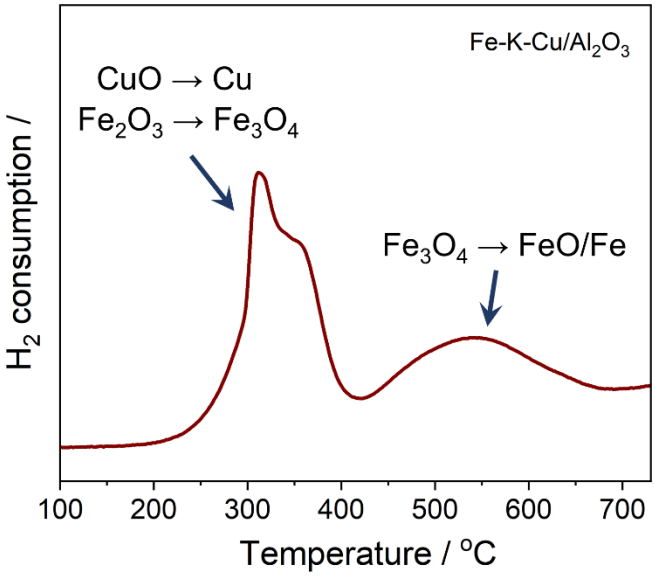

Figure S14. TPR-H_2 curve of Fe-K-Cu/γ-Al_2O_3 catalyst.

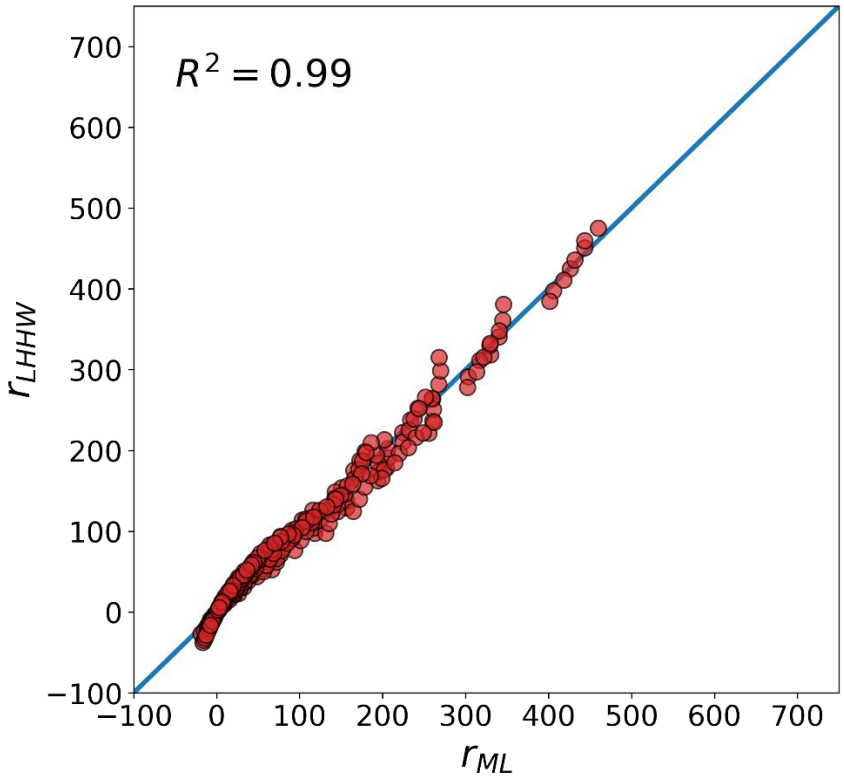

Figure S15. Parity plot of the rate of the RWGS reaction estimated by the KCNODE model versus those estimated by the LHHW model (equation S.9).

Tables

Table S1. Values of parameters used for simulating the plug flow reactor for CO_2 hydrogenation to methane.

Parameter	Value	Dimension
$k_{RWGS,ref}$	81.3	$mol \cdot g^{-1} \cdot s^{-1} \cdot bar^{-1.5}$
a_{RWGS}	16.3	-
$E_{a,RWGS}$	115	$kJ \cdot mol^{-1}$
$k_{FT,ref}$	63.9	$mol \cdot g^{-1} \cdot s^{-1} \cdot bar^{-2}$
a_{FT}	9.07	-
b_{FT}	2.44	bar^{-1}
$E_{a,FT}$	67.8	$kJ \cdot mol^{-1}$
T_{ref}	573.15	K
ρ_c	1.0	$g \cdot cm^{-3}$

Table S2. Catalyst loading list for the setup.

Reactor number	Heating set number	Reaction temperature, °C	Catalyst loading, mg
1	1	310	100
4			630
5	2	290	100
6			250
7			630
8			1630
10	3	270	100
11			630
14	4	250	250
15			1630

Table S3. Reaction conditions used in the present study. Time on stream was 15 hours for each condition.

Condition number	Flow rate, $cm^3 \cdot min^{-1}$	Gas composition, mol. %				Pressure, bar
		CO_2	CO	H_2	N_2	
1	18.3	20.0	-	60.0	20.0	15
2	**45.8**	**20.0**	**-**	**60.0**	**20.0**	**15**
3	114.4	20.0	-	60.0	20.0	15
4	45.8	32.0	-	48.0	20.0	15
5	45.8	11.4	-	68.6	20.0	15
6	**45.8**	**20.0**	**-**	**60.0**	**20.0**	**15**
7	45.8	16.0	4.0	60.0	20.0	15
8	45.8	13.2	6.8	60.0	20.0	15
9	**45.8**	**20.0**	**-**	**60.0**	**20.0**	**15**
10	45.8	20.0	-	60.0	20.0	20
11	45.8	20.0	-	60.0	20.0	10
12	**45.8**	**20.0**	**-**	**60.0**	**20.0**	**15**

Table S4. Activity of the Fe-K-Cu/γ-Al_2O_3 catalyst for different particle sizes. Reaction condition: pressure – 15 bar; temperature – 300 °C; CO_2:H_2:N_2 – 1:3:1; GHSV – 5 100 $cm^3 \cdot h^{-1} \cdot g^{-1}$; time on stream – 20 h. Before catalytic test, the catalyst was reduced in H_2 at 400 °C for 4 hours.

Particle size, mm	CO_2 conversion
0.08-0.20	26.0
0.20-0.32	26.7
0.32-0.40	26.8

Table S5. The list of parameters used for estimating criteria for the validation of diffusion and heat transfer limitations.

	Parameter	Dimension	Value
r_{obs}	measured reaction rate	$mol \cdot g^{-1} \cdot min^{-1}$	-
ρ_b	bulk catalyst density	$g \cdot cm^{-3}$	0.65
$R_{catalyst}$	catalyst particle radius	mm	0.07
n	reaction order	-	2
X	conversion	-	-
k_d	mass transfer coefficient [a]	$m \cdot s^{-1}$	0.061
C	bulk concentration of reactant	$mol \cdot m^{-3}$	-
Sh	Sherwood number [a]	-	-
Re	Reynolds number [b]	-	-
Sc	Schmidt number [c]	-	-
D	diffusion coefficient	$cm^2 \cdot s^{-1}$	0.5*
u_{feed}	gas feed velocity	$m \cdot s^{-1}$	-
ρ_{feed}	gas feed density	$kg \cdot m^{-3}$	-
μ	dynamic viscosity	$kg \cdot m^{-1} \cdot s^{-1}$	$2.5 \cdot 10^{-5}$
E_a	activation energy	$kJ \cdot mol^{-1}$	50
ΔH	reaction heat	$kJ \cdot mol^{-1}$	150
k_g	heat transport coefficient	$kJ \cdot m^{-2} \cdot s^{-1} \cdot K^{-1}$	2.0
R	gas constant	$J \cdot mol^{-1} \cdot K^{-1}$	8.31
T	temperature	K	-
$d_{reactor}$	reactor diameter	mm	7.04
L_{bed}	catalyst bed length	cm	-
Pe_{ax}	Peclet number [e]	-	-

* at 300 °C and atmospheric pressure. The values at different temperature and pressure were re-

Diffusion coefficient was calculated in each case according to the following formula:

$$D(P,T) = D(P_0,T_0)\frac{P_0 \cdot T^{1.5}}{P \cdot T_0^{1.5}}$$

Table S6. Elemental composition and textural characteristics of as-prepared catalysts.

Sample	Composition, wt. %			Specific surface area, $m^2 \cdot g^{-1}$	Pore volume, $cm^3 \cdot g^{-1}$	Pore size, nm
	Fe	K	Cu			
γ-Al_2O_3	-	-	-	216	0.46	7
Fe-K-Cu/γ-Al_2O_3	8.0 (10)*	1.9 (2.5)*	0.8 (1.0)*	193	0.38	6

* theoretical content in brackets

Table S7. The form of LHHW models used for modeling the RWGS reaction using the values of the RWGS reaction rates calculated by the KCNODE model. The values of the loss function, coefficient of determination R^2, and estimated parameters are also presented.

Expression	R^2	loss function	Values of parameters	Literature link
$\frac{k\left(p_{CO_2}p_{H_2} - \frac{p_{CO}p_{H_2O}}{K_{eq}}\right)}{p_{H_2}^{0.5}\left(1 + a\cdot p_{CO} + b\cdot\frac{p_{H_2O}}{p_{H_2}^{0.5}} + c\cdot p_{CO_2}\right)^2}$	0.986	$1.71\cdot10^2$	k = $1.6\cdot10^{-1}$ mmol min^{-1} g^{-1} $bar^{-1.5}$ a = 2.2 bar^{-1} b = 4.2 $bar^{-0.5}$ c = 0.16 bar^{-1}	Present work
$\frac{k\left(p_{CO_2}p_{H_2} - \frac{p_{CO}p_{H_2O}}{K_{eq}}\right)}{\left(1 + a\cdot p_{CO} + b\cdot p_{H_2O} + c\cdot p_{CO_2} + d\cdot p_{H_2}\right)^2}$	0.985	$1.80\cdot10^2$	k = $1.3\cdot10^{-1}$ mmol min^{-1} g^{-1} bar^{-2} a = 3.4 bar^{-1} b = 2.2 bar^{-1} c = 0.21 bar^{-1} d = 0.075 bar^{-1}	Hakeem et al. [8] Choi et al.[9]
$\frac{k\left(p_{CO_2}p_{H_2} - \frac{p_{CO}p_{H_2O}}{K_{eq}}\right)}{\left(1 + a\cdot p_{CO} + b\cdot p_{H_2O} + c\cdot p_{CO_2}\right)^2}$	0.972	$3.39\cdot10^2$	k = $5.5\cdot10^{-2}$ mmol min^{-1} g^{-1} bar^{-2} a = 2.2 bar^{-1} b = 1.4 bar^{-1} c = 0.16 bar^{-1}	Hakeem et al. [8]
$\frac{k\left(p_{CO_2}p_{H_2} - \frac{p_{CO}p_{H_2O}}{K_{eq}}\right)}{p_{CO} + a\cdot p_{H_2O} + b\cdot p_{CO_2} + c\cdot p_{H_2}}$	0.964	$4.36\cdot10^2$	k = $7.1\cdot10^{-3}$ mmol min^{-1} g^{-1} bar^{-2} a = 0.82 b = 0.052 c = 0.015	Panzone et al.[10]
$\frac{k\left(p_{CO_2}p_{H_2} - \frac{p_{CO}p_{H_2O}}{K_{eq}}\right)}{p_{H_2}^{0.5}(p_{CO} + a\cdot p_{H_2O} + b\cdot p_{CO_2})}$	0.944	$6.72\cdot10^2$	k = $2.2\cdot10^{-2}$ mmol min^{-1} g^{-1} $bar^{-1.5}$ a = 0.84 b = 0.11	Saeidi et al.[11]
$\frac{k\left(p_{CO_2}p_{H_2} - \frac{p_{CO}p_{H_2O}}{K_{eq}}\right)}{\left(1 + a\cdot p_{CO} + b\cdot p_{H_2O}\right)^2}$	0.935	$7.81\cdot10^2$	k = $2.5\cdot10^{-2}$ mmol min^{-1} g^{-1} bar^{-2} a = 1.6 bar^{-1} b = 0.98 bar^{-1}	Hakeem et al. [8]
$\frac{k\left(p_{CO_2}p_{H_2} - \frac{p_{CO}p_{H_2O}}{K_{eq}}\right)}{p_{CO} + a\cdot p_{H_2O} + b\cdot p_{CO_2}}$	0.930	$8.39\cdot10^2$	k = $7.5\cdot10^{-3}$ mmol min^{-1} g^{-1} bar^{-2} a = 0.83 b = 0.107	Riedel et al.[12]
$\frac{k\left(p_{CO_2}p_{H_2} - \frac{p_{CO}p_{H_2O}}{K_{eq}}\right)}{p_{H_2}^{0.5}\left(1 + a\frac{p_{H_2O}}{p_{H_2}}\right)^2}$	0.782	$2.62\cdot10^3$	k = $4.9\cdot10^{-2}$ mmol min^{-1} g^{-1} $bar^{-1.5}$ a = 6.6	Brübach et al.[13]
$\frac{k\left(p_{CO_2}p_{H_2} - \frac{p_{CO}p_{H_2O}}{K_{eq}}\right)}{p_{H_2}^{0.5}\left(1 + a\cdot\frac{p_{CO}p_{H_2O}}{p_{H_2}^{0.5}}\right)}$	0.586	$4.98\cdot10^3$	k = $3.7\cdot10^{-2}$ mmol min^{-1} g^{-1} $bar^{-1.5}$ a = 30 $bar^{-1.5}$	Yang et al.[14]

References

[1] D.E. Mears, Diagnostic criteria for heat transport limitations in fixed bed reactors, Journal of Catalysis 20(2) (1971) 127-131. https://doi.org/https://doi.org/10.1016/0021-9517(71)90073-X.

[2] H.S. Fogler, Elements of chemical reaction engineering, 5 ed., Prentice Hall, Philadelphia, PA, 2016.

[3] J. Zieliński, I. Zglinicka, L. Znak, Z. Kaszkur, Reduction of Fe_2O_3 with hydrogen, Applied Catalysis A: General 381(1) (2010) 191-196. https://doi.org/https://doi.org/10.1016/j.apcata.2010.04.003.

[4] O.A. Bulavchenko, A.A. Pochtar', E.Y. Gerasimov, A.V. Fedorov, Y.A. Chesalov, A.A. Saraev, V.A. Yakovlev, V.V. Kaichev, Chemical and texture promoters in Cu-Fe-Al oxide nanocomposite catalysts for combustion of solid fuel gasification products, Applied Catalysis A: General 590 (2020) 117364. https://doi.org/https://doi.org/10.1016/j.apcata.2019.117364.

[5] J. Antony, 6 - Full Factorial Designs, in: J. Antony (Ed.), Design of Experiments for Engineers and Scientists (Second Edition), Elsevier, Oxford, 2014, pp. 63-85. https://doi.org/https://doi.org/10.1016/B978-0-08-099417-8.00006-7.

[6] J.J. Moré, The Levenberg-Marquardt algorithm: Implementation and theory, in: G.A. Watson (Ed.) Numerical Analysis, Springer Berlin Heidelberg, Berlin, Heidelberg, 1978, pp. 105-116.

[7] N. Fischer, R. Henkel, B. Hettel, M. Iglesias, G. Schaub, M. Claeys, Hydrocarbons via CO_2 Hydrogenation Over Iron Catalysts: The Effect of Potassium on Structure and Performance, Catalysis Letters 146(2) (2016) 509-517. https://doi.org/10.1007/s10562-015-1670-9.

[8] A.A. Hakeem, M. Li, R.J. Berger, F. Kapteijn, M. Makkee, Kinetics of the high temperature water–gas shift over Fe_2O_3/ZrO_2, Rh/ZrO_2 and $Rh/Fe_2O_3/ZrO_2$, Chemical Engineering Journal 263 (2015) 427-434. https://doi.org/https://doi.org/10.1016/j.cej.2014.10.104.

[9] Y. Choi, H.G. Stenger, Water gas shift reaction kinetics and reactor modeling for fuel cell grade hydrogen, Journal of Power Sources 124(2) (2003) 432-439. https://doi.org/https://doi.org/10.1016/S0378-7753(03)00614-1.

[10] C. Panzone, R. Philippe, C. Nikitine, L. Vanoye, A. Bengaouer, A. Chappaz, P. Fongarland, Catalytic and Kinetic Study of the CO_2 Hydrogenation Reaction over a Fe–

K/Al_2O_3 Catalyst toward Liquid and Gaseous Hydrocarbon Production, Industrial & Engineering Chemistry Research 60(46) (2021) 16635-16652. https://doi.org/10.1021/acs.iecr.1c02542.

[11] S. Saeidi, S. Najari, F. Fazlollahi, M.K. Nikoo, F. Sefidkon, J.J. Klemeš, L.L. Baxter, Mechanisms and kinetics of CO_2 hydrogenation to value-added products: A detailed review on current status and future trends, Renewable and Sustainable Energy Reviews 80 (2017) 1292-1311. https://doi.org/https://doi.org/10.1016/j.rser.2017.05.204.

[12] T. Riedel, G. Schaub, K.-W. Jun, K.-W. Lee, Kinetics of CO_2 Hydrogenation on a K-Promoted Fe Catalyst, Industrial & Engineering Chemistry Research 40(5) (2001) 1355-1363. https://doi.org/10.1021/ie000084k.

[13] L. Brübach, D. Hodonj, P. Pfeifer, Kinetic Analysis of CO_2 Hydrogenation to Long-Chain Hydrocarbons on a Supported Iron Catalyst, Industrial & Engineering Chemistry Research 61(4) (2022) 1644-1654. https://doi.org/10.1021/acs.iecr.1c04018.

[14] J. Yang, Y. Liu, J. Chang, Y.-N. Wang, L. Bai, Y.-Y. Xu, H.-W. Xiang, Y.-W. Li, B. Zhong, Detailed Kinetics of Fischer−Tropsch Synthesis on an Industrial Fe−Mn Catalyst, Industrial & Engineering Chemistry Research 42(21) (2003) 5066-5090. https://doi.org/10.1021/ie030135o.

7. Curriculum Vitae

Aleksandr Fedorov

born: 23.04.1991.
email: fizorg103@gmail.com
Scopus 57539202100
Languages: Russian, English

Research Interests

Heterogeneous Catalysis, Reaction Engineering,
Mathematical Modelling, Machine Learning, Statistical Analysis.

Area of Expertise

Catalysis: CO_2 hydrogenation, CO oxidation, catalytic combustion of fuels and sludges in fluidized bed.
Physical Chemistry: analysis of XRD, TPR/TPD, XAS, XPS data, chemical thermodynamics.
Data Analysis and Modelling: kinetic modelling of catalytic reactions, mathematical modelling of chemical thermodynamics and industrial plants, artificial neural networks, statistical and correlation analysis of physicochemical and catalytic data.

Employment

2021-2024 **Researcher**, Leibniz-Institut für Katalyse e.V. (Rostock, Germany)
Department of Catalyst Discovery and Reaction Engineering

2014-2021 **Researcher**, Boreskov Institute of Catalysis (Novosibirsk, Russia)
Laboratory of Catalytic Processes of Renewables

2011-2014 **Laboratory Assistant**, Boreskov Institute of Catalysis (Novosibirsk, Russia)
Laboratory of Catalytic Processes of Renewables

Education

2021-2024 **PhD Student**, Leibniz-Institut für Katalyse e.V. (Rostock, Germany)
Thesis: *CO_2 Fischer-Tropsch Synthesis: Unleashing the Power of Data Science and Machine Learning for Sustainable Hydrocarbon Production*
Supervisor: Dr. David Linke

2008-2014 **Specialist Degree in Chemistry,** Novosibirsk State University (Novosibirsk, Russia)
Thesis: *Investigation of Cr- and Fe-based Deep Oxidation Catalysts for Fluidized Bed*
Supervisor: Prof. Dr. Yakovlev V.A.

2006-2008 **High School Certificate,** Specialized Educational Scientific Center of Novosibirsk State University (Novosibirsk, Russia)

Hobbies and Interests

Author of Instagram channel with scientific animation (@sexyscience103),
Baduk (5k, OGS)

Articles:

1. **Fedorov A.**, Perechodjuk A., Linke D. Kinetics-constrained neural ordinary differential equations: artificial neural network models tailored for small data to boost kinetic model development, *Chemical Engineering Journal*, 2023, doi:10.1016/j.cej.2023.146869.
2. **Fedorov A.**, Linke D. Data analysis of CO_2 hydrogenation catalysts for hydrocarbon production, *Journal of CO_2 Utilization*, 2022, doi:10.1016/j.jcou.2022.102034.
3. **Fedorov A.**, Lund H., Kondratenko V.A., Kondratenko E.V., Linke D. Elucidating reaction pathways occurring in CO_2 hydrogenation over Fe-based catalysts, *Applied Catalysis B: Environmental*, 2023, doi:10.1016/j.apcatb.2023.122505.
4. **Fedorov A.V.**, Shamanaev I.V. Crystal structure representation for neural networks using topological approach, *Molecular Informatics*, 2017, doi:10.1002/minf.201600162.
5. **Fedorov A.V.**, Dubinin Y.V., Yeletsky P.M., Fedorov I.A., Shelest S.N., Yakovlev V.A. Combustion of sewage sludge in a fluidized bed of catalyst: ASPEN PLUS model, *Journal of Hazardous Materials,* 2021, doi:10.1016/j.jhazmat.2020.124196.
6. **Fedorov A.V.**, Kukushkin R.G., Yeletsky P.M., Bulavchenko O.A., Chesalov Y.A., Yakovlev V.A. Temperature-programmed reduction of model CuO, NiO and mixed CuO–NiO catalysts with hydrogen, *Journal of Alloys and Compounds*, 2020, doi:10.1016/j.jallcom.2020.156135.
7. **Fedorov A.**, Saraev A., Kremneva A., Selivanova A., Vorokhta M., Šmíd B., Bulavchenko O., Yakovlev V., Kaichev V. Kinetic and mechanistic study of CO oxidation over nanocomposite Cu-Fe-Al oxide catalysts, *ChemCatChem*, 2020, doi:10.1002/cctc.202000852.
8. **Fedorov A.V.**, Gulyaeva Y.K. Strength statistics for porous alumina, *Powder Technology*. 2019, doi:10.1016/j.powtec.2018.11.098.
9. **Fedorov A.V.**, Yazykov N.A., Bulavchenko O.A., Saraev A.A., Kaichev V.V., Yakovlev V.A. CuFeAl nanocomposite catalysts for coal combustion in fluidized bed, *Nanomaterials*, 2020, doi:10.3390/nano10051002.
10. **Fedorov A.V.**, Tsapina A.M., Bulavchenko O.A., Saraev A.A., Odegova G.V., Ermakov D.Y., Zubavichus Y.V., Yakovlev V.A., Kaichev V.V. Structure and chemistry of Cu-Fe-Al nanocomposite catalysts for CO oxidation, *Catalysis Letters*, 2018, doi:10.1007/s10562-018-2539-5.
11. Fedorova E.A., Kraußer L., Weiß J., **Fedorov A.**, Brückner A., Kondratenko E.V., Kubis C. Operando DRIFTS Investigations on Surface Intermediates and Effects of Potassium in CO_2 Hydrogenation over a K-Fe/$YZrO_x$ Catalyst, *ChemCatChem*, 2024, doi:10.1002/cctc.202301697.

12. Kraleva E., **Fedorov A.**, Kreyenschulte C., Fedorova E., Armbruster U., Wohlrab S., Morphological and structural differences of Fe-Zn-Al oxide nanocomposites obtained from citrate decomposition and microemulsion method, *Journal of Alloys and Compounds*, 2023, doi:10.1016/j.jallcom.2023.169093.
13. Kaichev V.V., Saraev A.A., **Fedorov A.V.**, Gerasimov E. Yu. The origin of size effect in oxidation of CO on supported palladium nanoparticles, *Catalysts*, 2023, doi:10.3390/catal13111435.
14. Bulavchenko O.A., Pochtar A.A., Gerasimov E.Y., **Fedorov A.V.**, Chesalov Y.A., Saraev A.A., Yakovlev V.A., Kaichev V.V. Chemical and texture promoters in Cu-Fe-Al oxide nanocomposite catalysts for combustion of solid fuel gasification products, *Applied Catalysis A: General*, 2020, doi:10.1016/j.apcata.2019.117364.
15. Kremneva A.M., **Fedorov A.V.**, Bulavchenko O.A., Knyazev Y.V., Saraev A.A., Yakovlev V.A., Kaichev V.V. Effect of calcination temperature on activity of Fe_2O_3-Al_2O_3 nanocomposite catalysts in CO oxidation, *Catalysis Letters*, 2020, doi:10.1007/s10562-020-03250-8.
16. Saraev A.A., Tsapina A.M., **Fedorov A.V.**, Trigub A.L., Bulavchenko O.A., Vinokurov Z.S., Zubavichus Y.V., Kaichev V.V. CuFeAl-composite catalysts of oxidation of gasification products of solid fuels: in situ XAS and XRD study, *Radiation Physics and Chemistry*, 2020, doi:10.1016/j.radphyschem.2018.11.025.
17. Bulavchenko O.A., Vinokurov Z.S., Saraev A.A., Tsapina A.M., Trigub A.L., Gerasimov E.Y., Gladky A.Y., **Fedorov A.V.**, Yakovlev V.A., Kaichev V.V. The Influence of Cu and Al additives on reduction of iron(III) oxide: in situ XRD and XANES study, *Inorganic Chemistry*, 2019, doi:10.1021/acs.inorgchem.8b03403.
18. Selishcheva S.A., Smirnov A.A., **Fedorov A.V.**, Bulavchenko O.A., Saraev A.A., Lebedev M.Y., Yakovlev V.A. Highly active CuFeAl-containing catalysts for selective hydrogenation of furfural to furfuryl alcohol, *Catalysts*, 2019, doi:10.3390/catal9100816.

Book:

1. Parmon V.N., Yakovlev V.A., Sorokina K.N., Chesnokov V.V., Bulushev D.A., Yashnik S.A., Gromov N.V., Dubinin Y.V., **Fedorov A.V.**, Samoylova Y.V., Milushina A.S., Anisimov O.A., Bolotov V.A., Golub F.S., Griboskii A.G., Chernous Y.D., Shamirzaev V.T., Boltenkov V.V., Taran O.P., Medvedeva T.B. New physical and catalytic processes for deep processing of hydrocarbon raw materials and biomass for solving the problems of environmental, clean and resource-saving energy, Monograph, 2020, Publishing: Novosibirsk State University (In Russian).

Patents:

1. **Fedorov A.V.**, Ermakov D.Y., Dubinin Y.V., Yazykov N.A., Yakovlev V.A. Catalyst for sludge burning and method for preparing this catalyst, EA042079B1, 11.01.2023.
2. **Fedorov A.V.**, Ermakov D.Y., Dubinin Y.V., Yazykov N.A., Yakovlev V.A. Deep oxidation catalyst and method for catalytic combustion of sludge from municipal wastewater treatment plants, RU2750801C1, 25.09.2020.
3. **Fedorov A.V.**, Ermakov D.Y., Dubinin Y.V., Yazykov N.A., Yakovlev V.A. Method for preparing deep oxidation catalyst and method for catalytic combustion of sludge from municipal wastewater treatment plants, RU2750799C1, RU2750800C1, RU2750802C1, 25.09.2020.
4. **Fedorov A.V.**, Selishcheva S.A., Smirnov A.A., Yakovlev V.A. Method of producing selective hydrogenation furfural, RU2689417C1, 28.05.2019.
5. **Fedorov A.V.**, Selishcheva S.A., Smirnov A.A., Yakovlev V.A. Selective hydrogenation catalyst for furfural, RU2689418C1, 27.11.2018.
6. **Fedorov A.V.**, Ermakov D.Y., Yakovlev V.A., Yazykov N.A., Simonov A.D., Parmon V.N. Method of preparing deep oxidation catalyst, RU2591955C1, 25.03.2015.
7. **Fedorov A.V.**, Yazykov N.A., Yakovlev V.A., Ermakov D.Y., Simonov A.D., Parmon V.N. Catalyst deep oxidation, RU2577253C1, 25.03.2015.
8. Selishcheva S.A., **Fedorov A.V.**, Smirnov A.A., Yakovlev V.A. Method of obtaining furfuryl alcohol by selective hydrogenation of furfural, RU2680799C1, 27.11.2018.
9. Yazykov N.A., Simonov A.D., Dubinin Y.D., **Fedorov A.V.**, Fedorov I.A., Yakovlev V.A., Parmon V.N. Fuel combustion method, RU2649729C1, 04.04.2018.
10. Simonov A.D., Yazykov N.A., Dubinin Y.D., **Fedorov A.V.**, Fedorov I.A., Yakovlev V.A., Parmon V.N. Catalytic heat generator, RU195265U1, 21.01.2020.
11. Selishcheva S.A., **Fedorov A.V.**, Smirnov A.A., Yakovlev V.A. Method of obtaining furfuryl alcohol by selective hydrogenation of furfural, RU2680799C1, 27.11.2018.
12. Romanenko A.V., Bukhtiyarova M.V., Gulyaeva Y.K., Dubinin Y.D., **Fedorov A.V.**, Tyunyaev A.A., Gulyaev R.V., Voropaev I.N. Carrier, dehydrogenation catalyst, preparation method, RU2801222C2, 03.08.2023.
13. Simonov A.D., Yazykov N.A., Dubinin Y.D., Fedorov I.A., Yakovlev V.A., **Fedorov A.V.** Fuel combustion method, RU2647744C1, 19.03.2018.

Talks:

1. **Fedorov A.**, Linke D. Data analysis of CO_2 hydrogenation catalysts for hydrocarbon production, *55. Jahrestreffen Deutscher Katalytiker,* 27-29 June 2022, Weimar, Germany.
2. **Fedorov A.**, Lund H., Kondratenko V., Kondratenko E., Linke D. An unexpected pathway of CO_2 hydrogenation into hydrocarbons over Fe-based catalysts, *56. Jahrestreffen Deutscher Katalytiker,* 15-17 March 2023, Weimar, Germany.
3. **Fedorov A.**, Perechodjuk A., Linke D. Machine learning for small data: Accelerated kinetic model development for CO_2 hydrogenation into hydrocarbons, *Annual Meeting on Reaction Engineering 2023,* 15-17 May 2023, Frankfurt am Main, Germany.
4. **Fedorov A.**, Perechodjuk A., Wohlrab S., Linke D. Extracting knowledge from literature by data science for development of highly-selective CO_2 Fischer-Tropsch catalysts, *Sustainable Aviation Fuels - Design, Production and Climate Impact,* 24-27 May 2023, Bad Honnef, Germany.
5. **Fedorov A.**, Perechodjuk A., Linke D. Breaking barriers to kinetic modeling of CO_2 hydrogenation to hydrocarbons using machine learning, *15th European Congress on Catalysis,* August 27 – September 1, 2023, Prague, Czech Republic.

Posters:

1. **Fedorov A. V.**, Bulavchenko O.A., Saraev A.A., Tsapina A.M., Vinokurov Z.S., Yakovlev V.A., Kaichev V.V. Synthesis and catalytic properties of Cu-Fe-Al oxide nanocomposites - a catalyst for CO Oxidation, *14th European Congress on Catalysis*, 18-23 August 2019, Aachen, Germany.
2. **Fedorov A. V.**, Ermakov D.Y., Yazykov N.A., Yakovlev V.A., Spherical CuO-Fe_2O_3-Al_2O_3 catalysts for fuel combustion in a fluidized bed, *13th European Congress on Catalysis*, 27-31 August 2017, Florence, Italy.